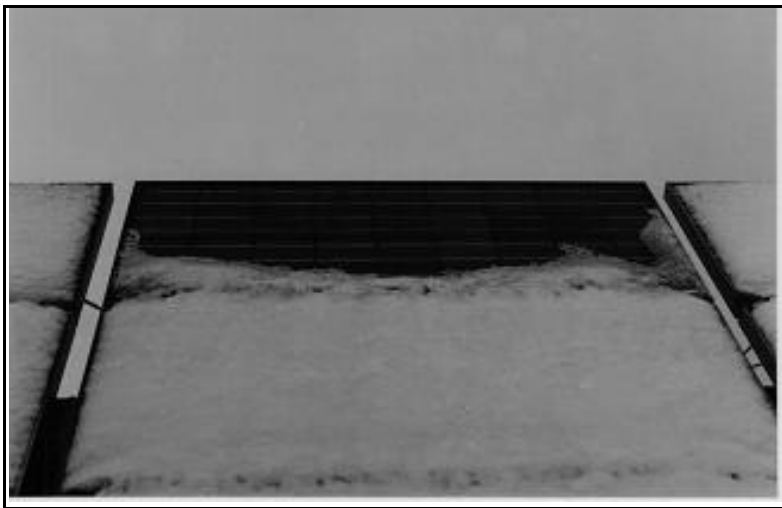


***Snow and Ice Accumulation
on Photovoltaic Arrays:
An Assessment of the TN Conseil
Passive Melting Technology***



***Snow and Ice Accumulation
on Photovoltaic Arrays:
An Assessment of the TN Conseil
Passive Melting Technology***

Michael Ross

Report Prepared for

The Science Institute of the Northwest Territories

and

The Energy Diversification Research Laboratory

September, 1995

Division Report EDRL 95-68 (TR)

CITATION

Ross, M. M. D., Snow and Ice Accumulation on Photovoltaic Arrays: An Assessment of the TN Conseil Passive Melting Technology, report # *EDRL 95-68 (TR)*, Energy Diversification Research Laboratory, CANMET, Natural Resources Canada, Varennes, September 1995, 273 pp.

Copies of this report may be obtained through the following:

*Energy Diversification Research Laboratory
CANMET / Natural Resources Canada
1615 Montée Ste-Julie
P.O. Box 4800
Varennes, Québec
J3X 1S6
Tel: (514) 652-4621
Fax: (514) 652-0999*

DISCLAIMER

This report is distributed for informational purposes and does not necessarily reflect the views of the Government of Canada nor constitute an endorsement of any commercial product or person. Neither Canada nor its ministers, officers, employees or agents makes any warranty in respect to this report or assumes any liability arising out of this report.

NOTE

Funding for this project was provided by the Energy Diversification Research Laboratory through the Panel on Energy Research and Development and Canada's Green Plan and the Science Institute of the Northwest Territories as part of the joint NRCan/SINT "PV for the North" program.

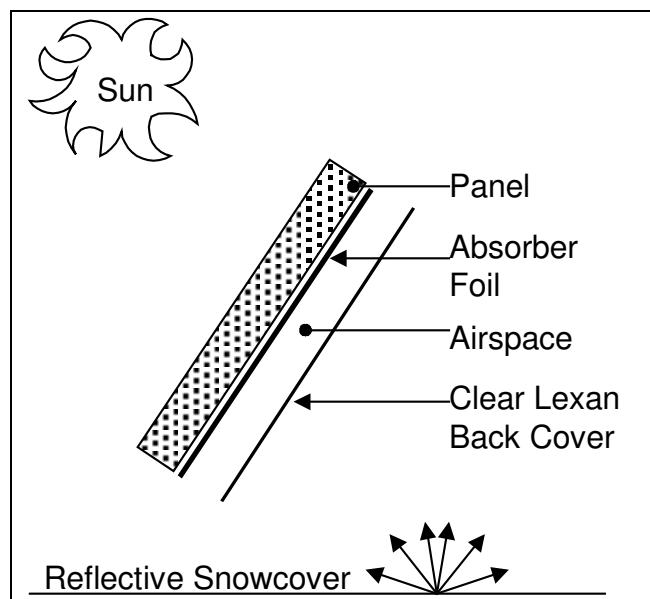
EXECUTIVE SUMMARY

Background

In Canada, photovoltaic (PV) systems are usually located at remote sites, where their low-maintenance, high-reliability characteristics make them the least-cost power supply option. However, during winter, snow and ice can accumulate on PV panels, thereby reducing electrical output for extended periods of time. This can result in the technology being unable to meet the load's power requirements, undermining the PV system's reliability. Such a failure often necessitates a visit to the site, which can be prohibitively costly at the more remote sites, especially those with helicopter access. In order to lower the probability of system outages, battery banks for PV systems are currently oversized, adding considerably to the cost of the system.

Working in conjunction with the EDRL and the Institut de recherche d'Hydro-Québec (IREQ), the Montréal firm TN Conseil has developed a passive technology that melts snow and ice from the face of a PV panel. This technology consists of a black absorber foil bonded to the rear of the panel, a one cm air cavity which insulates against heat loss, and a clear Lexan back cover sheet. The absorber foil collects the solar radiation that is incident on the rear face of the panel, and in combination with the back cover, elevates the temperature of the panel, promoting snow and ice removal. In this way, the technology is somewhat like a solar thermal stagnating air collector, utilizing the radiation which is reflected off the snowcover on the ground behind the panel.

In this report, the problem of snow and ice accumulation on PV panels is reviewed, and the solution proposed by TN Conseil is investigated.



The TN Conseil Technology

Snow and Ice Accumulation on PV Arrays

Snow and ice can accumulate on a PV array in a number of physical forms:

- dry snow deposition;
- wet snow accretion;
- rime, which occurs when supercooled water droplets impinge on a structure and freeze before forming a continuous liquid layer;
- glaze, which occurs when rain or supercooled water droplets impinge on a

- structure and freeze after forming a continuous liquid layer;
hoarfrost, which occurs when supercooled or supersaturated water vapour encounters a nucleating surface and forms crystals.

Snow, rime, glaze, and hoarfrost are very unpredictable, both from year to year and from site to site. Whether they are a problem at a particular PV site depends on many site-specific factors that can not be deduced from commonly available meteorological data. Simple models for the accumulation of rime and snow are presented in this report, mainly to identify for the reader the principal factors affecting the rate of accumulation. Qualitative information on snow and ice accumulation is available, on the other hand, from experts in the field of atmospheric icing of structures and from PV installers and users, eighteen of whom were contacted for this report. Even so, several PV installers pointed out that it is difficult to know whether snow or ice accumulation is a problem at remote PV systems, since oversized battery banks power the load even when the panels fail for an extended period of time.

Rime causes serious problems at many PV installations, particularly those, such as telecommunication systems, located on ridges and mountain tops at elevations greater than 650 m. Rime may accumulate in the late autumn and not melt off until the spring, effectively "turning off" the PV power system for the winter. Riming of PV panels can occur in mountainous regions throughout Canada, including Devon Island, Ellesmere Island, the Yukon, northeastern Labrador, the Gaspé, the north shore of the St. Lawrence, Cape Breton Island, and the Coastal, Cariboo, Selkirk, and Stikine Mountains of British Columbia. It also occurs in Arctic areas prone to winter fogs.

In general, snow melts off, slides off, or blows off PV panels fairly quickly, and thus presents less of a threat to PV installations than rime. A wet snowfall followed by very cold weather appears most likely to result in a long-lived deposit of snow on the array. Large panel tilt angles are quite effective in preventing snow accumulation; nevertheless, PV installers reported some snow accumulation problems on the Prairies and in Québec.

Glaze does not appear to be a serious problem in the operation of PV arrays in Canada, since it transmits considerable light and, in most places, is followed by warm temperatures. An exception to this may be Newfoundland, and the Avalon region especially, where glaze is more severe, more frequent, and longer-lasting than elsewhere. It is highly improbable that hoarfrost poses a threat to the winter operation of PV panels.

Presently, many panels in rime-prone areas are mounted vertically and located at the most windswept sites possible, with the expectation that this will encourage shedding and wind removal of rime. However, these two measures also maximize the flux of supercooled water droplets onto the panels, thus maximizing rime accumulation. Experts on rime accumulation suggested that, when possible, less windy sites should be chosen. Additionally, lower panel tilt angles should be experimented with.

The problem of snow and rime accumulation has been approached in a number of ways. The

most common practice is to drastically increase the capacity of the battery bank. It is not uncommon for rime-prone systems in British Columbia to have "three month autonomy", or the ability to power the load for three months from batteries alone. This increases the capital costs of the system, but installation, operating, and maintenance costs may be far more significant at remote sites accessible only by helicopter. Soltek Solar Energy Ltd., of Victoria, British Columbia, has developed a solar panel for flush mounting directly onto comshells. Wind, carrying water droplets, may flow around, rather than into, the comshell. Users report that this reduces, but does not eliminate, rime accumulation. Icephobic coatings, which purportedly reduce the adhesion of ice and snow to glass, wear off quickly and are unanimously dismissed by researchers and field personnel alike.

Pertinent Properties of Snow and Ice

The classification of snow and the properties of snow pertinent to the problem of snow accumulation on PV panels are reviewed in this report. Properties examined are density, effective thermal conductivity, latent heat of fusion, albedo, solar radiation transmission and emissivity. The transmission of solar radiation through snow can be modelled by the Bouguer-Lambert law; thus, the level of radiation penetrating a layer of snow decreases with thickness in an exponential manner. The properties of rime are poorly documented and must be inferred from those of snow.

Electrical Performance of a Snow or Ice Covered PV Array

Snow or ice cover "shades" cells in the array and thus limits their ability to generate electricity. The electrical performance of a uniformly covered array will be linearly related to the level of solar radiation penetrating the snow cover. However, the electrical performance of a nonuniformly covered array will be nonlinearly related to the average level of solar radiation penetrating the snow cover.

In a series string of cells, the current passing through the cells is limited by the most severely shaded cell. The less-shaded cells force this cell to operate at a current above its short circuit current, and thus the cell becomes reverse-biased, acts like a resistive component, and dissipates electrical energy as heat.

To reduce the degradation in electrical performance associated with shading a small portion of a module, most modules have one or more bypass diodes in parallel with the cells. These bypass diodes shunt current past a string of cells if the string becomes seriously shaded. Thus, the bypass diodes limit the effect of shading on the module. Nevertheless, shading by snow or ice can have a serious impact on the module output: in an experiment on a Siemens M55 and an Astropower APC4716 module, shading one cell in the module by 60 to 75 % reduced the irradiance of the panel by only 2 % but reduced the peak power output by 40 to 50 %.

A model for the effects of partial shading of the PV array would provide a better basis for studying the effect of snow or ice on the array's electrical performance, but was not developed for this study.

Solar Energy Incident on the Rear Face of a Panel

In order to predict the thermal performance of the TN Conseil technology, the radiation incident at the rear face of the panel must be modelled. For most arrays the beam radiation incident on the rear of the panel during the winter will be insignificant; the diffuse radiation on the rear face of the panel can be modelled with the Perez model or a modified Temps and Coulson model with Klucher modulating function. However, the principal component of the radiation on the rear face will be ground-reflected radiation. A model for this, accounting for the shadow of the array (for both beam and diffuse radiation) is developed.

The model for ground-reflected radiation was compared with four measurements of the radiation incident on the rear face of the 20 kW roof-top array at the EDRL when there was snow on the ground. For this array, the average error for the model that does not account for the shadow of the array was 90 %, whereas the model that accounted for the shadow was, on average, 25 to 30 % in error.

A sensitivity analysis was performed on the model. On the rear face of the array, the incident diffuse radiation was only 5 to 15 % of the intensity of the incident ground-reflected radiation. The radiation incident on the rear face of an array was found to be 8 to 34 % of magnitude of the total radiation incident on the front face of an array, with 24 % a typical value. For most small and medium-sized arrays (up to one kW), the shadow of the array does not significantly affect the radiation incident on the rear face of the array.

Thermal Performance of a PV Panel with the TN Conseil Snow Removal Technology

The thermal performance of the TN Conseil technology without snowcover was studied in two ways. First, two panels, equipped with the TN Conseil technology and installed in the rooftop array at the EDRL, were monitored. Second, mathematical models of the steady-state thermal behaviour of a Siemens M55 panel, with and without the TN Conseil technology, were developed. When compared with the monitored data, the models tended to overestimate the monitored readings by three to four °C, with a standard deviation of about four °C. The models appeared to be less accurate at lower windspeeds and higher insulations, but equally accurate at all ambient air temperatures.

As expected, both the models and the monitored data showed that the TN Conseil-modified panels operate at temperatures significantly higher than those of unmodified panels. With moderate to strong insolation levels, the monitored TN Conseil-modified panels operated at temperatures 15 to 30 °C higher than the unmodified panels. The models showed that the operating temperature is principally affected by the insolation on the front and back of the panel, the ambient air temperature, and the windspeed, which has a nonlinear effect.

The models were used to compare various options for the absorber foil and the plastic back cover. The standard TN Conseil technology, as described above, was found to have the highest temperature, the unmodified panel the lowest temperature, and all panel configurations with a plastic back cover operating at higher temperatures than all panels without such a back cover. However, the models predict only the average temperature of the panel, and the monitored panels revealed the existence of significant temperature variations at different locations on the TN Conseil-modified panel. Free convection results in the top half of the panel being up to 10 °C warmer than the bottom half, and the panel's aluminum frame acts as a heat sink and depresses the temperature of the panel in the vicinity of the frame.

Snow and Ice Removal from Photovoltaic Panels

Mathematical models were used to investigate the the rate of snow and ice removal from a Siemens M55 panel with and without the TN Conseil technology. For a given windspeed and insolation level, the TN Conseil modified panel initiates snow or ice removal at an ambient temperature much lower than that required for melting by an unmodified panel. For example, the model indicates that with peak sun and a 10 m/s wind, a 10 cm thick rime or dense snow accumulation will start melting at an ambient air temperature of -23 °C on the TN Conseil modified panel but only at -3 °C for an unmodified panel; the TN Conseil panel performs even better at lower windspeeds and with thinner accumulations. Furthermore, the TN Conseil-modified panel has a significantly higher melting rate than the unmodified panel. For example, for an ambient air temperature of -5 °C and peak sun insolation, the modelled melting rate for rime on the unmodified panel is about 0.25 cm/hr whereas the melting rate for the TN Conseil modified panel is about 0.7 cm/hr.

The models reveal that the contributions of the Lexan back cover and the black absorber foil to the snow removal performance of the TN Conseil technology are very different. The Lexan cover limits heat losses and thus raises the temperature of the panel to the snow's melting point. The black absorber foil maximizes the energy gains and increases the melt rate. A system with one or the other component, but not both, would not function well, especially for accumulations that are well-attached to the panel.

One aspect of the TN Conseil modified panels melting performance that is not reflected in the models is the modified panel's tendency to form a ledge of densified snow or ice at the bottom lip of the panel. This ledge partially shades the panel and provides a foothold for further snow or ice accumulation. It is hypothesized that this ledge arises either from the temperature gradients along the panel or from the TN Conseil panel initiating melting under marginal conditions such that the ledge freezes onto the panel overnight. The use of Lexan Thermoclear, a corrugated transparent plastic, in place of the Lexan back cover sheet and associated air cavity, is proposed as a way to reduce the temperature gradients across the panel and decrease the modified panel's tendency to form an ice ledge. In addition, very simple mathematical models of the panel frame show that anodizing the aluminum black instead of silver, or more effectively, insulating the frame against heat loss, will also reduce the temperature gradients.

It is possible that rime will accumulate on the rear as well as the front surface of the panel. Rime accumulation on the rear face of the panel will decrease the radiation incident on the black absorber foil and reduce the efficacy of the TN Conseil system considerably, especially for thicker rime deposits. A solution to this problem, referred to as a "rime shield", has been proposed during the course of this investigation but is not described in this report.

Simulation of System Performance at Four Sites

A computer program that models the melting performance of the unmodified and TN Conseil modified panels at four sites across Canada using actual weather data was developed. A rime or snow accumulation of a certain thickness was assumed to exist on the panels on January 1, and the program determined how long it would take for the deposit to be removed, assuming no further accumulation occurred. For rime, it was assumed that an equally thick accumulation existed on both the front and the back of the panel. The initial accumulation was assumed to be very dense with high thermal conductivity and poor solar radiation transmission-- a type of accumulation which is rare but represents the most serious threat to PV systems.

The modelled performance for a site at Bagotville, Quebec, suggests that the TN Conseil modification is highly effective for snow, reducing the average time required for snow removal by about 95 % (if shedding occurs) to 80 % (if complete melt-off occurs). For rime, the model suggests that the TN Conseil technology is somewhat less effective. For mountainous sites in B.C. and Newfoundland, the average time to shedding was reduced by about 30 to 40 % and the average time to melting by about 20 to 30 %. The technology was less effective at a site just above the Arctic Circle in the Northwest Territories. However, if the parameters used to model the rime accumulation are incorrect, these results probably underestimate the improvement realizable with the TN Conseil technology.

The times required for melting and shedding for the TN Conseil panel with the rime shield are only slightly better than those for the TN Conseil panel without the rime shield. This is misleading, however, since it was assumed that rime would be removed from the rear face of the panel at the same rate that it was removed from the front face of the panel. In reality, however, the air cavity in the TN Conseil technology insulates the panel sufficiently well that the Lexan back cover does not heat up. This suggests that rime will not remove itself from the rear of the TN Conseil technology, and therefore the performance of the TN Conseil Technology without the rime shield will degrade over the winter as rime accumulates on the rear face.

The large number of assumptions and unknowns required to model the removal of rime and snow from the panel suggest that the results presented above can be used only as a rough comparison of thermal performance. A more accurate assessment will require experimentation, preferably in the field, at rime-prone sites.

Summer Battery Charging Performance

The TN Conseil technology will elevate panel temperatures during summer as well as winter. Hotter panels operate at lower voltages, suggesting that during the summer a single panel or parallel arrangement of panels might not be able to fully charge a 12 V battery. Mathematical models of the thermal behaviour of the panel were used to determine whether this would be a problem.

According to the models, during worst-case summer conditions of very low wind, peak sun, and high ambient air temperatures, the M55 panel and other 36 cell panels will be able to charge the battery, although the rate of charging may be lower. Under worst-case conditions, the M75 and other panels with 33 or fewer cells may be unable to fully charge the battery. However, in locations where snow and ice accumulation is a concern, it is unlikely that worst-case conditions will persist for the duration of the summer. At the EDRL, the highest monitored temperature reached by the TN Conseil-modified panels was 78 °C. At this temperature, an M55 module would be capable of full charging.

Observed Short-term Operation of the Snow Removal Technology

The snow removal performance for March 6 and 7, 1995, of panels with and without the TN Conseil technology is examined. Results are presented in graphs of monitored panel current and temperature and a chronological series of photographs.

TABLE OF CONTENTS

1. INTRODUCTION.....	1
2. SNOW AND ICE ACCUMULATION ON PV PANELS.....	4
2.1 Introduction.....	4
2.2 Types of Snow and Ice Accumulation	6
2.2.1 Particulate Accretion: Rime and Glaze.....	7
2.2.1.1 Definitions and Properties.....	7
2.2.1.2 Formation: Theory and Field Experience	7
2.2.2 Deposition of Water Vapour: Hoarfrost.....	12
2.2.3 Snow Deposition and Accretion	12
2.2.3.1 Particulate Accretion: Wet Snow.....	13
2.2.3.2 Deposition: Dry Snow.....	16
2.2.3.3 Wet and Dry Snow Retention	20
2.3 Snow and Ice Accumulation by Region.....	21
2.3.1 Northern Canada	23
2.3.2 British Columbia and Albertan Rockies	23
2.3.3 Prairies	24
2.3.4 Ontario	24
2.3.5 Québec	25
2.3.6 Maritimes	25
2.3.7 Other Countries.....	27
2.4 Overview of the Problems Caused by Snow and Ice to PV Installations	27
2.5 Approaches to the Problem of Snow and Ice Accumulation	27
3. PERTINENT PROPERTIES OF SNOW, RIME, AND GLAZE.....	30
3.1 Snow	30
3.1.1 Classification of Snow	30
3.1.2 Effective Thermal Conductivity.....	31
3.1.3 Latent Heat of Fusion.....	32
3.1.4 Optical Properties of Snow	32
3.1.4.1 Albedo.....	32
3.1.4.2 The Bouger-Lambert Law	37
3.1.4.3 Solar Radiation Extinction Coefficient.....	38
3.1.5 Emissivity	40
3.2 Rime and Glaze.....	40

4. ELECTRICAL PERFORMANCE OF A SNOW OR ICE COVERED ARRAY	44
4.1 Effect of Partial Shading on Module Performance	44
4.1.1 Effect on a Single Cell	44
4.1.2 Effect on a Series Arrangement of Cells.....	45
4.1.3 Effect on a Module.....	46
4.2 Measured Effects of Shading	46
4.2.1 Observations	46
4.2.2 Application to Snow and Ice Cover on Panels.....	59
4.3 Modelling the Effects of Partial Shading due to Snow or Ice Cover	60
5. SOLAR ENERGY INCIDENT ON THE REAR OF A PANEL.....	61
5.1 Introduction.....	61
5.2 Diffuse Radiation Incident on the Rear Face of the Array.....	63
5.2.1 Temps and Coulson Model with Klucher Modulating Function	64
5.2.2 The Perez Model	65
5.3 Ground-Reflected Radiation Incident on the Rear Face of the Array	67
5.3.1 Ground-Reflected Radiation Without Accounting for Shading.....	67
5.3.2 Ground-Reflected Radiation Accounting for Shading.....	67
5.3.2.1 Assumptions.....	68
5.3.2.2 Diffuse Radiation on a Point on the Ground.....	68
5.3.2.3 Beam Radiation on a Point on the Ground	72
5.3.2.4 Radiation on the Rear Surface of the Array	74
5.3.2.5 Implementation	75
5.4 Comparison of Model and Experimental Results	75
5.5 Application of Model Accounting for Shading to Various Installations	77
6. THERMAL PERFORMANCE OF A PV PANEL WITH THE TN CONSEIL SNOW REMOVAL TECHNOLOGY.....	82
6.1 Monitored Performance	82
6.1.1 Panel Configuration and Monitoring	82
6.1.2 Unmodified versus TN Conseil	83
6.1.3 Nickel vs Copper Absorber.....	84
6.1.4 With vs Without Lexan Back Cover.....	86
6.1.5 Panel Temperature Gradients.....	86
6.2 Modelled Performance.....	91
6.2.1 Description of the Models.....	91
6.2.1.1 Model of Unmodified Panel.....	91
6.2.1.2 Model of Standard TN Conseil Technology	93
6.2.1.3 Model of Black Tedlar Back without Back Cover.....	93
6.2.1.4 Model of Black Nickel Foil Back without Back Cover	95
6.2.1.5 Model of Lexan Thermoclear	95
6.2.1.6 Model of Black Tedlar Back with Back Cover	95
6.2.2 Equations for Heat Transfer And Other Energy Flows.....	95
6.2.2.1 Radiation	97

6.2.2.2 Conduction.....	97
6.2.2.3 Convection.....	98
6.2.2.4 Other Energy Flows	101
6.2.3 Solar Radiation Transmission and Absorption	101
6.2.3.1 Front Panel.....	102
6.2.3.2 Back Panel without Cover	104
6.2.3.3 Panel with Lexan Back Cover.....	104
6.2.3.4 Panel with Thermoclear Back Cover	105
6.2.4 Parameters Used in the Models.....	106
6.2.5 Ground and Sky Temperatures.....	109
6.2.6 Sensitivity Analysis of Models	110
6.2.6.1 Unmodified Panel	110
6.2.6.2 Standard TN Conseil Technology.....	112
6.2.6.3 Discussion.....	114
6.2.7 Comparison of Modelled and Observed Performance.....	116
6.2.8 Comparison of Predicted Thermal Performance for Different Models	121
6.2.9 Model Deficiencies	126
7. SNOW AND ICE REMOVAL FROM PHOTOVOLTAIC PANELS	127
7.1 Background	127
7.1.1 Natural Mechanisms of Snow and Ice Removal.....	127
7.1.2 Observed Snow Removal.....	128
7.2 Modelled Panel Performance.....	129
7.2.1 Description of Model.....	129
7.2.2 Impact of Accumulation Thickness on Panel Surface Temperature.....	130
7.2.3 Critical Temperature Assumption.....	133
7.2.4 Complete Melting Assumption.....	138
7.2.5 Discussion on the Operation of the TN Conseil Technology	143
7.3 Ice Ledge Development	144
7.3.1 Observations	144
7.3.2 Use of Thermoclear.....	146
7.3.3 Frame Modifications.....	147
7.3.3.1 Background.....	147
7.3.3.2 Models of the Frame	147
7.3.3.3 Results.....	151
7.3.3.4 Discussion.....	152
7.4 Rime Icing Considerations.....	154
7.4.1 Background.....	154
7.4.2 Probability of Rear Face Rime Icing.....	155
7.4.3 Impact of Rear Face Rime Icing on Thermal Performance.....	155
7.4.4 Modification to Panel Installation.....	156

8. SIMULATION OF SYSTEM PERFORMANCE AT FOUR SITES	163
8.1 Introduction.....	163
8.2 Method	164
8.2.1 Weather Data	164
8.2.2 Use of the Thermal Model	166
8.2.3 Software Description	168
8.3 Results.....	168
8.4 Discussion.....	184
8.4.1 Why the Shedding and Melt-off Times seem Very Long	184
8.4.2 Performance for Rime versus Snow.....	184
8.4.3 Shedding versus Complete Melt-off Times	185
8.4.4 Melting Performance in the Far North.....	185
8.4.5 Utility of the Rime Shield.....	185
8.4.6 Interpreting the Results	186
8.4.7 Further Work.....	186
9. SUMMER BATTERY CHARGING PERFORMANCE	187
9.1 Introduction.....	187
9.2 Worst-Case Meteorological Conditions.....	187
9.3 Method of Investigation	188
9.4 Results.....	190
9.5 Effect of Charge Controller Temperature Derating	195
9.6 Maximum Monitored Temperatures	195
9.7 Conclusions.....	195
10. OBSERVED SHORT-TERM OPERATION OF THE SNOW REMOVAL TECHNOLOGY	198
10.1 Background	198
10.2 Photographs of Panels	198
10.3 Monitored Data	202
10.3.1 Insolation Levels	202
10.3.2 Wind Speed.....	202
10.3.3 Temperature	202
10.3.4 Current	205
CONCLUSIONS.....	207
REFERENCES	212
APPENDIX A: ICING ON WIRES AND STRUCTURES.....	218
APPENDIX B: MATHCAD FILE: FRONTPAN.MCD	222
APPENDIX C: MATHCAD FILE: DIFFUNCM.MCD	229
APPENDIX D: MATHCAD FILE: LEXAN.MCD.....	240
APPENDIX E: C PROGRAM TO SIMULATE RIME SHEDDING AND MELTOFF FROM TN PANEL AT NORMAN WELLS AND DANIELS HARBOUR	248

LIST OF FIGURES

1.1 The TN Conseil Snow Removal System.....	3
2.1 Relation between Types of Icing and Meteorological Conditions	9
2.2 Measurement of the Angle of Repose.....	19
2.3 Freezing Precipitation, Excluding Snow, by Region in Canada	22
2.4 Rime Icing of Panels in Gros Morne National Park, Newfoundland.....	26
2.5 Soltek Solar Energy Ltd. Flush Mount Panels for Comshells	26
3.1 Effective Thermal Conductivity of Snow	33
3.2 Albedo of Snow	35
3.3 Comparison of Bouger-Lambert and Giddings-LaChapelle Models for Radiation Transmission Through Snow	39
3.4 Extinction Coefficient for Snow	41
3.5 Fraction of Incident Solar Radiation Transmitted through Snow, Ice, and Rime	43
4.1 The Function of the Bypass Diode.....	47
4.2 Astropower Module with No Shading	49
4.3 Astropower Module with One Cell 60 to 70 % Shaded.....	50
4.4 Astropower Module with Two Cells 45 to 50 % Shaded	51
4.5 Astropower Module with Four Cells 50 to 60 % Shaded	52
4.6 Astropower Module with Nine Cells 50 to 60 % Shaded	53
4.7 Siemens Module with No Shading	54
4.8 Siemens Module with One Cell, Outer Row, 65 to 75 % Shaded	55
4.9 Siemens Module with Two Cells, Outer Row, 45 to 50 % Shaded	56
4.10 Siemens Module with One Cell in Outer Row and One Cell in Inner Row, Each 45 to 50 % Shaded	57
4.11 Siemens Module with One Cell in Each Row 45 to 50 % Shaded	58
5.1 View Factor of Surface i onto Surface j.....	69
5.2 Cartesian Coordinate System at a Point on the Ground.....	69
5.3 Definition of Cartesian Coordinate System for Beam Radiation Shadow Model	73
6.1 Comparison of Monitored Panel Temperatures, February 22 through March 8, 1995: Nickel Foil and Copper Foil with Lexan Cover vs Unmodified Panel	85
6.2 Effect of Lexan Cover on Panel Temperature, March 28 through April 8, 1995, No Snow Cover.....	87
6.3 Placement of Thermocouples on Rear Face of TN Conseil Panel	88
6.4 Measured Temperature Gradient at Foil, Absolute.....	89
6.5 Measured Temperature Gradient at Foil, Relative.....	90
6.6 Model of Unmodified Panel.....	92
6.7 Model of Standard TN Conseil Technology	94
6.8 Model of Lexan Thermoclear	96
6.9 Modelled Effect of Windspeed on Panel Surface Temperature, $T_{amb} = 0^{\circ}\text{C}$, Insolation $= 700 \text{ W/m}^2$ front and 200 W/m^2 back	115
6.10 Model Error as a Function of Insolation	118
6.11 Model Error as a Function of Windspeed	119

6.12 Model Error as a Function of Ambient Air Temperature	120
6.13 Comparison of Modelled Panel Surface Temperature, $T_{amb} = -10\text{ }^{\circ}\text{C}$, Wind = 3 km/hr, Back Insol = Front/3	122
6.14 Comparison of Modelled Panel Surface Temperature, $T_{amb} = -10\text{ }^{\circ}\text{C}$, Wind = 10 km/hr, Back Insol = Front/3	123
6.15 Comparison of Modelled Panel Surface Temperature, $T_{amb} = -10\text{ }^{\circ}\text{C}$, Wind = 25 km/hr, Back Insol = Front/3	124
6.16 Comparison of Modelled Panel Surface Temperature, $T_{amb} = -10\text{ }^{\circ}\text{C}$, Wind = 10 km/hr, Back Insol = Front/5	125
7.1 Modelled Effect of Snow Cover Thickness on Critical Air Temperature for Melting (Unmodified Panel)	131
7.2 Modelled Effect of Snow Cover Thickness on Heat Conduction and Solar Radiation Penetration, Fresh Light Snow (Unmodified Panel)	132
7.3 Modelled Critical Ambient Air Temperature to Initiate Melting for Light, Fresh Snow	134
7.4 Modelled Critical Ambient Air Temperature to Initiate Melting for Slightly Densified Snow	135
7.5 Modelled Critical Ambient Air Temperature to Initiate Melting for Moderately Dense Snow	136
7.6 Modelled Critical Ambient Air Temperature to Initiate Melting for Rime	137
7.7 Modelled Melting Rate for Slightly Densified Snow 5 cm Thick, Wind of 5 m/s	140
7.8 Modelled Melting Rate for Moderately Densified Snow 5 cm Thick, Wind of 5 m/s	141
7.9 Modelled Melting Rate for Rime 5 cm Thick, Wind of 5 m/s	142
7.10 Ice Ledge	145
7.11 Cross-Section of Frame	148
7.12 Schematic Representation of the Frame Models	150
7.13 Modelled Temperature of Frame for Various Configurations (Without Snow)	153
7.14 Modelled Effect of Rime: Wind 10 m/s, Front Insolation 1000 W/m^2 , Back 250 W/m^2	158
7.15 PV Panel With Rime Shield	159
8.1 Modelled Time to Shedding, Bagotville, Qc., for Eight cm Snowcover on January 1	171
8.2 Modelled Time to Melt-off, Bagotville, Qc., for Eight cm Snowcover on January 1	172
8.3 Modelled Time to Shedding, Daniels Harbour, Nfld., for Five cm Rime Deposit on January 1	174
8.4 Modelled Time to Melt-off, Daniels Harbour, Nfld., for Five cm Rime Deposit on January 1	175
8.5 Modelled Time to Shedding, Norman Wells, NWT, for Five cm Rime Deposit on January 1	177
8.6 Modelled Time to Melt-off, Norman Wells, NWT, for Five cm Rime Deposit on January 1	178
8.7 Modelled Time to Shedding, Prince George, B.C., for Five cm Rime Deposit on January 1	180
8.8 Modelled Time to Melt-off, Prince George, B.C., for Five cm Rime Deposit on January 1	181
9.1 Modelled Maximum Ambient Air Temperature for Full Battery Charging with	

Unmodified Panel, M55 and M75	191
9.2 Modelled Maximum Ambient Air Temperature for Full Battery Charging with TN	
Conseil Panel, M55 with 1000 W/m ² on Front.....	193
9.3 Modelled Maximum Ambient Air Temperature for Full Battery Charging with TN	
Conseil Panel, M75 with 1000 W/m ² on Front.....	194
9.4 Modelled Maximum Ambient Air Temperature for Full Battery Charging at Various	
Charge Controller Temperature Deratings (D _{cc}).....	196
10.1 Performance of TN Conseil-Modified Panels on March 6 and 7	199
10.2 Windspeed, March 6 and 7, 1995	203
10.3 Temperature of Panels and Ambient Air, March 6 and 7, 1995	204
10.4 Cumulative Normalized Amp-Hrs, March 6 and 7, 1995.....	206

LIST OF TABLES

2.1 Some Examples of Documented Snow Accumulation on Arrays	13
3.1 Densities of Various Types of Snowcover.....	31
3.2 Albedo of Various Types of Snowcover.....	37
3.3 Extinction Coefficients for Various Types of Snowcover	40
4.1 Effect of Partial Shading on the Series String of Cells in an Astropower Panel	48
4.2 Effect of Partial Shading on Siemens M55 Panel with Two Overlapping Bypass Diodes	59
5.1 Global Radiation on the Horizontal for March 10, 1995	76
5.2 Validation of Ground-Reflected Radiation Model based on Measurements at Varennnes	78
5.3 Modelled Irradiance of Rear Face of Various Array Installations	80
6.1 Parameters for Glass and EVA	106
6.2 Parameters for Cell, Polyester, Tedlar, and Absorber Foil	107
6.3 Parameters for Lexan and Thermoclear	108
6.4 Summary of Sensitivity Analysis of Model of Unmodified Panel, Without Snow	110
6.5 Sensitivity Analysis of Model of Unmodified Panel, Without Snow	111
6.6 Summary of Sensitivity Analysis of Model of Panel with TN Conseil Technology, Without Snow	112
6.7 Sensitivity Analysis of Model of TN Conseil Panel, Without Snow	113
6.8 Comparison of Thermal Model and Monitored Performance.....	117
7.1 Parameters for Frame Models	152
7.2 Effect of Rime on Front and Back of Panel	157
8.1 Parameters for Snow Removal.....	167
8.2 Parameters for Rime Removal	169
8.3 Modelled Snow Melt-off Times in Bagotville, Québec.....	170
8.4 Modelled Rime Melt-off Times in Mountains Near Daniels Harbour, Nfld.	173
8.5 Modelled Rime Melt-off Times in Mountains Near Norman Wells, NWT.	176
8.6 Modelled Rime Melt-off Times in Mountains Near Prince George, BC.....	179
8.7 Modelled Time to Shed for Different Sites and Different Technologies.....	182
8.8 Modelled Time to Complete Melt-off for Different Sites and Different Technologies.....	183
8.9 Shedding and Melt-off Times as a Percentage of Time Required for Unmodified Panel	183

CHAPTER 1

INTRODUCTION

One of the strengths of photovoltaic (PV) systems is their high reliability in severe environments. PV systems have no moving parts and no easily broken components. At a remote site, this is advantageous: a maintenance visit to the site may entail a helicopter flight -- an expensive proposition. For this and other reasons, PV is used at many remote sites across Canada.

During winter, however, snow and ice may accumulate on PV panels. While this accumulation does not harm the panels, it blocks sunlight's path to the solar cells, and can reduce the electrical output of the panels significantly. During these times, the power requirements of the load must be met by the battery bank. If the accumulation remains on the array for a sufficiently long period, the battery will be depleted. This has a number of ramifications: the life expectancy of the battery is lowered, the probability of electrolyte freezing rises, and, in a worst-case scenario, the PV system fails to meet the load's power requirements. For most remote sites, this failure is unacceptable.

In order to diminish the probability of the PV system being unable to meet the load's power requirement, battery banks for PV systems are oversized. This extra capacity is in addition to the extra capacity required by the variability of insolation levels. This raises the cost of the system considerably, especially since the batteries must be replaced several times during the lifetime of the system.

Working in conjunction with the EDRL and Hydro-Québec, TN Conseil, a Montréal firm, has developed a technology, with neither moving parts nor electrical power requirement, that melts snow from the face of a PV panel (see Figure 1.1) This technology consists of two components: a black absorber foil bonded to the rear of the panel and a transparent Lexan cover that goes over this absorber foil. Between the absorber foil and the Lexan back cover is a one cm air gap.

The air gap enclosed by the Lexan back cover insulates the panel from convective heat loss at its rear face. When snow or ice accumulates on the front, both the front and the back are well insulated, and the panel temperature rises high above the ambient air temperature. This is aided by the black absorber foil, which collects solar radiation incident on the rear face of the panel. During the summer, this radiation is weak, but during the winter, when rays are reflected off the snowcover on the ground, this radiation can be significant. The additional energy collected in this way melts the snow or ice from the front of the panel.

In this report, the problem of snow and ice accumulation on PV panels is overviewed, and the solution proposed by TN Conseil is assessed. The report has five aims:

1. To provide background information on snow and ice and the mechanisms by which they accumulate on PV panels (Chapters 2 and 3).
2. To identify the locations in Canada where snow and ice accumulates on PV panels, and overview the effects of this accumulation on the performance of the panel (Chapters 2 and 4).
3. To determine the efficacy of the TN Conseil snow removal technology under various conditions (Chapters 5 through 8 and Chapter 10).
4. To identify possible improvements that could be made to the TN Conseil technology (Chapters 6 through 8).
5. To assess whether the TN Conseil technology will negatively impact the performance of the panel by raising its temperature during the summer (Chapter 9).

Ideally, this report would include an economic analysis. Such an analysis would use the decrease in the loss-of-load probability to estimate the reduction in battery capacity-- and thus cost-- allowed by the TN Conseil technology. However, the variability and unpredictability of rime and snow accumulation makes the determination of a loss-of-load probability nearly impossible at this time. A rough measure of the economic worth of the technology should become apparent after it has been tested in the field for several years.

For those readers who wish to read only the parts of this report that discuss concepts, results and conclusions, the following sections are recommended.

Chapter 2: all sections.

Chapter 4: Section 4.1, 4.2.

Chapter 5: Section 5.1, 5.5.

Chapter 6: Section 6.1, 6.2.7, 8, 9.

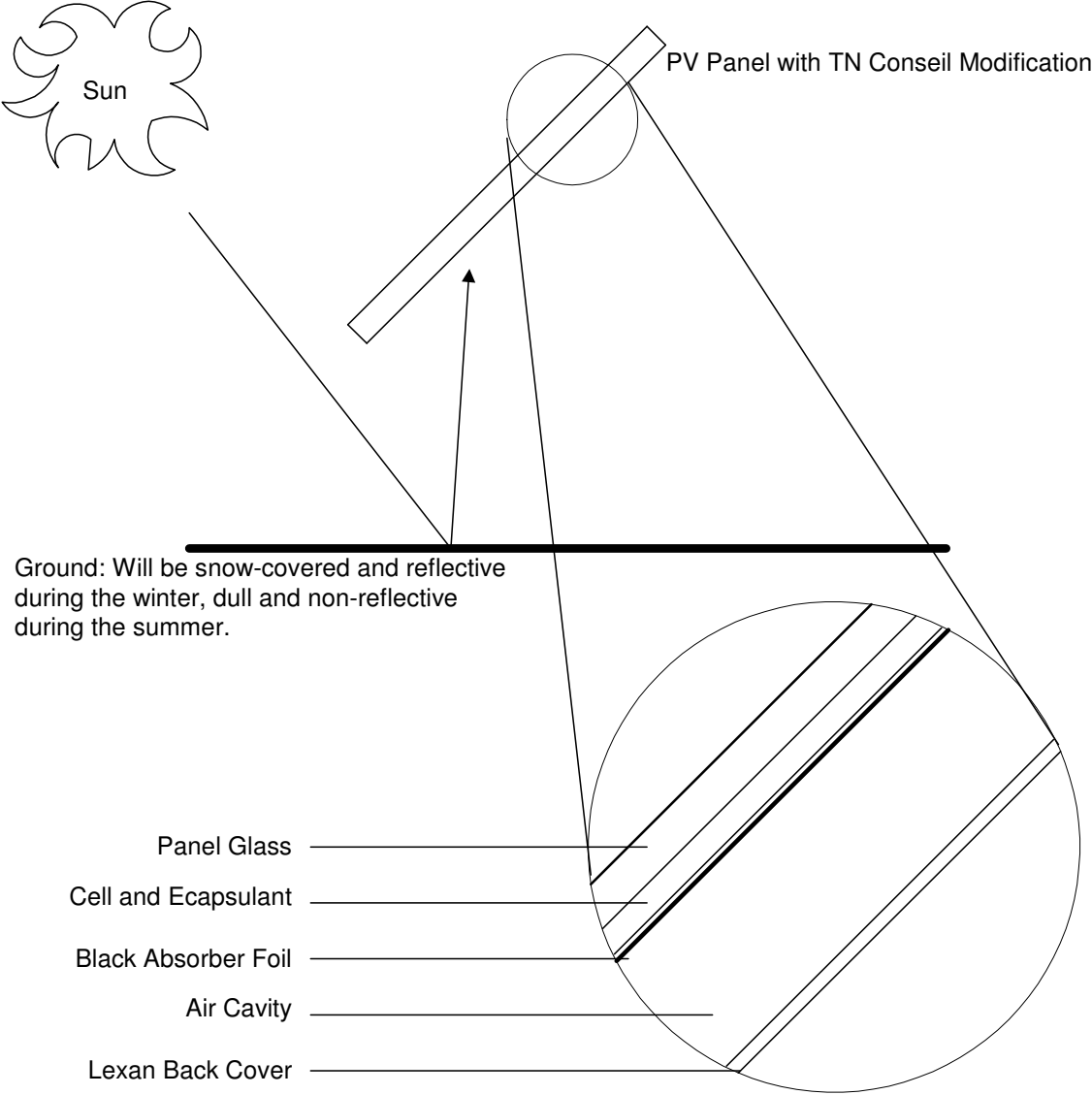
Chapter 7: Section 7.1.1, 2; 7.2.2, 3, 4; 7.3.1, 2; 7.3.3.1, 3, 4.

Chapter 8: Section 8.1, 3, 4.

Chapter 9: Section 9.1, 4, 6, 7.

Chapter 10: all sections.

Figure 1.1 The TN Conseil Snow Removal System



CHAPTER 2

SNOW AND ICE ACCUMULATION ON PV PANELS

2.1 Introduction

It is a commonly held belief in much of the photovoltaic industry that ice and snow present no particular problem to the operation of an array. It is assumed that panel slope angles are too steep, winds too strong, melting rates too rapid, and snow and ice too slippery for any serious interruption of array operation. For the majority of the time and for the majority of PV installations this may well be true. But the experience of many people actually relying on PV installations demonstrates that this is not the case for all installations, and that for certain locations and certain conditions, ice and snow can seriously reduce the output of a PV array for extended periods of time.

Determining where ice and snow accumulation will occur, and with what frequency, is an unsolved problem. Snow and ice accumulation is a function of microphysical climatic conditions, generally determined by the site; whether an installation becomes encrusted in snow and ice can not be predicted from commonly collected meteorological data. Further, panel encrustation is, in certain installations, a low probability, high cost event. In such cases, the weather conditions that affect an array are freak occurrences¹. Thus, while the mean accumulation on a panel for, say, the month of January, averaged over a number of years, might be very low, the one year for which significant icing does occur belies the photovoltaic system's claim to high reliability. At installations where reliability is paramount, the operation of the array during this one bad year will dictate the design-- and cost-- of the system.

This chapter aims to describe the types of snow and ice accumulation that can occur, the

¹One user reported that a site that had survived many years without a snow/ice problem was, for the winter of 1994-1995, completely covered in ice and snow [Jarvis].

meteorological conditions and physical siting that lead to these conditions, and to suggest where, in Canada, photovoltaic installations are at risk of serious snow and ice accumulation. Regarding the latter, only guidelines, and not a definitive assessment, can be presented; the susceptibility of a particular site to snow and ice can be better estimated by either a local veteran of PV installations (or similar structures) or an expert on climatology². Models of snow and ice accumulation are introduced, in the hope that this sheds some light on the physical factors affecting accumulation. The methods presently enlisted to cope with this problem are also reviewed.

There appears to be very little literature on the problem of snow and ice accumulation on PV arrays. A study [Nentwich et al., 1993] on the operation of three high elevation and Nordic sites in Europe does not mention any snow or ice problems at the German or Finnish installations, and concludes that snow cover on the panels at the Loser, Austria plant caused less than a three percent reduction of the annual electricity output³. It is not a design consideration discussed in a paper [Schadel, 1991] on a PV-powered repeater station to be located 3300 m above sea level, "at the top of " Muttler Mountain, in Switzerland. An article [Jantsch et al., 1991] on the effect of tilt angle on PV system performance contains a picture of a snow covered array, with the caption "Realistic energy losses in winter", but does not elucidate. Earlier studies on a large PV installation in the Swiss Alps [Real, 1982] found that "snow and ice accumulation have only a small impact on the overall energy output", although the author cautioned that "the location is a more dry area, and not very typical for the Swiss Alps. The northern part is more humid, the southern part more dry" [Real]. Two studies on snow accumulation on solar thermal collectors report a problem, but are limited in their applicability since they report only on several American cities for one or two winters. One study [O'Rourke, 1979] indicates that snow melts off soon after it has fallen; the other [Corotis et al, 1979] documents the adverse effects of snow and ice on thermal collectors in the Chicago area for eighteen sites during the winter of 1979, which was considered particularly harsh. Unfortunately, the physical configuration of most sites in that study was significantly different from that of a typical PV installation, and as a result few conclusions can be extrapolated. The study did confirm, however, that "practically no data exists regarding the accumulation of snow and ice at solar collector installations"-- a situation that does not appear to have been ameliorated.

Fortunately, other sources of information are far more helpful. There exists a body of literature on the nature of ice and wet snow accretion on structures, electrical transmission lines, and ships, some of which is applicable to PV installations. Most power utilities and telephone companies

²Such work is done by the Atmospheric Environment Service of Environment Canada [Morris].

³However, it is noted that "owing to a single event of excessive high frozen snow at the Loser plant, module frame damage occurred on certain module types" [Nentwich et al., 1993, p. 64]. Snow and ice accumulation are highly variable, and, as shown by this anecdote, it is always the worst-case scenario one must prepare for.

have a great deal of experience with remote structures, and have groups who possess a good practical understanding of the problem. The Canadian Atmospheric Environment Service is well versed in this domain. Further, some results from civil engineering studies of snow accumulation on roofs are of interest, although in general this work occupies itself with estimating the maximum snow load under worst case conditions, rather than the actual snow load at a given time.

Whether or not any given snowfall or icing event leads to an obstructing layer on the face of a PV array, and whether this obstructing layer persists, is a function not only of the local conditions, but also the state of the array itself. Most obviously, the array will often be at a temperature other than the ambient air temperature; it is conceivable that the array will be above freezing when the ambient air temperature is well below. The temperature of the array is influenced by radiation gains and losses to/from the environment and wind (convective cooling); in general it will be warmer than air temperature during the day and colder during a clear night, when radiation losses to the sky will become significant. On a cloudy night, the sky losses will be low and the array temperature will closely match ambient air temperature. In the neighbourhood of the array, the wind field will be affected by the array itself (as well as any other structures, outcroppings, trees, etc.). For example, a wind blowing onto the back of the array will probably cause an eddy at the front of the array, into which airborne snow will tend to accumulate. Windswept mountaintops, usually largely free of ice and snow, may become sites of enormous accumulations once a obstruction is situated there [Jarvis]. In addition, a layer of accumulation on the face of an array may facilitate further snow and ice build-up, even in conditions that would not lead to accumulation were the face of the array clear.

2.2 Types of Snow and Ice Accumulation

Snow accumulation is the most obvious manner by which the confluence of cold temperatures and moisture can obstruct the face of a PV array, but it is certainly not the only mechanism, nor probably the most problematic. Broadly, a layer of frozen moisture on a PV array can be either accretion, which "results from the impingement of water droplets or wet snow, or of sublimation on an object, the energy balance favouring ice formation" [McKay et al., 1969, p. 928], or dry deposition, the phenomenon whereby falling dry snow flakes or drifting, dry snow particles settle on a surface⁴. Accretion can be further subdivided into wet snow accretion, sublimation (hoarfrost), and particulate accretion of soft rime, hard rime, and glaze. This chapter groups the various forms of accretion and accumulation based on the state of the water when it reaches the surface of the array: rime and glaze are in the liquid phase, snow is largely in the solid phase, and hoarfrost is in the vapour phase.

2.2.1 Particulate Accretion: Rime and Glaze

⁴This is the definition of deposition from [Kobayashi, 1987, p. 239], modified to apply to dry snow only. This dichotomy between dry deposition and accretion, which is not generally useful to snow and ice researchers, is exclusive to this report.

2.2.1.1 Definitions and Properties

Glaze, hard rime, and soft rime all stem from the impingement of droplets of liquid water upon a cold surface, where the droplets subsequently freeze. The droplets may be from fog, cloud, or freezing rain or drizzle. The temperature of the droplets, the rate of impingement, and the properties of the surface determine the nature of the resulting accretion.

Glaze results when the droplets, upon impact, do not freeze entirely, and form a liquid layer that flows over the surface before freezing. A clear and smooth ice, glaze may contain a small number of air pockets [Boyd, 1968: American Meteorological Society, 1959]. It is hard, highly adhesive, and has a specific gravity of 0.8 to 0.9 [McKay, 1969].

If the droplets do not freeze entirely upon impact, yet do not have sufficient time to form a continuous film of water, hard rime is formed. It is less transparent and less adhesive than glaze, granular and amorphous in nature, can be milky or opaque depending on its porosity, and can grow into the wind as glazed cones or feathers [Boyd, 1968: American Meteorological Society, 1959]. It has a specific gravity of 0.6 to 0.9 [Farzaneh, 1990].

Soft rime is the result of droplets that freeze very rapidly upon the surface; it is white, opaque, composed of fine granules, somewhat like frost in structure, even less adhesive than hard rime, and has a specific gravity of about 0.3 to 0.6⁵. It grows into the wind, often in the shape of a feather or a cone [Boyd, 1968: American Meteorological Society, 1959].

2.2.1.2 Formation: Theory and Field Experience

When water vapour cools and the vapour pressure is above the triple point, water droplets are produced by condensation. In the absence of substrates or airborne nucleants, the water droplets can cool well below the equilibrium freezing point without actually freezing; such droplets exist in a metastable (supercooled) state down to temperatures as low as -40 degrees C, at which point homogenous nucleation (freezing without nucleant or substrate) occurs [Lock, 1990, p. 59, p. 178].

⁵In the literature, different authors cite different densities for glaze, hard rime, and soft rime. The ranges used here are close to those of most authors; the exception is [Minsk, 1980], who states that the specific gravity of hard rime is 0.1 to 0.6 and that of soft rime is 0.01 to 0.08.

The growth of these droplets is limited by the finite amount of water vapour contained in the local atmosphere. Eventually the droplets must compete for the remaining water vapour. Large droplets, under the influence of gravity and aerodynamic drag, tend to fall faster than small ones. By coalescence and collision these large drops assimilate the small, a process enhanced by any local air turbulence [Lock, 1990, p. 181].

The mean size and concentration of droplets thus created vary widely. Cumulonimbus clouds have a low concentration of comparatively large droplets; the mean droplet radius in these clouds is 20 micrometres, which is comparable to a thick fog. Very thick fogs and freezing drizzle have mean droplet radii of about 100 micrometres. Freezing rain droplets can be much larger. The largest drops are the first to succumb to homogenous nucleation, but droplets up to 120 micrometres in radius can reach the homogenous nucleation threshold without freezing [Lock, 1990, p. 181].

When these supercooled droplets strike a surface they freeze, with the rate of their phase change determining the type of accretion. A supercooled droplet ΔT below the triple point will have a sensible heat deficit of the product of ΔT and the specific heat capacity of water. If this deficit exceeds the latent heat of freezing the mass of water contained in the droplet, the droplet will freeze instantly⁶. This rarely occurs under natural conditions, but if the temperature of the environment is below the equilibrium freezing point, further heat can be dissipated by the substrate and the local air [Lock, 1990, p. 185]. The rate of this heat loss is dependent upon the temperature of the environment and the coefficient of thermal conduction of the surface [McKay, 1969]. If the heat loss is rapid, the rate of droplet freezing will exceed the rate of droplet impingement and rime will occur. If the heat loss is slow, such that the rate of impingement exceeds that of freezing, there will be sufficient time for the water in the droplet to spread over the face of the surface and form a continuous film, which freezes into the homogenous ice known as glaze. Since the site of a glaze accretion is completely wetted prior to freezing, glaze tends to adhere to its substrate better than does rime, and for similar reasons, hard rime adheres better than soft [Minsk, 1980].

A number of factors affect the rate of droplet impingement and their rate of heat loss to the environment. The mass and concentration of the droplets obviously influences the flux of water onto a surface, as does the mean velocity of the droplets, due to gravity and air velocity with respect to the surface. In addition, smaller droplets are more likely to be deflected around an object by wind. Thus, impingement is maximized when a high concentration of large droplets is being blown by a strong wind onto a surface perpendicular to the trajectory of the droplets. These conditions favour glaze accretion. Glaze tends to form at temperatures above -3°C , with winds between 1 and 20 m/s, hard rime between -3 and -8 degrees C and winds of 5 to 10 m/s, and soft rime at -5 to -25 degrees C and winds of 1 to 5 m/s [Minsk, 1980] [Farzaneh, 1989] (see Figure

⁶The ratio of sensible heat deficit to latent heat of fusion for the droplet is referred to as the Stefan number.

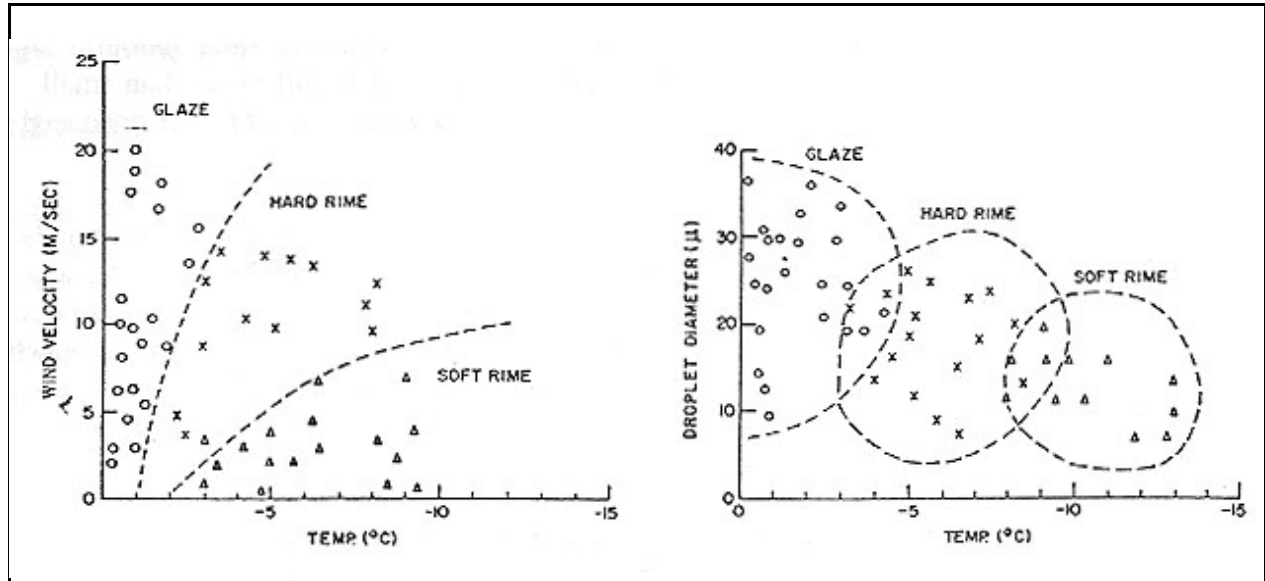


Figure 2.1 Relation between Types of Icing and Meteorological Conditions
from [McKay et al., 1969; Kuroiwa, 1965]

2.1). The rate of heat loss to the environment is related not only to the temperature of the environment but also the thermal conductivity of the surface: the higher the thermal conductivity and the lower the temperature, the greater the rate of heat loss. The surface of a PV panel consists of glass and aluminum. Glass has a thermal conductivity of about 1 W/m/K, which is between that of steel (approximately 20 W/m/K) and snow (0.05 to 0.8 W/m/K). The thermal conductivity of aluminum (200 W/m/K) is very high [Reynolds et al., 1977, pp. 659-660] [Mellor, 1977, p. 35]. Thus the rime forming on the aluminum frame should be more fragile and less dense than that forming on the glass surface. Further, the bond between the rime and the frame should be weaker⁷.

The intensity, I , or growth rate of the mass of an accretion per unit cross sectional area is [Makkonen, 1981]:

$$I = E_c E_a v W \quad (2.1)$$

where E_c is the dimensionless collision efficiency, the ratio of droplets that collide with the array surface per unit time to all those that would have collided with the surface per unit time had the array not affected the wind field around it,

⁷Both these predictions are supported by pictures taken at the Lookout Hills RCMP repeater station, Gros Morne National Park, Newfoundland.

E_a is the dimensionless accretion efficiency, the ratio of the icing intensity to the mass flow of the impinging water,
 v is the particle speed relative to the surface, which for droplets in cloud and fog is essentially the wind speed,
 and W is the liquid water content.

Unfortunately, the practical application of this equation is precluded by the difficulty of ascertaining E_c , which varies with wind speed, wind direction, array configuration, and site topography.

For rime accretions E_a is unity, since all impinging water freezes on the array. During glazing, on the other hand, some water will flow off the array surface, and E_a will be less than unity. The degree to which this occurs is determined by a detailed heat balance of the water film on the array surface.

In very cold climates, like those of the prairies, the occurrence of particulate accretion appears to be bimodally distributed, with peaks in the autumn and late winter or early spring. In more temperate climates, like that of Southern Ontario or Avalon, Newfoundland, particulate accretion is most likely in December or January [McKay, 1969].

The conditions leading to the formation of glaze and rime are also related to topography and vegetative cover [McKay, 1969]. In Canada glaze tends to occur in valleys or flat areas [Morris].

In practice, it is questionable whether glaze poses much of a threat to the operation of photovoltaic arrays. In a ten year study of glaze accumulation on structures in the United States, the most substantial recorded deposit was five centimetres in thickness⁸ [Boyd, 1968]. Such a deposit would not severely diminish solar radiation striking the surface of the array; not only would the array continue to operate, but the absorbed radiation would heat the array and tend to melt off the glaze within a period of days. In general, glaze is most common in the southern parts of Canada, where temperatures tend to be moderate. While users of photovoltaic arrays report snow and rime accumulations, no such problems are reported for glaze. Although glaze in combination with other forms of precipitation may seriously affect array performance, it appears that glaze alone is a minor threat to array performance.

The occurrence of particulate accretion in general and rime in particular is strongly related to elevation. Higher elevations have, on average, a greater number of hours of freezing precipitation [McKay, 1969]. Temperature decreases with increasing elevation, creating conditions more susceptible to rime accretion and, equally important, retention [Jarvis]. As a rule of thumb,

⁸The guy wires of one Newfoundland tower, however, were observed to have an accumulation twenty-five centimetres in diameter [Boyd, 1968].

temperature drops 6.5 ° C for every 1000 m increase in elevation [ASHRAE, 1993]. While high elevation is, in general, a necessary condition for rime accretion, it is not a sufficient one. A dry plateau at a high elevation will not be conducive to rime accumulation; the rime accretion occurs at elevations considerably higher than the surrounding areas-- that is, on mountains and hills. An air mass encountering a mountain must rise to pass over the mountain; as it does so it will cool, water vapour will condense, and the resulting droplets may become supercooled. The existence of these supercooled water droplets is a prerequisite of rime formation. In reality, any hill which is clad in fog or cloud during the winter will be prone to riming; such hills tend to be over 650 m⁹ [Morris].

Hard rime tends to form at the very top of mountains and along ridges, and it is here that riming is most severe. Not only will these locations be cool and have an environment of supercooled water droplets, but the wind, and therefore the flux of water onto the array, will be at its maximum here. An air mass, rising over a mountain, will blow over the top at velocities significantly greater than its velocity lower down the mountain, due to the simple fact that a wind blowing into a mountain has nowhere to go [Morris].

Soft rime may occur in wooded regions relatively sheltered from the wind. Forested mountainous areas, in cloud, are cited as typical locations for soft rime [Boyd, 1968].

Rime grows only on the windward side of a substrate; at this surface it can accrete at a rate of up to four cm/hour [Boyd, 1968]. Glaze, on the other hand, can flow from the windward to the leeward side of a substrate and can form icicles [Minsk, 1980]. There is some disagreement as to whether rime can occur when there is no wind, but researchers who maintain that rime icing can occur in calm conditions [Shellard, 1974] are at variance with the majority of their colleagues. It is probably safe to conclude that at very low wind speeds riming will not be significant.

The humidity of the air mass encountering a mountain will also be a factor determining the severity of rime accretion. Field personnel report that riming is worst within sixty to one hundred kilometres of the ocean [Waszkiewicz] [Egles]. It is unclear whether the ocean must be open (free of ice) for this criterion to apply; in any case, there will be periods during the autumn when the ocean will be open and mountain-top conditions will be prime for heavy riming [Morris]. Locations downwind of open lakes and rivers are also at risk [Jarvis]. Proximity to open water is not, however, an absolute prerequisite for riming, and many exceptions have been documented.

Rime accumulations appear to densify with time. This probably results from an episodic or diurnal freeze-thaw cycle. Rime undergoing this densification can become sufficiently hard and well-bonded that it can be removed from the panel only by chipping with a screwdriver [Waszkiewicz].

2.2.2 Deposition of Water Vapour: Hoarfrost

⁹Many PV-powered telecommunication systems are situated on mountaintops.

Hoarfrost is the phenomenon commonly known as frost; it also goes by the name of hoar. It is a deposit of white, interlocking ice crystals in a feathery and rather fragile mass [McKay, 1969]. It has a low density in comparison with rime [Boyd, 1968]. Some researchers claim that it has poor adhesive qualities [Boyd, 1968] [McKay, 1969]. While this may pertain to the self-adhesion of hoarfrost, the attachment of frost to car windows suggests that it is not true of adhesion to a substrate [Morris].

Hoarfrost forms in a manner not unlike that of dew formation, but with lower temperatures [Boyd, 1968]. Water vapour at temperatures below that of the triple point can be in a metastable state. Upon encountering a nucleating surface, the water vapour grows a hoar crystal [Lock, 1990, p. 167]. The surface must be below freezing, and the colder the temperature of the surface, the more prone the surface is to hoarfrost [Morris]. Hoarfrost occurs in still air or low wind conditions. It has been suggested that objects of small diameter are especially susceptible to hoarfrost [Boyd, 1968: American Meteorological Society, 1959]

Usually hoarfrost accretions are very thin and light [Boyd, 1968] [Lock, 1990, p. 215]. The growth of the accretion will be limited by the amount of water vapour in the air. Cold air tends to contain little water vapour [Minsk, 1980]. The thinness of the hoarfrost layer and its low density suggest that it will have little strength and transmit a large fraction of incident solar radiation. This affords many opportunities for wind to remove it and the sun to melt it off¹⁰. It is highly improbable that hoarfrost presents any problem to the winter operation of photovoltaic panels.

2.2.3 Snow Deposition and Accretion

Snow does accumulate on photovoltaic arrays, as can be seen in Table 2.1. Further, under certain conditions it can remain on the arrays for considerable periods of time. This section examines the nature of snow accumulation on photovoltaic panels, with separate treatment of wet snow accretion and dry snow deposition, due to the dissimilarities in the physics of these phenomena. Additionally, the fate and evolution of snow cover on an array are discussed.

¹⁰Hoarfrost accumulation on the photovoltaic panels at the Energy Diversification Research Laboratory completely disappeared within minutes of being exposed to the sun.

Table 2.1. Some Examples of Documented Snow Accumulation on Arrays

Location	Tilt deg	Temp deg C	Wind km/h	Accumulation	Notes
Germany	50	?	?	full	picture in [Jantsch et al., 1991]
Germany	70	?	?	partial	ditto
EDRL, Feb. 9	45	-6	20	partial	wind from behind array, dry dendritic snow
EDRL, Feb. 21	45	-2	?	full	snow did not melt on impact
EDRL, Feb. 27	45	-4 to -10	5 - 10	full	
EDRL, Feb. 28	45	-4	5 - 10	full	
Boucherville	60	-5	?	full	picture in [TN Conseil, 1993, p. 8]

2.2.3.1 Particulate Accretion: Wet Snow

Wet snow has a surface layer of liquid water. This provides a mechanism by which snow, usually a material with very low friction adhesion properties, can adhere to snow or other surfaces very effectively. Once it has reached the surface, it will either melt or freeze into a snow-ice mixture, depending on heat losses to the environment.

For snow to adhere to a vertical surface, the surface of the snow particle must be wet [Makkonen, 1989]. There are two ways that a snow particle may become wet. It may collide with an airborne droplet of water, which will either wet the snow directly or, through riming of the particle, cause heat transfer sufficient to induce melting of the snow. This latter mechanism can raise the temperature of a snow particle 0.3 to 0.5 ° C [Stewart et al., 1990]. Alternatively, there may be a heat transfer to the environment in the absence of a collision with a water droplet. Snow, forming in a cold air mass, may fall through a warm air layer, allowing convective heat transfer from the air. Although radiative heat transfer with the environment may be ignored, evaporative heat transfer, by sublimation, may not. Thus, in the absence of a collision between the snow particle and a liquid droplet, the positive heat flux to the snow particle that is a necessary and sufficient condition for surface wetting occurs when the sum of convective and evaporative heat transfers to the snow particle is greater than zero [Makkonen, 1989].

The positive heat flux criterion for surface wetting of a snow particle is equivalent to the criterion that the wet bulb temperature must be above zero ° C. This results from the physical similarity of a wet bulb thermometer and a snow particle-- if evaporative losses do not bring the wet bulb thermometer below zero ° C, they will not do so for a snow particle either. This criterion is satisfied at air temperatures above a critical threshold, which is a function of relative humidity.

This critical temperature varies more or less linearly between zero ° C at 100 % relative humidity and 3.5 ° C at 50 % relative humidity (the relative humidity during a snow storm can be as low as 50 %). Air pressure plays a minor role in this relationship. At lower air pressures, as in mountains, the critical air temperature for a given relative humidity will be slightly higher [Makkonen, 1989].

The above analysis applies only to a dry accretion surface. Snow particles will adhere to a wet accretion surface-- for example, a photovoltaic panel with melted snow or rain on it-- even when the above criterion is not satisfied. However, if there is already an accretion of snow or rime on the substrate, the criterion for the wetness of a snow particle applies to the wetness of the accretion surface (the exposed surface of the snow or ice on the substrate), regardless of the temperature of the underlying substrate. This is due to the fact that a melting snow deposit will be uniformly at zero ° C and can not sustain a temperature gradient across it [Makkonen, 1989]. Thus, if the wetness criterion above is satisfied, a snow- or rime-covered panel will accumulate further wet snow upon it regardless of the temperature of the array. Over time, of course, the rate of melting may exceed the rate of accretion and a net loss of snow cover will occur.

Given that the above criterion is satisfied, a relation for the rate of wet snow accretion can be developed. The equation for intensity, I , of wet snow accretion is the same as that for rime and glaze accretion (Equation 2.1), with the substitution of E_s , sticking efficiency, for E_a , accretion efficiency, and the definition of W as the mass concentration of snow in the air [Makkonen, 1989]:

$$I = E_c E_s v W \quad (2.2)$$

For small objects the collision efficiency for small particles will be nearly unity [Wakahama et al., 1977]. Unfortunately, for larger objects such as photovoltaic arrays, this is not the case¹¹, and as with rime and glaze accretion, this hinders the practical application of this equation.

The local topography will affect W . For instance, a clearing in a forest will accumulate a great deal of snow, in the same way that a snow fence develops an accumulation on its leeward side. Regardless of its direction, wind blowing over the forest will create eddies in the clearing. Snow will tend to drop into these eddies and accumulate more heavily than elsewhere. However, if the clearing is sufficiently large the snow will tend to drop at the edges of the clearing, and the centre of the clearing will be relatively free of snow [Morris].

¹¹Personal observation at the Energy Diversification Research Laboratory photovoltaic array.

Despite the highly adhesive nature of wet snow, the sticking efficiency is not near unity. Wet snow particles generally bounce off the surface upon impact, and often dislodge other accreted snow particles in the process. [Wakahama et al., 1977] reports that for snow accretion on cylinders, the sticking efficiency decreases with increasing radius. Photovoltaic arrays and other planar surfaces could be considered as cylinders with infinite radii. However, by virtue of the fact that arrays do accumulate wet snow deposits it is clear that the sticking efficiency is not zero, as might be inferred from the above relationship. This supports the intuitive notion that increasing the surface area affords opportunities for bouncing and dislodged snow particles to re-impact the surface. This is confirmed by studies on bouncing of dry snow particles [Kobayashi, 1987]. Fortunately, reasonable results yield from a simple empirical relation for sticking efficiency based on wind velocity [Makkonen, 1989; Admirat et al., 1986]:

$$E_s = c/v_w \quad (2.3)$$

where c is one m/s
and v_w is the velocity of the wind (m/s).

The fall velocity of snow particles is approximately one m/s; when the wind speed exceeds one m/s, v_w is approximately equal to v , the velocity of the particles relative to the surface. When the wind speed is less than 1 m/s, v is approximately the fall velocity of the snow particles, and it has been found that under these conditions E_s is approximately unity [Makkonen, 1989; Admirat et al., 1986]. Thus in either case the intensity can be recast as

$$I = E_c c W \quad (2.4)$$

with W in g/m^3 and I in $\text{gm}^{-2}\text{s}^{-1}$.

Further, an empirical relation between mass concentration of snow and the "observed visibility" exists [Makkonen, 1989; Stallabrass, 1978]:

$$W = 2100 v_m^{-1.29} \quad (2.5)$$

where v_m is the "observed visibility" in m.

This allows the intensity of wet snow accretion to be estimated by [Makkonen, 1989]:

$$I = 2100 E_c v_m^{-1.29} \quad (2.6)$$

This is a primitive model, but the development of a significantly more accurate model will require a great deal of work. The relation was developed assuming that the angle of incidence of the snow particles on the surface, θ , is zero °. For other angles of incidence a factor of $\sin\theta$ should be included; additionally, the sticking efficiency may be a function of θ , and the nature of the accreting surface [Makkonen, 1989].

Observations of meteorological conditions during wet snow accretion suggest that the wet snow accretion criterion given above is not strictly accurate. Studies of snow in Japan have concluded that wet snow accumulates between temperatures of -1 and +1 °C¹²; the lower bound of -1 °C is clearly at variance with the criterion. In another study all accretion events occurred at temperatures below the freezing point [Stewart et al., 1990], again contradicting the criterion.

The relation for sticking efficiency supports the intuitively appealing notion that, neglecting complicating factors such as eddy currents, an array in strong wind does not accumulate snow. Other research has also supported this [McKay, 1969], and suggested that most wet snow accretion (at least on overhead transmission lines) occurs at wind speeds less than 3 m/s¹³. However, reports of heavy, wet snow accretion on overhead transmission lines at temperatures of 0 to 2 °C and wind speeds of 10 to 20 m/s belie the assertion that high winds will necessarily clear a surface of snow. During these "cyclone" events the free water content of the snow particles is very high; the phenomenon is attributed to the very high cohesion of snow with a high free water content. The high wind speeds appear to provide aerodynamic lift to counteract the weight of the wet snow deposits, but this may apply only to cylindrical deposits such as those on transmission lines [Wakahama et al., 1977]. In any case, these cyclone events may be a phenomenon of the late spring only and may not be of concern to photovoltaic panel users.

2.2.3.2 Deposition: Dry Snow

Due to the low friction and cohesion of dry snow on glass, a snow particle without a wet surface will not accumulate on a vertically-mounted panel. It will, however, accumulate on panels with lesser tilt angles, at least under certain conditions. Predicting these conditions is especially difficult, although some rough estimates can be made.

Dry snow particles often bounce when they impact the glass face of a photovoltaic panel or any other hard surface. This occurs even at relative velocities well below the saltation wind speed (the wind speed necessary to initiate snow drifting) [Kobayashi, 1987]. After bouncing, the snow particle follows a trajectory determined by gravity, the wind field at the surface of the array, and the momentum of the particle immediately after its collision with the surface. For panel tilt angles less than 90 °, the snow particle will probably return to the array surface, where it will have the opportunity to bounce again. Under many conditions, especially when the wind is not very strong, the snow particle will have less momentum on each subsequent impact, until it either does not bounce, and sticks to the array, or bounces so feebly that the motion of the bounce is negligible compared with the motion of the particle sliding down the array.

The most important parameters in this process are temperature, the wind field around the array¹⁴,

¹²From Shoda, quoted by [Kuroiwa, 1965], in turn quoted by [McKay, 1969, p. 929]

¹³ibid.

¹⁴Note that the discussion of the role of the local topography on the mass

and the panel tilt angle. At temperatures just below freezing, snow particles are fairly adhesive. Adhesive particles appear less likely to bounce and, when sliding down the glass, are more likely to come to a halt on the array surface. The overall collection efficiency of falling snow (ratio of amount collected to amount falling in the same area) is high at temperatures above -1 degree C, falls rapidly at temperatures between -2 and -3 ° C, and is uniformly low below -3 ° C [Kobayashi, 1987]. The wind field plays a significant role in determining the relative velocity of a snow particle impacting the array, both on the first impact and on subsequent bounces. Higher velocities are less likely to result in the snow particle sticking to the array. Further, the wind field may carry the particle away from or tangential to the panel, decreasing the number of collisions and therefore the collection efficiency. The panel tilt angle is significant in determining the tendency of a particle to stay at rest on the panel surface. The forces on a snow particle on the surface of the panel are a wind (or air resistance) force, which is a function of the wind field, the drag coefficient of the particle and its surface area; a component of the force of gravity, normal to the surface, equal to the product of the weight of the particle and the cosine of the tilt angle; a component of the force of gravity, tangential to the surface, which is the product of the weight of the particle and the sine of the tilt angle; and a friction force, which is a function of the particle velocity, particle temperature, particle surface area, panel and particle surface irregularities, and the sum of the normal components of the gravity force and the wind force¹⁵. When the magnitude of the friction force exceeds that of the vector sum of the tangential components of the wind force and the gravity force, the particle will decelerate and tend to come to rest. Therefore, when the wind is weak, the principal tangential force (inciting acceleration) will vary with the sine of the tilt angle, and the friction force (inciting deceleration) will vary with the cosine of the tilt angle.

When dry snow does accumulate, it tends to do so as the growth of "embryonic" areas of snow accumulation [Kobayashi, 1987]. Several particles sticking to the surface of the array in close proximity to one another will provide an irregularity at the surface on which sliding and bouncing particles will be more likely to accumulate. As long as conditions remain conducive to accumulation, these "islands" grow in area and thickness, eventually assimilating other islands and covering the entire panel surface. On a photovoltaic panel, the aluminum frame is not usually flush with the glass surface, and the joint of the frame and the glass at the bottom of the panel is a natural location for these "islands".

Snow will be more likely to accumulate on a panel already covered in snow, rime, or hoarfrost, since the such surfaces are more irregular than glass. One indicator of the likelihood of the accumulation of new snow on existing snow cover is the angle of repose. The angle of repose for snow is the angle between the horizontal and the surface of a cone of snow formed by snow

concentration of wet snow in the air in Section 2.2.3.1 pertains also to dry snow.

¹⁵The friction and adhesion of snow is exceedingly complicated; for example, unlike most other engineering materials, with snow crystals the surface area of the particle affects the coefficient of kinetic friction [Barnes et al., 1971].

falling from a hopper onto an elevated disk, measured when the cone has reached steady state (see Figure 2.2). When the cone is at steady state, snow falling on the cone rolls down the cone and falls off the disk. Before reaching steady state, when the angle of the surface of the cone is less than the angle of repose, snow accumulates on the cone. Thus, the angle of repose approximates the critical tilt angle; at tilt angles less than this snow will accumulate on an already snow-, rime-, or hoarfrost-covered array.

The angle of repose is determined by the mutual adhesion of the snow particles (itself dependent on temperature) and the surface irregularities¹⁶ of the particles [Kuroiwa, 1967]. On pulverized snow particles of 0.5 to 0.6 mm diameter, the angle of repose below -20 ° C is about 45 °; this rises to 50 ° at -6 ° C and at -3.5 ° C the angle of repose is about 55 °, whence it increases rapidly with rising temperature^{17 18}. There appears to be little dependence on particle size for pulverized particles from 5 mm down to 0.42 mm in diameter. Natural snow crystals of dendritic form exhibit an even higher angle of repose for a given temperature, probably due to their more significant surface irregularities. At -35 ° C the angle of repose is about 63 °, at -12 ° C it is "steeper", and at -4 ° C it approaches 90 ° [Kuroiwa, 1967].

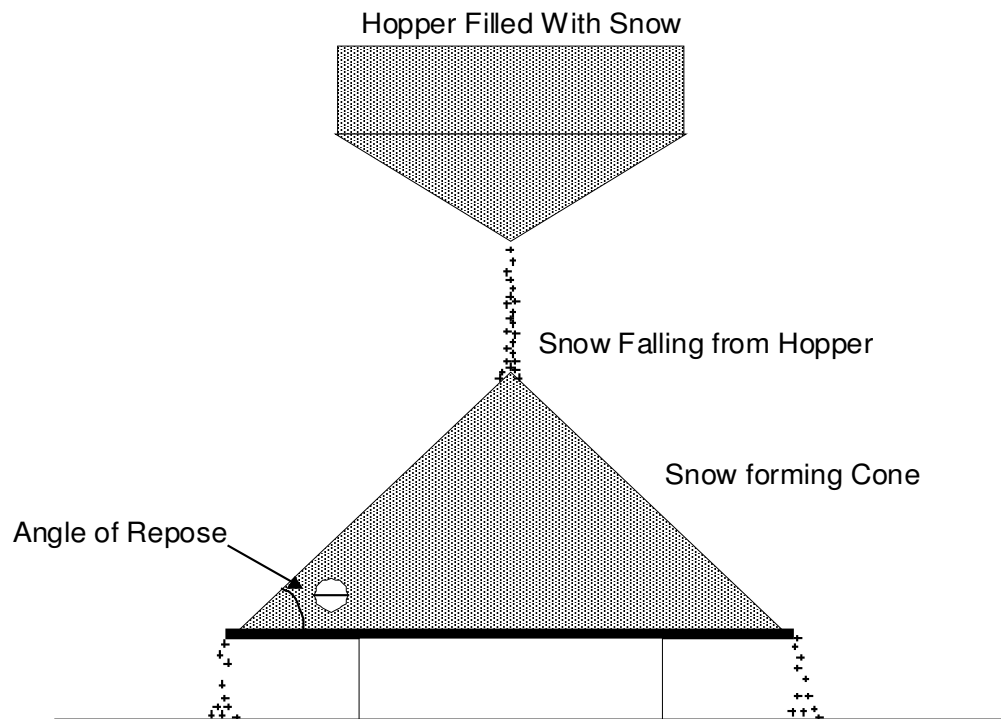
These results are not strictly applicable to the problem of finding the critical tilt angle for dry snow deposition unless the snow already covering the array is of the same type as that which is falling. Further, dendritic crystals tend to have extremely high surface irregularities compared with other snow crystals, and pulverized snow grains are more regular than most natural snow crystals [Kuroiwa, 1967]. Probably the results cited above bracket the critical tilt angle for dry snow accumulation on a covered array.

¹⁶One measure of surface irregularity for a snow particle is the ratio of the area of a circle just large enough to circumscribe a two dimensional image of the particle to the actual projected area of the particle [Kuroiwa, 1967].

¹⁷For wet snow particles, the angle of repose is essentially 90 °, which is in agreement with the findings reported in Section 2.2.3.1 [Kuroiwa, 1967].

¹⁸This is for accumulation in an environment nearly saturated with respect to ice; dryer environments will lead to lower angles of repose for a given temperature [Kuroiwa, 1967].

Figure 2.2 Measurement of the Angle of Repose



2.2.3.3 Wet and Dry Snow Retention

Snow that has come to rest on a photovoltaic panel may or may not remain there. If the temperature of the panel reaches zero ° C, the snow will tend to melt off. This is treated in Chapter 7 after a thermal model of the panel of a panel has been developed. However, tilt angle and climatological conditions also affect the retention of snow on a panel.

Tilt angle is an important determinant of the retention of snow on a panel. The principal force motivating snowcover to slide off a panel is due to gravity. Specifically, it is the tangential component of this force, equal to the product of the snow weight and the sine of the panel tilt angle, that is responsible for snow shedding. Thus, the tendency of the panel to shed snow cover will be related to the sine of the tilt angle. A study of unheated glass roofs in a wooded area near Ottawa, Ontario [Taylor, 1987] indicates that over three winters the ratio of actual roof to National Building Code ground load was 0.1 to 0.4 at a tilt angle of 20 °, whereas for 35 ° the ratio was 0.05 to 0.1.

If wet snow has accumulated on an array and the temperature drops, the liquid water in the accretion may freeze. This is particularly threatening to photovoltaic arrays, since there will be strong adhesion between the panel surface and the snow particles and between individual snow particles. This applies also to an array wetted by rain prior to snowfall, a combination of snow and rain, or rain falling on snow accumulation. The most long-lived snow accumulation at the Ontario Hydro photovoltaic installation at Trout Lake (well north of Thunder Bay) had as its genesis a freak December rain, followed by snow, followed by dropping temperatures¹⁹ [Drewes]. Thus, a wet snow followed by a long cold stretch is a potent meteorological combination for PV arrays.

It is less obvious that dry snow accumulations will remain on the panel surface for long periods of time: there is no wetting from which a strong adhesive bond between particles and between panel and snow can result, and the snow particles seem vulnerable to wind removal. Nevertheless, there exist several mechanisms which promote the self-adhesion of dry snow and thereby prolong the sojourn of the snow on the panel [Langham, 1981]. Metamorphism is the sublimation of parts of deposited snow crystals, the movement of the resultant water vapour, and the redeposition of the water at a different location. Generally, the sublimation occurs at the expense of small particles and surface irregularities (like the arms of dendritic snow crystals) and results in rounded, larger, heavier snow particles which have lower air drag coefficients and are less likely to blow away. Sintering is the formation of bonds at the points of contact between snow crystals. With time, "necks" of ice tend to build at these points by a process similar to metamorphism. Sintering increases the strength of the snow cover and further inhibits wind removal. It is likely that firnification, the strengthening and hardening of snowcover by a freeze-thaw cycle, will occur on a photovoltaic panel. Snow cover strengthens and densifies with the formation of hoar crystals at the surface of the accumulation (surface hoar) and in the air spaces

¹⁹Even so, the accumulation remained on the panel only one and half weeks.

between snow particles deep within the snowcover (depth hoar) [Boyd et al., 1968]. Overburden densification, the compaction of snow cover under the weight of the snow on top of it, is also possible.

2.3 Snow and Ice Accumulation by Region

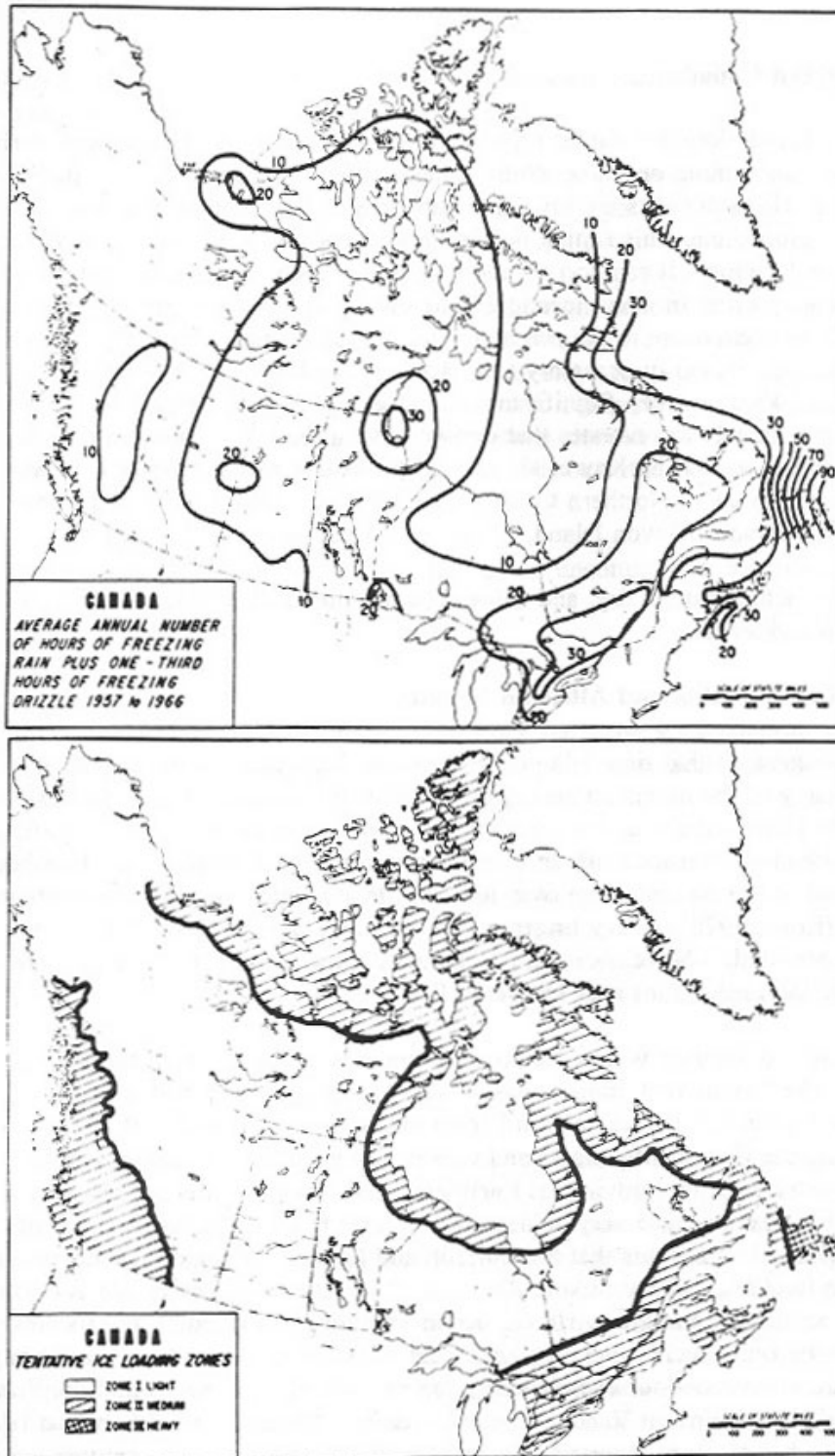
At present, theory and collected data are insufficient to provide any reliable estimate of the threat posed by snow and ice to photovoltaic systems installed at arbitrary locations within Canada. However, comparative evidence exists. Much of the information presented here is based on the personal experience of eighteen PV installers, PV end-users, and snow and ice experts contacted for this report. Unfortunately, even stating a broad range for the annual probability of an accumulation which persists for a given period of time is beyond this report.

The potential for glaze, and to a certain extent, rime accretion can be estimated by the mean annual number of hours of freezing precipitation (excluding snow) of all types. This measure has been presented graphically by [McKay et al., 1969], [Boyd, 1970] and [Boyd et al., 1968] (see Figure 2.3). Eastern Newfoundland has the highest incidence of ice accretion, followed by Northern Nova Scotia and Eastern New Brunswick, the Gulf of St. Lawrence, South Eastern Ontario, Southern Quebec, and the rest of the Maritimes. These maps would indicate a higher potential for icing in British Columbia were weather stations located at elevation, and not only in valleys and inlets [McKay et al., 1969]. [Boyd, 1970] also presents a table summarizing reports of icing on wires and other structures by province (see Appendix A).

Determining the potential for snow accumulation is more difficult. While freezing precipitation will adhere to an inclined surface, snow will do so only under certain conditions, as discussed above. Simply knowing where heavy snow fall occurs is not sufficient, since a photovoltaic array will shed its snowcover rapidly if temperatures are near freezing. Conversely, low temperatures are a poor indicator of snow accumulation hazard since sufficient snow fall must accompany the low temperatures. A better indicator is the frequency of snow fall at relatively high temperatures (to allow for adhesion) followed by a long cold period.

It must be pointed out that while riming is a recognized and recurring problem at some installations, persistent snow accumulation is not well-documented. Of all the people surveyed for this report, only two said that snow accumulation and retention was definitely a problem [Bergevin] [LaPlace]. On the other hand, as was pointed out by [Kociuba], most remote sites are rarely visited during winter and have oversized battery banks. This suggests that a relatively long lasting snow cover could go unnoticed as long as it was not so long-lived as to cause system failure.

Figure 2.3 Freezing Precipitation, Excluding Snow, by Region in Canada (from [Boyd, 1970])



Top: Index of Severity of Freezing Precipitation; Bottom: Tentative Ice Loading Zones

2.3.1 Northern Canada

"The arctic is notorious for winter fogs and many of these undoubtedly deposit rime" [Boyd, 1970, p. 6]. Soft riming on photovoltaic panels, densifying into strong ice deposits, has been documented. These deposits are several centimetres thick, and may not clear themselves from PV panels before June. This riming occurs on glaciers, and is not necessarily confined to mountainous locations. It can accumulate at a rate of 5 cm a day. The severity of the problem is highly site specific; in many locations rime either does not accumulate on PV panels or clears itself with exposure to the sun and wind. The atmosphere within 60 km of the coast generally has the humidity necessary to permit riming. Baffin Island appears to be particularly problematic. [Waszkiewicz]. Significant riming on a wind turbine on a mountain near Whitehorse [Morris] demonstrates that despite having the lowest number of hours of freezing precipitation in Canada [McKay et al., 1970], the Yukon poses a problem as well. Mountainous regions in Northern Canada include much of the Yukon, the Torngat mountains in Northern Labrador, Devon Island, Ellesmere Island, and Baffin Island.

The arctic is actually quite dry, and snow accumulation and drifting do not appear to be a problem [Waszkiewicz].

2.3.2 British Columbia and Albertan Rockies

There is no question that rime icing causes serious disruptions in the operation of photovoltaic arrays in many of the mountainous regions of British Columbia [Egles] [Dodd] [Jarvis]. Not only are the mountain elevations conducive to rime accretion, but they are sufficiently cold that rime does not soon melt off. In extreme cases, riming lasts from late October to early May [Jarvis]. Rime accumulation over four centimetres thick is not uncommon on some structures [Boyd, 1970]. Heavy fingers of rime and ice extending over 30 cm into the wind have been reported; a November rime accumulation measuring 50 cm thick occurred at a site (at an elevation of 2000 m) near Osoyoos [Boyd, 1970].

From location to location within the province there is a great deal of variation in the severity of riming. The "windswept, moist, coastal" areas are especially problematic [Egles]. As a rule, the province's weather moves eastward from the ocean. Moist wind off the ocean rises upon encountering the Coastal Mountains and causes heavy riming, especially within 100 km of the coast. The interior of the province is fairly arid, and few problems are reported there. However, because it is also very cold, accumulations that happen to arise can be very persistent [Jarvis]. It appears that the Cariboo and Selkirk Mountains, which are immediately west of the Rockies, and the Stikine Range, in the north, pose further obstacles to the eastbound air masses and heavy riming occurs. Moving east through the Rockies, the atmosphere becomes increasingly dry, and riming is less frequent. More northern parts of the province are more prone to severe riming; the problem is extreme around the Prince George area [Egles]. Mountains on Vancouver Island reach 2100 m, so it is likely that riming occurs there, although it was not reported as a problem. In certain locations daytime temperatures and insolation levels are sufficiently high to melt off rime

accumulations [Waszkiewicz] but this is certainly not true for many locations [Egles]. As expected, there are no reports of riming in the many valleys of the province [Morris].

There were no reports of snow problems, although it is difficult to interpret this result, since it appears that in most areas where snow accumulations are heavy, panels have been mounted vertically. For off-vertical panels one user in Banff National Park indicated that as long as the panel was mounted in an unshaded area snow melted off in a period of days [Gilbride]. Indubitably the region receives enough snow that under the right conditions it could be a serious problem; some locales regularly receive annual snowfalls of five to nine metres [Morris], a figure that gives credibility to the otherwise unbelievable report of snow drifting over panels mounted on an eight metre high pole [Gilbride]. Temperatures low enough to facilitate snow retention are more common at high elevations than in the valleys; at these elevations, however, winds, and therefore wind removal, will be stronger than in the protected valleys [Dodd] [Boyd, 1970].

Heavy glazing, mainly from freezing rain and drizzle, is not uncommon in the Fraser Valley but it is warm and such accumulations melt away in days.

2.3.3 Prairies

It has been suggested that the Prairies are too cold and dry for snow accumulation [Waszkiewicz], but PV installers working in the province report snow accumulation and retention at certain locations, even on panels with tilt angles of 45 to 60 ° [LaPlace].

Although heavy, wet snow and glaze accretions on vertical surfaces have been documented [McKay et al., 1969] [Wakahama et al., 1977], these have generally occurred in the late spring and would not have seriously impacted array performance. Surprisingly, rime can and does occur on the Prairies, but it is thin (two cm thick) and reportedly on wires (objects of small radius) only. Probably this occurs when moist air blows up a long, gentle slope [Morris].

2.3.4 Ontario

Riming and snow accumulation were not reported for the province, but it seems likely that conditions in parts of Ontario are not unlike those of the Prairies: by inference, snow accumulation could occur. In the south of the province, temperatures are probably high enough that snow will melt off; the panels at the Hugh Macmillan installation in Toronto-- admittedly a warm locale-- are mounted at 30 ° but still shed snow within a day or two [Drewes]. In the far north of the province it may be too cold, and snow too dry, for serious accumulation to occur [Drewes]. Rime accumulations may occur on some of the hills north of Lake Superior, but this is probably limited to accretions less than one centimetre thick [Morris]. Southern Ontario, near the Great Lakes, has a lot of freezing rain and glaze [McKay et al., 1969], but that alone should not pose much of a problem to photovoltaic installations.

2.3.5 Québec

Mountains in Québec are prone to riming; many reports, including one at Saguenay (November 13, 1969 at 1000 m elevation) of 20 cm thickness (see Appendix A), come from the north shore of the St. Lawrence and the Sept-Iles area [Bergevin]. The Chic Choc Mountains in the Gaspé Peninsula rise to over 1000 m; probably riming occurs here also. Hydro-Québec is reluctant to install transmission lines at elevations greater than 500 m because they have had serious riming (greater than two cm thick) in the past [Morris].

Snow accumulation problems are also reported. Principally these are wet snow accretions that freeze onto the panels. Dry snow deposition is also a problem around Lac St-Jean, where many installations receive heavy snowfalls and, being located in forested valleys, are sheltered from wind [Bergevin].

At lower elevations glazing and freezing rain are observed.

2.3.6 Maritimes

Accretions in the Maritimes are characterized by glaze. Eastern Newfoundland and Avalon have by far the highest incidence of freezing precipitation [McKay et al., 1969]. Glaze deposits 35 centimetres thick in Lascie, Newfoundland [Boyd, 1970] and 25 cm thick in Antigonish, Nova Scotia [Boyd, 1970] [McKay et al., 1969] have been observed. Further, in contrast to many other regions across Canada, in Newfoundland glazing is not uncommon in the dead of winter and is not necessarily accompanied by a warm front (as tends to be the case in Nova Scotia [Stewart et al., 1990]). Thus, glaze deposits will persist for periods of weeks [Haldar]. In the Avalon region, Newfoundland and Labrador Hydro design for a 2 to 5 cm glaze accumulation for a 50 year return period [Haldar].

Rime is a serious problem in mountainous parts of Newfoundland [Boyd, 1970]. The Long Mountains are especially bad; some test sites accumulate 20 to 25 cm rime deposits on tower guy wires [Haldar]. The winds on the coastal mountains can be very high (gusts to 150 km/hr) and temperatures very low (remaining below -20 C for months), completely encrusting panels in rime for extended periods of time during some winters (see Figure 2.4)[Kennedy] [Frampton].

The western coast of Newfoundland has a reputation for storms of snow mixed with freezing rain [Haldar].

Nova Scotia and New Brunswick are characterized by glaze deposits [Boyd, 1970], and Nova Scotia receives a high percentage of its freezing precipitation as freezing rain [Stewart et al., 1990]. In hilly regions of Nova Scotia there are reports of rime; the mountains on Cape Breton Island rise to 550 m and probably experience moderate riming.



Above:
Figure 2.4 Rime Icing of Panels in Gros Morne National Park, Newfoundland



Left:
Figure 2.5 Soltek Solar Energy Ltd. Flush Mount Panels for Comshells

2.3.7 Other Countries

Apparently conditions in the Russian arctic are very similar to those in the Canadian arctic, and similar riming problems exist [Waszkiewicz]. Mountain riming of PV panels definitely occurs in Washington State, probably occurs in Alaska, and possibly occurs in Oregon [Egles] [Dodd].

2.4 Overview of the Problems Caused by Snow and Ice to PV Installations

In addition to blocking solar radiation, snow and ice present a variety of threats to PV installations.

The weight of snow and ice accumulation, especially in combination with wind, presents a formidable challenge to structures, and these structures sometimes fail [Kalmbach]. It appears that PV panels themselves are sufficiently strong to withstand this loading.

Ice and rime that accumulates on towers and guy wires does fall and may be carried by wind. Falling ice deposits can crack panels, and panels must be situated and oriented (preferably vertically) to minimize this risk [Jarvis].

Snow can drift over arrays. Some PV systems are installed in the spring and summer with little consideration for their winter operation; if these arrays are too close to the ground snow will drift over them [Laplace].

The repeated freezing and thawing of water, and its accompanying expansion and contraction, can cause damage to panels, especially the frame. In addition, if the panel frame is made of aluminum and is not sufficiently strong, the bottom part of the frame may be deformed by sliding snow.

The abrasive nature of blowing snow may also be a minor problem. When snow is very cold, as it is in the arctic, it has properties in some ways not unlike those of sand. When being carried by a strong wind, blowing snow can effectively strip paint off exposed surfaces [Frampton].

2.5 Approaches to the Problem of Snow and Ice Accumulation

The problem of snow and ice accumulation on PV panels is approached in a number of ways. The fact that Canadian PV systems are, in most cases, reliable during the winter months indicates that the preventative measures currently employed are generally effective. But for the installations where these preventative measures are not sufficient, there exist few feasible solutions to the problem.

Snow accumulation is already dealt with in a most elegant manner: PV panels are mounted at a tilt angle that encourages snow removal. In locations where snow accumulation is a problem, the panel can be tilted past the angle that would be optimal for the latitude. Thus, many panels at

around 55 ° latitude are tilted at 60 to 75 ° to the horizontal [LaPlace] and in the far north most panels are mounted vertically [Waszkiewicz] [Kalmbach]. For most locations this solution works well; while reducing the summer output below the optimal, it boosts winter output by removing snow more rapidly. Interestingly, most rime-prone sites also have vertically mounted panels; when winds are high and the fall velocity of the particle is negligible in comparison, this presents the maximum area, projected onto a plane normal to the wind field, for rime to accrete on. In theory, this should exacerbate rime accretion [Makkonen, 1981], although in practice there may be other factors at play.

In locations where this solution is not effective, especially those for which riming is a problem, the standard practice is to drastically increase the capacity of the battery bank. It is not uncommon for systems in the mountains of British Columbia to have "three month autonomy"--the ability to operate on power from batteries alone for a period of three months [Dodd]. This increases the capital cost of the system. However, many of these systems are remote and the capital cost is a small proportion of the total cost of the system, which may require helicopter access at \$ 700 an hour [Egles]. Although the operators of these systems may be hesitant to decrease the autonomy of their systems [Egles] [Jarvis], rime removal technology still interests them. Such technology represents another layer of defense against system failure and would help keep the batteries from being deeply discharged, as is the case at present [Dodd].

It is agreed that good siting of the array is very important, although there is disagreement on what, exactly, characterizes a good site. Most people in the PV industry believe that the array should be placed in a windswept site, since this will maximize wind removal. Theoretically, this should also maximize the flux of liquid water onto the panel, and at sites where conditions are appropriate, should maximize rime accretion. Contradicting this, [Boyd et al., 1968] recommends avoiding exposed locations and [Morris] suggests avoiding siting the panels along ridges or mountain tops whenever possible; unfortunately this is precisely where telecommunications equipment, a common application for remote PV systems, is sited. With respect to the Arctic, [Waszkiewicz] counsels avoiding low-lying areas where moist air will accumulate, but also maintains that wind-exposed sites are best.

It appears that a smooth, aerodynamic structure with few irregularities provides fewer opportunities for rime to accumulate. With this in mind, Soltek Solar Energy Ltd. (Victoria, B.C.) has developed a PV strip that is mounted directly on the vertical exterior walls of comshells (see Figure 2.5). Users report that this appears to decrease rime accretion, but does not eliminate it. It seems that most fibreglass comshell-mounted panels perform better than panels in racks or on poles, although those panels on aluminum comshells seem to have the worst performance [Dodd]. The reason for this is unknown; [Dodd] speculated that the dark color of fibreglass comshells and their tendency to vibrate in the wind (properties not shared by the aluminum comshells) are responsible for this. An alternate hypothesis is that wind may be more likely to flow around the tall, slender fibreglass comshells than the low, squat aluminum ones. If this were the case, collision efficiency would be decreased, and riming would be lessened. This explanation would also apply to the poor performance of rack- and pole-mounted panels.

Noting that the frame of the PV panel accumulates rime, [Jarvis] reported that black anodized frames hasten rime removal from the panel itself. But he indicated that a cover of ice, not in contact with the panel itself but attached to surrounding structure, sometimes develops. To deter snow accumulation, it is important that the bottom lip of the frame and any supporting structure not pose a serious obstacle to sliding snow [Drewes]. Therefore, the frame should be as nearly flush with the glass surface as possible. Removing the bottom lip of the frame has met with some success [TN Conseil, 1993]. It is important that there is sufficient space at the bottom of the array such that snow can slide off without forming a pile that reaches the panels [LaPlace] [Corotis et al., 1979].

Icephobic coatings, which makes it difficult for ice to bond to a glass surface, have been developed. These tend to wear off quite quickly, and in this study were unanimously dismissed by researchers and field personnel alike [Lock, 1990, p. 220] [Egles] [Drewes] [Jarvis] [Frampton].

The literature on rime and glaze removal methods is not very illuminating, pointing out that "baseball bats, sledge hammers, axes, hammers, picks and other impact instruments...icephobic coatings and heated surfaces have been experimented with" [Minsk, 1980, p. 16].

Where system reliability is paramount and riming is serious, PV systems are augmented by other power sources, notably potash primary batteries and remotely actuated diesel and gasoline generators [Jarvis]. Obviously these add considerably to the system cost.

In an effort to heighten radiation absorption and wind vibration, dark-colored garbage bags have been attached to the rear face of some single-panel installations in the Arctic [Waskiewicz].

When systems are not remote, the option of manual clearing is available and often employed. It is not universally endorsed; though field personnel come daily to the Ontario Hydro grid-tied system at Trout Lake, they are instructed not to clear the array. The rationale for this is based on the observations that the array clears itself quickly and that, in general, human error is often responsible for the breakage of equipment [Drewes].

CHAPTER 3

PERTINENT PROPERTIES OF SNOW, RIME, AND GLAZE

In order to assess the performance of a snow or ice covered PV panel, several thermal and optical properties of the snow or ice that is covering the panel must be known. Unfortunately, snow and ice are very complex phenomena, and exhibit great variations in their properties. This complicates the study of the interactions between a PV panel and the snow or ice accumulated on it.

More information exists on the properties of snow than on the properties of rime and glaze. Most of the quantitative data necessary for the models used in this investigation is unavailable for glaze and rime. For these forms of accretion, it is necessary to extrapolate from the information on snow.

3.1 Snow

3.1.1 Classification of Snow

The formation of snow crystals and, subsequently, the formation of snowcover, are highly complex processes, and the variability of snow particles and snowcover reflects this. Classification systems for snow crystals recognize ten or more categories of snow crystal, and numerous subdivisions within each category. During snowfall, snow crystals collide and form aggregates. Fallen snow evolves through metamorphism, sintering, riming (which can also occur during snowfall) and various other processes (see Section 2.2.3.3). As a result, "snowcover" is a term that denotes not just one phenomenon, but a whole range of phenomena having a wide range of properties.

Classification systems for snowcover have responded to this complexity in a variety of ways. The system adopted by the International Commission on Snow and Ice of the International Association of Scientific Hydrology recognized a large number of primary features: specific

gravity or density, free water content, level of impurities, grain shape, grain size, temperature of the snow, strength and hardness. Later classification systems have focussed on the level of metamorphism exhibited by the snowcover [Langham, 1981].

In this study, only several properties of snowcover are pertinent. Unfortunately, these properties are not tabulated according to the classification systems mentioned above. Rather, each researcher tends to find a set of pertinent features by which to classify the snow, and then presents results as a function of these features. For the thermal and optical properties of interest here, researchers tend to classify snow by density, mean snow grain size, whether it is "wet" or "dry" and, in certain cases, the age of the snow and level of impurities it contains.

Density appears to be the most common classifying feature and is relied upon to capture much of the natural variation that gives rise to the complex classification systems mentioned above. The densities of various types of snow are listed in the Table 3.1.

Table 3.1 Densities of Various Types of Snowcover

Snow Type	Density (kg/m³)
Wild snow	10 to 30
Ordinary new snow immediately after falling in the still air	50 to 65
Settling snow	70 to 90
Very slightly toughened by wind immediately after falling	63 to 80
Average wind-toughened snow	280
Hard wind slab	350
New firn snow	400 to 550
Advanced firn snow	550 to 650
Thawing firn snow	600 to 700

from [McKay et al., 1981]

3.1.2 Effective Thermal Conductivity

In order to model the thermal characteristics of a snow-covered PV panel, the transfer of heat through the snow must be quantified.

Snow, being an agglomeration of a solid and a fluid or fluids, transfers heat in a more complicated manner than either a solid or a fluid alone. Solids transfer heat by conduction caused by lattice vibrations, fluids by convection and conduction stemming from molecular collisions. In dry snow, heat transfer involves [Mellor, 1977]:

- a) conduction in the network of ice grains and bonds,
- b) conduction across air spaces or pores,
- c) convection and radiation across pores (probably negligible), and
- d) vapour diffusion through the voids.

In practice, all heat transfer through snow is treated as conduction, and an effective thermal conductivity is used. The effective thermal conductivity accounts for all the above types of heat transfer through snow. Most of the variation in the effective thermal conductivity for different snow types can be related to the density of the snow. Figure 3.1 shows the effective thermal conductivity for snow as a function of density. The effective thermal conductivity is also related to the temperature of the snow, though this has not been considered in this study.

The measured values for the effective thermal conductivity in Figure 3.1 show considerable scatter: the values measured depend on the method of measurement and the condition of the snow at the time of measurement. [Langham, 1981] cautions that "considerable care should be exercised in applying this..., since it is difficult to determine whether the thermal regime encountered in the field problem will correspond to the regime under which the curve was developed."

3.1.3 Latent Heat of Fusion

The latent heat of fusion for snow is the same as that for water: the mass of the air in snow can be ignored, and the mass of the snow can be treated as a mass of ice. Therefore, the latent heat of fusion for snow is approximately 333 kJ/kg at standard atmospheric pressure and zero °C [Lide, 1994].

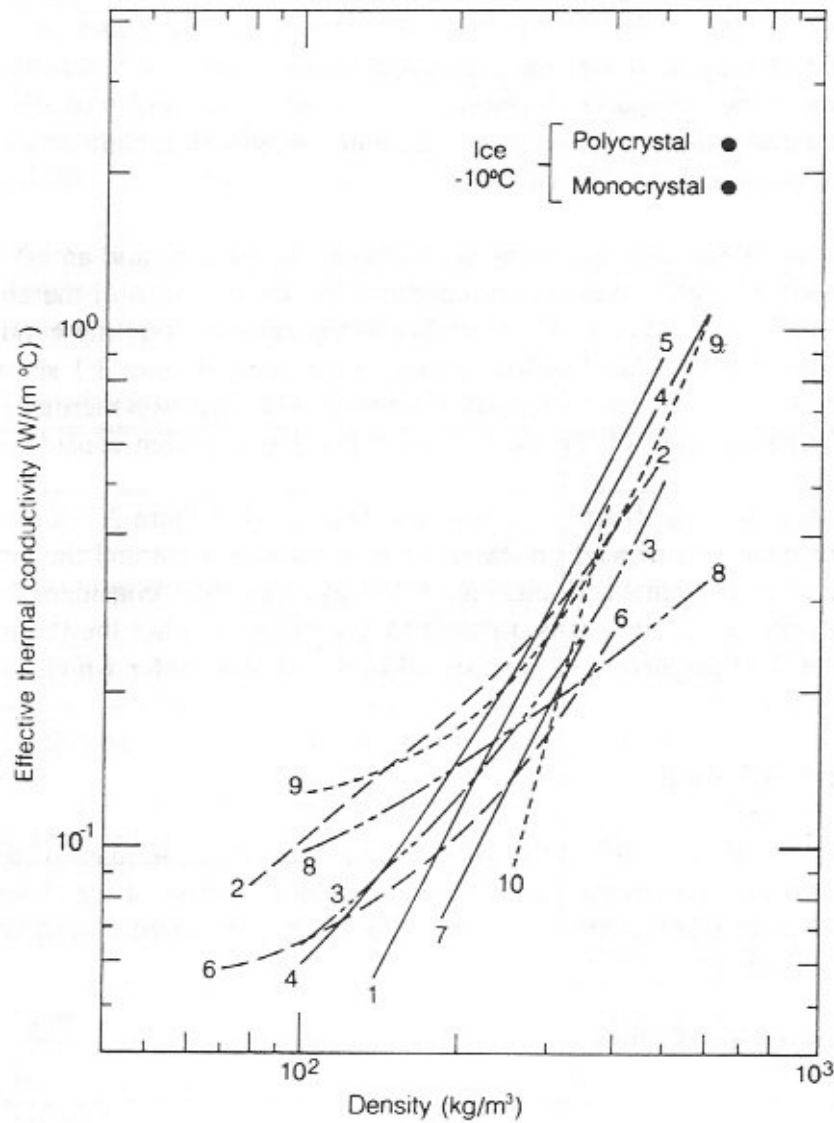
3.1.4 Optical Properties of Snow

3.1.4.1 Albedo

[Langham, 1981] defines albedo as "the ratio of the intensities of reflected radiation to incident radiation calculated using radiation intensities averaged over the short-wave radiation spectrum", which typically includes the wavelengths from 0.3 to 3 microns. Strictly speaking, the reflection of light from snowcover is a function of, among other variables, wavelength, but over the short-wave spectrum, spectral selection is not significant (see Figure 3.2a) and the use of an average reflectance value is valid [Mellor, 1977]. This is supported by the fact that snow appears white when illuminated by white light.

Figure 3.1 Effective Thermal Conductivity of Snow

Figure 3.1a From [Mellor, 1977]



Effective thermal conductivity of snow as a function of density. Data from 1 Abels (1892); 2 Jansson (1901); 3 Van Dusen (1929); 4 Devaux (1933); 5 Kondrat'eva (1945); 6 Yosida and others (1955); 7 Bracht (1949); 8 Sulakvelidze (1959) (-20°C); 9 Pitman and Zuckerman (1967) (-5°C); 10 Jaafar and Pigot (1970). The data for ice is from Glen (1974). (Adapted from Mellor, 1977).

Figure 3.1b From [Langham, 1981]

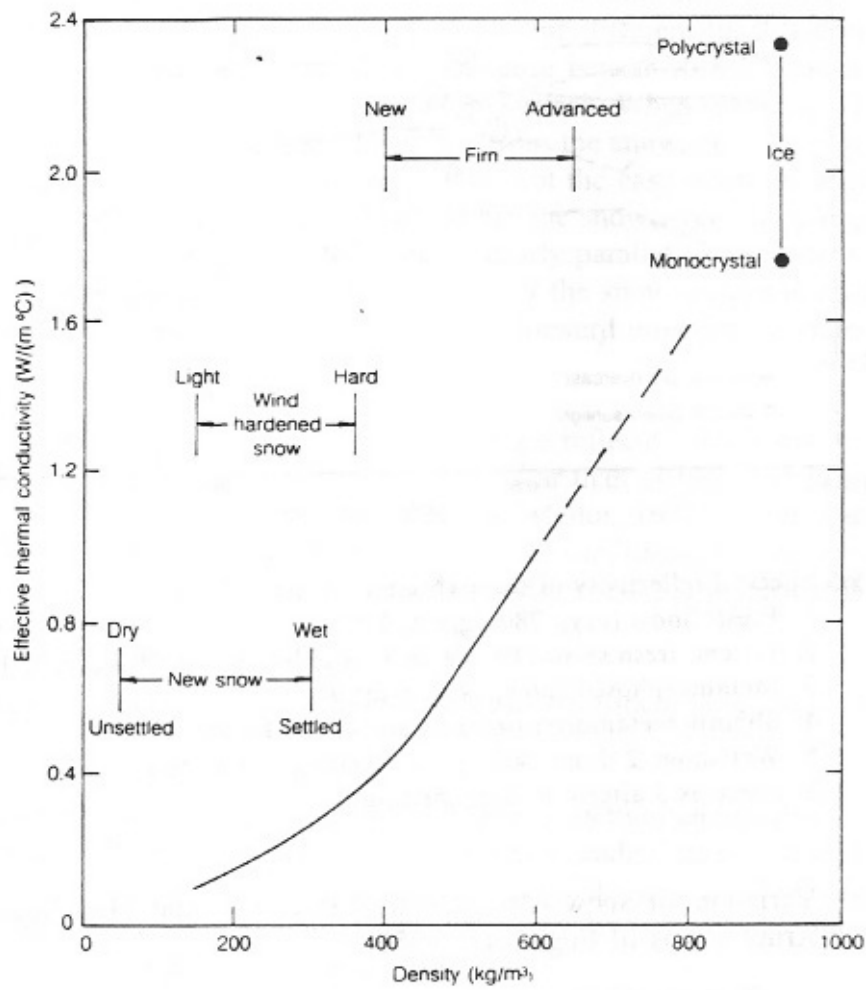
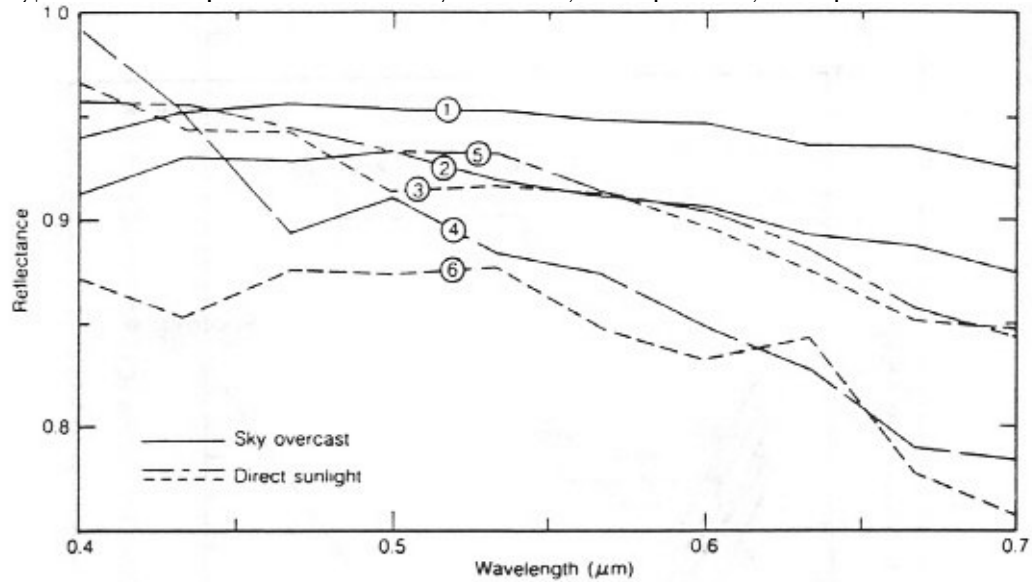


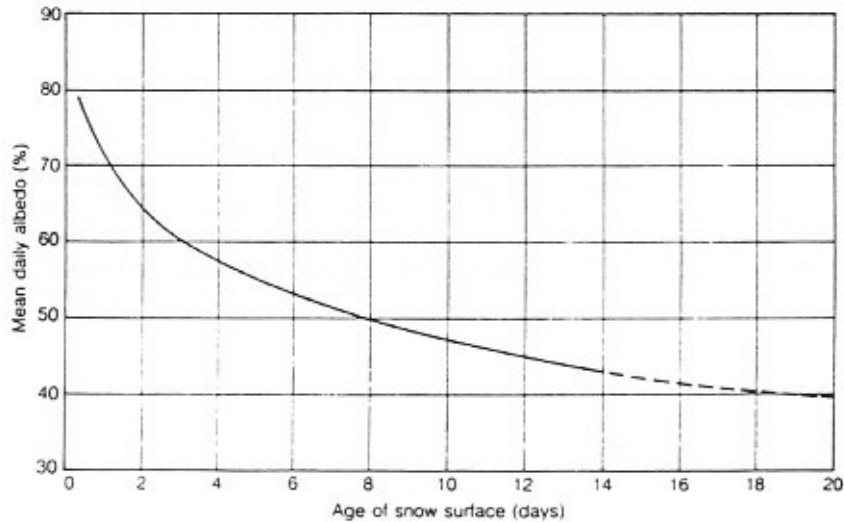
Figure 3.2 Albedo of Snow

Figure 3.2a Spectral Reflectivity of Snow, from [Mellor, 1966]



1. Fresh snow (dry), 280 kg/m³, 0° C.
2. 1-2cm, fresh snow (100 kg/m³) on older snow (400 kg/m³), 0° C.
3. Metamorphosed snow, 430 kg/m³, 0° C.
4. Slightly metamorphosed new snow, 200 kg/m³, 0° C.
5. Wet snow, 2 d old, 400 kg/m³, melting during test.
6. Same as 5 after 4 h more melting.

Figure 3.2b Variation of Snow Albedo with Age During the Melt Season, from [U.S. Army Corps of Engineers, 1956]



Solar radiation penetrates the surface of snowcover; "contrary to general belief, reflection at the surface of snow grains plays little part..."[Langham, 1981]. Once in the snow, the light is scattered, with most of the scattered rays being diverted only several degrees [Warren, 1982].

The albedo of snow is a function of sun angle. This is due to both the direction of the beam radiation and the spectral composition of the radiation being different for different sun angles. When the sun is low in the sky, and the angle of incidence is near 90 °, a beam that penetrates the snow surface remains fairly close to the surface. When scattering of the beam occurs, the scattered beams are more likely to escape from the snow, since they must travel only a short distance to reach the snow surface. This is not the case when the angle of incidence is small, and the scattering occurs deep within the snowcover. More importantly, when the angle of incidence is high, and the beam is nearly parallel to the snow surface, the probability of the beam being scattered in the direction of the snow surface is greater. This is a result of the scattering occurring most strongly in the forward direction, as stated above [Warren, 1982].

Snow is neither a perfectly specular nor a perfectly diffuse reflector. For a smooth snow surface and beam radiation, the snow will be more specular than diffuse, and for diffuse radiation the surface will be more diffuse than specular [Mellor, 1977]. In this study it is assumed that snow is a perfectly diffuse reflector under all conditions; this assumption simplifies the modelling of ground-reflected radiation considerably. It is unclear how much error this introduces.

Albedo is a function of grain size, also. Albedo decreases with increasing grain size [Mellor, 1977].

As snow ages, its albedo changes. Aging snow undergoes structural changes which alter its scattering characteristics [Male et al., 1981]. The result is a gradual reduction in the albedo. This is shown in Figure 3.2b; it should be noted that this graph is for a period of time during the melt season. Further, the introduction of impurities into the snow or onto the snow surface further reduces the albedo [Langham, 1981].

For snowcover that is not very deep, the reflectance of the underlying surface affects the albedo of the snowcover. [McKay et al., 1981] reports that for snowcover depths of less than 12 cm, the reflectance of the underlying surface is important. This figure will depend on the type of snow.

Table 3.2 lists the albedo for snow under various conditions. Figure 3.2a should also be consulted. For comparison, the albedo of bare soil is around 20 %.

Table 3.2 Albedo of Various Types of Snowcover

Snow Type	Albedo (%)	Source
Exposed with continuous snowcover	80	1
Exposed with changing (melting) snowcover	55	1
Wet, after snowmelt	15	1
Compact, dry, clean, sun angle 30.3 °	86	2
Compact, dry, clean, sun angle 25.1 °	95	2
Clean, wet, fine grain	64	2
Wet, clean granular	62	2
Porous, very wet, greyish color	46	2
Very porous, grey, full of water, sea ice visible	43	2
Dry packed snow	78 to 93	3
Moist snow	73 to 78	3
Wet snow	56 to 72	3
Coniferous forest with snowcover	12	1

1 [McKay et al., 1981: Kondratyev, 1954 quoting P. P. Kuz'min]

2 [Male et al., 1981: Kondratyev, 1954 quoting P. P. Kuz'min]

3 [Mellor, 1977: Bryazgin et al., 1969]

3.1.4.2 The Bouger-Lambert Law

The electrical output of a PV panel and the panel temperature are both functions of (among other variables) the solar radiation striking the surface of the panel. A layer of snow on the face of the panel diminishes the radiation which reaches the PV cells. Therefore, in modelling the electrical and thermal performance of a snow-covered PV panel, it is necessary to have a model for the penetration of solar radiation through snow.

The transmission through snow of monochromatic radiation at a wavelength λ , contained in the solar spectrum, can be modelled by the Bouger-Lambert Law [Mellor, 1977]:

$$I_{\text{Bouger}}(x) = I_0 e^{-\kappa x} \quad (3.1)$$

where υ is the extinction coefficient,
 x is the depth below the snow surface,
 I_0 is the radiation intensity at the surface,
and I_{Bouger} is the radiation intensity at depth x .

In general, υ is a function of wavelength and the type of snow.

The Bouger-Lambert Law can be applied to the entire solar spectrum by choosing an average value for υ . The value of the extinction coefficient does not vary greatly over the solar spectrum; more error is likely to be introduced when estimating the extinction coefficient on the basis of snow properties.

The Giddings-LaChapelle model [O'Neill et al., 1972], gives the radiation penetration at depth x when a plate is placed at this depth. Since solar radiation penetration through snow is largely a scattering phenomenon the reflectance of the plate affects the radiation intensity at its surface. This model more accurately reflects the situation of a PV panel under snow. However, the use of this model requires the empirical determination of at least one experimental coefficient, and this is not feasible for our study.

Figure 3.3 shows a comparison of the Bouger-Lambert Law and the Giddings-LaChapelle model. The coefficients for the Giddings-LaChapelle model are from [O'Neill et al., 1972]. The extinction coefficient for the Bouger-Lambert Law was chosen on the basis of the description of the snow and its density given in [O'Neill et al., 1972]; it was chosen prior to the comparison of the two.

In this case, the two models are in poor agreement for snow depths less two cm; at snow depths greater than two cm both models give essentially the same result-- virtually no radiation penetration. Penetration is very low because the snow being modelled is wet and dense.

The Bouger-Lambert Law gives acceptable accuracy for the prediction of solar radiation penetration through snowcover on the face of a PV panel; further, the Giddings-LaChapelle model requires parameters which are unavailable. Therefore, the Bouger-Lambert Law is used in this study to predict the solar radiation transmission through the snowcover on the front of the panel.

3.1.4.3 Solar Radiation Extinction Coefficient

Application of the Bouger-Lambert Law requires estimation of the extinction coefficient on the basis of snow properties. Relevant properties are the same as those for the albedo. Attenuation of light in snow is due primarily to refraction and diffraction of the light, and secondarily due to absorption.

Figure 3.3 Comparison of Bouguer-Lambert and Giddings-LaChapelle Models for Radiation Transmission Through Snow

$I_0 := 1$ Assume Incoming radiation has unit intensity
 $w := 0.1622$ Parameters given by O'Neill and Gray for G-L model
 $b := 0.42$
 $v := 100$ Estimate of extinction coefficient for same snow type
 $x := 0, 0.0025, 0.06$

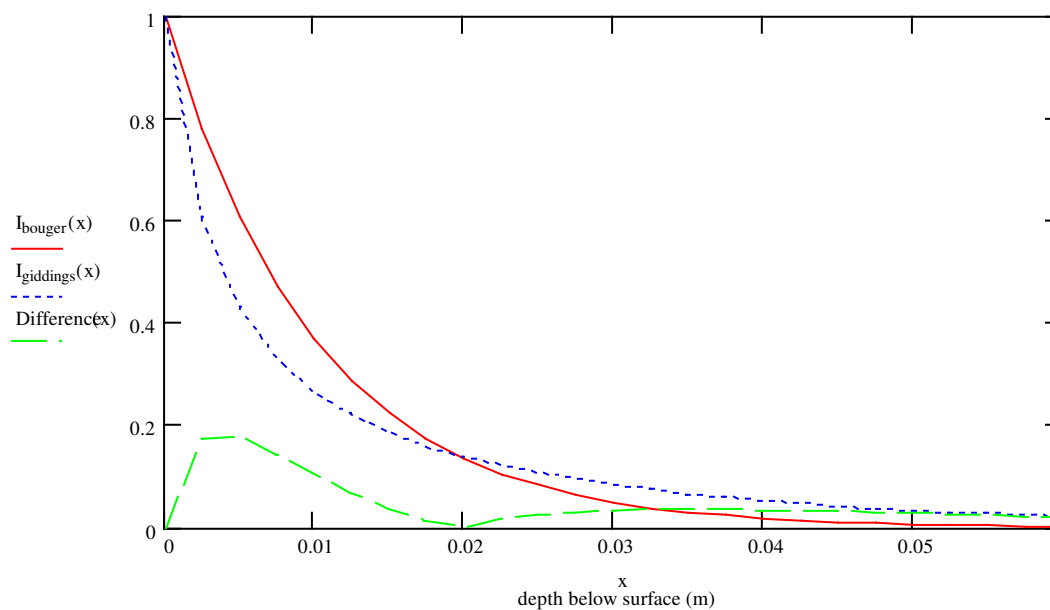
$$I_{\text{bouger}}(x) := I_0 \cdot e^{-v \cdot x}$$

Bouguer-Lambert

Giddings-LaChapelle(in metres)

$$I_{\text{giddings}}(x) := \frac{I_0 \cdot w \cdot e^{-b \cdot 100 \cdot x} \cdot (1 + \tanh(b \cdot 100 \cdot x))}{\left[1 + \frac{w}{2} \cdot \left[1 + \frac{e^{-b \cdot 100 \cdot x} \cdot \left(1 - \frac{w}{2} \right)}{\left(\frac{w}{2} \right) \cdot \cosh(b \cdot 100 \cdot x) + \sinh(b \cdot 100 \cdot x)} \right] \right] \cdot \left(\frac{w}{2} + \tanh(b \cdot 100 \cdot x) \right)}$$

$$\text{Difference}(x) := |I_{\text{giddings}}(x) - I_{\text{bouger}}(x)|$$



Fraction of visible wavelengths transmitted to a semi-infinite black surface at depth x (m) below the snow surface. See [O'Neill et al., 1972]

Figure 3.4 contains values for the solar radiation extinction coefficient for various types of snow according to a number of researchers. In addition, values for the extinction coefficient for various types of snow are listed in Table 3.3.

Table 3.3 Extinction Coefficients for Various Types of Snowcover

Snow Description	Extinction Coefficient (m^{-1})	Source
Soft new snow	10 ± 2	[Maguire, 1975]
Hard powder snow	50 ± 5	[Maguire, 1975]
Hard powder snow	27 to 45	[Maguire, 1975; Thomas, 1963]
Snow	20	[Adams, 1981]

There is a great deal of variation in these results, both between researchers and between snow under different conditions. Because the extinction coefficient is used in an exponential function, this variation greatly affects the radiation transmission. This can be seen in Figure 3.5, which shows solar radiation transmission as a function of snow thickness and solar radiation extinction coefficient. As a consequence, estimating the extinction coefficient may introduce significant error to the models of snow-covered panels.

3.1.5 Emissivity

The emissivity, or emittance, of snow is very high. Values around 0.97 to 1.0 are reported [Male et al., 1981]. The emissivity tends to decrease with decreasing grain size and decreasing temperature [Mellor, 1977], but this has not been accounted for in this study.

3.2 Rime and Glaze

This study is concerned not only with the accumulation of snow on the surface of the PV panels, but also with the accretion of rime and glaze. Thus, the thermal conductivity, latent heat of fusion, solar radiation transmission, and emissivity of rime and glaze must also be known.

Since glaze is simply ice, its properties are easily obtained. The thermal conductivity for ice is given in Figure 3.1. The latent heat of fusion for ice is given in Section 3.1.3; the specific gravity of ice is 0.917 [Lide, 1994]. The emissivity of ice is 0.97 [Mellor, 1977]. The solar radiation transmission for ice can be modelled with the Bouger-Lambert law; extinction coefficients range from 2 m^{-1} for clear ice to 20 m^{-1} for cloudy ice [Maguire, 1975].

Figure 3.4 Extinction Coefficient for Snow

Figure 3.4a As a function of wavelength according to different investigators [Mellor, 1977]

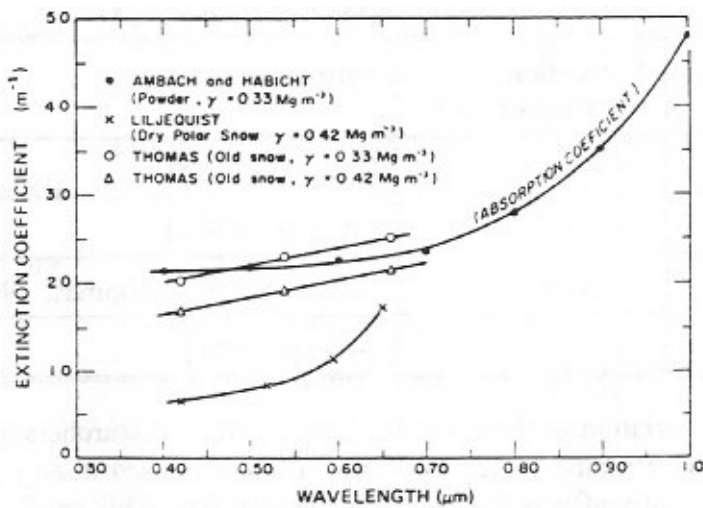


Figure 3.4b As a function of grain size and density [Mellor, 1966]

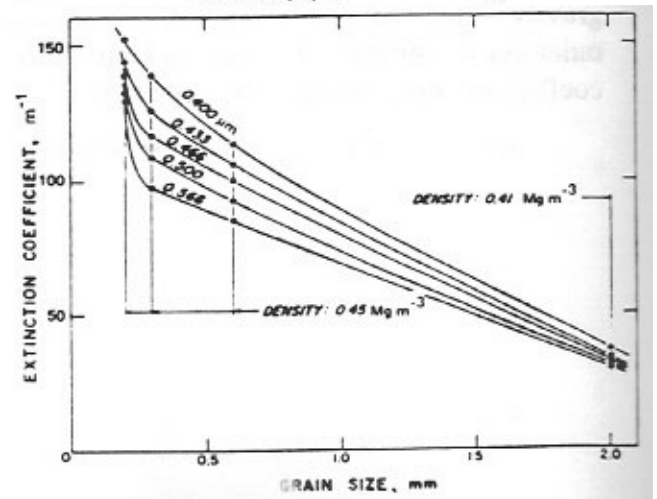
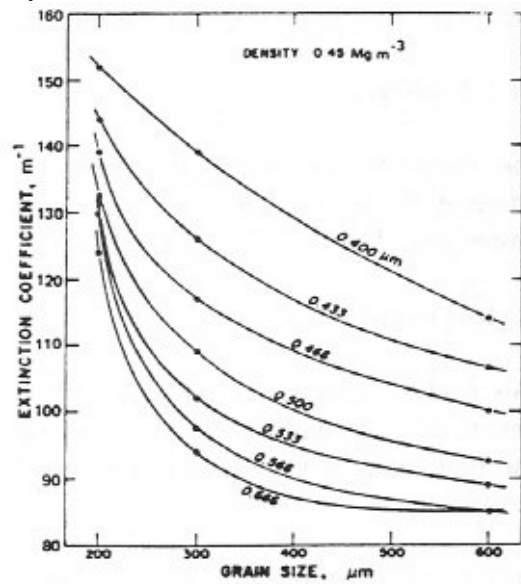
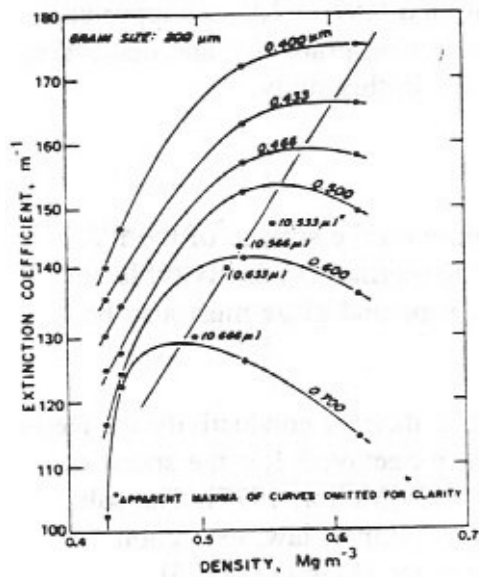


Figure 3.4c As a function of wavelength [Mellor, 1966]

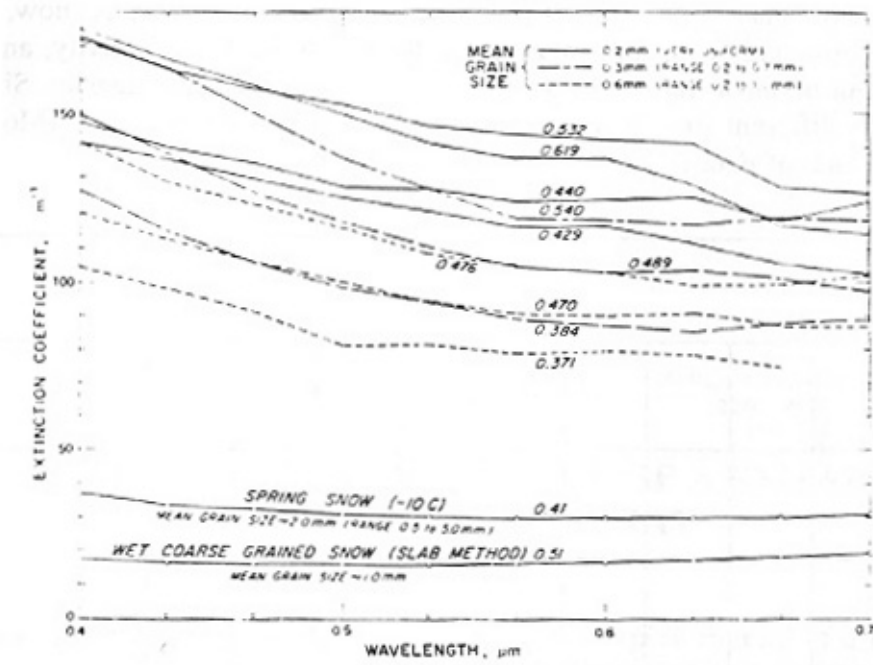
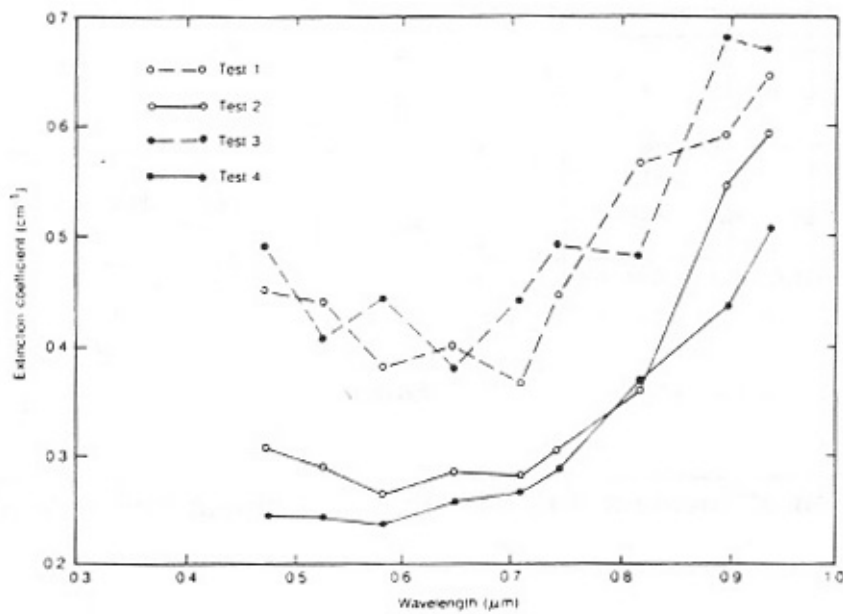


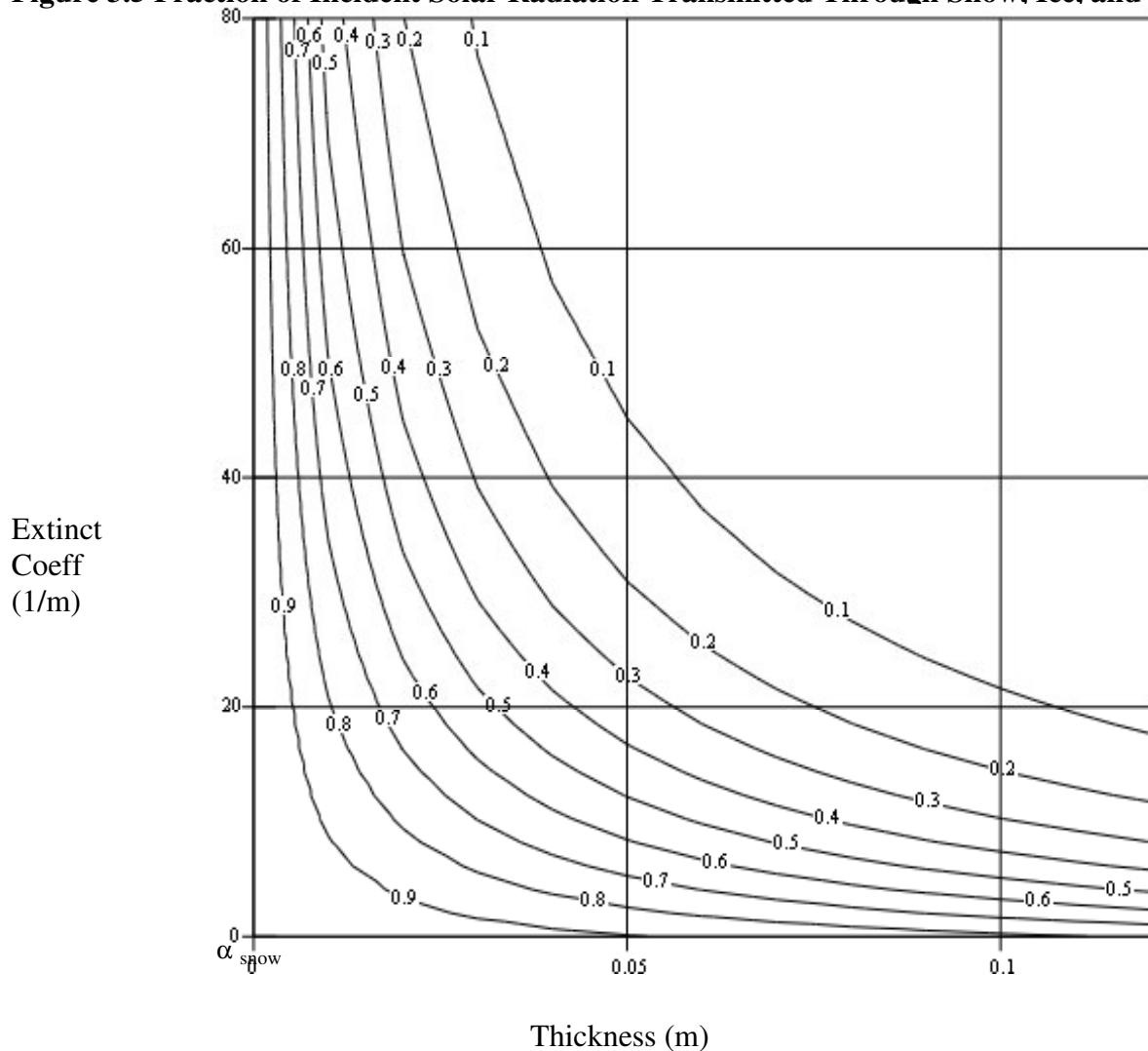
Figure 3.4d As a function of wavelength [Male et al., 1981]

	Condition	Density g/cm ³	Foreign Matter mg/Litre	Particle Size μm
Test 1	Wet	284	51	0.302
Test 2	Wet	338	29.8	0.475
Test 3	Dry	284	50.5	0.259
Test 4	Wet	180	15.5	0.167



The properties of rime are poorly documented. Obviously, the latent heat of fusion is the same as that for snow. Since rime contains the same constituent materials as snow, a reasonable first approximation for the emissivity, effective thermal conductivity, and extinction coefficient of snow may be estimated from snow of the same density. Since the structure of snow is different from that of rime, this will introduce some error [Morris]. Unfortunately, the lack of data for rime leaves few alternatives.

Figure 3.5 Fraction of Incident Solar Radiation Transmitted Through Snow, Ice, and Rime



CHAPTER 4

ELECTRICAL PERFORMANCE OF A SNOW OR ICE COVERED ARRAY

In order to assess the impact of snow or ice cover on the performance of a PV panel, the degradation in the electrical output of the array must be determined. The current and power output of a uniformly covered array will decrease linearly with the decrease in solar radiation penetrating the snowcover. On an array that is not uniformly covered, however, the decrease in output is nonlinearly related to the decrease in total radiation reaching the array.

4.1 Effect of Partial Shading on Module Performance

In general, snow, and presumably rime and ice, melt and shed irregularly from the face of a PV panel. Sometimes much of the panel clears after a short interval, but a minor portion of the panel, usually an upward-facing crescent at the bottom, remains covered for a longer period of time (see Section 7.1.2). This results in different irradiation levels for different cells in the module.

4.1.1 Effect on a Single Cell

For a single cell, the short-circuit current varies in direct proportion to the insolation level. The effect of insolation level on open circuit voltage is much less pronounced; the open circuit voltage of the cell is reduced in proportion to the logarithm of the reduction in radiation intensity [Siemens Solar Industries, 1990]. The shape of the IV curve stays relatively constant with changing insolation levels.

4.1.2 Effect on a Series Arrangement of Cells

For a series arrangement of cells, the effect of diminished insolation levels is more complicated. If all cells are shaded exactly the same amount, the behaviour of the series string is the same as that of a single cell. But if some cells are shaded more than others, the performance of the entire series arrangement is tied closely to the irradiance of the most heavily shaded cell. This is due to the fact that, in a series arrangement, each cell must conduct the same current. For any operating voltage below the open-circuit voltage, shading the cell decreases the current it will conduct. The least-irradiated cell will limit the current for the entire string.

The decrease in the current in the entire string, however, is not as great as the decrease in the current that would be observed for the least irradiated cell were it isolated from the other cells. The less shaded cells in the series arrangement force the more heavily shaded cells to operate at a current higher than their short-circuit current. Thus, there is a "negative" voltage drop across the shaded cells, and electrical power, equal to the voltage drop across the cell multiplied by the operating current of the entire series arrangement, is dissipated as heat in the cell. This can be thought of as a transfer of energy from the less shaded cells to the more shaded cells. This transfer of energy not only decreases the useful energy that can be extracted from the series string of cells, but also causes "hot spots" in the string.

The short-circuit current of the entire series string can be found quite simply. Consider a cell in isolation from the string. Since the sum of the voltage drops around the circuit must be zero, the short-circuit current of the combination of the string and the cell is that current at which the magnitude of the voltage of the cell equals the magnitude of the voltage of the rest of the string. If the cell is partially shaded and has a short-circuit current that is lower than that of the string, the potential across the cell will oppose the potential across the string as a whole: in a sense it will be reverse-biased.

For all cells in the string, and for currents other than the short circuit current, this operation corresponds to the addition of the individual cell IV curves:

$$V_{string}(I) = \sum_{x=1}^n V_{cell}(I) \quad (4.1)$$

where V_x is the operating voltage of x, where x is the entire string or an individual cell,
I is current (Amps),
and n is the number of cells in the series arrangement.

This provides V_{string} as a function of I; since this is a one-to-one function, the string IV curve is simply the inverse of $V_{string}(I)$.

4.1.3 Effect on a Module

Most PV panels consist of a series string of cells in parallel with one or more bypass diodes. These diodes exist to prevent a heavily shaded module from "dragging" down the output of an array. If several modules are connected in series, then the result is another series arrangement of cells. If there were no bypass diodes, shaded cells in one module would limit the current of the entire array in the manner described above.

The bypass diode is placed in parallel with the string of cells (see Figure 4.1). Under normal operating conditions-- i.e., without any shading-- the diode is reverse-biased and conducts no current. If the string becomes shaded and is forced to operate at a current above its short-circuit current it will become reverse-biased. In this situation the diode is forward-biased, and will conduct current. The diode will have a voltage drop across it, which for most diodes will be approximately 0.7 V. Thus, the string will be reverse-biased, but only by 0.7 V; this limits the power loss in the string, and permits a higher current to pass.

Most modules have either one or two bypass diodes. If there is one bypass diode, as is the case in Astropower modules, it spans all cells in the module. If there are two, as there are in Siemens panels, the diodes overlap, with each diode spanning two-thirds of the cells in the module, and two-thirds of the cells being spanned by both diodes.

4.2 Measured Effects of Shading

4.2.1 Observations

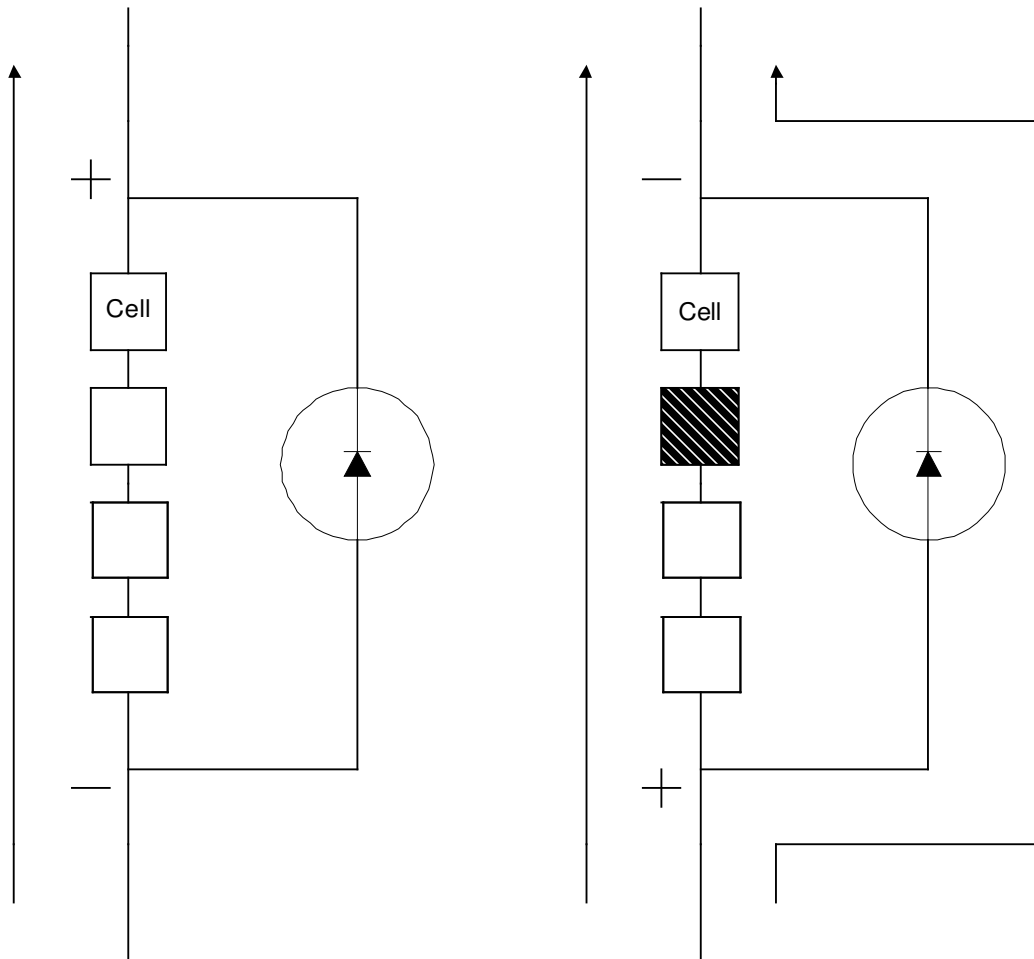
Two modules were tested under various conditions of partial shading. One was an Astropower APC4716 with the bypass diode removed; this panel contained a series string of 36 cells. The other panel was a Siemens M55 panel with two bypass diodes, each spanning 24 cells.

Various cells on the panels were partially shaded, using cardboard attached to the face of the panel. When snow is covering a cell, the irradiance of the entire cell is reduced by a certain fraction. To simulate this, an equivalent fraction of the area of the cell was perfectly shaded-- i.e., kept dark-- by a covering of cardboard.

A Spi-Array Tester 750, from Spire Corporation, was used to determine the IV curve of the panel under natural sunlight. The tests were done on cloudless days to ensure strong, constant insolation.

A hand-held multimeter was used to verify the short-circuit current on some of the tests. In some tests this was done immediately prior to taking the IV curve with the Spi-Array Tester. This caused heating of the shaded cells, whereas the open circuit configuration did not. Raising the cell temperature altered the ability of the shaded cells to conduct current, and therefore made it difficult to closely compare the results. It was not recorded which tests were preceded by a

Figure 4.1 The Function of The Bypass Diode



a) Unshaded Operation: No current passes through bypass diode

b) With Shaded Cell: Current passes through cells and bypass diode

measurement of the short-circuit current. Thus, results are presented to demonstrate the effects of shading, and not as a definitive characterization of the performance of partially shaded modules.

Plots of the results for the Astropower module demonstrate the degradation in performance for a series string of cells. Each plot shows the actual IV curve that was taken and also the same curve translated to standard conditions of 25 ° C cell temperature and 1000 W/m² insolation²⁰. Figure 4.2 shows the IV curve with no shading. Figure 4.3 demonstrates that with just one cell 60 to 70 % shaded, the curve has been radically altered. While the short-circuit current and the open circuit voltage are approximately the same as those of the unshaded case, the fill factor is much lower for this curve. As a result, the peak power has been reduced almost 45 %. In Figure 4.4 two cells are shaded 45 to 50 %; the peak power has dropped about 25 % from the level of the unshaded case. With four cells 50 to 60 % shaded (Figure 4.5), the peak power is reduced about 40 %; with nine cells 50 to 60 % shaded (Figure 4.6), the reduction in peak power is almost 55 %. These results are summarized in Table 4.1.

Table 4.1 Effect of Partial Shading on the Series String of Cells in an Astropower Panel

Shading Conditions	% reduction in radiation on panel	% reduction in peak power
Unshaded	0	0
One cell 60 to 70 %	2	43
Two cells 45 to 50 % each	3	24
Four cells 50 to 60 % each	6	39
Nine cells 50 to 60 % each	14	53

Similar reductions in the peak power for the Siemens M55 panel were found, and are summarized in the table below. Comparing the IV curve for the unshaded panel (Figure 4.7) with the IV curves for the partially shaded panel configurations (Figures 4.8, 4.9, 4.10, and 4.11²¹), one sees that the bypass diode results in a "stepped" IV curve, with the step occurring at the point at which the bypass diode begins to conduct current.

²⁰ A standard procedure developed by the Jet Propulsion Laboratory and implemented in the software accompanying the Spi-Array Tester was used for this transformation.

²¹ In these diagrams "outer row" refers to a series string of cells that are spanned by one bypass diode only, and "inner row" to a series string of cells that are spanned by two bypass diodes. In the Siemens module there are, therefore, two outer rows and one inner row.

Figure 4.2 Astropower Module with No Shading

Site: AS1	System: AS1	Name: AS1			
Date: 04-24-95	Module: AS1	Misc: -0.000			
Time: 13:32:12					
Irradiance(W/m2)	860.0	Peak Power(Watts)	34.8	Actual	25°C
Cell temp(°C)	43.0	I at Peak(Amps)	2.3		46.0
Isc(Amps)	2.7	V at Peak(Volts)	14.8		2.8
Voc(Volts)	19.2	Fill Factor(%)	67.8		16.6

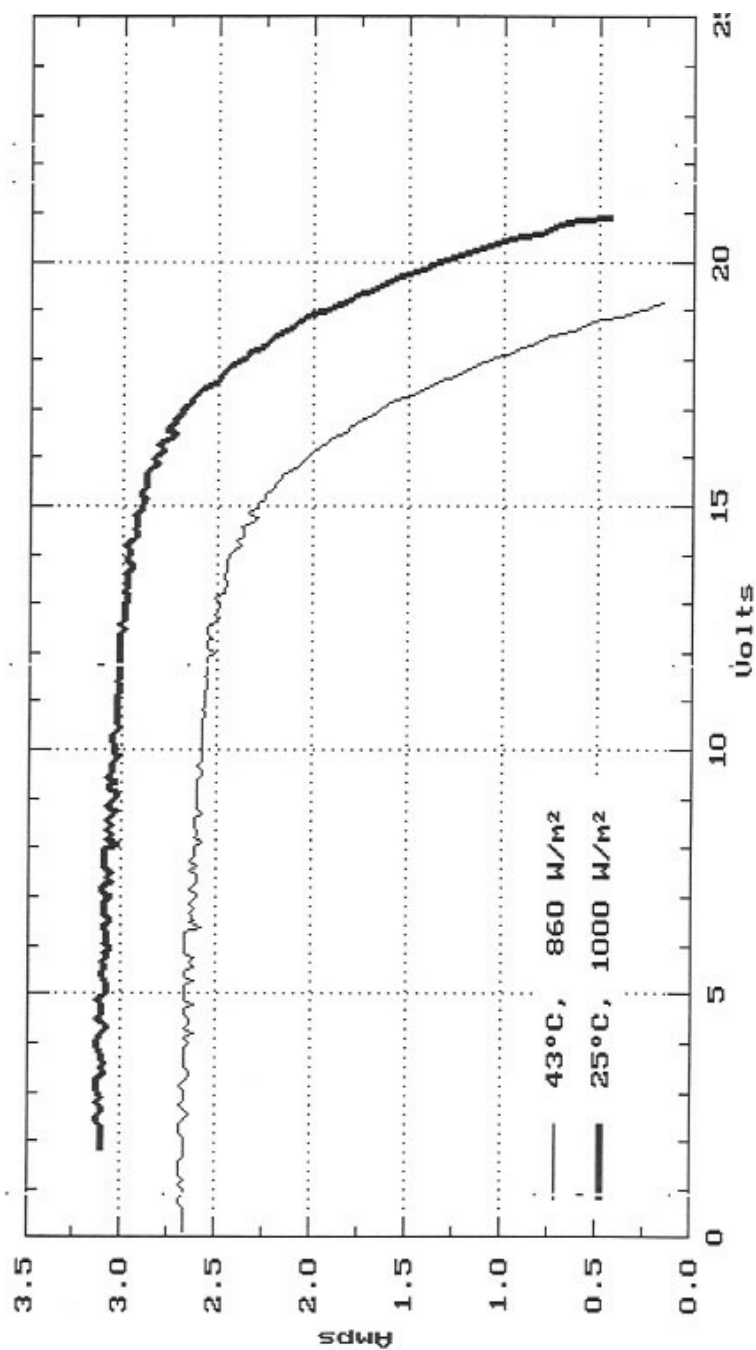


Figure 4.3 Astropower Module with One Cell 60 to 70 % Shaded

Site: AS3	System: AS3	Name: AS3			
Date: 04-24-95	Module: AS3	Misc: -0.000			
Time: 13:41:09					
Irradiance(W/m2)	840.0	Peak Power(Watts)	17.4	Actual	25°C
Cell temp(°C)	43.0	I at Peak(Amps)	1.4	26.2	
Isc(Amps)	2.4	U at Peak(Volts)	12.5	1.7	
Voc(Volts)	19.2	Fill Factor(%)	38.0	15.4	

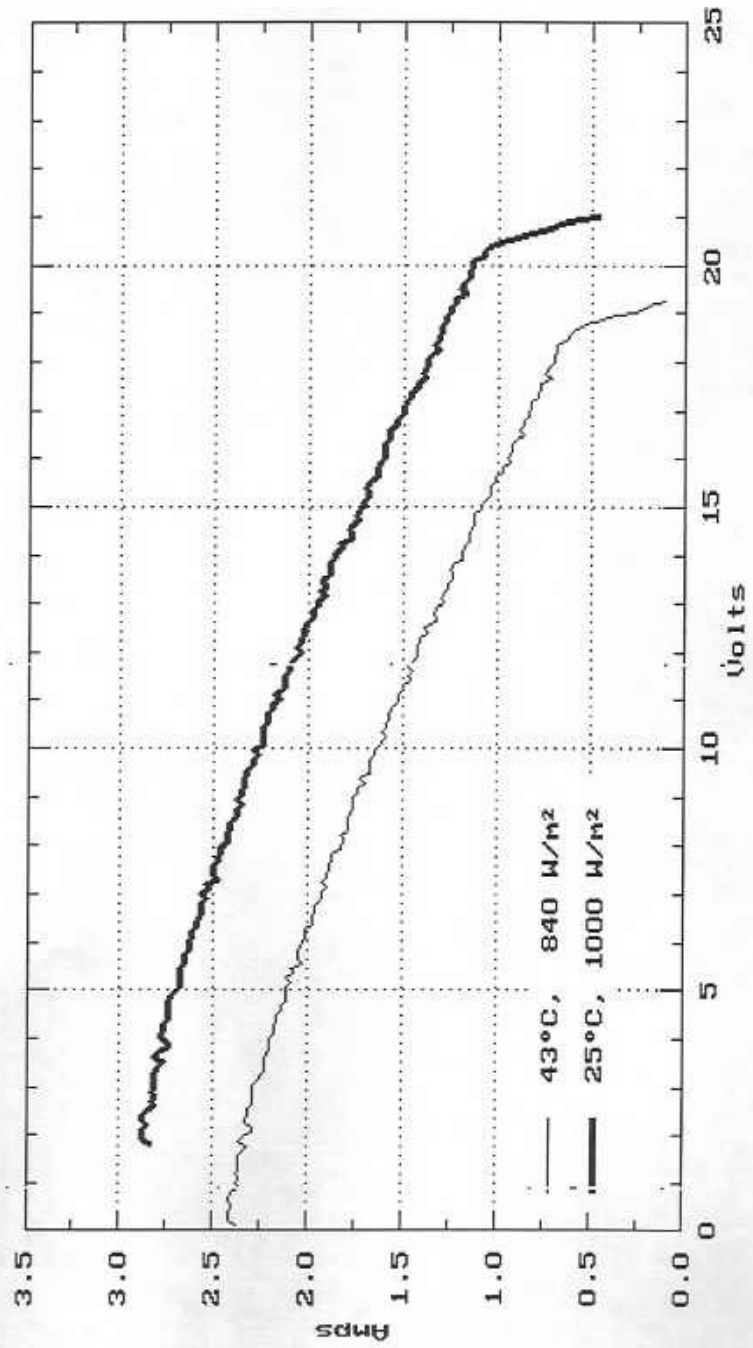


Figure 4.4 Astropower Module with Two Cells 45 to 50 % Shaded

Site: AS4	System: AS4	Name: AS4			
Date: 04-24-95	Module: AS4	Misc: -0.000			
Time: 13:45:39					
Irradiance(W/m2)	830.0	Peak Power(Watts)	25.2	Actual	25°C
Cell temp(°C)	42.0	I at Peak(Amps)	1.5		34.8
Isc(Amps)	1.9	U at Peak(Volts)	16.4		1.9
Voc(Volts)	19.0	Fill Factor(%)	69.6		18.2

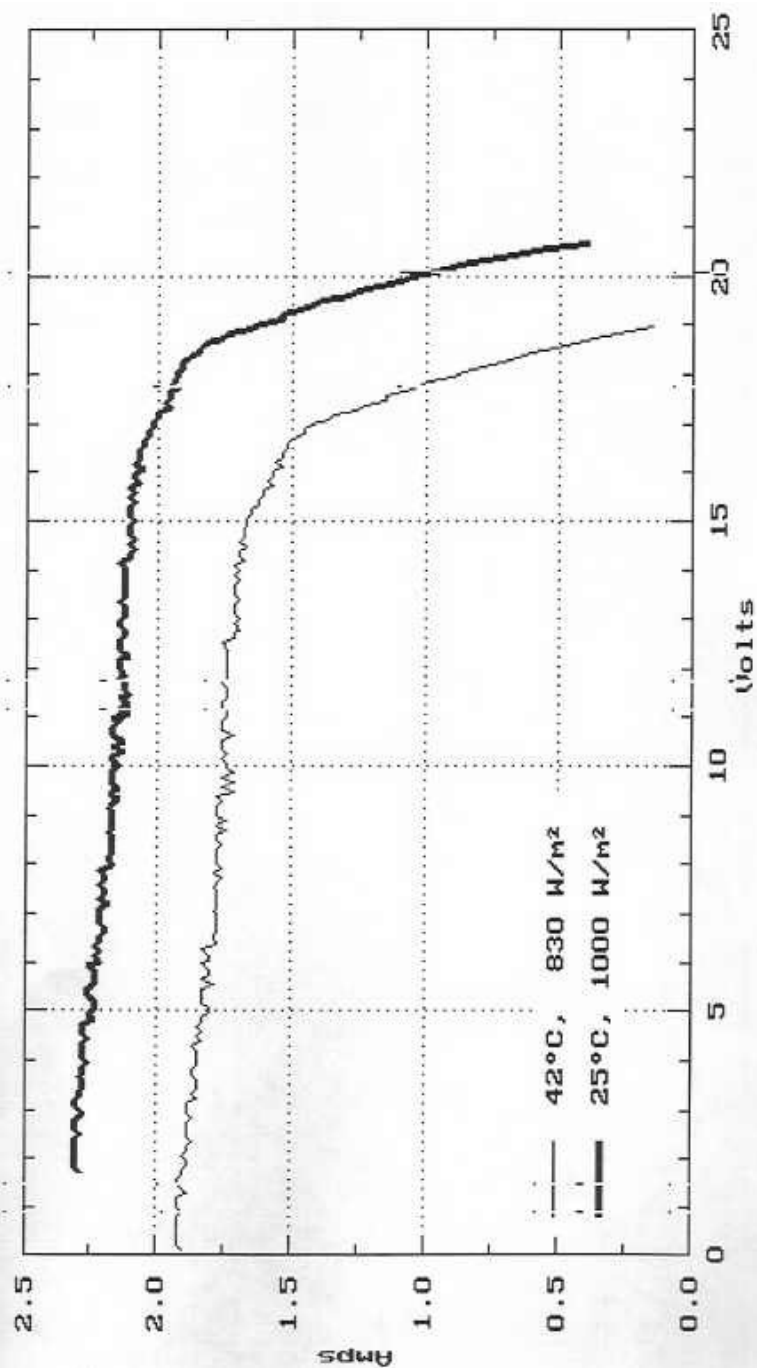


Figure 4.5 Astropower Module with Four Cells 50 to 60 % Shaded

Site: AS6	System: AS6	Name: AS6			
Date: 04-24-95	Module: AS6	Misc: -0.000			
Time: 13:53:56					
Irradiance(W/m2)	820.0	Peak Power(Watts)	20.1	Actual	25°C
Cell temp(°C)	42.0	I at Peak(Amps)	1.2		1.5
Isc(Amps)	1.5	U at Peak(Volts)	15.6		18.2
Voc(Volts)	18.8	Fill Factor(%)	72.0		

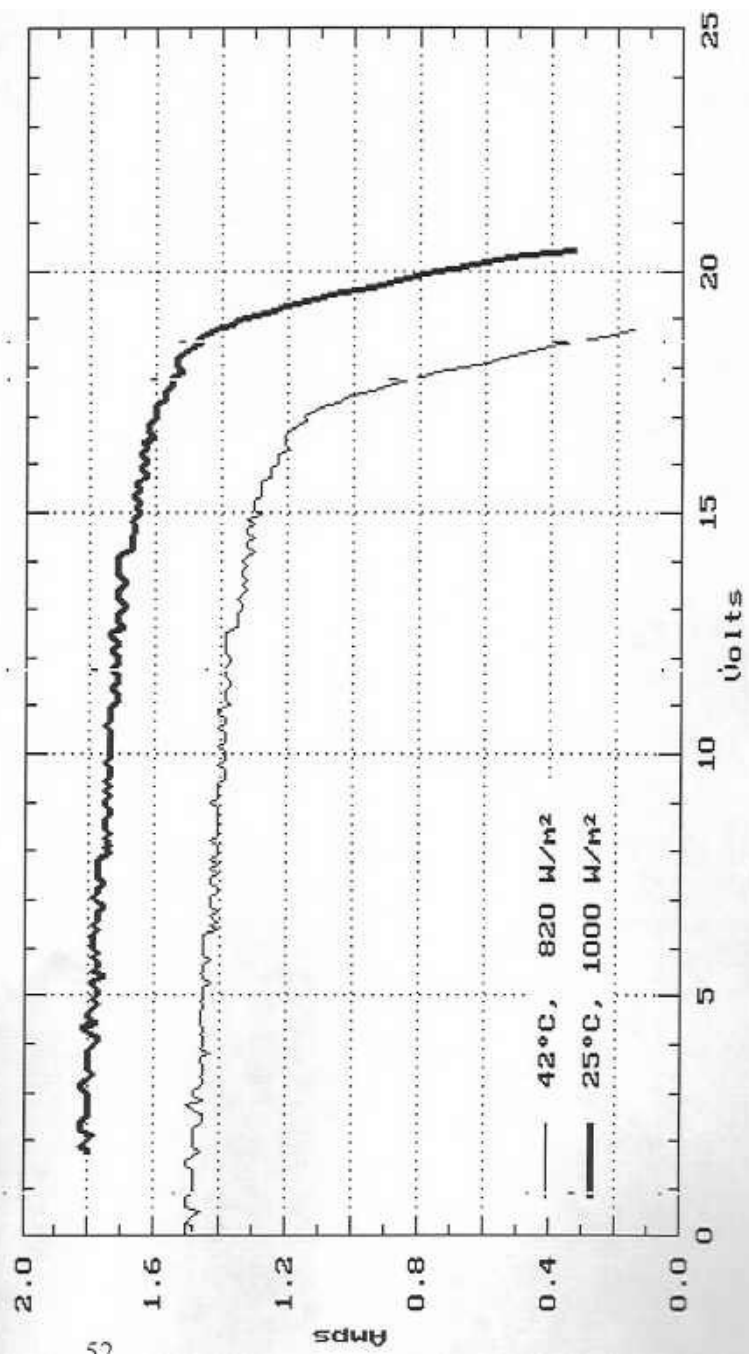


Figure 4.6 Astropower Module with Nine Cells 50 to 60 % Shaded

Site: AS8	System: AS8	Name: AS9
Date: 04-24-95	Module: AS8	Misc: -0.000
Time: 14:06:01		
Irradiance(W/m2)	750.0	Peak Power(Watts)
Cell temp(°C)	40.0	I at Peak(Amps)
Isc(Amps)	1.0	U at Peak(Volts)
Voc(Volts)	18.8	Fill Factor(%)
		Actual
		25°C
		14.5
		0.9
		1.2
		16.8
		18.2
		80.7

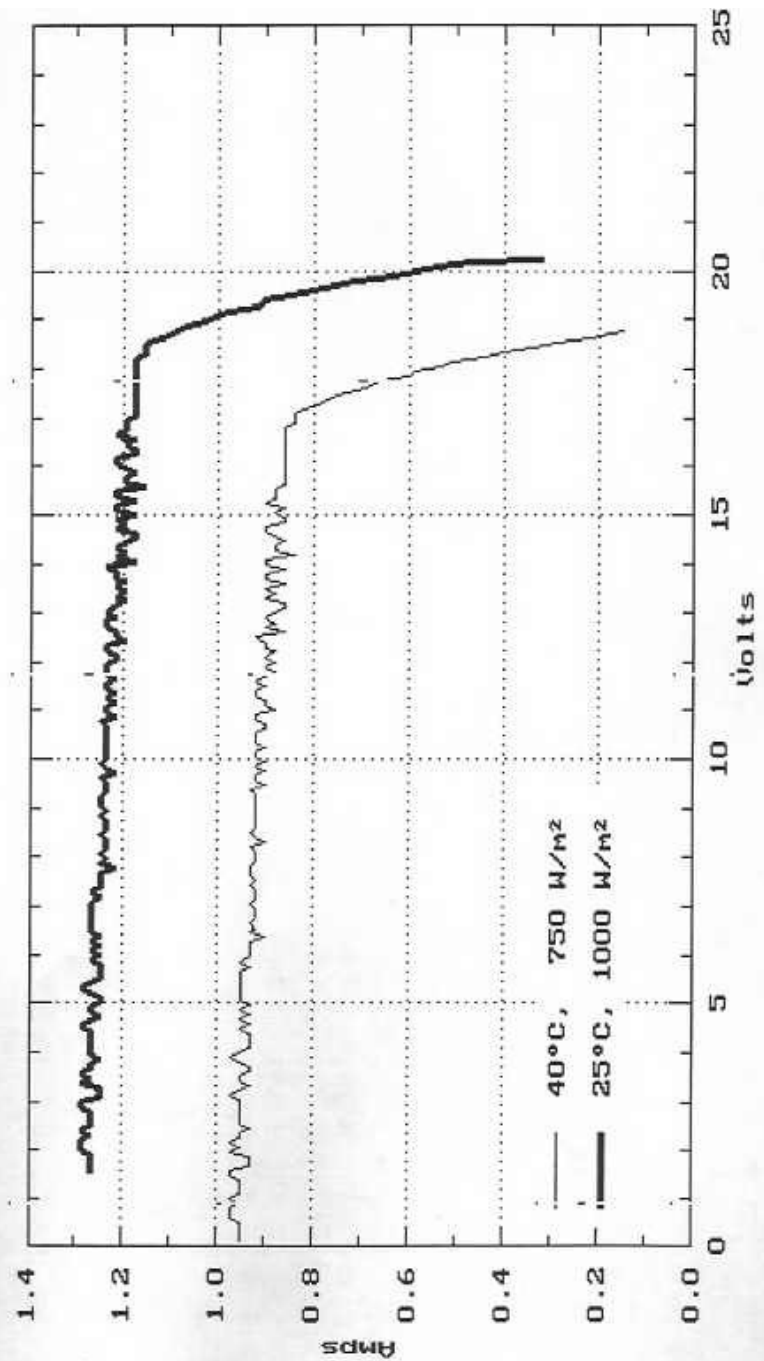


Figure 4.7 Siemens Module with No Shading

Site: M551	System: M551	Name: M551			
Date: 04-24-95	Module: M551	Misc: -0.000			
Time: 12:08:18					
Irradiance(W/m2)	1040.0	Peak Power(Watts)	54.1	Actual	25°C
Cell temp(°C)	45.0	I at Peak(Amps)	3.2	58.5	
Isc(Amps)	3.5	U at Peak(Volts)	17.0	3.1	
Voc(Volts)	21.3	Fill Factor(%)	72.4	18.8	

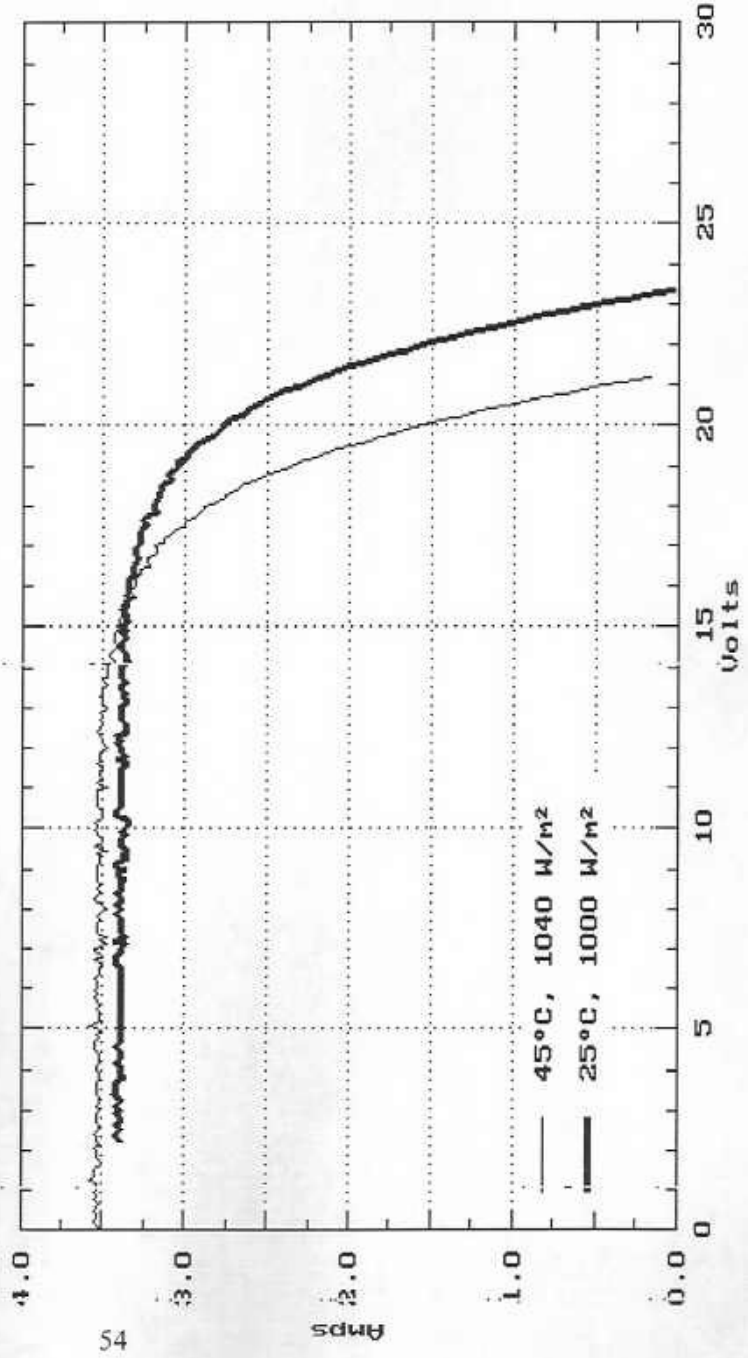


Figure 4.8 Siemens Module with One Cell, Outer Row, 65 to 75 % Shaded

Site: M559	System: M559	Name: M559			
Date: 04-24-95	Module: M559	Misc: -0.000			
Time: 13:06:20					
Irradiance(W/m2)	970.0	Peak Power(Watts)	24.9	Actual	25°C
Cell temp(°C)	44.0	I at Peak(Amps)	2.2		30.6
Isc(Amps)	3.3	U at Peak(Volts)	11.5		2.4
Voc(Volts)	20.4	Fill Factor(%)	37.2		12.6

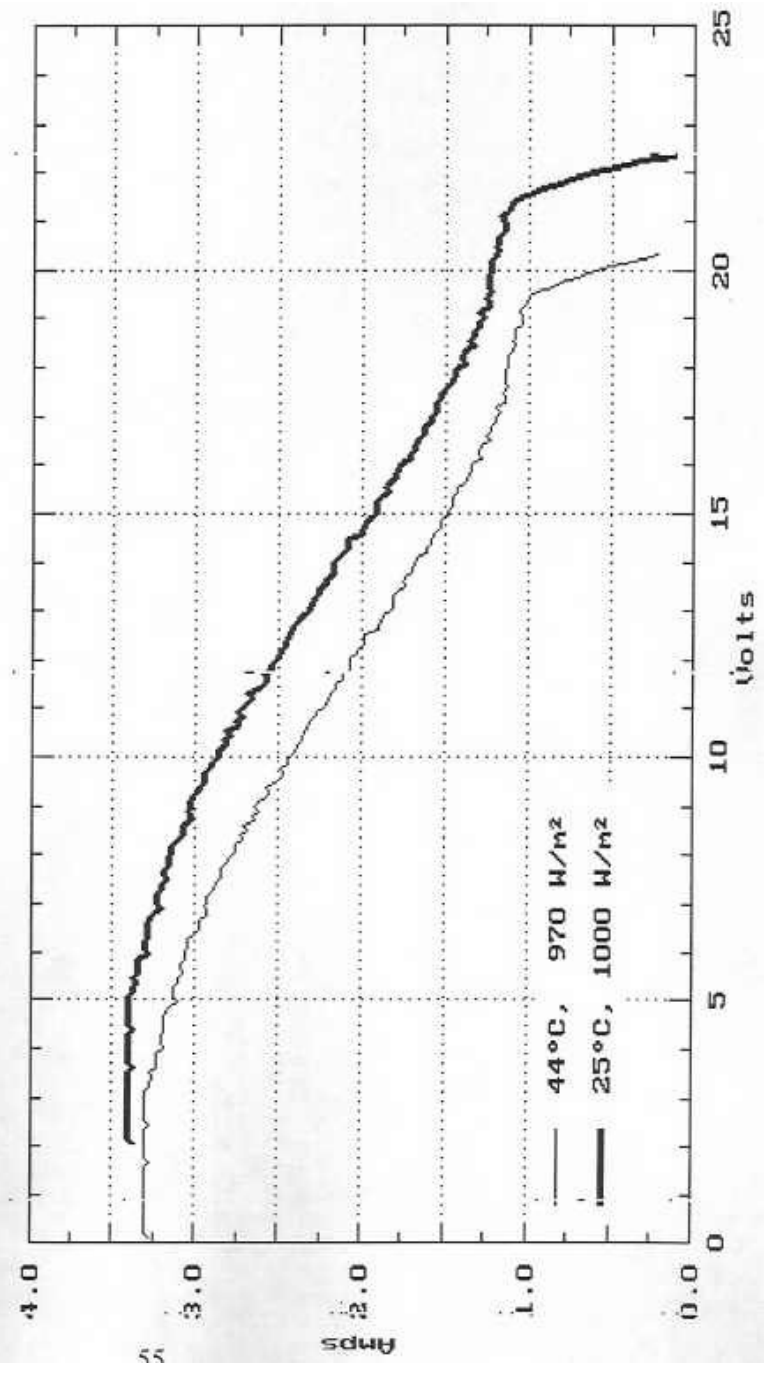


Figure 4.9 Siemens Module with Two Cells, Outer Row, 45 to 50 % Shaded

Site: M553	System: M553	Name: M553			
Date: 04-24-95	Module: M553	Misc: -0.000			
Time: 12:20:17					
Irradiance(W/m2)	1020.0	Peak Power(Watts)	38.3	Actual	25°C
Cell temp(°C)	45.0	I at Peak(Amps)	2.1		41.1
Isc(Amps)	3.5	U at Peak(Volts)	18.7		2.0
Voc(Volts)	21.1	Fill Factor(%)	52.1		20.8

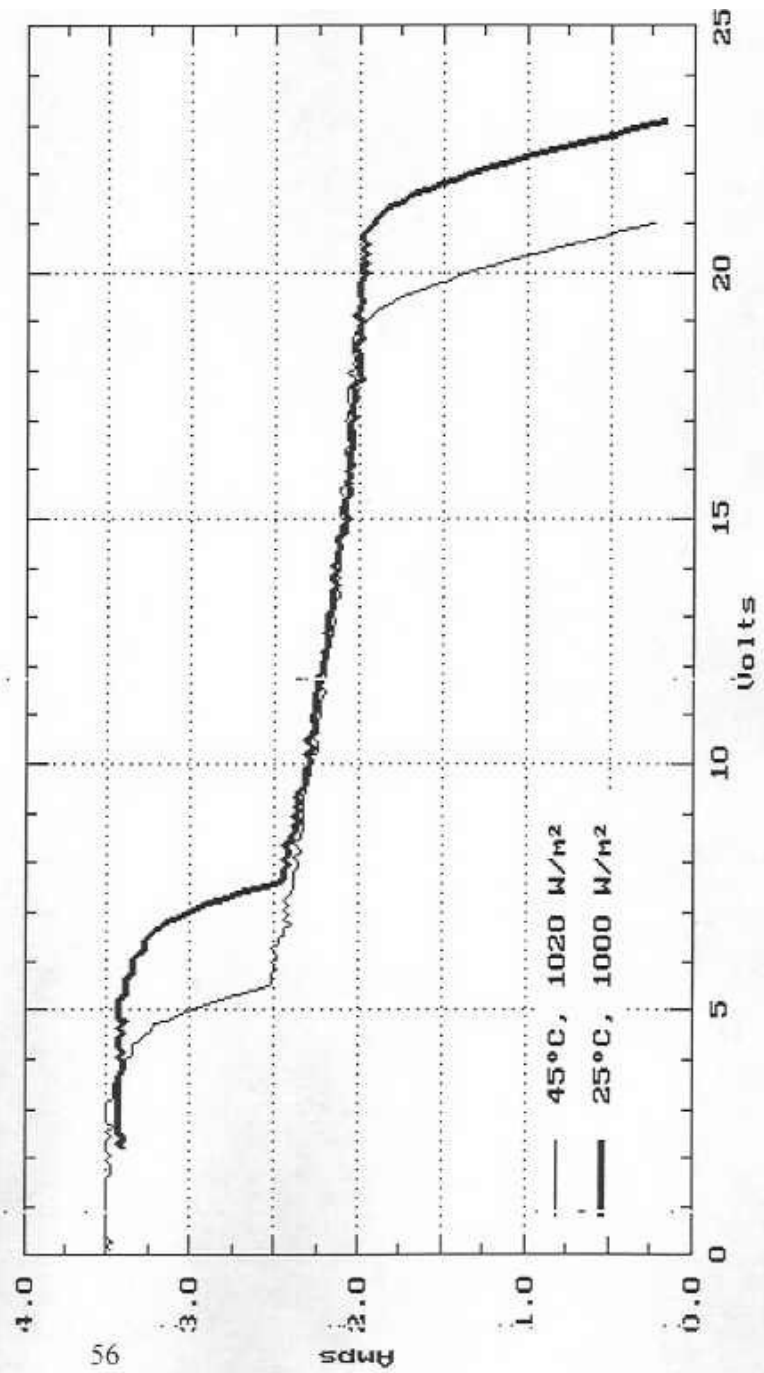


Figure 4.10 Siemens Module with One Cell in Outer Row and One Cell in Inner Row, Each 45 to 50 % Shaded

Site: M5510	System: M5510	Name: M5510			
Date: 04-24-95	Module: M5510	Misc: -0.000			
Time: 13:10:37					
Irradiance(W/m2)	960.0	Peak Power(Watts)	33.3	Actual	25°C
Cell temp(°C)	43.0	I at Peak(Amps)	1.8	39.4	
Isc(Amps)	3.4	V at Peak(Volts)	18.2	2.0	
Voc(Volts)	20.2	Fill Factor(%)	48.5	20.0	

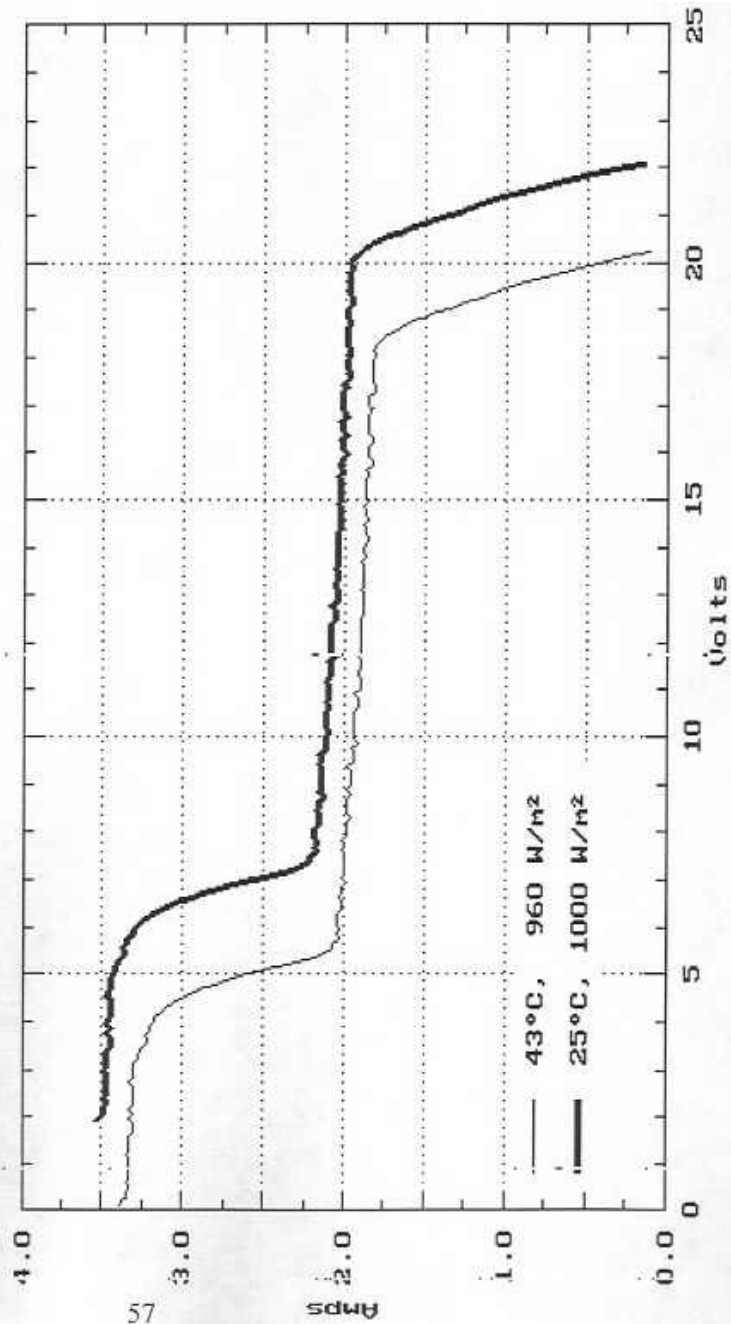


Figure 4.11 Siemens Module with One Cell in Each Row 45 to 50 % Shaded

Site: M555	System: M555	Name: M555			
Date: 04-24-95	Module: M555	Misc: -0.000			
Time: 12:39:56					
Irradiance(W/m2)	1000.0	Peak Power(Watts)	34.0	25°C	37.6
Cell temp(°C)	44.0	I at Peak(Amps)	1.8		1.8
Isc(Amps)	2.3	U at Peak(Volts)	18.8		20.8
Voc(Volts)	21.1	Fill Factor(%)	68.8		

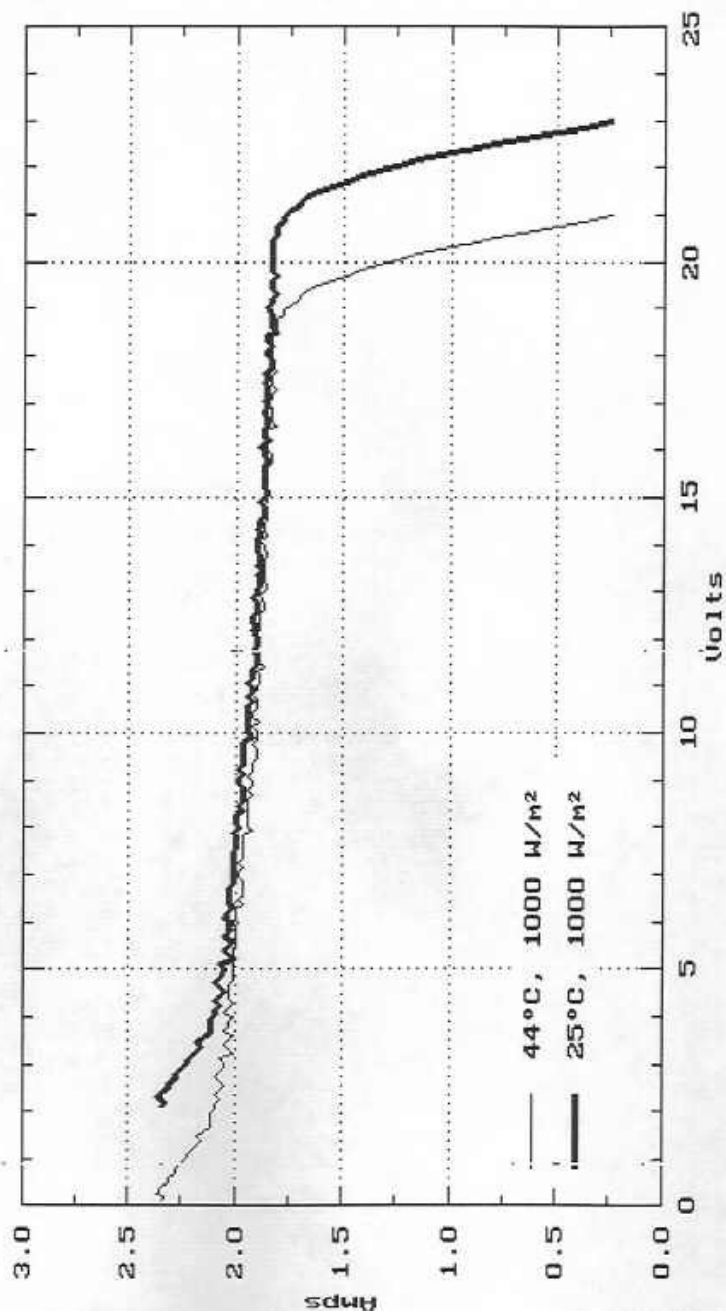


Table 4.2 Effect of Partial Shading on Siemens M55 Panel with Two Overlapping Bypass Diodes

Shading Conditions	% reduction in radiation on panel	% reduction in peak power
Unshaded	0	0
One cell, outer row, 65 to 75 %	2	48
Two cells, outer row, 45 to 50 % each	3	30
One cell, outer row, 45 to 50 % One cell, inner row, 45 to 50 %	3	33
Three cells, one in each row, 45 to 50 % each	4	36

It should be noted that these results support the assertion that the percent reduction in panel output is more closely related to the decrease in the radiation on the most heavily shaded cell than the decrease in the radiation on the entire panel.

4.2.2 Application to Snow and Ice Cover on Panels

It is clear from these results that a relatively small patch of snow or ice cover that shades a portion of the panel will seriously decrease the power output of the panel. The reduction in power will be roughly similar to the findings tabulated above. However, because the thermal situation of a snow-covered panel is quite different from that of the panels in the tests above, the effect may not be exactly the same.

In the tests above, immediately prior to characterization, the panel was either short-circuited or open-circuited. In the case of the former, the shaded cells were permitted to heat themselves to an equilibrium temperature before the IV curve was taken. In the case of the latter, all cells were essentially at the panel open-circuit temperature.

In a snow or ice covered panel, however, current will be conducted in the panel but the snow or ice cover will diminish the heating of the cell that will occur due to shading. Heat that in the above tests raised the temperature of the shaded cells would, in a snow- or ice-covered panel, heat or melt the snow or ice instead. Further, melting snow or ice will ensure that the front surface of the panel does not exceed zero ° C; this will limit the temperature increase of the cell. Since the electrical behaviour of a semiconductor is a function of its temperature, this will alter the IV curve of the panel.

The electrical energy that is dissipated as heat in the shaded cells does fulfill a useful function in the case of the snow or ice covered panel. The heat will be used either to raise the snow temperature or to melt the cover.

4.3 Modelling the Effects of Partial Shading due to Snow or Ice Cover

As stated in Section 4.2.2, the IV characteristics of a panel shaded with a cardboard shield may not match those of a panel shaded by snow or ice. A model of a partially shaded panel would permit a more complete investigation than that presented above. As part of this study, an attempt to create such a model was started. Unfortunately, several factors complicated this approach, and no results are presented here.

Section 4.1.2 indicated that the IV curve of a series arrangement of cells can be determined by simply adding the IV curves of the cells in the series string. These series strings can then be treated as "blocks", completely characterized by their IV curves. Then normal circuit analysis techniques can be used to model the circuit comprised of these blocks, the load, and any bypass diodes which might exist.

Several complications arise. The IV characteristics of the cell in the negative bias region-- that is, when the cell is behaving like a load rather than a generator-- must be known. Different cells behave differently in this region; for some current varies almost linearly with voltage while for other others avalanche multiplication dominates, producing an exponential curve. It is difficult to measure the IV characteristics of the cell in this region, because the cell heats up considerably, and this changes drastically the "resistance" of the cell. Simple electrical models of the panel do not reflect this coupling between the temperature of cell and its ability to conduct.

To successfully model the effects of shading by snow or ice, the following must be done:

- 1) A model of the IV curve of a typical cell in both the forward and negative bias regions must be obtained; this model must account for the temperature of the cell.
- 2) A model of the panel's IV curve must be assembled from the IV curves for the cells and the characteristics of the bypass diodes and the load.
- 3) The electrical model for the panel must be incorporated into a thermal model of the panel. Such a thermal model would take the form of the models presented in Section 6 and Section 7.
- 4) The electrical model and the thermal model must be applied iteratively until a steady-state solution is reached.

The snow/ice removal models of Section 7 are very crude. They do not reflect the fact that snow and ice removal from the face of the panel is not uniform. Therefore, at this point in time it did not make sense to develop such a highly involved model for the effects of partial shading of a PV panel. However, such a model could be used for many purposes other than investigating the behaviour of snow or ice covered panels. Shading of panels due to leaves, bird droppings, dirt, and obstructions are all areas where such a model would be helpful. In addition, the model could be used to assess the performance of modules with various configurations of bypass diodes under various conditions.

CHAPTER 5

SOLAR ENERGY INCIDENT ON THE REAR OF A PANEL

5.1 Introduction

The TN Conseil snow removal technology is essentially a stagnating solar collector mounted on the rear face of the PV panel. Its efficacy, therefore, is to a certain extent dependent upon the solar radiation incident on the back of the panel.

Solar radiation can be modelled in three components: beam radiation, diffuse radiation, and ground-reflected radiation. Beam radiation, also referred to as direct radiation, is the radiation received from the sun which has not been scattered by the atmosphere nor reflected off the ground. Diffuse radiation is the solar radiation which has had its direction changed by the atmosphere, but still comes from the direction of the sky. Ground-reflected radiation is all that radiation which reflects off the ground and then strikes the surface, coming from the direction of the ground²².

In general, beam, diffuse, and ground-reflected radiation will be incident upon the rear face of a photovoltaic array; in this way the rear face is essentially no different from the front face of the array. However, several factors particular to the TN Conseil snow removal technology and the installations where it will be used dictate a treatment quite different from the typical problem of determining the radiation incident on the face of a photovoltaic array:

- 1) Most of the radiation incident on the front face of a PV array will be beam and diffuse radiation; because the array is oriented in the general direction of the sun and the sky, the

²² This rather complicated definition is necessary to differentiate between ground-reflected radiation and that radiation which strikes the ground, is reflected back into the sky, and is then scattered by the atmosphere such that it approaches the surface from the direction of the sky. The latter is designated diffuse radiation, and is accounted for by diffuse radiation models in a "horizon-brightening" term.

ground-reflected component of incident radiation will be low. This is especially true if the array's surroundings consist of vegetation, concrete, asphalt, rock, or other "dark" coloured surfaces, which all have a low albedo, or ratio of reflected to incident radiation²³. In contrast to this, the TN Conseil snow removal technology faces towards the ground and away from the sun. Further, for the periods of time when there is snow on the array, there will almost certainly be snow on the ground, and snow has a very high albedo. Thus, in most configurations, ground-reflected radiation will account for the majority of the radiation incident on the back of the array.

- 2) A significant portion of the area "viewed" by the back face of the array lies below or behind the array. For most array configurations this area will be shaded from both diffuse and beam radiation by the array itself. Thus, when calculating the ground-reflected radiation, it may be necessary to account for the shadow of the array on the ground.
- 3) Arrays in the northern hemisphere facing due south (i.e., surface azimuth angle of zero degrees) will not have beam radiation strike their rear face between the autumnal equinox and the vernal equinox of the following year. Immediately following the vernal equinox and prior to the autumnal equinox the sun's rays will strike the rear face of the array during late afternoon and early morning only. At these times, the angle formed by the normal to the array's rear face and the incident radiation will be large-- in the neighbourhood of 90 °. The component of the incident radiation directed onto the surface will be proportional to the cosine of this angle, and thus will be much diminished for angles approaching 90 °. Likewise, even those installations with a non-zero surface azimuth angle will receive very little energy on their rear face from beam radiation because, for small surface azimuth angles at least, beam radiation will reach the rear face during either early morning or late afternoon only. Thus, beam radiation incident on the rear face of the array can be ignored in a first approximation for most array installations, at least from mid-September until late March.

With beam radiation on the rear of the array assumed to be insignificant, total irradiance of the rear face of the array, G_T (in W/m^2), can be approximated by:

$$G_T = G_d + G_{gr} \quad (5.1)$$

where G_d is the total diffuse irradiance of the rear face (W/m^2),
and G_{gr} is the total irradiance from ground-reflected radiation (W/m^2).

²³This is the simplest definition of albedo. In general, albedo is a function not only of the surface material, as implied here, but also of the incident angle of the radiation and its wavelength. As it is used here, albedo refers to the ratio of reflected radiation to incident sunlight, measured at several angles of incidence and then averaged.

5.2 Diffuse Radiation Incident on the Rear Face of the Array

While the sun is clearly the brightest feature of the daytime sky, the rest of the sky is not dark, and the radiation received from other parts of the sky, designated diffuse radiation in the preceding section, is not insignificant. Even ignoring the sun, the dome of the sky is not uniformly bright, either spatially-- from one point in the sky to the next-- or temporally-- from one time and set of atmospheric conditions to the next. Solar energy research has fostered the development of a number of models, accounting for this anisotropy of the sky, which predict the diffuse radiation on an arbitrarily oriented surface.

Diffuse radiation from the anisotropic sky dome can be treated as the sum of three radiation sources [Duffie et al., 1991, pp. 91-92]. The first of these is the "isotropic" sky dome, or the base level of radiation from any point in the sky. Superimposed upon this are the two other sources. One of these sources is the "circumsolar diffuse radiation", or a bright region around the sun resulting from forward scattering of the sun's rays by the atmosphere. The other source is a band of bright sky around the horizon, called "horizon brightening". The existence of horizon brightening can be explained in two ways. An observer looking at the horizon is gazing through a larger air mass than one looking overhead. This larger air mass scatters more incoming radiation [Iqbal, 1983, p. 311]. In addition, ground reflected radiation, headed skyward, is scattered by the atmosphere and redirected towards the earth, appearing as horizon brightening [Duffie et al., 1991, p. 92]. When the albedo is high, as it will be when there is snowcover, the upwell of radiation is significantly greater, and radiation "ricochets" back and forth between the ground and the atmosphere [Iqbal, 1983, pp. 154-155], possibly strengthening this effect.

The relative importance of each of these three components is strongly related to atmospheric clearness and cloud conditions [Duffie et al., 1991, pp. 91-92]. The clearness of the sky is represented by a dimensionless parameter known as the hourly clearness index, k_t , which is defined as the ratio of global radiation on a horizontal surface to extraterrestrial radiation on a horizontal surface, for the period of an hour. Clearer skies-- or, equivalently, a clearness index tending towards unity-- result in a diminished isotropic component and accentuated circumsolar and horizon brightening components, relative to total diffuse radiation. This appeals to common sense, since a heavily clouded sky appears uniformly dull.

Another parameter related to atmospheric conditions that appears in the diffuse radiation models is the dimensionless diffuse fraction, k_d , which is defined as the ratio of diffuse radiation on the horizontal to global radiation on the horizontal. The diffuse fraction is treated by most models as an empirically derived function of the clearness index.

Three of the more common models that can be used to estimate the diffuse radiation incident on the rear face of the panel are the Temps and Coulson model with modulating function by Klucher, the Hay and Davies model with modifications by Klucher and Reindl (HDKR), and the Perez models. Each of these models account for all three components-- isotropic, circumsolar, and horizon brightening-- of diffuse radiation. Initially this study used the Temps and Coulson

model with Klucher modulating function [Klucher, 1978]. This is the model used in Watsun [Watsun, 1992, pp. 6.1-6.9]. The model is simple to implement and was thought to be sufficiently accurate for our purposes. However, it became clear that the model contained an inaccuracy, and although a modification to the Temps, Coulson and Klucher model would have resolved this problem, it was decided that another model would be used. In a comparison of the Perez and the HDKR model, "for surfaces with γ [surface azimuth angle, which is 180° for a north-facing surface] far from zero degrees in the northern hemisphere...the Perez model is suggested."²⁴[Duffie et al., 1991, p. 102]. Thus, the Perez model was used in this study.

5.2.1 Temps and Coulson Model with Klucher Modulating Function

The Temps, Coulson, and Klucher model multiplies the global radiation on a horizontal surface by a view factor to account for the portion of the sky "seen" by the array, a factor to account for horizon brightening term, and another factor to account for circumsolar radiation [Watsun, p 6.1-9]:

$$G_d = G_{d,h} S \left[1 + F \sin^3 \frac{\beta_R}{2} \left[1 + F \cos^2(\theta_R) \sin^3(\theta_z) \right] \right]$$

where G_d is the diffuse irradiance on the rear of the array (W/m^2),
 $G_{d,h}$ is the diffuse irradiance on a horizontal surface (W/m^2),
 S is the sky view factor, $((1+\cos(\beta))/2)$
 β_R is the slope of the rear face of the array, which will be equal to the slope of the front face of the array, β , plus $\pi/2$ radians (radians),
 F is the Klucher modulating function, equal to $1-k_d^2$,
 θ_R is the angle of incidence of radiation on the rear face (radians),
and θ_z is the zenith angle (radians).

The Temps and Coulson model was intended for clear skies only; the Klucher modulating function, F , decreases the circumsolar and horizon brightening terms when conditions are cloudy. The first factor following the sky view factor is the horizon brightening term. The remaining factor is the circumsolar diffuse term.

It soon became apparent that this model is ill-suited to the study of radiation incident on the back face of an array-- a surface with slope, β , more than 90° and surface azimuth angle, γ , of 180° . The model predicts that the rear face of an array, with the array facing due south, would receive more radiation than the rear face of an identically sloped array facing due north. Given that horizon brightening is modelled as being of uniform intensity in all compass directions, this suggests that the Temps, Coulson and Klucher model sees a circumsolar region around not only

²⁴This suggestion was echoed by Professor Alfred Brunger, Solar Thermal Engineering Centre, University of Waterloo in a personal communication on April 28, 1995.

the sun, but in exactly the opposite direction also. Inspection of the equation shows this to be the case: when the angle of incidence, θ , is obtuse (the rear of the array can not "see" the sun) the circumsolar term should be unity, but in the model it will be greater than unity. This is not an accurate reflection of physical reality.

The Temps, Coulson, and Klucher model could be modified such that the factor that accounts for circumsolar radiation is set to unity whenever the angle of incidence becomes obtuse. However, by the time that this modification became obvious, the Perez model had already been implemented for this study. Since the Perez model is considered a more accurate model in most cases, the Temps, Coulson, and Klucher model was not further investigated.

5.2.2 The Perez Model

The Perez model, similar in form to the Temps, Coulson, and Klucher model, deals with horizon brightening and the circumsolar region in a more sophisticated manner, employing a set of empirically derived factors dependent upon the clearness of the atmosphere, the zenith angle and a brightness factor [Duffie et al., 1991, p. 99-101][Perez et al., 1990]:

$$G_d = G_{d,h} \left(1 - F_1\right) \frac{1 + \cos b_R}{2} + F_1 \frac{a}{b} + F_2 \sin b_R$$

where G_d is the diffuse irradiance on the rear of the array (W/m^2),
 $G_{d,h}$ is the diffuse irradiance on a horizontal surface (W/m^2),
 F_1 is the circumsolar brightness coefficient,
 F_2 is the horizon brightness coefficient,
 β_R is the slope of the rear face of the array (radians), which will be equal to the slope of the front face of the array, β , plus $\pi/2$ radians,
 a is defined equal to $\max[0, \cos \theta_R]$,
and b is defined equal to $\max[\cos(85^\circ), \cos \theta_z]$.

The coefficients are defined as:

$$F_1 = \max \left[0, \left(f_{11} + f_{12} D + q_z f_{13} \right) \right]$$

$$F_2 = f_{21} + f_{22} D + q_z f_{23}$$

where Δ , "brightness", is defined equal to $(m (G_d / G_{on}))$ (dimensionless),
 m , the air mass, is given by²⁵ [Watsun, 1992, pp. 6.1-6.3]

²⁵ The air mass, m , can be approximated by $1/\cos \theta_z$ for θ_z , the zenith angle, from 0 to 70°.

$$m = \frac{1}{\cos q_z + 0.15 \cdot 93.885 - \frac{180}{p} q_z^{-1.253}}$$

G_{on} is the extraterrestrial radiation measured on a plane normal to the radiation, given by $G_{sc}(1 + 0.033\cos(360n / 365))$, with the cosine taken in degrees (W/m^2),
 G_{sc} is the solar constant, defined equal to $1367 W/m^2$,
 n is the day of the year,
and f_{11} , f_{12} , f_{13} , f_{21} , f_{22} , and f_{23} are irradiance brightness coefficients.

The values of the irradiance brightness coefficients are chosen from a table on the basis of the value of a brightness index, ϵ . This table is contained in matrix form in the Mathcad file "frontpan.mcd" located in Appendix B; each row of the matrix corresponds to the irradiance brightness coefficients for a range of the brightness index. The brightness index is given by:

$$\epsilon = \frac{\frac{G_d + G_{b,n}}{G_d} + 1.041 q_z^3}{1 + 1.041 q_z^3}$$

where $G_{b,n}$ is the normal incidence beam irradiance (W/m^2):

$$G_{b,n} = G_h \frac{(1 - k_d)}{\cos q_z}$$

It is encouraging to note that when the angle of incidence on the rear face of the panel, θ_R , is obtuse, $a = \max[0, \cos \theta_R]$ is zero, a/b is zero and the circumsolar contribution to diffuse radiation is zero. Thus the Perez model does not fail in the same way that the Temps, Coulson, and Klucher model failed.

However, for a PV installation at a northern latitude during the winter θ_z will often exceed 70° -- that is, the sun will be very low in the sky.

5.3 Ground-Reflected Radiation Incident on the Rear Face of the Array

As noted above, for many PV installations on which snow is likely to accumulate, the ground-reflected radiation will be the dominant component of radiation incident on the rear face of the array. This ground-reflected radiation results from both beam and diffuse radiation striking the ground and reflecting back up to the array; it is, therefore, subject to the shading of the ground underneath the array by the array itself. In addition, the radiation reflected off the ground will be a function of the albedo of the surface below the array.

The models of ground-reflected radiation presented here require three important simplifying assumptions. First, it is assumed that either the irradiation of the ground is perfectly diffuse (uniform from all directions) or that the ground is a perfectly diffuse reflector (reflects equally independent of direction). Obviously, neither of these conditions will in general be true-- the beam component of incoming radiation certainly does not satisfy the first clause and the fact that snow appears "shiny" from some angles precludes the second. Nevertheless, as discussed in Section 3.1.4.1, this assumption can, and of necessity, will be made. Second, the snow is treated as a grey, or nonselective, surface-- radiation absorption is independent of wavelength. Third, the rear face of the array is assumed to be a diffuse surface, absorbing radiation independently of angle of incidence.

5.3.1 Ground-Reflected Radiation Without Accounting for Shading

An unobstructed surface mounted above a uniformly illuminated horizontal plane extending to infinity in all directions will have a ground-reflected irradiance of [Watson, pp. 6.1-6.10]:

$$H_{gr} = H_h \rho \frac{1 - \cos(\beta)}{2}$$

where H_h is the total (diffuse plus beam) irradiance of a horizontal surface (W/m^2),
 ρ is the dimensionless albedo of the ground,
and β is the slope of the surface (for the rear of an array this will be β_R , an angle greater than 90°).

5.3.2 Ground-Reflected Radiation Accounting for Shading

The array shades the ground under itself, and thus diminishes the radiation that will be reflected off the ground and onto the rear surface of the array. The array shades both beam and diffuse radiation. For beam radiation this results in a well-defined shadow; for diffuse radiation, for which the source is the entire sky, the shadow is region of decreased illumination without clear demarcation.

The model for the radiation incident on the rear of the array, accounting for shading by the array, has three parts:

- 1) The insolation due to diffuse radiation for a point on the ground is calculated.
- 2) The insolation due to beam radiation for a point on the ground is calculated.
- 3) The reflected radiation incident on a point on the rear surface of the array is calculated.

5.3.2.1 Assumptions

Many assumptions have been made in the development of the model. In addition to those stated in Section 5.3, these assumptions are:

- the ground or snow surface underneath the panel forms a horizontal plane extending to the horizon on all sides.
- there are no obstructions on this plane except the panels themselves.
- the array faces due south, with the upper and lower edges of each panel perfectly horizontal.
- the back face of the array reflects no light back onto the ground that is subsequently reflected onto the rear surface of the panel.
- the sun is a point source at infinite distance from the array, such that its rays are parallel.
- the sky is isotropic, with the exception of the point where the sun is located.

5.3.2.2 Diffuse Radiation on a Point on the Ground

The diffuse irradiance of a point on the ground, $G_{g,d}$, in W/m^2 , will be:

$$G_{g,d} = G_{h,d} F_{sky} \quad (5.9)$$

where $G_{h,d}$ is the diffuse irradiance (W/m^2) of an unobstructed horizontal surface,
and F_{sky} is the dimensionless view factor of the sky for the point on the ground.

For a point on the ground which sees only the array and the sky,

$$F_{sky} + F_{array} = 1 \quad (5.10)$$

where F_{array} is the dimensionless view factor of the array.

Thus, the principal task in determining the diffuse irradiance of a point on the ground is the determination of F_{sky} through the calculation of F_{array} .

F_{ij} , the view factor for radiation departing from surface i and intercepting surface j , as shown in Figure 5.1, is given by [Incropera et al., 1990]:

Figure 5.1 View Factor of Surface i onto Surface j

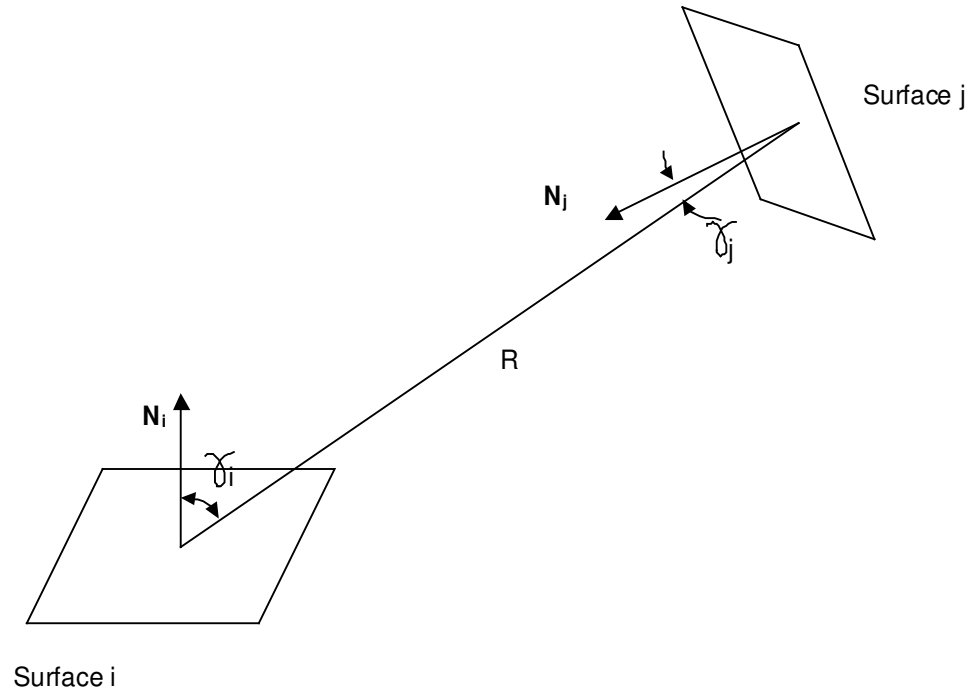
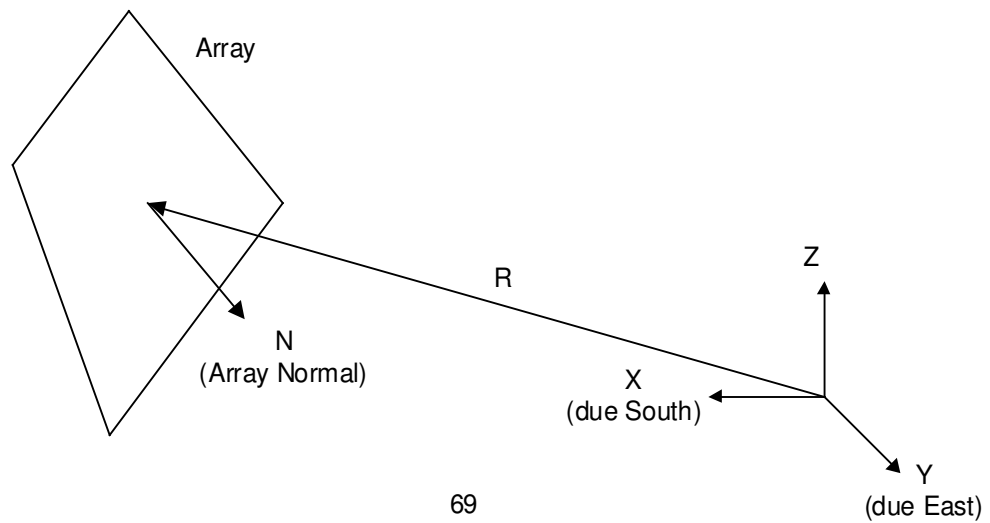


Figure 5.2 Cartesian Coordinate System at a Point on the Ground



$$F_{ij} = \frac{1}{A_i} \iint_{A_j} \frac{\cos(\gamma_i) \cos(\gamma_j)}{R^2} dA_j dA_i \quad (5.11)$$

where A_x is the area of surface x,
 γ_x is the angle formed by a line drawn between points on the two surfaces and the normal to surface x,
and R is the length of the line drawn between the points on the two surfaces.

From this equation it can be reasoned intuitively that, for a point on the ground, the view of the array will be:

$$F_{array} = \int_{A_{ground}} \frac{\cos(\gamma_{ground}) \cos(\gamma_{array})}{R^2} dA_{array} \quad (5.12)$$

If a three-dimensional coordinate system is placed with its origin at the point on the ground, as shown in Figure 5.2, relations to convert from Cartesian to spherical coordinates can be substituted into the above equation. These relations are:

$$\rho = \sqrt{x^2 + y^2 + z^2} \quad (5.13)$$

$$\phi = \cos^{-1}\left(\frac{z}{\rho}\right) \quad 0 \leq \phi \leq \pi \quad (5.14)$$

It can be seen that γ_{ground} is equivalent to ϕ and R is equivalent to ρ . In addition, for a point on the array, z is not an independent variable. Rather, it is related to x by:

$$z = b - \tan(\beta) x \quad (5.15)$$

where b is the value of x where the plane of the array cuts through the ground,
and β is the slope of the array.

The unit normal to the rear face of the array (see Figure 5.2) is the vector \mathbf{N} :

$$\mathbf{N} = \mathbf{i} N_x + \mathbf{j} N_y + \mathbf{k} N_z \quad (5.16)$$

where \mathbf{i} is the unit vector in the x direction,
 \mathbf{j} is the unit vector in the y direction,
 \mathbf{k} is the unit vector in the z direction,
 N_x is equal to $-\sin(\beta)$,

N_y is zero,
and N_z is equal to $-\cos(\beta)$.

γ_{array} is the angle between the unit normal to the rear face of the panel and the negative of the vector, \mathbf{R} , from the origin of the coordinate system on the ground to the point (x, y, z) on the rear face of the array. Thus,

$$\cos(\gamma_{array}) = \frac{\mathbf{N} \cdot (-\mathbf{R})}{|\mathbf{N}| |\mathbf{R}|} \quad (5.17)$$

$|\mathbf{N}|$ is equal to 1 and $|\mathbf{R}|$ is equal to ρ . Therefore,

$$\begin{aligned} \cos(\gamma_{array}) &= \frac{-\mathbf{N} \cdot \mathbf{R}}{\rho} \\ &= \frac{-N_x R_x - N_y R_y - N_z R_z}{\rho} \\ &= \frac{x \sin(\beta) + z \cos(\beta)}{\rho} \end{aligned} \quad (5.18)$$

With this we can simplify the equation for F_{array} :

$$\begin{aligned} F_{array} &= \int_{A_{array}} \frac{\cos(\gamma_{ground}) \cos(\gamma_{array})}{\rho^2} dA_{array} \\ &= \int_{A_{array}} \left(\frac{z}{\rho} \right) \left(\frac{x \sin(\beta) + z \cos(\beta)}{\rho} \right) dA_{array} \\ &= \int_{A_{array}} \frac{z(x \sin(\beta) + z \cos(\beta))}{\rho^2} dA_{array} \end{aligned} \quad (5.19)$$

This integral is over the area of the array; it should be noted that since the array is an inclined plane, an element of area is not simply $dx dy$, but rather:

$$dA_{array} = \left(\frac{dx}{\cos(\beta)} \right) dy \quad (5.20)$$

In addition, it should be noted that using the equation above, F_{array} will be negative when the z-intercept of the point on the ground is negative, i.e., when the point on the ground is in front of the array and beyond the line of intersection of the ground and the plane of the array. This results from the cosine of an obtuse angle being negative; the angle between $-\mathbf{R}$ and \mathbf{N} is obtuse for such points on the ground. The view factor should always be positive, however, so the absolute value is taken. With the expression $(b - x \tan(\beta))$ substituted for z , the equation for F_{array} becomes:

$$F_{array} = \frac{1}{\pi \cos(\beta)} \iint_{\text{surface}} \frac{[b - x \tan(\beta)] [x \sin(\beta) + (b - x \tan(\beta)) \cos(\beta)]}{\rho^4} dy dx$$

where $\rho = \sqrt{x^2 + y^2 + (b - x \tan(\beta))^2}$ (5.21)

This integral can be evaluated numerically for a particular array configuration and point on the ground.

5.3.2.3 Beam Radiation on a Point on the Ground

The beam irradiance of a point on the ground, $G_{g,b}$, in W/m^2 , will be:

$$G_{g,b} = G_{h,b} \Gamma \quad (5.22)$$

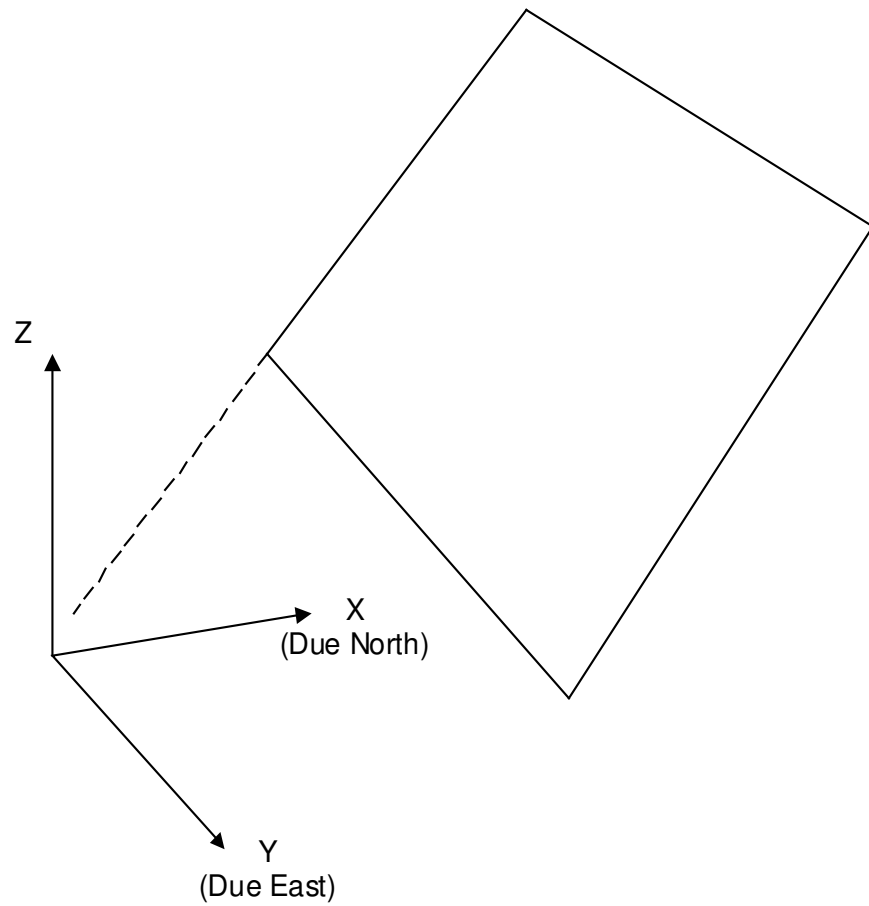
where $G_{h,b}$ is the intensity of beam radiation on a horizontal surface, in W/m^2 ,
and Γ is an indicator function that equals zero if the point on the ground is in the shadow of the array and one otherwise.

Let the array be defined in relation to a Cartesian coordinate system with its origin located at the point on the ground, in the plane of the array, nearest the array's bottom left hand corner, as shown in Figure 5.3. For this coordinate system, the x and y axes will be in the plane of the surface of the ground and be parallel to the projection of the edges of the array onto the ground. It has been assumed that the array faces due south; the positive x axis points due north, the positive y axis points due east, and the positive z axis points towards the sky.

The shadow of the array will form a parallelogram on the ground. The sun, a corner of the array, and the corresponding corner of the array shadow will all lie on a line. The position of the sun in the sky will be defined by a zenith angle, θ_z , and a solar azimuth angle, γ_s ; equations for these variables as functions of time, date, latitude, and longitude can be found in [Duffie et al., 1991, pp. 13-16], or the Mathcad file "diffuncm.mcd" in Appendix C.

To find x_s and y_s , the coordinates of a corner of the shadow, the following system of equations must be solved:

Figure 5.3 Definition of Cartesian Coordinate System for Beam Radiation Shadow Model



$$x_s = x_a - \rho \sin(\theta_z) \cos(\gamma_s) \quad (5.23)$$

$$y_s = y_a + \rho \sin(\theta_z) \sin(\gamma_s) \quad (5.24)$$

where x_a is the x coordinate of the corner of the array corresponding to the corner of the shadow,

y_a is the y coordinate of the corner of the array corresponding to the corner of the shadow,

z_a is the z coordinate of the corner of the array corresponding to the corner of the shadow,

and ρ is equal to:

$$\rho = \sqrt{(x_s - x_a)^2 + (y_s - y_a)^2 + z_a^2}$$

When the coordinates of the four corners of the shadow have been located in this way, the indicator function can be determined as a function of position on the ground,

$$\Gamma = \Gamma(x, y, 0) \quad (5.25)$$

In order to do this, recognize that because the top and bottom edges of the array are parallel to the plane of the ground, the shadow of these edges will be parallel to the y - axis, and defined by $x = x_{s, \text{ top edge}}$ and $x = x_{s, \text{ bottom edge}}$, respectively. In contrast, for inclined arrays, the shadows of the east and west edges of the array will not be parallel to the x - axis. $\Gamma(x, y, 0)$ will be zero except at those locations where $x_{s, \text{ top edge}} \leq x \leq x_{s, \text{ bottom edge}}$ and (x,y) lies in between the lines formed by the shadows of the east and west edges of the array. The latter criterion can be evaluated in the following manner:

Let

$$\Delta x = x_{s, \text{ top edge}} - x_{s, \text{ bottom edge}}$$

$$\Delta y = y_{s, \text{ top west corner}} - y_{s, \text{ bottom west corner}} = y_{s, \text{ top east corner}} - y_{s, \text{ bottom east corner}}$$

Then (x,y) lies in between the lines formed by the shadows of the east and west edges of the array if

$$y_{s, \text{ bottom west corner}} + \Delta y \frac{x - x_{s, \text{ bottom}}}{\Delta x} \leq y \leq y_{s, \text{ bottom east corner}} + \Delta y \frac{x - x_{s, \text{ bottom}}}{\Delta x} \quad (5.26)$$

5.3.2.4 Radiation on the Rear Surface of the Array

Section 5.3.2.2 and 5.3.2.3 detailed the method for calculating the diffuse and beam radiation incident on a point on the ground. From this, the ground-reflected radiation incident on a point on the rear face of the array must be determined. This problem is very similar to the one of

finding the view factor of the array for a point on the ground. Here, however, we are essentially finding the view factor of the ground for a point on the array. This is done by considering each element of the ground, $dx dy$, separately; we find the view factor for this element and multiply by the radiation reflected by the element.

For this section, the Cartesian coordinate system introduced in Section 5.3.2.3 will be adopted.

A point on the ground $(x, y, 0)$ will reflect radiation with an intensity, $G_r(x, y)$ given by:

$$G_r(x, y) = G_{g, d}(x, y) \rho_d + G_{g, b}(x, y) \rho_b \quad (5.27)$$

where ρ_d is the albedo for diffuse radiation,
and ρ_b is the albedo for beam radiation.

The irradiance, G_p , of a point (x_p, y_p, z_p) on the rear face (in W/m^2) will be:

$$G_p(x_p, y_p, z_p) = \iint_{y \geq 0} \frac{z_p \left[(x - x_p) \sin \theta_p^2 + z_p \cos \theta_p^2 \right] G_r(x, y)}{\left[(x - x_p)^2 + (y - y_p)^2 + z_p^2 \right]^{3/2}} dx dy \quad (5.28)$$

Note that for the integral of x the lower limit will be zero, since the light reflected from the snow in front of (i.e., south of) the line of intersection of the plane of the array and the ground can not reach the rear face of the panel.

5.3.2.5 Implementation

The above procedure for computing the radiation incident on the rear face of the array is implemented in the Mathcad file "diffuncm.mcd" found in Appendix C. The procedure detailed above has been altered slightly in several places to reduce the computational burden. For example, the diffuse radiation incident on the ground is calculated and stored in a matrix rather than being recalculated each time it is required.

5.4 Comparison of Model and Experimental Results

Due to an incompatibility between the pyranometers and the data acquisition system, the data from the pyranometer mounted on the rear face of the array at the Energy Diversification Research Laboratory could not be used to assess the validity of the models developed above. However, on March 10, 1995, some readings were taken manually with a Licor LI 200SA pyranometer. On this day there was a thin cover of snow on the ground and an almost cloudless sky.

At 13:40 the global radiation on the horizontal, measured with the Licor, was $730 W/m^2$. At this

point in time the global radiation on a horizontal surface at the same longitude and latitude but outside the earth's atmosphere would be 822 W/m^2 . Thus, the ratio of terrestrial to extraterrestrial radiation on the horizontal was 0.89. If it is assumed that this ratio held constant for the readings, which were at 14:10, 14:35, and 14:50, the terrestrial global radiation on the horizontal can be estimated from the extraterrestrial radiation on the horizontal at these times. In this way, the values in the Table 5.1 were computed.

Table 5.1 Global Radiation on the Horizontal for March 10, 1995

Time	Global Radiation on Horizontal, Extraterrestrial (W/m^2)	Global Radiation on Horizontal, Terrestrial (W/m^2)
13:40	822	730
14:10	760	675*
14:35	693	615*
14:50	654	581*

* estimate

There are two PV arrays at the EDRL; one is on an upper roof and the other is on a lower roof. They both face due south, have a tilt angle of 45° , and have the same dimensions: they are composed of 42 columns of 6 panels, with each panel about one metre in the horizontal direction and 0.5 metres in the vertical direction. The bottom edge of the array is 1.7 m off the ground. The roofs are both horizontal.

Readings of the radiation on a north facing surface with a slope angle of 45° were taken at five different locations with the Licor pyranometer. For all these readings the pyranometer was facing south at a height of 2.62 m from the ground. At 14:10, readings were taken at the top array. One was taken very close to the rear of the array, approximately 0.5 metres, measured horizontally, from the panels. The other was taken at a point about 6 metres, measured horizontally, north of the panels. These readings were taken at a distance about 9 metres from the west end of the array. At 14:35, readings were taken at the lower array; these readings were taken at approximately the same locations, with respect to the array, as above. At 14:50 a reading was taken in an open, snowcovered field, free of shadows.

The upper and lower roofs have a number of obstructions other than the array. Both have HVAC vents and fume hood exhausts at various locations north of the array. The upper roof has a wall, about 1.5 m high, that runs around the edge of the roof. This wall is about 15 m north of the bottom edge of the array. A similar wall runs around the lower roof, but the wall that is 15 m north of the lower array runs up to the upper roof, and is thus about 5.5 m high. All these walls are dark brown.

The diffuse radiation incident on North facing surfaces at 45° to the horizontal was estimated using the Perez model. The diffuse radiation incident on the pyranometer was very low; it was approximately 21, 19, and 18 W/m^2 at 14:10, 14:35, and 14:50, respectively.

The snow cover was patchy on the upper roof, and gravel showed through the snowcover. In the field and on the lower roof the snowcover was about 7 to 10 cm thick and relatively uniform. The snowcover was several days old, and quite dry. The albedo of the snow in the open field was estimated on the basis of the equation for ground-reflected radiation, not accounting for shading (Eq. 5.8). According to this equation, the albedo was 0.7, which is reasonable for thin snowcover several days old. The albedo of the snowcover on the lower roof was assumed to be the same. The albedo of the snowcover on the upper roof was assumed to be 0.5.

The measured values of irradiation and the values predicted by both the model accounting for shading and the conventional model (Eq. 5.8) are given in Table 5.2. In addition, the error of the models, compared with the measured values, is given. The readings for the lower array are each entered twice in the table; for the second entry the integration limits for the model accounting for shading have been set to account for the back wall.

The measured values show that at this time of year, for an array of this size, the effect of the array's shadow on the irradiation of the rear of the array is very significant. The readings taken under the arrays were approximately half those taken at locations more distant from the array. These more distant locations were near the edge of the array's shadow for beam radiation.

Since the albedo was estimated on the basis of the reading in the unobstructed field, the error for conventional model was zero. Since there is no shadow in this field, one would expect that the model accounting for shading would predict the same value as the conventional model. However, this is only true when the integration limits over the ground are set to infinity. This calculation takes prohibitively long, and the calculation limits were instead set to boundaries 150 m behind the array and 50 m from either end of the array. This results in the two percent error observed in the prediction of the model accounting for shading.

While both models are very inaccurate for these readings, the model that accounts for shading is much less inaccurate. The average error for the conventional model (Eq. 5.8) for the four readings on the upper and lower roofs was about 90 %. For the model accounting for shading, the average error was about 25 to 30 %, depending on whether or not the integration limits were set to account for the back wall on the lower roof. Both models tended to overestimate the ground-reflected radiation, especially in the shadow of the array.

5.5 Application of Model Accounting for Shading to Various Installations

The model of ground-reflected radiation, accounting for the shadow cast by the array, was used to predict the irradiation of the rear face of various array installations. A typical array configuration was chosen, and then the time of day, day of the year, array size, height, latitude,

Table 5.2 Validation of Ground-Reflected Radiation Model based on Measurements at Varennes											
						Ground Reflected		Total Radiation		Model Error	
	Rad on		Total Rad	Diffuse on		Without	With	Without	With	Without	With
Time	Horiz	Location	Measured	Back	Albedo	Shadow	Shadow	Shadow	Shadow	Shadow	Shadow
	W/m ²		W/m ²	W/m ²		W/m ²	W/m ²	W/m ²	W/m ²	%	%
14:10	675	Under Top Array	135	21	0.5	288	165	309	186	129%	38%
14:10	675	Distant from Top Array	245	21	0.5	288	239	309	260	26%	6%
14:35	615	Under Bottom Array	145	19	0.7	367	216	386	235	167%	62%
14:35	615	Distant from Bottom Array	290	19	0.7	367	305	386	324	33%	12%
14:35	615	Under Bot Arr: w/ Back Wall	145	19	0.7	367	185	386	204	167%	41%
14:35	615	Dist f. Bot Arr: w/ Back Wall	290	19	0.7	367	242	386	261	33%	-10%
14:50	580	Unobstructed	365	18	0.7	347	341	365	359	0%	-2%

tilt angle, and diffuse fraction were varied. While the analysis was not comprehensive, the results give an indication of the effect of each variable.

The "typical" array was assumed to be a one kW array located at 50 ° N. The panel tilt angle was 65 °. The array was four metres from east to west and two metres along its diagonal edge. The bottom edge of the array was 1.5 m off the snow surface. The typical day was February 5; the typical time was 13:30. The diffuse fraction (ratio of diffuse to beam radiation) was assumed to be 0.3. The ground albedo was assumed to be 0.8.

For each different time, day, or latitude, the global radiation on the horizontal was estimated on the basis of the global radiation on a surface, parallel to the ground, at the same latitude but outside the earth's atmosphere. The terrestrial radiation on the horizontal was assumed to be 85 % of the value of the radiation on the horizontal outside of the earth's atmosphere; this is probably high.

The beam radiation on the front of the array and the diffuse radiation on the front and the back of the array were calculated for each run of the model. The diffuse radiation incident on the rear face of the array was only 5 to 15 % of the intensity of the ground reflected radiation. The ground reflected radiation incident on the rear of the array was calculated with both the model accounting for the array shadow and with the conventional model (Eq. 5.8). Since the irradiation of the rear face is not uniform, an average value and the standard deviation were computed for the output of the model accounting for shading. The total average irradiation of the rear face of the array was found from the sum of the average ground-reflected irradiation according to the model accounting for shading and the diffuse irradiation of the back; this was also expressed as a percentage of the total irradiation of the front panel.

The results are summarized in Table 5.3. The radiation incident on the rear of the array ranged from 8 % to 34 % of the front face value. For the typical case the back panel radiation was 24 % of the front panel radiation. There were a number of reasons for this variation.

The array tilt angle determines the rear face's view factor of the ground and the sky; a lower array tilt angle results in a larger view factor of the ground and therefore a higher ratio of back-to-front radiation.

When the solar azimuth angle is small and the zenith angle large, the radiation flux on the horizontal is small compared with the radiation flux on a vertical or inclined surface of the same size. When the radiation on the ground is comparatively low, the ground-reflected radiation is also low, and this is reflected in low ratios of back-to-front insolation. This is precisely the situation around midday during the winter months in the northern latitudes. At 13:30, the typical array at a latitude of 50 ° N and a slope of 65 ° had a back-to-front radiation ratio of 18 % on December 20 and 24 % on February 5. In early fall or early spring the ratio will be much larger, e.g., 33 % on March 20. At lower latitudes the ratio will also be much larger (32 % at 45 ° N and 45 ° tilt angle).

Table 5.3 Modelled Irradiance of Rear Face of Various Array Installations																	
Diffuse fraction 0.3 except where stated; ground reflectivity of 0.8; height of 1.5 m																	
clearness	0.85												Array Back Surface Radiation				
							Radiation		Array Front Surface Radiation				Conv mod		Model Accounting for Array Shadow		
Situation	lat/slope	latitude	n, day of	hours	Declin-	Hour ang	Extraterr	Terrestrial	Beam	Diffuse	Grnd-ref	Total	G-r	Ave G-r	G-r SD	Diffuse	Total
	degrees	radians	year	past noon	ation (rad)	(rad)	W/m^2	W/m^2	W/m^2	W/m^2	W/m^2	W/m^2	W/m^2	W/m^2	W/m^2	W/m^2	W/m^2
Typical	50/65	0.872665	36	1.5	-0.286274	0.392699	496.0394	421.6335	776	166	97	1039	240	220	9.5	28	248
20-Dec	50/65	0.872665	354	1.5	-0.409246	0.392699	338.7073	287.9012	774	135	66	975	164	152	1.5	20	172
20-Mar	50/65	0.872665	79	1.5	-0.014088	0.392699	802.4765	682.105	734	217	158	1109	388	326	12.5	40	366
12:00	50/65	0.872665	36	0	-0.286274	0	561.9273	477.6382	835	187	110	1132	272	238	5.1	31	269
15:00	50/65	0.872665	36	3	-0.286274	0.785398	308.4065	262.1455	608	110	61	779	149	141	1.1	18	159
H = 0.2	50/65	0.872665	36	1.5	-0.286274	0.392699	496.0394	421.6335	776	166	97	1039	240	142	19.4	28	170
H = 5	50/65	0.872665	36	1.5	-0.286274	0.392699	496.0394	421.6335	776	166	97	1039	240	224	1.4	28	252
Kd = 0.2	50/65	0.872665	36	1.5	-0.286274	0.392699	496.0394	421.6335	887	116	97	1100	240	216	5.3	23	239
Kd = 0.8	50/65	0.872665	36	1.5	-0.286274	0.392699	496.0394	421.6335	222	459	97	778	240	219	1.6	47	266
45/45	45/45	0.785398	36	1.5	-0.286274	0.392699	599.4202	509.5072	740	195	60	995	348	306	9.5	17	323
65/85	65/85	1.134464	36	1.5	-0.286274	0.392699	166.5306	141.551	776	82	52	910	62	58	0.4	16	74
100 W	50/65	0.872665	36	1.5	-0.286274	0.392699	496.0394	421.6335	776	166	97	1039	240	232	0.9	28	260
10 kW	50/65	0.872665	36	1.5	-0.286274	0.392699	496.0394	421.6335	776	166	97	1039	240	174	15.3	28	202

Arrays close to the surface of the snow allow less radiation to pass under them and strike the snow beneath them-- i.e., they cast a shadow directly underneath themselves. As a result, they receive less ground-reflected radiation on their rear face. For the typical array, the back-to-front radiation ratio was 16 % when the height of the bottom edge of the array was 0.2 m above the snow surface, and 24 % for heights of 1.5 m or more. A larger array must be higher off the snow surface to achieve the same back-to-front radiation ratio. At 1.5 m, a 1.2 m (east-west) by 1 m (diagonally) array has a back-to-front ratio of 25 %, a 4 m by 2 m array has a back-to-front ratio of 24 %, and a 42 m by 3 m array has a back-to-front ratio of 19 %.

Under cloudy skies the sky behind the array will be bright in comparison with the ground and the stark shadow for beam radiation will not be important. Thus, when there is a high diffuse fraction, the ratio of back-to-front radiation is high (34 % for the typical array with an 80 % diffuse fraction).

The shadow of the array was significant only when the shadow was large and close to the array. Thus, the shadow was important when the array was large compared with its height above the ground, when the zenith angle was large and the solar azimuth angle was small, and when the array tilt angle was not near the vertical. For most small to medium-sized arrays, it appears that the shadow cast by the array is relatively unimportant during winter months in northern latitudes. For larger arrays, and especially during the autumn and spring, the shadow will be important.

The standard deviation of the irradiation over the rear face of the array was generally quite small (less than 4 % of the average value). The standard deviation was slightly larger when the array was large and close to the ground.

CHAPTER 6

THERMAL PERFORMANCE OF A PV PANEL WITH THE TN CONSEIL SNOW REMOVAL TECHNOLOGY

The thermal performance of the TN Conseil snow removal technology was studied in two ways. First, two unmodified panels and two TN Conseil modified panels were installed in the roof-top array of the Energy Diversification Research Laboratory and their temperatures and short-circuit currents were monitored. Second, simple thermal models of the panels were developed. These models allowed the performance of several variations of the TN Conseil Technology to be compared, and provided a tool for investigating the performance of the TN Conseil Technology for conditions other than those observed at the EDRL.

This chapter treats only the thermal performance of the panels in the absence of snow; the snow melting and removal capabilities of the panels are investigated in the Chapter 7. There are several reasons for this. Most importantly, the thermal performance of the panels without snow should be a good indicator of the panel performance with snow, and thus provides a good basis for comparison. In addition, snow and ice are complex phenomenon that complicate the investigation of the thermal performance of the panels, and introduce significant error. Further, the monitored data collected at the EDRL did not include the thickness of snow cover on the panels, the snow density, the extinction coefficient, or the melt rate. Therefore, while the models of thermal performance presented here can be validated against monitored data, the same can not be done for the snow melting models presented in the next chapter.

6.1 Monitored Performance

6.1.1 Panel Configuration and Monitoring

Four panels were monitored. All the panels were Astropower Canada Ltd. APC4716 modules with a short circuit current of around three amps, an open circuit voltage of about 21 V, and a maximum power point output of about 45 Watts. The modules measure approximately 95 cm by

45 cm, including their frame. All of the panels were essentially short-circuited, with a very small shunt resistance-- nominally $0.1\ \Omega$ -- introduced between the terminals to facilitate the measurement of the short-circuit current. Two of the panels, referred to as the "Control" panels, were unmodified. The two remaining panels were outfitted with the TN Conseil snow removal system. One of these ("TN 1") had a copper foil as the selective surface on the rear of the panel and the other ("TN 2") had a nickel foil. Part of the way through the monitoring period the rear Lexan cover of TN 1 was removed so that the efficacy of the panel with absorber foil but no cover could be investigated.

The panels were mounted in the roof-top array at the EDRL in Varennes, which is on the south shore of the St. Lawrence River, just east of Montréal, Québec. The surrounding area is flat, windy cropland. The array is mounted at 45° and faces due south. It consists of 252 Astropower modules, mounted in six rows of 42 panels. The modules are mounted such that their major axis of symmetry is parallel to the plane of the ground. There are no obstructions in front of the array, but behind the array there are several vents and chimneys. The surface underneath the array consists of grey gravel traversed by light-grey cement walkways. A metre-high wall at the perimeter of the roof seemed to prevent thick snow cover from accumulating on the gravel; much of the time the gravel was bare or merely dusted in snow. The four monitored panels were located in the top row of the array. TN 1 was located adjacent to Control 1 and TN 2 was located adjacent to Control 2.

A number of variables were monitored. The short-circuit current and temperature of the panels were measured. The temperature was measured by a thermocouple fastened with a piece of metallic tape to the rear face of the panel; on the TN panels the absorber foil was applied over this. The difference between the temperature of the rear face of the panel and the temperature of the front glass face is generally limited to several degrees C; the panel is less than 0.5 centimetres thick. The thermocouple was mounted at a location roughly equidistant from the four corners of the panel. The wind speed, wind direction, ambient air temperature, and relative humidity were monitored at a weather station located on the roof. In addition, Eppley pyranometers mounted on the horizontal, at 45° to the horizontal, and at the back of the array measured insolation levels. While these pyranometers were correctly calibrated, an incompatibility between the data acquisition system and the amplifiers for the pyranometers introduced significant error into their readings. This error appeared to be nonlinearly related to insolation level. This problem was detected and corrected about half-way through the monitoring period. All the monitored data was recorded every fifteen minutes; the value recorded was the average for the fifteen minute period.

6.1.2 Unmodified versus TN Conseil

Under all conditions but those of very low insolation levels, the measured temperature of the TN Conseil panels was considerably higher than the temperature of the unmodified panels; under moderate-to-strong insolation levels, the temperature of the TN Conseil panels exceeded that of the unmodified panels by 15 to 30°C -- a result apparently unaffected by ambient air temperature.

This can be observed in Figure 6.1, which shows the difference in the temperatures of the TN Conseil panels and the control panels under a wide range of operating conditions. The panels were covered in snow on February 27, 28 and March 6, and 7. February 24 was exceedingly overcast, with insolation levels rarely straying above 300 W/m^2 on the array face; on February 26 and March 2 the insolation levels exceeded 1000 W/m^2 on the array face. At times of high front panel insolation, the insolation on the rear face of the panels was about 150 W/m^2 . Wind speeds ranged from calm air to fifty-five kilometres per hour.

It is interesting to note that on most nights the TN Conseil panels operated at temperatures several degrees C below the control panels. At night, all PV panels tend to radiate heat to their environment, in particular to the sky, and therefore are cooler than the ambient air temperature²⁶.

This heat loss causes the panel temperature to drop below the ambient air temperature. Counteracting this radiative heat loss is a convective heat gain. Because the TN Conseil panels are better insulated against convective heat loss or gain, they are colder at night than the unmodified panels.

6.1.3 Nickel vs Copper Absorber

The temperature of the TN Conseil panel with the nickel absorber foil was significantly higher than that of the panel with the copper absorber foil. Under conditions of moderate-to-strong insolation, the nickel foil panel was about 10°C hotter than the copper foil panel. This can be observed in Figure 6.1.

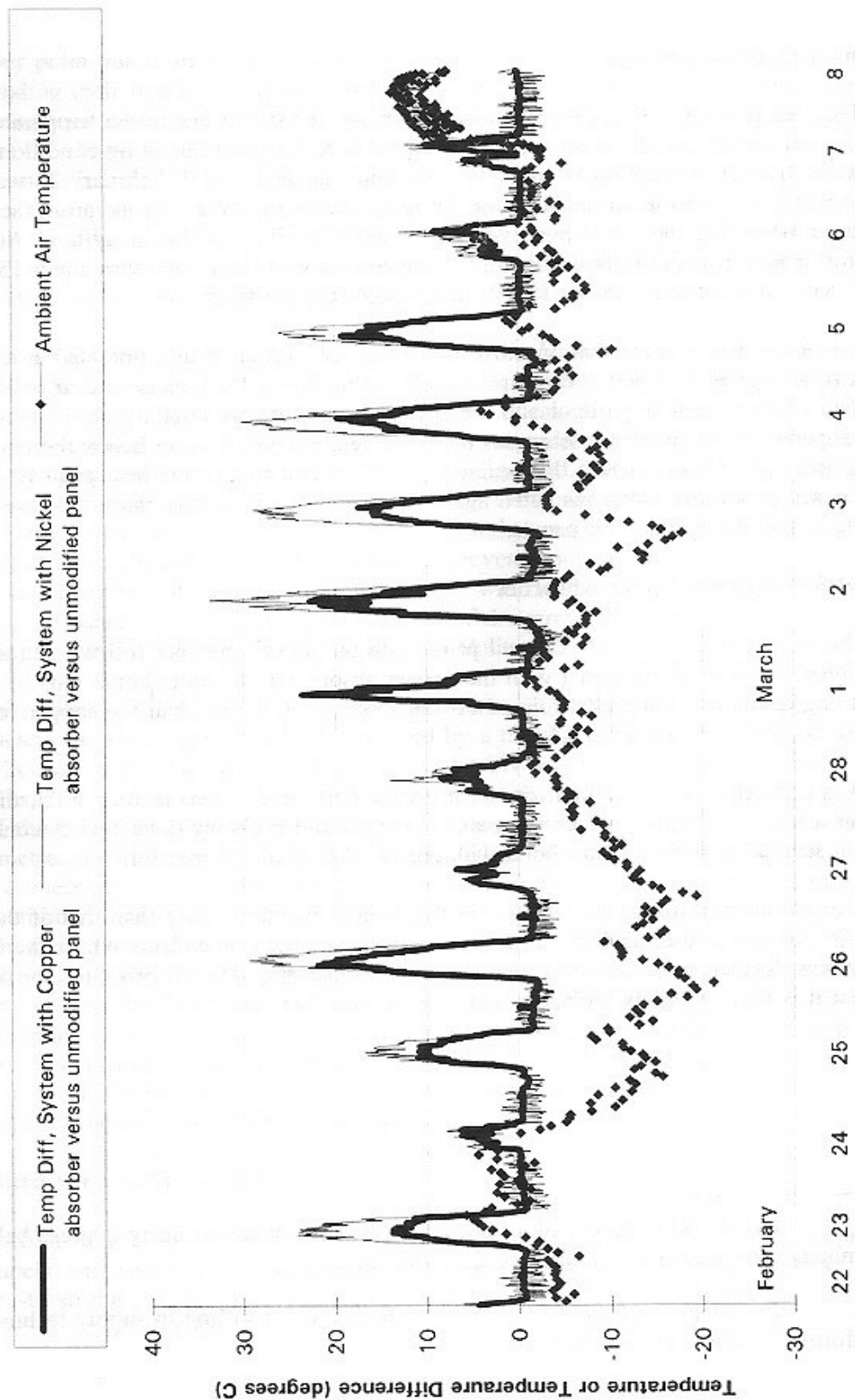
This difference in thermal performance can be attributed to two factors. First, the nickel foil has a highly selective surface whereas the copper foil probably does not²⁷. Second, the nickel foil seemed to form a better bond with the panel than the copper foil.

Because the performance of the nickel foil is demonstrably better than that of the copper foil, it is strongly recommended that the copper foil no longer be considered for the TN Conseil system; further, the nickel foil seems to approximate the ideal absorber foil sufficiently well that it is hard to justify trying to find a better absorber foil.

²⁶The sky may have a black-body temperature twenty to thirty degrees below the ambient air temperature [Duffie et al., 1991, p. 158].

²⁷The supplier of the copper foil was unable or unwilling to supply technical information about the product.

Figure 6.1 Comparison of Monitored Panel Temperatures, February 22 through March 8, 1995: Nickel Foil and Copper Foil with Lexan Cover vs Unmodified Panel



6.1.4 With vs Without Lexan Back Cover

As mentioned previously, the TN Conseil panels operate at a temperature higher than that of the unmodified panels for two reasons: one, they are better insulated against convective heat loss, and two, they absorb ground-reflected radiation incident on the back of the panel more efficiently. To investigate the relative importance of the insulative effect, the Lexan back cover was removed from TN 1 (the copper foil panel). Unfortunately, the results for this experiment are confounded by two other variables: first, by the time the Lexan back-cover was removed, there was no longer any snow cover on the ground, and ground-reflected radiation was low as a result. Second, the panel without the Lexan back-cover was equipped with the copper foil whereas the panel with the back panel had the (superior) nickel foil.

Under conditions of strong insolation, the panel with the Lexan back cover operated at a temperature about 20 °C higher than the panel without the Lexan cover (see Figure 6.2). This difference is sufficiently large that it can not be attributed to low back panel insolation, nor the inferiority of the copper foil, nor the combination of the two. Clearly, the effect of the Lexan back cover is significant.

6.1.5 Panel Temperature Gradients

The fact that warm air within the cavity between the panel and the Lexan back cover is free to move suggests that free convection will occur within the cavity and the panel will be hotter at the top of the panel than at the bottom. Additionally, the aluminum frame that surrounds the panel is a good heat sink, and one would expect that the temperature of the panel at points located near the frame would be lower than at points distant from the frame. To gauge the importance of these effects, six thermocouples were affixed to the face of the nickel absorber foil of TN 2. These thermocouples were affixed with metallic tape and their temperatures were measured using a hand-held multimeter. The approximate placement of the thermocouples is shown in Figure 6.3.

The temperature of the panels was measured on several occasions (see Figures 6.4 and 6.5). The top of the panel operated at a temperature significantly higher than the bottom of the panel. The magnitude of this difference was roughly related to the difference between the average panel temperature and the ambient air temperature-- at elevated panel temperatures the gradient was exaggerated. When panel temperatures were considerably higher than the ambient temperature (15 to 20 °C or more) the top of the panel was seven to 10 °C hotter than the bottom of the panel. The temperature gradient was most pronounced in the bottom half of the panel; that is, the temperature at the center of the panel was only slightly lower than the temperature at the top of the panel. In addition, locations on or near the vertical axis of symmetry of the panel were hotter than those distant from it. Stated another way, the thermocouples close to the left edge of the panel (viewed from the rear) were cooler than those on the centre line of the panel.

Figure 6.2 Effect of Lexan Cover on Panel Temperature, March 28 through April 8, 1995, No Snow Cover

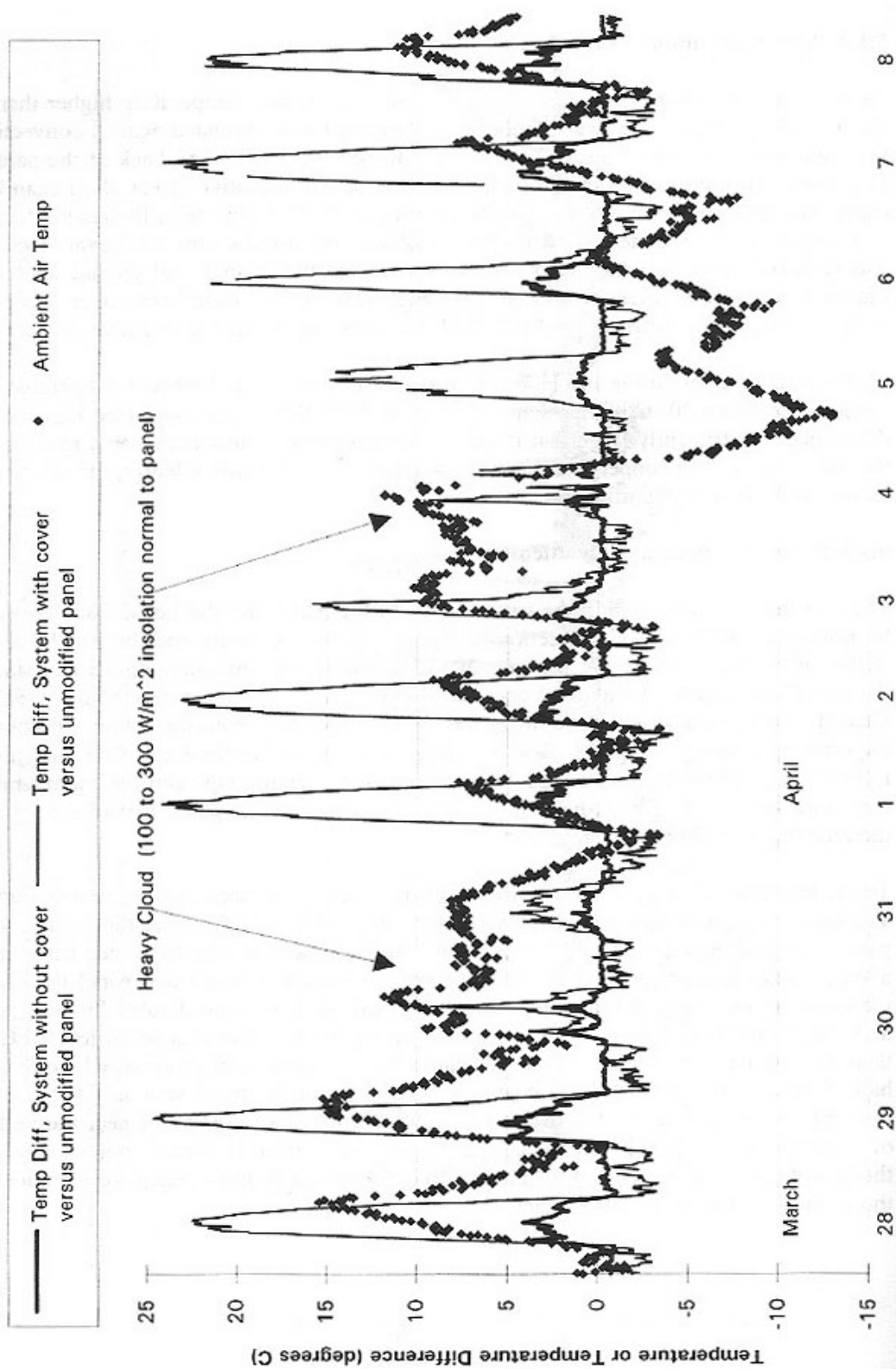


Figure 6.3 Placement of Thermocouples on Rear Face of TN Consell Panel

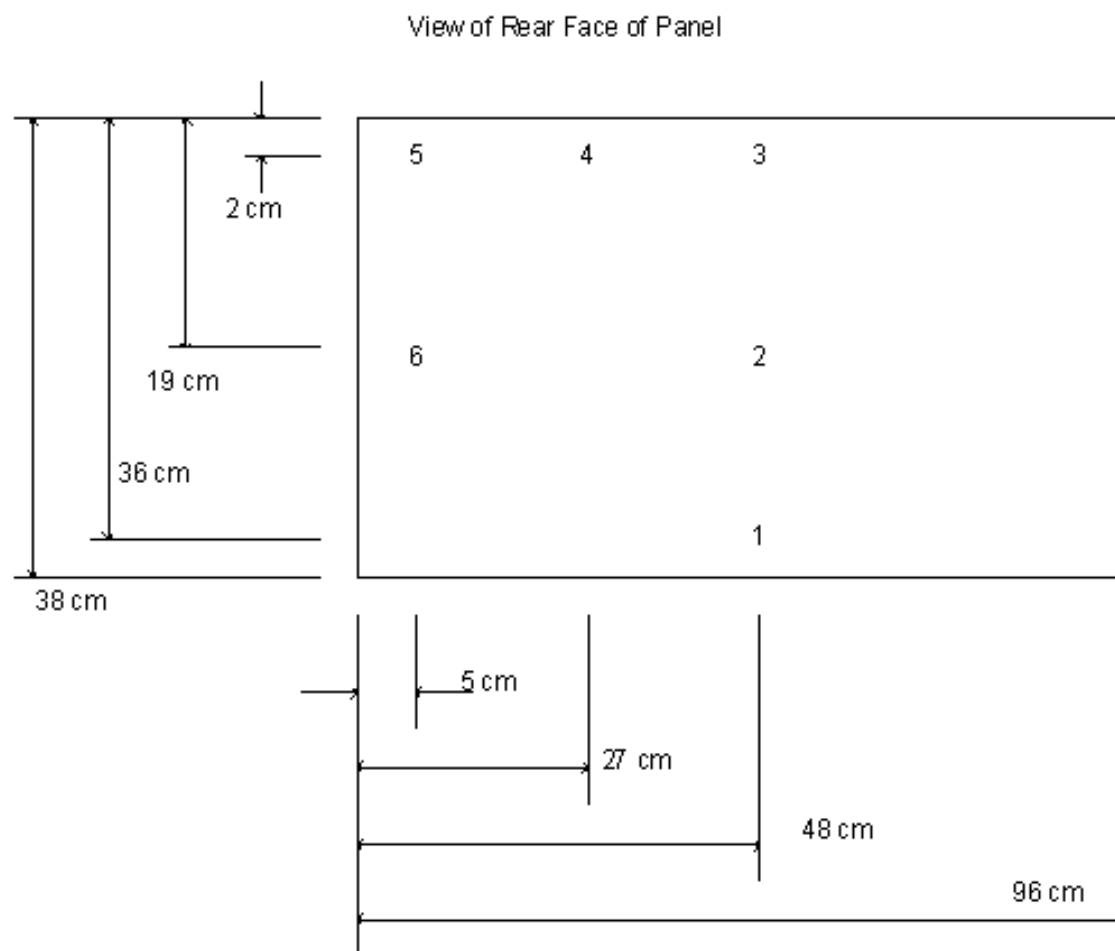


Figure 6.4 Measured Temperature Gradient at Foil, Absolute

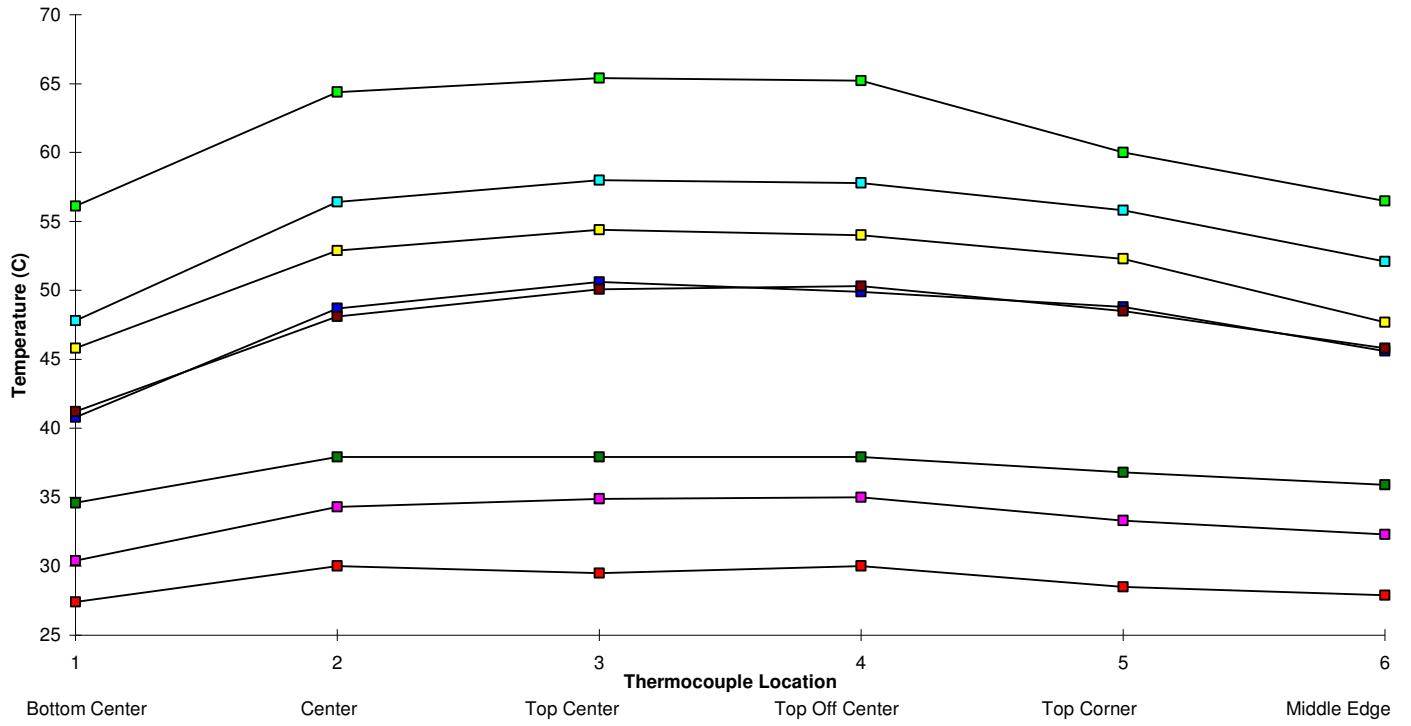
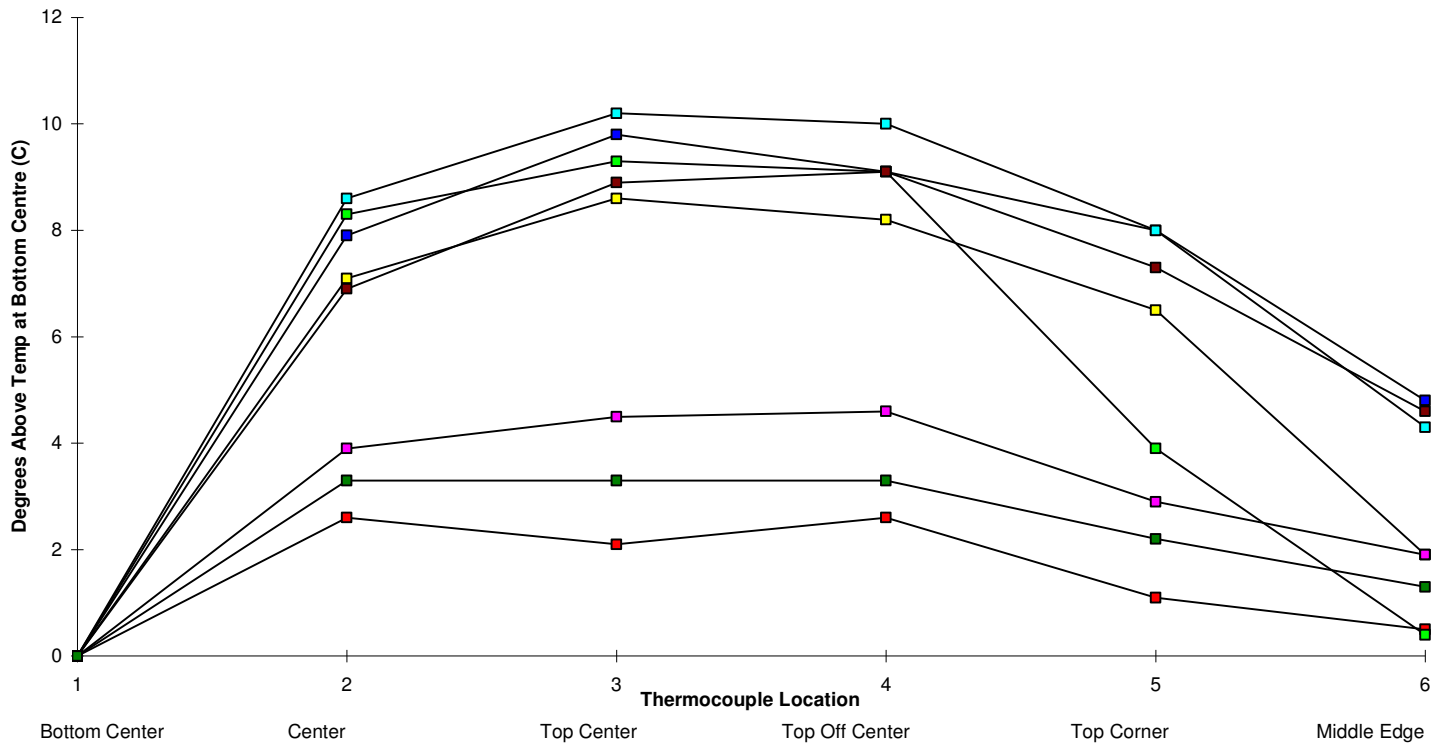


Figure 6.5 Measured Temperature Gradient at Foil, Relative



6.2 Modelled Performance

6.2.1 Description of the Models

In order to develop a better understanding of the workings of the TN Conseil technology and to find a basis for comparing several variations of the snow removal system, six simple thermal models were developed. These models are one-dimensional: they consider only the heat flow through the different layers of the panel, and ignore differences in the temperature of the panel at different locations on the panel (discussed in Section 6.1.5). The models assume steady-state operation of the panels; this is probably a good assumption since weather conditions change relatively slowly and the panels do not have a high thermal mass.

The models are based on the Siemens M55 panel. From front to back, this panel consists of low iron glass, clear ethylene vinyl acetate (EVA), the cell, another layer of EVA, and a Tedlar-Polyester-Tedlar sandwich. By volume, mass, and thermal mass the panel is dominated by the glass.

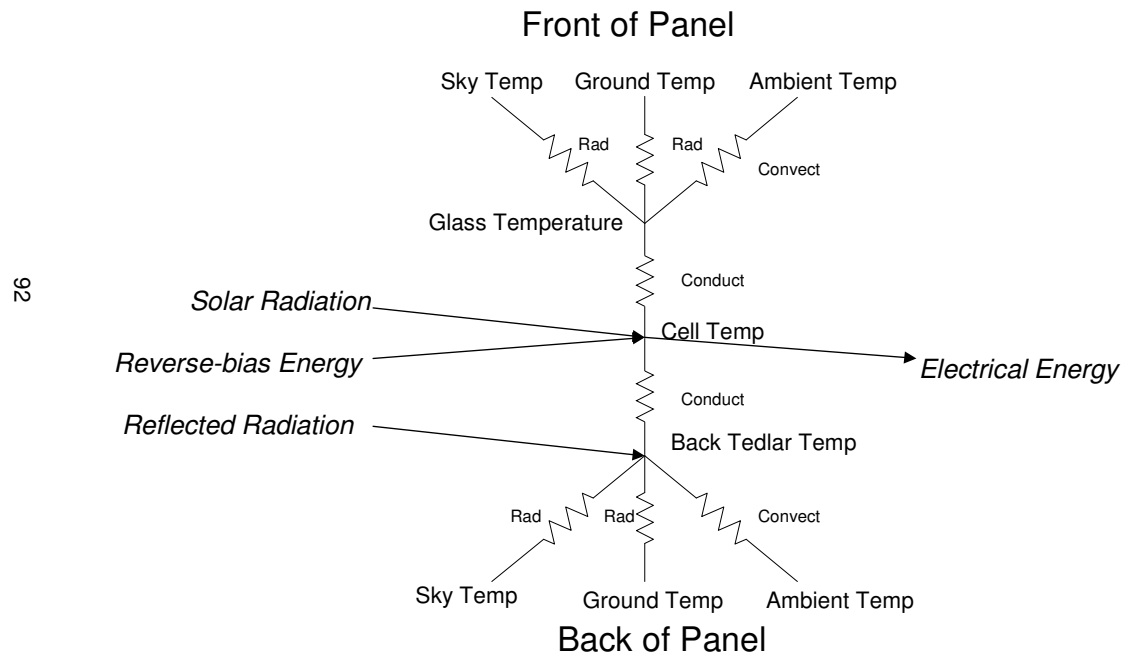
6.2.1.1 Model of Unmodified Panel

The model of the unmodified panel provides a point of reference for the comparison of all the various panel configurations.

A schematic representation of the model is shown in Figure 6.6. In this diagram, each node represents the temperature and each path between nodes indicates that heat transfer can occur between the nodes. The paths contain a resistor which indicates that the rate of heat transfer will be inversely related to some resistance to heat transfer. The resistors are labelled "Conduct" for heat transfer by conduction, "Convect" for heat transfer by convection, and "Rad" for heat transfer by radiation. Each arrow represents an energy flow (in a form other than heat), to or from the environment.

Sunlight shining on the front of the array penetrates the glass and the EVA and is absorbed at the cell. This is represented in the schematic by the arrow, incident on the node representing the cell temperature, labelled "Solar Radiation". It is assumed that all the solar radiation that is reflected and refracted by the front panel is returned to the environment, and does not heat up the glass or the EVA. Also incident on the cell temperature node is an energy flow denoted as "Reverse-bias Energy". This refers to the electrical energy that is converted to internal energy when a shaded cell is forced to operate in its negative-bias region by unshaded cells connected in series with the shaded cell. The arrow departing from the cell temperature node, labelled "Electrical Energy", refers to the electrical energy generated by the PV cell that is "used" by the load. The arrow incident on the back Tedlar temperature node, labelled "reflected radiation", represents the short-wave radiation that strikes the back panel and is absorbed by the Tedlar. It is assumed that the Tedlar is opaque.

Figure 6.6 Model of Unmodified Panel



The node "Glass Temperature" represents the temperature at the front surface of the glass. From this node, there is heat transfer in the form of radiation to/from the sky and to/from the ground, by convection to/from the ambient air, and by conduction through the glass and EVA to/from the cell. From the cell, heat is transferred by conduction to/from the glass and to/from the "Back Tedlar Temperature" node, which represents the temperature at the rear surface of the panel. Infra-red radiation through glass, EVA, Tedlar, and polyester is ignored; glass is more-or-less opaque to long-wave radiation [Duffie et al., 1991, p. 231], and while certain plastics, such as Tedlar, are transparent to some parts of the infra-red spectrum, the temperature gradients across these very thin layers will not cause much heat transfer by radiation. The back Tedlar temperature node, like the front surface of the glass, transfers heat to/from the ground and sky by radiation, and to/from the ambient air by convection.

6.2.1.2 Model of Standard TN Conseil Technology

The model of the standard TN Conseil snow melting technology is simply the model of the unmodified panel with some alterations to account for the adhesive, the foil, and the Lexan cover added to the rear of the panel (see Figure 6.7). The model assumes that the nickel absorber foil is used.

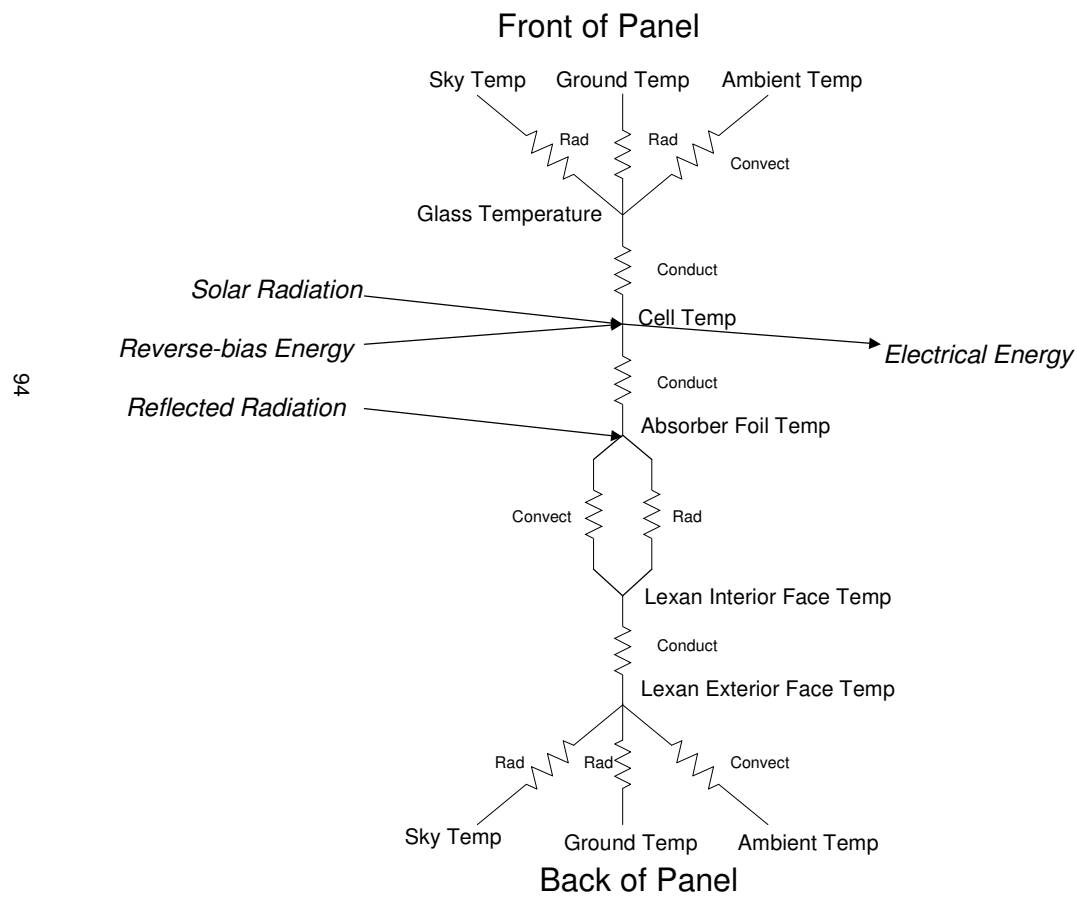
The radiation and convection transfers to/from the back Tedlar temperature node in the unmodified panel model are now found at the "Lexan Exterior Face Temperature" node. Between this node and the "Lexan Interior Face Temperature" node heat is transferred by conduction. Lexan is largely opaque to infra-red. Across the air cavity (between the Lexan interior face node and the "Absorber Foil Temperature" node) there is heat transfer by natural convection and radiation.

The reflected radiation incident on the absorber foil has a different magnitude than the term of the same name in the unmodified panel model. This results from the low reflectivity of the absorber foil and the reflection and absorption due to the Lexan cover. It is assumed that all the radiation not absorbed at the absorber foil is returned to the environment and does not heat the Lexan sheet.

6.2.1.3 Model of Black Tedlar Back without Back Cover

This model is identical to that of the unmodified panel except that the Tedlar backing on the panel is black instead of white, the latter being the standard color on Siemens panels. The black Tedlar backing absorbs more incident radiation than the white Tedlar backing; thus, a Siemens panel manufactured with a black Tedlar backing may be the cheapest option for improving the snow melting performance of the panel. While Siemens does not presently manufacture panels with black Tedlar backing, it might be able to do so.

Figure 6.7 Model of Standard TN Conseil Technology



6.2.1.4 Model of Black Nickel Foil Back without Back Cover

This model represents the next cheapest option for improving the snow melting performance of the Siemens panel: the standard panel with the black nickel absorber foil that is found in the TN Conseil technology. In other words, it is the standard TN Conseil system without the Lexan back cover. This model demonstrates the relative importance of the Lexan back cover.

6.2.1.5 Model of Lexan Thermoclear

As discussed in Section 6.1.5, free convection in the air cavity of the standard TN Conseil technology results in a temperature gradient up the panel surface. This has potentially negative implications for melting-- snow and ice will melt more quickly from the top of the panel than from the bottom. To diminish this temperature gradient and equalize temperatures around the panel, free convection in the air cavity must be reduced. One way to do this is to divide the air cavity into smaller compartments using baffles running parallel to the bottom and top edges of the panel. This configuration is closely approximated by Lexan Thermoclear, a material containing two parallel Lexan sheets, about a centimetre apart, with regularly spaced transparent Lexan ribs connecting the two sheets. The result is something like transparent corrugated cardboard. Lexan Thermoclear comes in various thicknesses, each having different spacing between the Lexan sheets and between the ribs.

From the glass to the nickel absorber foil the model of the panel with Lexan Thermoclear is identical to that of the standard TN Conseil-modified panel (see Figure 6.8). Instead of an airspace and Lexan back cover, however, the panel has Lexan Thermoclear mounted snugly against the nickel foil. In addition to heat transfer by conduction to/from the cell temperature node, there is conduction from the nickel absorber foil through the interior sheet of Lexan in the Lexan Thermoclear. Between the two Lexan sheets there is heat transfer by radiation, conduction through the ribs, and convection. There is heat transfer by conduction through the exterior Lexan sheet, and from the exterior face of the exterior Lexan sheet there is heat transfer by radiation to the ground and sky and by convection to the ambient air.

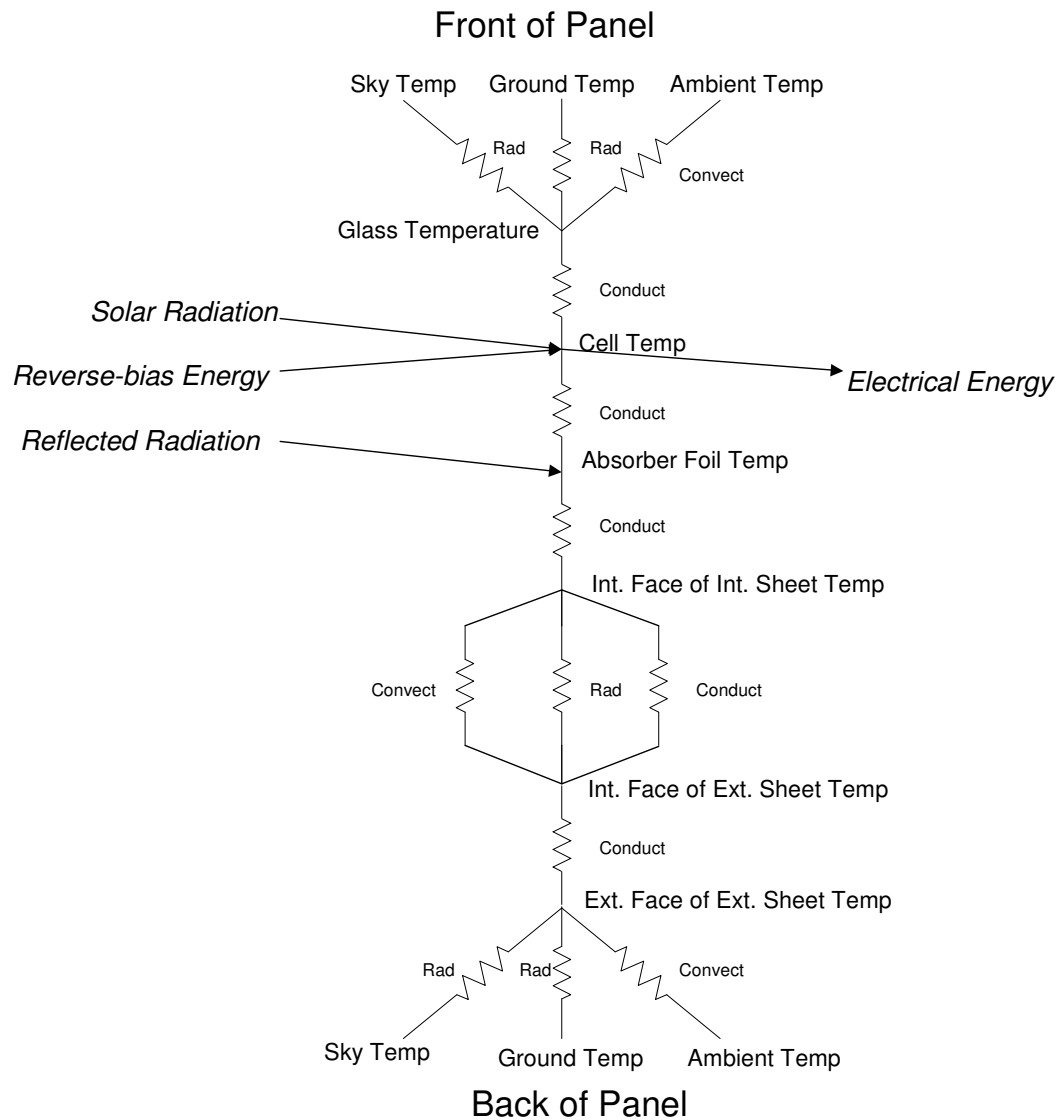
6.2.1.6 Model of Black Tedlar Back with Back Cover

This model is for an option slightly cheaper than the standard TN Conseil System. If the panels were manufactured with black Tedlar backing, a possibility raised in Section 6.2.1.3, the nickel absorber foil could be dispensed with while the Lexan back cover was retained. Thus, this model is the same as that for the standard TN Conseil Technology, but without the nickel foil and its adhesive at the back surface of the panel.

6.2.2 Equations for Heat Transfer And Other Energy Flows

The models presented above are all fairly similar, and they share the same heat transfer and energy flow terms. Rather than presenting the equations for the models explicitly, the individual

Figure 6.8 Model of Lexan Thermoclear



terms representing each form of energy transfer are described below. All equations for heat and energy flows are given per unit area (W/m^2).

6.2.2.1 Radiation

Heat transfer by radiation to the ground or sky from the front or back surface of the panel is given by [Duffie et al., 1991, p. 157]:

$$q_{\text{panel}} = F \epsilon_{\text{panel}} s (T_{\text{env}}^4 - T_{\text{panel}}^4) \quad (6.1)$$

where q_{panel} is the heat transfer due to radiation (W/m^2) from the panel surface to the ground or sky,
 F is the panel's view factor of the sky or ground, which for the front panel are S and $1 - S$, respectively, and for the back panel are $1 - S$ and S , respectively, where S is the sky view factor from Eq. 5.2 in Section 5.2.1.
 ϵ_{panel} is the emittance of the panel surface in question,
 σ is the Stefan-Boltzmann constant, equal to $5.6697 \times 10^{-8} \text{ Wm}^{-2}\text{K}^{-4}$,
 T_{env} is the temperature of the ground or sky, in K,
and T_{panel} is the temperature of the panel surface in question, in K.

Heat transfer by radiation across the air cavity is given by [Duffie et al., 1991, p. 157]:

$$q_{\text{cav}} = \frac{s (T_{\text{in}}^4 - T_{\text{ex}}^4)}{\frac{1}{\epsilon_{\text{in}}} + \frac{1}{\epsilon_{\text{ex}}} - 1} \quad (6.2)$$

where q_{cav} is the heat transfer due to radiation (W/m^2) from the interior to the exterior surfaces bounding the air cavity,
 T_{in} is the temperature of the interior surface bounding the cavity, in degrees K,
 T_{ex} is the temperature of the exterior surface bounding the cavity, in degrees K,
 ϵ_{in} is the emittance of the interior surface bounding the cavity,
and ϵ_{ex} is the emittance of the exterior surface bounding the cavity.

For the radiation across the Lexan Thermoclear, the radiation transfer term is multiplied by the fraction of the cavity that is not obstructed by the Lexan ribs.

6.2.2.2 Conduction

All conduction terms take the form [Reynolds et al., 1977, p. 543]:

$$q = \frac{k}{L} (T_1 - T_2) \quad (6.3)$$

where q is the heat transfer by conduction (W/m^2) from node 1 to node 2,
 k is the thermal conductivity of the material(s) ($\text{Wm}^{-1}\text{K}^{-1}$) between node 1 and node 2,
 L is the thickness (m) of the material(s), or, equivalently, the distance from node 1 to node 2,
and T_x is the temperature of node x , in degrees K.

When there exist n or more materials of different thermal conductivities between node 1 and node 2, an effective thermal conductivity is calculated from:

$$k_{\text{eff}} = \frac{L_{\text{tot}}}{\frac{L_1}{k_1} + \frac{L_2}{k_2} + \dots + \frac{L_n}{k_n}} \quad (6.4)$$

where k_{eff} is the effective thermal conductivity ($\text{Wm}^{-1}\text{K}^{-1}$) of the n materials,
 L_x is the thickness (m) of material x ,
 k_x is the thermal conductivity of material x ($\text{Wm}^{-1}\text{K}^{-1}$),
and L_{tot} is the sum of L_x for $x = 1, 2, \dots, n$.

For the conduction of heat across the Lexan Thermoclear ribs, the conduction term is multiplied by the fraction of the air cavity occupied by the ribs.

6.2.2.3 Convection

All heat transfers by convection take the form [Reynolds et al., 1977, p. 555]:

$$q = h(T_1 - T_2) \quad (6.5)$$

where q is the heat transfer by convection (W/m^2) from node 1 to node 2,
and h is the convective heat transfer coefficient ($\text{Wm}^{-2}\text{K}^{-1}$).

Heat transfer by convection from the front or back of the panel is given by the above equation with T_1 set to the surface temperature, T_2 set to the ambient air temperature and h set to h_{wind} [Watsun Simulation Laboratory, 1992, pp. 6.2-6.6: Mostrel et al., 1982]:

$$h_{\text{wind}} = \begin{cases} 5.0 & V < 0.45 \\ 0.6 + 6.64 \sqrt{V} & V \geq 0.45 \end{cases} \quad (6.6)$$

where V is the wind velocity, in m/s.

For heat transfer across the air cavity due to natural convection, h_{cav} is found from the dimensionless Nusselt number, Nu [Reynolds et al., 1977, p. 556]:

$$h_{cav} = \frac{Nu \cdot k_{air}}{t_{cav}} \quad (6.7)$$

where k_{air} is the thermal conductivity of air ($W m^{-1} K^{-1}$),
and t_{cav} is the thickness of the cavity (m).

For the determination of Nu , the dimensionless Rayleigh number, Ra , must be found [Advanced Glazing System Laboratory, 1992, p. 14]:

$$Ra = \frac{r_{air}^2 t_{cav}^3 g \beta_{air} c_p \Delta T}{m_{air} k_{air}} \quad (6.8)$$

where ρ_{air} is the density of air (kg/m^3),
 g is acceleration due to gravity, equal to $9.81 m/s^2$,
 β_{air} is the isobaric compressibility or thermal expansion coefficient of air (K^{-1}), which is assumed to be equal to the inverse of T_m (K), the mean air temperature in the cavity,
 c_p is the specific heat of air at constant pressure ($J kg^{-1} K^{-1}$),
 ΔT is the temperature difference between the two surfaces bounding the cavity (K),
and μ_{air} is the viscosity of air ($kg m^{-1} s^{-1}$).

Treating air as an ideal gas [Reynolds et al., 1977, p. 96]:

$$r_{air} = \frac{P_{atm}}{RT_m} \quad (6.9)$$

where P_{atm} is the atmospheric air pressure, assumed equal to $101325 N/m^2$,
and R is the ideal gas constant for air at low pressures, assumed equal to $286 J kg^{-1} K^{-1}$.

Empirical relations for k_{air} , μ_{air} , and c_p as functions of T_m , all taken from [Advanced Glazing System Laboratory, 1992, p. 18], can be found in the Mathcad model "lexan.mcd" in Appendix D.

Except at night and other times of very low insolation, the absorber foil (or black Tedlar surface) will be hotter than the Lexan back cover. For the systems with the Lexan back cover, this creates an inclined cavity with the heated plate as the top surface. This is a thermally stable configuration, and the average heat transfer across the air cavity can be found simply by scaling the result for the vertical cavity to reflect the tilt angle. In practice, this is accomplished by scaling the Nusselt number [Advanced Glazing System Laboratory, 1992, p. 16; Arnold et al., 1974]²⁸:

$$Nu = 1 + (Nu_v - 1) \sin(\beta + 90) \quad (6.10)$$

where Nu_v is the Nusselt number for a vertical cavity of the same dimensions and at the same operating conditions,
and β is the panel tilt angle (degrees).

Nu_v is found from [Advanced Glazing System Laboratory, 1992, p. 15]:

$Nu_v = \max [Nu_1, Nu_2] \quad (6.11)$ <p>where</p> $Nu_1 = \begin{cases} 0.0673838 Ra^{\frac{1}{3}} & 50000 < Ra < 10^6 \\ 0.028154 Ra^{0.4134} & 10000 < Ra < 50000 \\ 1 + 1.7596 \cdot 10^{-10} Ra^{2.2985} & Ra < 10000 \end{cases}$ $Nu_2 = 0.242 \frac{Ra^{0.272}}{A}$

where A is the aspect ratio of the cavity, defined as the dimension of the panel along its vertical axis of symmetry (its length or width, depending on how it is mounted) divided by t_{cav} .

The above equations are valid for $100 < Ra < 2 \cdot 10^7$ and $5 < A < 110$. For the Siemens M55 panel mounted with its minor axis of symmetry parallel to the ground, the aspect ratio will be approximately 120; it is assumed that this does not introduce significant error, especially since under most conditions the Rayleigh number for the TN Conseil system results in Nu_1 being greater than Nu_2 .

²⁸This scaling law was developed and verified for a cavity aspect ratio of six [Arnold et al., 1974], and the aspect ratios for the TN Conseil System are between forty and one-hundred-twenty. The inaccuracies introduced by this are unknown.

For the Lexan Thermoclear, the scaling law (Eq. 6.10) is applied to Nu_v for a cavity with parallel, horizontal slats. For this configuration, the Nusselt number can be found from [Duffie et al., 1991, p. 164; Meyer et al., 1978]:

$$Nu_v = \max[1.1 C_1 C_2 Ra^{0.28}, 1] \quad (6.12)$$

where C_1 and C_2 are empirical coefficients based on the aspect ratio of the cavity.

6.2.2.4 Other Energy Flows

Other than the short-wave radiation incident on the front and back of the panel, the only energy flows that are not in the form of heat are the "Reverse Bias Energy" flow incident on the cell temperature node and the "Electrical Energy" flow departing from that same node. The reverse bias energy flow is useful for studying partially shaded modules; that was not investigated in the course of this study and was always set to zero. The electrical energy flow, E_{elec} , (W/m^2) is modelled as:

$$E_{elec} = \eta_{elec} S_{front} \quad (6.13)$$

where η_{elec} is the electrical efficiency of the panel,
and S_{front} is the solar radiation on the front surface of the panel (W/m^2).

The electrical energy flow was set to zero when modelling the panel at open circuit or short circuit conditions. At load, η_{elec} was assumed to be ten percent.

6.2.3 Solar Radiation Transmission and Absorption

Not all the solar radiation incident on the front and back of the panel is absorbed by the cell or the back panel surface: some is reflected back into space. The "Solar Radiation" and "Reflected Radiation" energy flows must reflect this: for example, for $1000 W/m^2$ insolation on the front panel, the radiation reaching the cell will be around $900 W/m^2$. The principal losses come from reflection in the transparent cover material and reflection at the cell or absorber surface; absorption by the transparent covers is very low since the covers are thin and have a low extinction coefficient.

Absorptivity, transmissivity, and reflectivity are functions of wavelength. In this analysis, however, they are treated as being independent of wavelength. Over the majority of the wavelengths contained in the solar spectrum, this is an excellent assumption for glass [Duffie et al., 1991, p. 216], Lexan²⁹, the nickel absorber foil³⁰, and the cell with antireflective coating

²⁹ from Product Data for Lexan and Lexan Thermoclear, GE Plastics, Structured Products Division, General Electric Company.

³⁰ Product data sheets, name of manufacturer proprietary information.

[Overstraeten et al., 1986, p. 256]. For the Tedlar back panel surfaces, the reflectivity, transmissivity, and absorptivity were specifically for the solar radiation spectrum.

The absorptivity and reflectivity of the cell with antireflective coating, the nickel absorber foil and the Tedlar back panel surface are assumed to be independent of the angle of incidence. It is unknown how much error this introduces.

6.2.3.1 Front Panel

Before light strikes the cell surface it must pass through glass and EVA. This will cause losses. The EVA is much thinner than the glass-- 460 microns versus three mm-- and losses due to absorption in the EVA can be ignored. Further, the index of refraction for EVA is about 1.48 whereas that for glass is about 1.53; since these are very close, as long as the two materials are in contact with one another there is very little reflection of the light passing from the one medium into the other. Thus, we can ignore the losses due to the EVA without introducing any significant error.

Light striking the glass at an angle of incidence of θ_{air} will have an angle of refraction within the glass of θ_{glass} , with angles measured with respect to the surface normal, given by Snell's law [Duffie et al., 1991, p. 217]:

$$\theta_{\text{glass}} = \arcsin(n_{\text{air}} \sin(\theta_{\text{air}}) / n_{\text{glass}}) \quad (6.14)$$

where n_x is the index of refraction of material x with respect to a vacuum.

The index of refraction for air, n_{air} , is assumed to be unity.

The reflection of unpolarized light striking the glass surface is given by relations developed by Fresnel [Duffie et al., 1991, p. 216]:

$$r_{\perp} = \frac{\sin^2(q_{\text{glass}} - q_{\text{air}})}{\sin^2(q_{\text{glass}} + q_{\text{air}})} \quad (6.15)$$

$$r_{\parallel} = \frac{\tan^2(q_{\text{glass}} - q_{\text{air}})}{\tan^2(q_{\text{glass}} + q_{\text{air}})} \quad (6.16)$$

where r_{\perp} is the reflection of the perpendicular component of the unpolarized light,
and r_{\parallel} is the reflection of the parallel component of the unpolarized light, with parallel and perpendicular defined in relation to the plane created by the incident beam and the surface normal.

The transmission of the glass accounting for losses due to reflection only, τ_r , is [Duffie et al., 1991, p. 216]³¹:

$$\tau_r = 1 - (r_{\perp} + r_{||}) / 2 \quad (6.17)$$

Bouguer's law describes the absorption of light in the glass [Duffie et al., 1991, p. 221]:

where τ_a is the fraction of
through the glass,
 K is the extinction
and L is the thickness of the glass (m).

$$\tau_a = e^{-\frac{KL}{\cos(\theta_{\text{glass}})}} \quad (6.18)$$

the incident light that is transmitted
ignoring losses due to reflection,
coefficient for the glass (m^{-1}),

From this, the overall transmission of the incident light through the glass, τ , can be found from the approximation [Duffie et al., 1991, p. 221]:

$$\tau = \tau_a \tau_r \quad (6.19)$$

The cell surface is not a perfect absorber. Some of the light that passes through the glass and strikes the cell is reflected back through the glass. Some of this reflected light, in turn, will be reflected back towards the cell when it reaches the glass surface; this continues ad infinitum. The transmittance-absorptance product, $(\tau \alpha)$, is the parameter used to describe the fraction of the energy incident on the glass surface that is ultimately absorbed [Duffie et al., 1991, p. 229]:

where α is the
with
and ρ_d is the reflectance
radiation, which can be estimated by

$$(\tau \alpha) = \frac{\tau \alpha}{1 - (1 - \alpha) \rho_d} \quad (6.20)$$

absorptance of the cell surface
antireflective coating,
of the glass surface for diffuse

³¹Eq. 6.17 is different from the relation given in [Duffie et al., 1991, p. 219] due to the absence of air between the glass and the cell surface; a fill gas exists between the cover and the absorber surface in a solar thermal collector.

$$\tau_a^2 (1 - \tau_r) \text{ for } \theta_{\text{air}} \text{ of } 60^\circ \text{ }^{32}.$$

The transmittance-absorptance product is clearly a function of the incident angle of the radiation. During most times of moderate to strong insolation, beam radiation will strike the glass surface at an angle of incidence less than 40° . The transmittance-absorptance product is essentially constant over the range of zero to 40° ; at 40° the value is no more than five percent lower than at zero degrees. Thus, most beam radiation can be treated as having the same transmittance-absorptance product as radiation that is normal to the surface. It has been determined that for a wide range of applications, diffuse radiation has the same transmittance as beam radiation of the same intensity at an angle of incidence of 60° [Duffie et al., 1991, p. 227]. Since the absorptance is considered independent of the angle of incidence, the transmittance-absorptance product for diffuse radiation can also be calculated as the transmittance-absorptance product for beam radiation incident at 60° .

The cell absorptance was assumed to be 0.97. This resulted in a transmittance-absorptance product of 0.92 for beam radiation and 0.87 for diffuse radiation.

6.2.3.2 Back Panel without Cover

It is assumed that the solar radiation transmission of the Tedlar and foil is zero. This is a good assumption for the black Tedlar, which has a rated solar transmittance of zero, and the nickel foil (solar transmittance unknown, but much less than five percent) and a reasonable one for the white Tedlar (seven percent solar transmittance).

The absorbed radiation is simply the product of the irradiance (W/m^2) and the absorptance of the foil or the Tedlar.

6.2.3.3 Panel with Lexan Back Cover

With several exceptions, the equations that appear in Section 6.2.3.1 can be used for the transmission and absorption of radiation incident on the rear of the panel; all variables with the "glass" subscript are equally pertinent to Lexan. However, the equations for τ_r and ρ_d are slightly different due to the fact that there is air between the Lexan and the panel, whereas the glass, EVA, and cell are in contact with one another.

The transmission of the back cover accounting only for losses due to reflection, τ_r , is [Duffie et al., 1991, p. 219]:

$$\tau_r = \frac{1}{2} \frac{1 - r_{\parallel}}{1 + r_{\parallel}} + \frac{1 - r_{\perp}}{1 + r_{\perp}} \quad (6.21)$$

³²This equation for ρ_d is different from the estimate given by [Duffie et al., 1991, p. 228] for the reason given in the previous footnote.

For the back cover, the reflectance for diffuse radiation, ρ_d , is estimated by $\tau_a - \tau$ for radiation incident at 60° [Duffie et al., 1991, p. 228].

All radiation on the back surface is assumed to be diffuse. Therefore, the radiation on the back surface is treated as beam radiation incident at 60° . For the Lexan cover with the nickel foil this results in a transmittance-absorptance product of 0.79; for the Lexan cover with the black Tedlar this yields 0.76.

6.2.3.4 Panel with Thermoclear Back Cover

The Lexan Thermoclear is modelled using the equations for a solar thermal collector with two identical covers separated by air. This implicitly assumes that the layer of Lexan sheet in the Thermoclear that is adjacent to the panel will not be in perfect contact with the Tedlar or absorber foil, but rather be separated from it by a very thin layer of air. The equations for a two cover system are the same as those found in Section 6.2.3.1, with the following exceptions and changes.

The transmittance, accounting only for reflection, becomes [Duffie et al., 1991, p. 219]:

$$t_r = \frac{1}{2} \frac{1 - r_{||}}{1 + 3r_{||}} + \frac{1 - r_{\perp}}{1 + 3r_{\perp}} \quad (6.22)$$

When calculating τ_a , the thickness, L , is the combined thickness of the two Lexan sheets.

The reflectance for diffuse radiation, ρ_d , should be estimated as for Eq. 6.22 in Section 6.2.3.3; this introduces a very small error.

Treating the Lexan Thermoclear as a two cover system ignores the effects of the ribs on light transmission. There are two principal effects. First, some off-normal incident radiation passing through the outer Lexan sheet into the air cavity will strike the ribs, at which point a fraction will be transmitted into the adjacent cavity, a fraction will be reflected, and the remainder absorbed in the rib. Second, some incident radiation passing through the outer Lexan sheet will pass immediately into the rib at the junction of the rib and the sheet.

In the case of the first effect, the radiation that strikes the rib and is reflected is not returned to space; rather, its angle of reflection is the same as its angle of incidence and it continues moving towards the panel. [Hollands et al., 1978] point out that the trajectories of the reflected and transmitted portions of the beam incident on the rib are the mirror images of each other, such that one can treat the wall like a mirror. Thus, in the case of the first effect the additional loss is only the radiation absorbed by the beam passing through the rib. Since the rib is thin and quite

transparent, this will be minor.

In the case of the second effect, if the angle of incidence relative to the sheet is large the radiation entering at the "top" of the rib will pass out of the rib and into the air cavity. If the angle of incidence is small, the beam will be internally reflected down the rib in the manner of a waveguide [Hollands et al., 1978]. In either situation, the additional loss is, once again, the radiation absorbed in the rib. For the radiation that is internally reflected, the path length through the rib may be quite long, and therefore the losses reasonably large. However, the rib occupies only about five percent of the cross-sectional area of the Thermoclear, and the radiation that is internally reflected in the rib will be correspondingly small. Therefore, the losses caused by the rib can be ignored.

A more accurate method of estimating the radiation passage through the Thermoclear could be developed using the methods presented in [Hollands et al., 1978]. The application of the method would require the empirical determination of several optical properties of the Lexan material.

For the Lexan Thermoclear of nominally 10 mm thickness used in conjunction with the nickel absorber foil, the transmittance-absorptance product calculated in the above manner is 0.72.

6.2.4 Parameters Used in the Models

The models require a large number of parameters to describe the physical properties of the materials that constitute the panel and the TN Conseil technology. The values used for these parameters and whence these parameters were obtained is listed below. It should be noted that accurate parameter values are very difficult to obtain; some of the values listed below, though from reliable sources, are probably somewhat inaccurate.

Table 6.1 Parameters for Glass and EVA

Parameter	Value	Source
Glass...		
...thickness	3 mm	Kim Mitchell, Siemens Solar Industries
...emittance	0.88	[Duffie et al., 1991, p. 260]
...extinction coefficient	4 m^{-1}	[Duffie et al., 1991, p. 221] for low iron glass; glass type confirmed with Kim Mitchell, Siemens Solar Industries
...index of refraction	1.526	[Duffie et al., 1991, p. 217]
...thermal conductivity	$1.00 \text{ Wm}^{-1}\text{K}^{-1}$	[Lide, 1994] for soda lime glass; AFG, Toronto confirmed that the value for low iron glass is the same
EVA...		
...thickness	460 microns	John Lovelace, Siemens Solar Industries

...index of refraction	1.48	Average value, from Dupont Hotline
...thermal conductivity	$0.288 \text{ Wm}^{-1}\text{K}^{-1}$	Dupont Hotline
Glass + EVA...		
...thickness	3.46 mm	Calculated
...thermal conductivity	$0.75 \text{ Wm}^{-1}\text{K}^{-1}$	Calculated

Table 6.2 Parameters for Cell, Polyester, Tedlar, and Absorber Foil

Parameter	Value	Source
Cell...		
...thickness	300 microns	Kim Mitchell, Siemens Solar Industries
...thermal conductivity	$83.5 \text{ Wm}^{-1}\text{K}^{-1}$	[Lide, 1994]
...solar absorptance	97 %	estimate based on [Overstraeten et al., 1986, p. 256]
Polyester...		
...thickness	76 microns	Mark Tribo, Solar App. Rep., Dupont
...thermal conductivity	$0.16 \text{ Wm}^{-1}\text{K}^{-1}$	Nancy Coup, ICI Americas Hotline
Tedlar		
...thickness	38 microns	Mark Tribo, Solar App. Rep., Dupont
...thermal conductivity	$0.14 \text{ Wm}^{-1}\text{K}^{-1}$	Mark Tribo, Solar App. Rep., Dupont
...solar transmittance (black)	0.0 %	Mark Tribo, Solar App. Rep., Dupont
...solar transmittance (white)	6.6 %	Mark Tribo, Solar App. Rep., Dupont
...solar reflectance (black)	7.4 %	Mark Tribo, Solar App. Rep., Dupont
...solar reflectance (white)	66.9 %	Mark Tribo, Solar App. Rep., Dupont
...solar absorptance (black)	93 %	Calculated based on above
...solar absorptance (white)	33 %	Calculated based on above; transmitted radiation is considered as absorbed
...emittance (black)	0.88	Mark Tribo, Solar App. Rep., Dupont
...emittance (white)	0.89	Mark Tribo, Solar App. Rep., Dupont

Foil Adhesive...		
...thickness	50 microns	Product data sheet (confidential)
...thermal conductivity	$0.29 \text{ Wm}^{-1}\text{K}^{-1}$	Guess based on thermal conductivity of silicone [Lide, 1994]
Foil...		
...thickness	13 microns	Pierre Hosatte, TN Conseil
...thermal conductivity	$89.9 \text{ Wm}^{-1}\text{K}^{-1}$	Product data sheet (confidential)
...absorptance	0.97	Average value, from product data sheet
...emittance	0.08	Range of 0.08 to 0.11 at 100 ° C from product data sheet
Cell+EVA+Tedlar+Polyester+Tedlar...		
...thickness	912 microns	Calculated based on above
...thermal conductivity	$0.349 \text{ Wm}^{-1}\text{K}^{-1}$	Calculated based on above
Cell+EVA+Tedlar+Polyester+Tedlar+Adhesive+Foil...		
...thickness	975 microns	Calculated based on above
...thermal conductivity	$0.350 \text{ Wm}^{-1}\text{K}^{-1}$	Calculated based on above

Table 6.3 Parameters for Lexan and Thermoclear

Parameter	Value	Source
Lexan Sheet...		
...thickness	2.8 mm	Hand measurement with calipers
...thermal conductivity	$0.19 \text{ Wm}^{-1}\text{K}^{-1}$	GE Plastics Hotline
...extinction coefficient	9 m^{-1}	Inferred from solar energy transmission data for Lexan Monolithic Sheet, GE Plastics
...emittance	0.7	GE Plastics Hotline

Thermoclear...		
...overall thickness	10 mm	GE Plastics data sheet
...sheet thickness (each)	610 microns	GE Plastics Fax
...rib thickness (each)	510 microns	GE Plastics Fax
...rib centre-to-centre spacing	1.1 cm	GE Plastics Fax

6.2.5 Ground and Sky Temperatures

While the emissivity of snow, at 0.97 to 1.0 [Male et al., 1981, p. 383], is very high, the high albedo of snow indicates that the solar absorptance of snow is very low. Thus, when skies are clear and there is a low sky temperature, as will often happen in the winter, the snow cover on the ground will cool to a temperature below the ambient air temperature. In the models above, this has been accounted for by setting the ground temperature, when snow is on the ground, to two °C below the ambient air temperature. When there is no snow cover the underlying ground is exposed. For most locations this will have a significant solar absorptance, such that when the sun is shining the ground will be at a temperature above the ambient air temperature. This has been approximated by setting the ground temperature for no snow cover to two degrees above the ambient air temperature. These are guesses, but the models are not very sensitive to ground temperature (see Section 6.2.6) so a large margin of error will not greatly affect the results.

The sky temperature is the temperature of a blackbody having the same radiation characteristics as the sky. On a clear, dry winter day it may be considerably lower than the ambient air temperature. If the dew point is known, the sky temperature, T_s (in K), can be found from the empirical relation [Duffie et al., 1991, p. 158; Berdahl et al., 1984]:

$$T_s = T_a (0.711 + 0.0056 T_{dp} + 0.000073 T_{dp}^2 + 0.013 \cos (15 t))^{0.25} \quad (6.23)$$

where T_a is the ambient air temperature (K),
 T_{dp} is the dew point temperature (°C),
and t is the number of hours after midnight.

The dewpoint can be calculated from wet-bulb temperatures or relative humidity measurements by standard psychrometric methods [ASHRAE, 1993] (see also "lexan.mcd" in Appendix D). The above equation was formulated on the basis of experimental data for dewpoints from -20 °C to 30 °C. The model, however, was used for dewpoint temperatures far below -20 °C.

When a dewpoint temperature was not available the sky temperature was assumed to be 20 °C or 25 °C below ambient air temperatures for clear sky conditions. Once again, this is a guess, but

the model is not very sensitive to sky temperature (see Section 6.2.6).

6.2.6 Sensitivity Analysis of Models

The models of the unmodified and standard TN Conseil panels were examined to determine their sensitivity to various parameters.

6.2.6.1 Unmodified Panel

The influence of wind, front panel insolation, back panel insolation, panel tilt angle, ambient air temperature, ground temperature, sky temperature, and cell efficiency were investigated (see Table 6.5). When one parameter was varied, all others were held constant. The "standard conditions" around which the parameters were varied were wind speed of three m/s, front panel insolation of 600 W/m², back panel insolation of 200 W/m², panel tilt angle of 45 °, ambient air temperature of zero ° C, ground temperature of two ° C, sky temperature of -20 ° C, and cell efficiency of 10 percent. A summary of results is found in Table 6.4.

Table 6.4 Summary of Sensitivity Analysis of Model of Unmodified Panel, Without Snow

Parameter	Range	Cell Temp (C)	ΔT (C)	Linear
wind speed	0 to 20 m/s	26.2 to 8.0	18.2	no
front insolation	100 to 1000 W/m ²	2.7 to 25.8	23.1	yes
back insolation	0 to 400 W/m ²	13.7 to 17.7	4.0	yes
panel tilt angle	0 to 90 °	15.8 to 15.7	0.1	no
ambient air temp	-20 to 20 ° C	-3.0 to 34.5	37.5	yes
ground temp	-5 to 10 ° C	14.9 to 16.8	1.9	yes
sky temp	-30 to 5 ° C	14.8 to 18.5	3.7	yes
cell efficiency	0 to 10 %	17.4 to 15.8	1.6	yes

Over the range of parameter values studied, the temperatures of the different layers in the panel were linearly related to all parameters except wind speed, which had a strong non-linear effect, and panel tilt angle.

The most important parameters were wind speed, front panel insolation, and ambient air temperature. Ground and sky temperature, back panel insolation and cell efficiency played a minor role. Tilt angle was unimportant.

Table 6.5 Sensitivity Analysis of Unmodified Panel Model, Without Snow											
Run	Wind	Front	Back	T a	T s	T g	Tilt	C Eff	T fr	T c	T bk
	m/s	W/m2	W/m2	C	C	C	deg	%	C	C	C
Wind 0	0	600	200	0	-20	2	45	10%	24.8	26.2	25.7
Wind 1	1	600	200	0	-20	2	45	10%	20.3	21.7	21.2
Wind 3 Typ	3	600	200	0	-20	2	45	10%	14.4	15.8	15.3
Wind 5	5	600	200	0	-20	2	45	10%	11.9	13.3	12.8
Wind 8	8	600	200	0	-20	2	45	10%	9.9	11.3	10.7
Wind 12	12	600	200	0	-20	2	45	10%	8.4	9.7	9.2
Wind 20	20	600	200	0	-20	2	45	10%	6.7	8	7.5
Front 100	3	100	200	0	-20	2	45	10%	2.3	2.7	2.8
Front 400	3	400	200	0	-20	2	45	10%	9.6	10.6	10.3
Front 1000	3	1000	200	0	-20	2	45	10%	23.7	25.8	24.9
Back 0	3	600	0	0	-20	2	45	10%	12.5	13.7	13.2
Back 40	3	600	40	0	-20	2	45	10%	12.9	14.2	13.6
Back 100	3	600	100	0	-20	2	45	10%	13.5	14.8	14.2
Back 400	3	600	400	0	-20	2	45	10%	16.2	17.7	17.3
F+B 0	3	0	0	0	-20	2	45	10%	-2.1	-2	-1.9
Tilt 0	3	600	200	0	-20	2	0	10%	14.3	15.8	15.3
Tilt 90	3	600	200	0	-20	2	90	10%	14.5	15.7	15.1
Amb -20	3	600	200	-20	-40	-18	45	10%	-4.4	-3	-3.5
Amb -5	3	600	200	-5	-25	-3	45	10%	9.7	11.1	10.6
Amb +5	3	600	200	5	-15	7	45	10%	19.4	20.4	19.9
Amb +20	3	600	200	20	0	22	45	10%	33.1	34.5	34
Grnd -5	3	600	200	0	-20	-5	45	10%	13.6	14.9	14.4
Grnd +10	3	600	200	0	-20	10	45	10%	15.4	16.8	16.3
Sky -30	3	600	200	0	-30	2	45	10%	13.4	14.8	14.4
Sky 0	3	600	200	0	0	2	45	10%	16.6	17.9	17.3
Sky 5	3	600	200	0	5	2	45	10%	17.3	18.5	17.9
C Eff 0	3	600	200	0	-20	2	45	0%	16	17.4	16.9
C Eff 0.05	3	600	200	0	-20	2	45	5%	15.2	16.6	16.1

Additionally, the operating temperature of the panel with no insolation incident on the panel was investigated. All parameters except front and back insolation were held at the standard operating conditions listed above. This simulates night-time panel temperatures for clear skies. The temperature of the panel was found to be approximately two ° C below ambient air temperature.

For all parameter variations, the temperatures of the three model nodes-- the glass surface, the cell surface, and the back Tedlar-- were within two ° C of one another.

6.2.6.2 Standard TN Conseil Technology

The influence of wind, front panel insolation, back panel insolation, panel tilt angle, ambient air temperature, air cavity aspect ratio, and cell efficiency were investigated (see Table 6.7). As in Section 6.2.6.1, when one parameter was varied, all others were held constant. The standard conditions were wind speed of three m/s, front panel insolation of 600 W/m², back panel insolation of 200 W/m², panel tilt angle of 45 °, ambient air temperature of 0 ° C, ground temperature of 2 ° C, sky temperature of -20 ° C, and cell efficiency of 10 percent. A summary of results is found in the Table 6.6.

Table 6.6 Summary of Sensitivity Analysis of Model of Panel with TN Conseil Technology, Without Snow

Parameter	Range	Cell Temp (C)	ΔT (C)	Linear
wind speed	0 to 20 m/s	46.9 to 17.4	29.5	no
front insolation	100 to 1000 W/m ²	9.8 to 47.2	37.4	yes
back insolation	0 to 400 W/m ²	23.0 to 39.0	16.0	yes
panel tilt angle	45 to 90 °	31.1 to 32.3	1.2	no
ambient air temp	-20 to 20 ° C	13.4 to 48.7	35.3	yes
aspect ratio	30 to 120	31.1	0	
cell efficiency	0 to 10 %	33.8 to 31.1	2.7	yes

For the range of parameter values tested, the only parameters with a nonlinear effect on the panel temperature were wind speed and panel tilt angle.

Wind speed, front and back panel insolation, and ambient air temperature have the largest effect on panel temperatures. Panel tilt angle and cell efficiency are of minor importance. Over the range of 30 to 120, the aspect ratio has no effect.

Table 6.7 Sensitivity Analysis of TN Conseil Panel, Without Snow												
T ground = T amb + 2 degrees C												
Tsky = T amb - 20 degrees C												
Run	Wind	Front	Back	T amb	Tilt	Asp Rat	C eff	T fr	T c	T fl	T li	T lo
	m/s	W/m^2	W/m^2	C	degrees	()	%	C	C	C	C	C
Wind 0	0	600	200	0	45	120	10	44.5	46.9	47.0	13.7	12.2
Wind 1	1	600	200	0	45	120	10	37.9	40.3	40.5	10.0	8.6
Wind 3	3	600	200	0	45	120	10	28.6	31.1	31.3	5.9	4.8
Wind 8	8	600	200	0	45	120	10	20.9	23.4	23.7	3.4	2.5
Wind 20	20	600	200	0	45	120	10	14.8	17.4	17.7	1.9	1.3
T amb -20	3	600	200	-20	45	120	10	10.9	13.4	13.6	-13.8	-14.9
T amb 20	3	600	200	20	45	120	10	46.2	48.7	48.9	25.6	24.4
Front 100	3	100	200	0	45	120	10	8.8	9.8	10.1	1.7	1.4
Front 1000	3	1000	200	0	45	120	10	43.5	47.2	47.3	9.3	7.6
Back 0	3	600	0	0	45	120	10	21.1	23.0	22.8	4.2	3.4
Back 100	3	600	100	0	45	120	10	24.9	27.1	27.1	5.0	4.1
Back 400	3	600	400	0	45	120	10	35.9	39.0	39.6	7.7	6.2
F + B 0 *	3	0	0	0	45	120	10	-3	-3	-3	-1	-1
Tilt 60	3	600	200	0	60	120	10	29.0	31.4	31.7	5.6	4.8
Tilt 90	3	600	200	0	90	120	10	29.8	32.3	32.5	5.0	3.8
AR 30	3	600	200	0	45	30	10	28.6	31.1	31.3	5.9	4.8
C Eff 0	3	600	200	0	45	120	0	31.1	33.8	34.0	6.5	5.2
* estimate for h of convective heat transfer across cavity of h = 2.												
With T amb = T sky = T ground												
Tilt 90	3	600	200	0	90	120	10	31.6	34.1	34.3	6.7	5.5
Tilt 45	3	600	200	0	45	120	10	31.6	34.1	34.3	6.7	5.4

The model is formulated on the assumption that the absorber foil is hotter than the Lexan cover; if this is not the case, the natural convection in the air cavity is unstable and the model can not be used without guessing a value for h_{cav} . It appears that the model is not sensitive to h_{cav} under most conditions; in one instance, varying h_{cav} over two orders of magnitude resulted in a change in cell temperature of just over two °C. When there is no insolation on the panel, radiative cooling brings the temperature of panel below that of the Lexan cover. The clear night conditions detailed in the previous section resulted in a cell temperature of roughly -3 °C when h_{cav} was estimated at two $Wm^{-2}K^{-1}$.

For all parameter variations, the temperatures of the glass surface, the cell surface, and the back absorber foil nodes were within four °C of one another.

6.2.6.3 Discussion

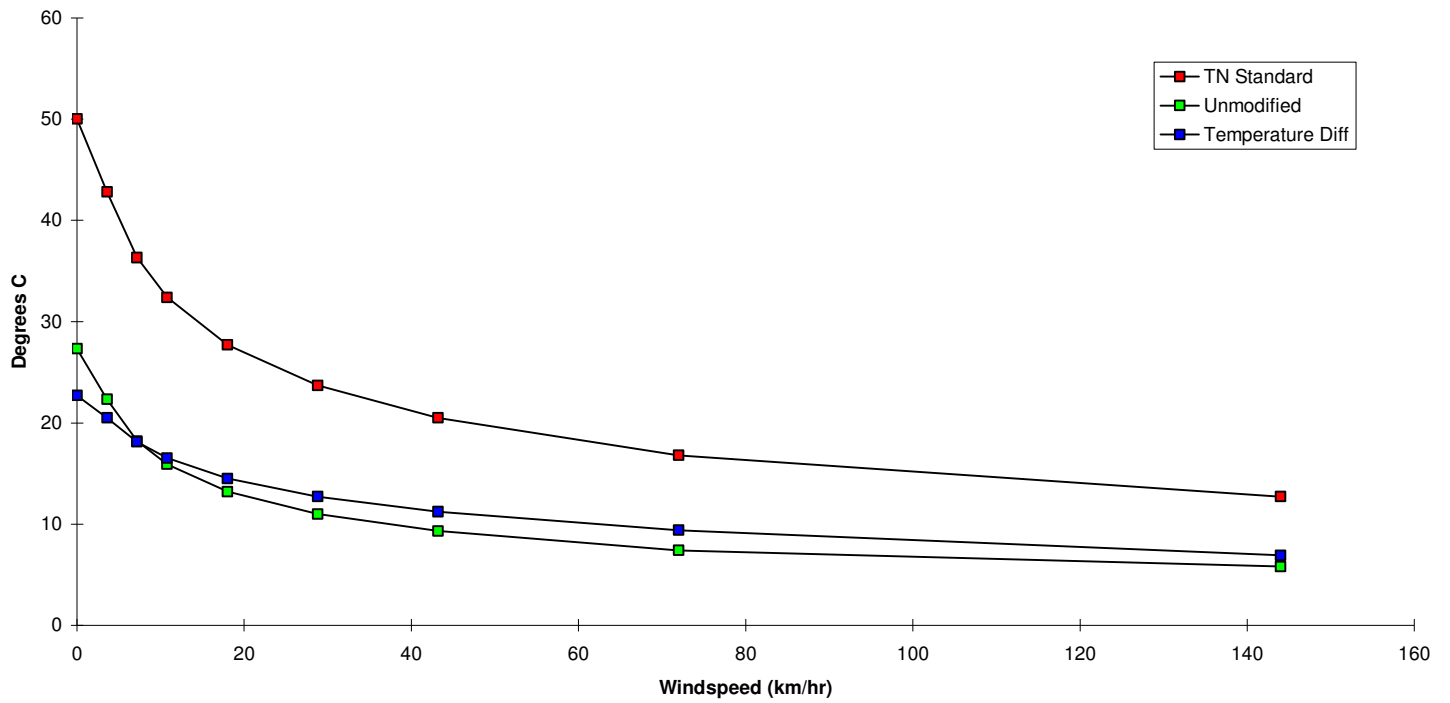
The addition of the black absorber foil and the back Lexan cover has two principle effects, both of which are expected. First, for daytime levels of insolation, it significantly raises the panel operating temperature. Second, it makes the level of insolation on the back panel an important operating parameter. It should be noted, however, that even with no insolation on the back panel the TN Conseil panel is considerably warmer than the unmodified panel when there are daytime levels of insolation on the front panel. This is due to the insulating effect of the back cover.

The model suggests that the TN Conseil panel will be cooler at night than the control panel. This is supported by the observations and argument contained in Section 6.1.2.

The wind speed is the only significant parameter with a non-linear effect on the thermal performance of the panel. In order to investigate the effect of wind on panel temperature, the panel surface temperature for a fixed ambient air temperature and panel insolation level was plotted as a function of wind speed (Figure 6.9). The temperature drops significantly upon increasing the wind speed from still air conditions, but the effect of wind decreases as the wind speed increases. Thus, for these particular conditions, the temperature of the TN Conseil panel drops about 37 °C for a change in wind speed of zero to 144 km/hr, with 50 percent of this decrease occurring between the wind speeds of zero and 12 km/hr.

For any increase in wind speed, the temperature of the TN Conseil panel drops more than that for the unmodified panel. In this sense, the TN Conseil panel is more sensitive to wind speed. However, for a given level of insolation, it is only at an infinite windspeed that the temperatures of the two panels converge, at the ambient air temperature. Thus, for daytime insolation conditions and any finite wind speed, the temperature of the TN Conseil panel will be higher than the temperature of the unmodified panel.

Figure 6.9 Modelled Effect of Windspeed on Panel Surface Temperature, $T_{amb} = 0\text{ C}$, Insolation = 700 W/m^2 front and 200 W/m^2 back



6.2.7 Comparison of Modelled and Observed Performance

To validate the models of this Chapter, their performance was compared with that of the panels installed at the roof-top array at Varennes (see Section 6.1.1). Unfortunately, the comparison is imperfect for two reasons. First, the models are for a Siemens M55 panel, whereas the panels on the roof are manufactured by Astropower. These panels are quite similar, however, so the performance of the two should be close. Second, as mentioned in Section 6.1.1, the pyranometers used to measure the front and back insolation levels were improperly interfaced for much of the winter. While the front panel insolation can be inferred from the short-circuit current of the panels, the rear panel insolation must be estimated from the ratio of the front to the back pyranometer readings and the correction factor by which the front pyranometer reading must be multiplied to equal the insolation level inferred from the panel short-circuit current. While these two complications prevent an exact comparison, the performance of the model should roughly correspond to that of the monitored panels.

The back panel temperatures predicted by the model for the unmodified panel and the TN Conseil panel were compared with the measured temperatures for sixteen different points in time during the period of February through early May. The modelled temperatures of the panel with black nickel foil back and no Lexan back cover was compared with the measured performance of the copper foil-backed panel, also without back cover, for twelve of these sixteen cases. It should be noted that the nickel foil results in higher operating temperatures than the copper foil (see Section 6.1.3). The sixteen test cases cover a vast range of operating conditions: ambient air temperatures from -17 to 23°C , wind speeds of two to 47 km/hr , and front-panel insolation levels from zero to 1060 W/m^2 .

The measured relative humidity was used to calculate the dewpoint and thence the sky temperature. A value for the diffuse fraction was guessed from a comparison of the actual level of insolation and the level of insolation that would occur if skies were perfectly clear. Fortunately, the diffuse fraction does not strongly affect the results: it affects only the fraction of the radiation incident on the front panel that is treated as incident at 60° , rather than $\text{zero}^{\circ}\text{C}$ (see Section 6.2.3.1).

The results are shown in Table 6.8. They are plotted as a function of insolation (Figure 6.10), wind speed (Figure 6.11) and temperature (Figure 6.12). The error is three to four $^{\circ}\text{C}$ for all three models, with a standard deviation of three to five $^{\circ}\text{C}$. All three models appear to overestimate the panel temperature; it is not known whether this bias is due to differences between the Siemens and the Astropower panels.

The error of the model compared with the measured results appears relatively independent of ambient air temperature but strongly related to wind speed and insolation. It also appears to increase significantly with decreasing wind speeds. This can not be attributed solely to the fact that at higher wind speeds the temperature of the panel tends to deviate less from the ambient air temperature; two of the three test cases for winds at or above 25 kilometres per hour had

Table 6.8 Comparison of Thermal Model and Monitored Performance															
Date	Time	T amb C	Wind km/hr	Insolation		R Hum %	Experimental Results			Model Results			Error C	No Lex C	Error C
				Front W/m^2	Back W/m^2		Control C	TN C	No Lex C	Control C	Error C	TN C			
2-Feb	9:45	-17	7	760	55	49	1	21		5	5	23	3	11	
26-Feb	15:45	-11	2	550	45	36	8	26		10	2	26	0	18	
2-Mar	12:35	-6	2	1060	175	50	23	55		37	15	69	14	56	
2-Mar	14:45	-4	12	820	155	42	17	42		16	-1	36	-6	23	
19-Mar	12:05	13	4	1030	55	35	39	63	47	45	6	68	5	50	2
28-Mar	9:30	8	9	740	45	45	18	35	26	25	8	41	7	31	5
2-Apr	5:15	-2	3	0	0	55	-9	-11	-9	-6	3	-8	2	-7	2
2-Apr	11:50	6	14	1010	55	22	20	43	29	28	8	47	4	33	4
3-Apr	10:50	9	25	810	70	21	20	36	25	23	3	37	1	27	2
4-Apr	16:20	3	38	450	50	68	7	14	8	9	2	16	3	11	3
5-Apr	13:15	-6	47	770	75	40	1	15	3	5	4	17	2	8	5
6-Apr	10:50	-3	14	810	60	35	15	35	21	15	-1	31	-4	20	-2
29-Apr	11:05	13	17	260	40	77	14	19	16	17	3	21	2	18	2
4-May	15:10	23	15	420	55	23	30	41	34	30	0	38	-3	33	-1
5-May	9:30	17	4	580	60	46	26	40	32	34	8	48	8	41	9
9-May	13:40	23	7	890	65	22	39	60	45	46	7	64	4	53	8
									Ave error:		4		3		3
									Stand dev:	3.9504		4.7125			3.1722

Figure 6.10 Model Error as a Function of Insolation

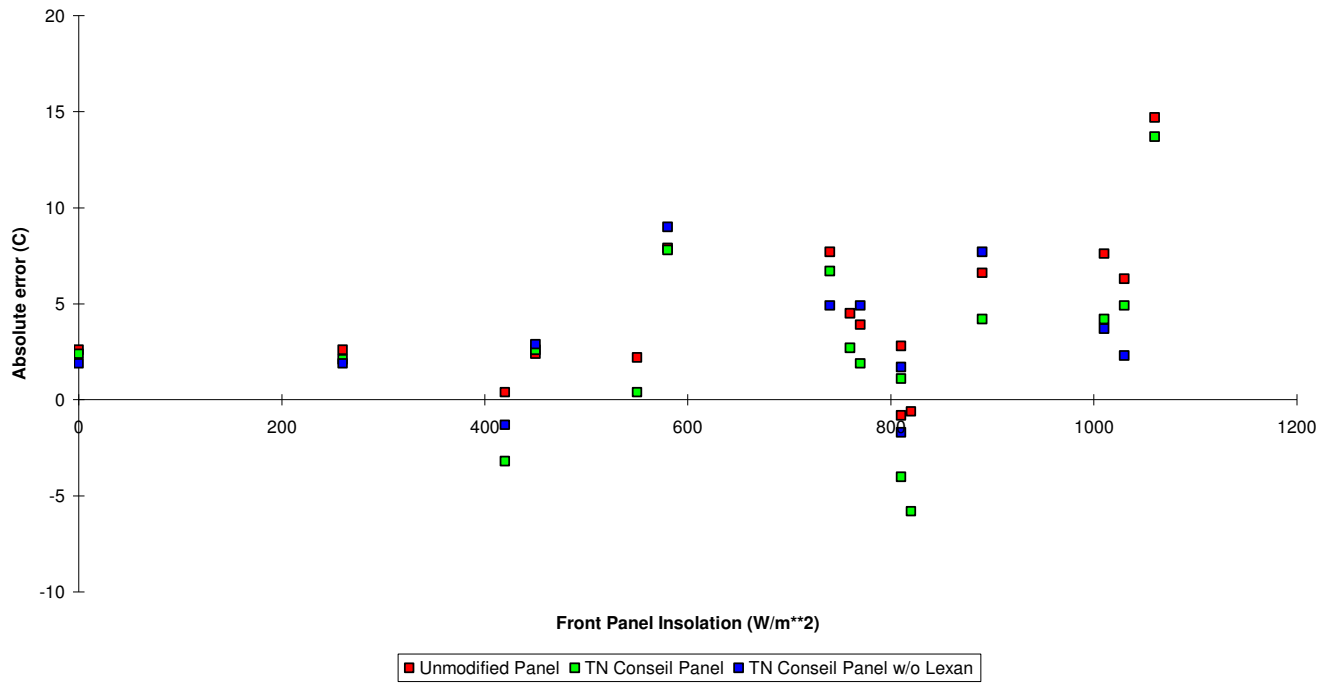


Figure 6.11 Model Error as a Function of Windspeed

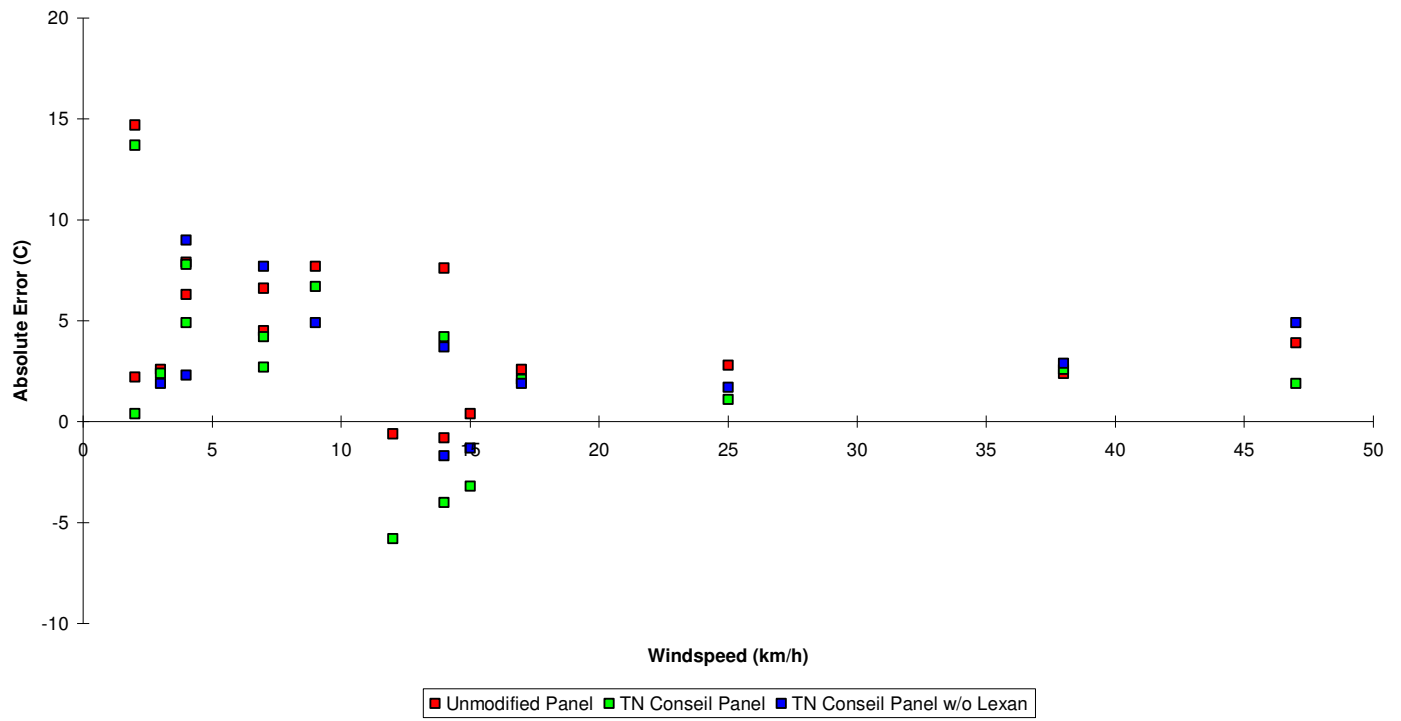
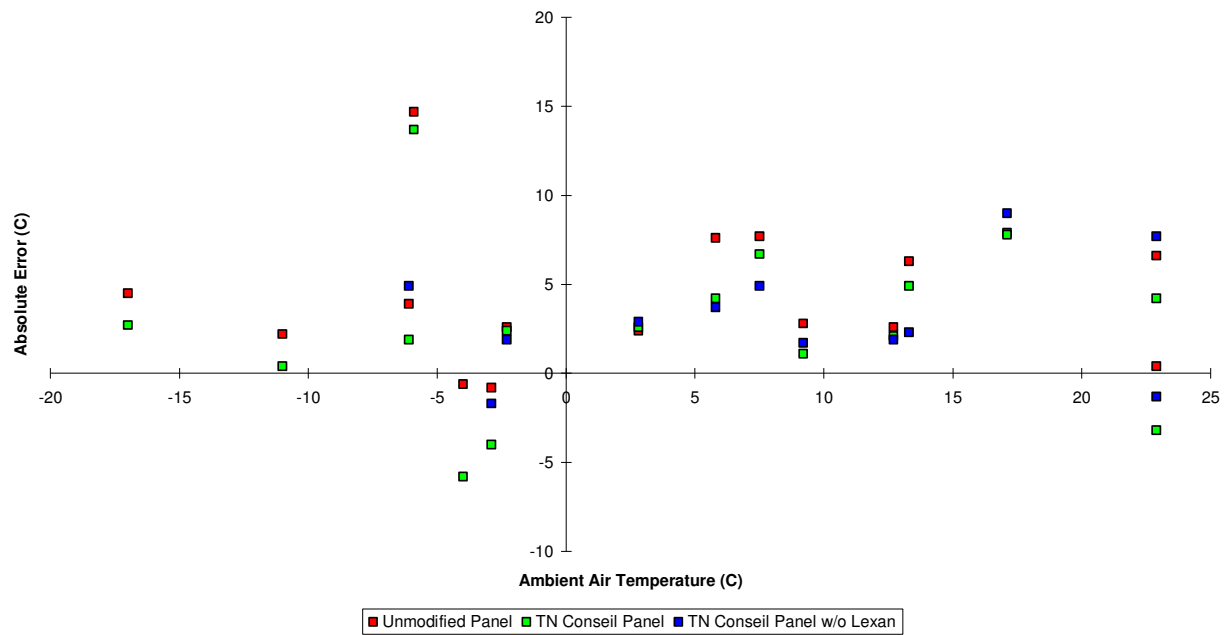


Figure 6.12 Model Error as a Function of Ambient Air Temperature



insolation levels exceeding 750 W/m^2 , resulting in panel temperatures much higher (up to 27°C for the TN Conseil panel) than ambient air temperature. The model appears to be increasingly inaccurate at higher insolation levels also; however, this may be an artifact of the estimates for insolation level. A 10 % error in the estimate will translate into 100 W/m^2 at a front panel insolation level of 1000 W/m^2 but only 40 W/m^2 at 400 W/m^2 . The former insolation level will heat the panel significantly more than the latter, and the error will reflect this.

6.2.8 Comparison of Predicted Thermal Performance for Different Models

The six models described in Sections 6.2.1.1 through Sections 6.2.1.6 were used to compare the predicted panel surface temperature for winds of 3, 10, and 25 km/hr. A back panel insolation level one-third that of the front panel insolation level was assumed; to investigate the importance of this fraction the models were also tested assuming a back panel isolation one-fifth that of the front panel insolation level, but for a wind speed of 10 km/hr only.

The results are presented in Figures 6.13, 6.14, 6.15, and 6.16. The results are given for an ambient air temperature of -10°C ; a different ambient air temperature would linearly shift the panel surface temperature. For insolation levels above 100 W/m^2 on the front panel, the panel with the highest surface temperature is the standard TN Conseil technology, followed by the black Tedlar back with Lexan, the Thermoclear, the nickel foil without Lexan, the black Tedlar without Lexan, and the unmodified panel. At very low insolation levels-- at night, for instance-- the models indicate that this ordering is reversed; an explanation for this is given in Section 6.1.2. The difference between the panel temperatures of various configurations increases linearly with increasing insolation levels.

The insulating effect of the Lexan back cover becomes increasingly apparent at higher wind speeds. In terms of panel temperatures, two groups emerge: the panels with a back cover and the Lexan Thermoclear operate at a range of high panel temperatures, and the panels without a back cover operate at a range of much lower temperatures.

Decreasing the back panel insolation level did not significantly alter the results. Panel temperatures stayed slightly closer to the ambient air temperature. This is not surprising since the front panel radiation is the principal energy flux in these tests. Were the front panel insolation very low, as is the case when there is snow or ice on the front of the panel, the effect of decreasing the back panel insolation level would be more noticeable.

The temperatures of the panels equipped with nickel foil are considerably higher than those of the panels with a black Tedlar back. This is due to both the lower solar absorptance and the higher emittance of the black Tedlar.

The Lexan Thermoclear-equipped panel operates at a lower temperature than the standard TN Conseil-modified panel because the two Lexan sheets in the Thermoclear decrease radiation transmission to the absorber foil and the ribs conduct heat across the air cavity.

Figure 6.13 Comparison of Modelled Panel Surface Temperature, $T_{amb} = -10\text{ C}$, Wind = 3 km/h, Back Insol = Front/3

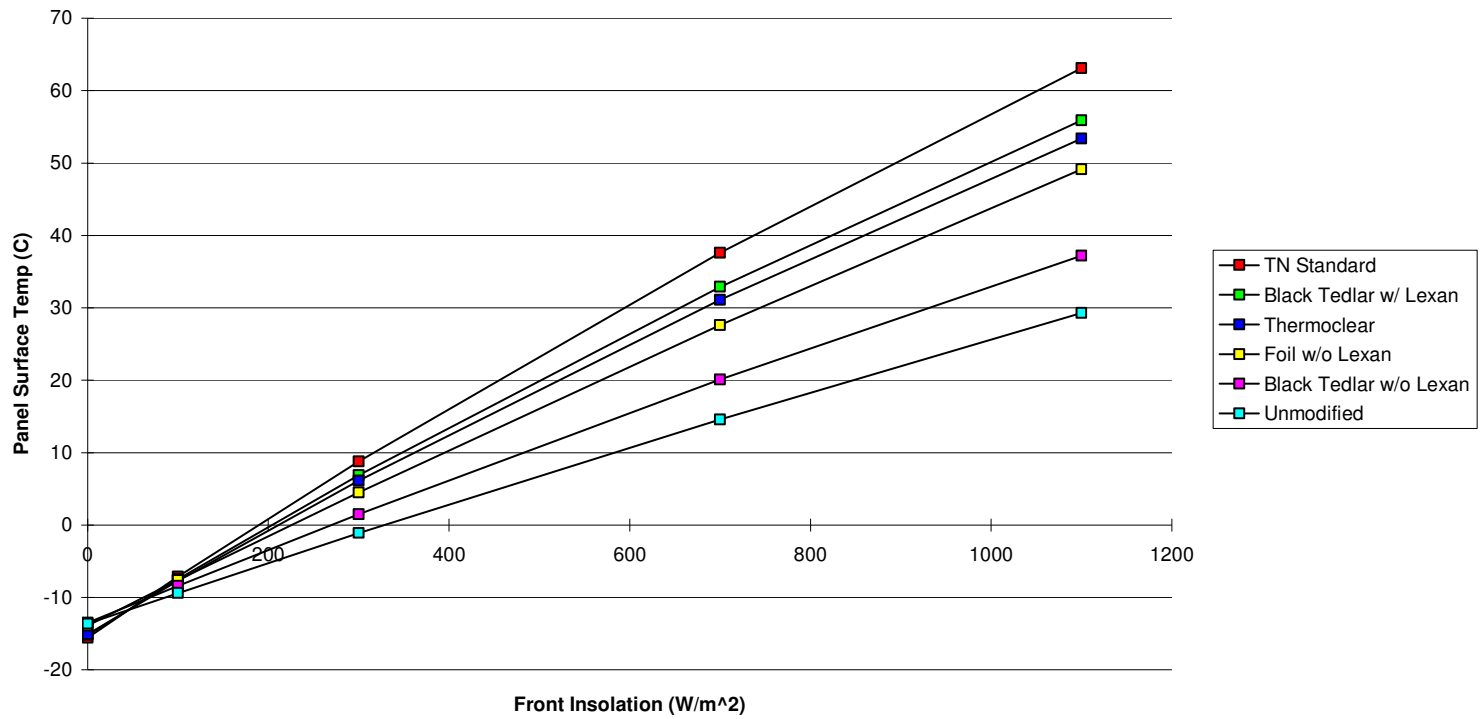


Figure 6.14 Comparison of Modelled Panel Surface Temperature, $T_{amb} = -10\text{ C}$, Wind = 10 km/h, Back Insol = Front/3

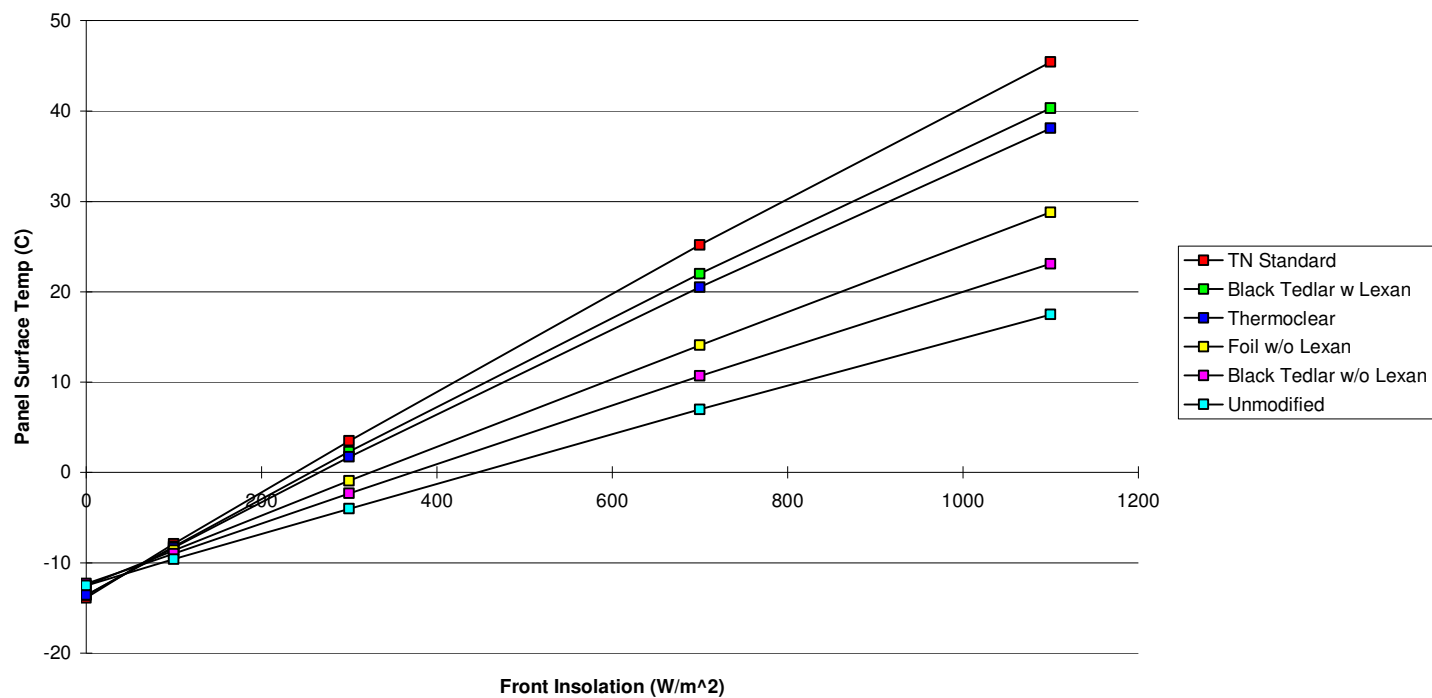


Figure 6.15 Comparison of Modelled Panel Surface Temperature, $T_{amb} = -10\text{ C}$, Wind = 25 km/h, Back
Insol = Front/3

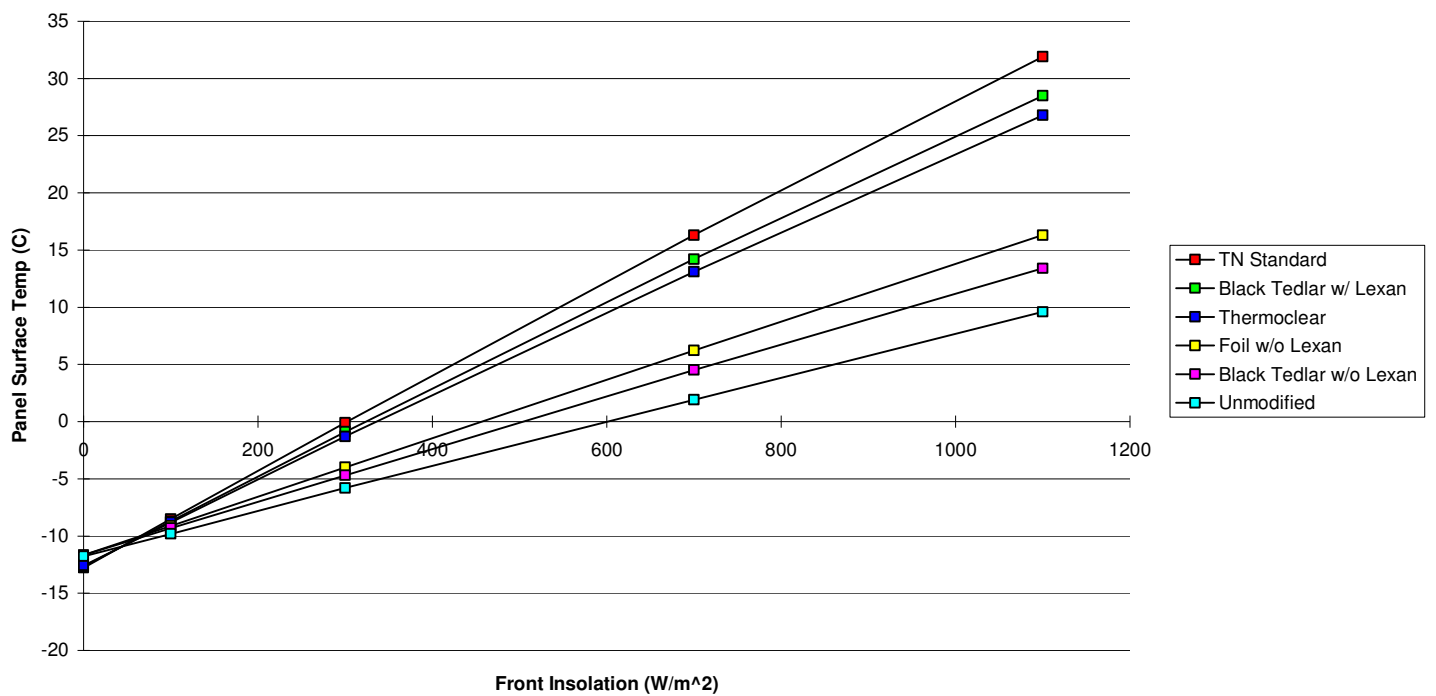
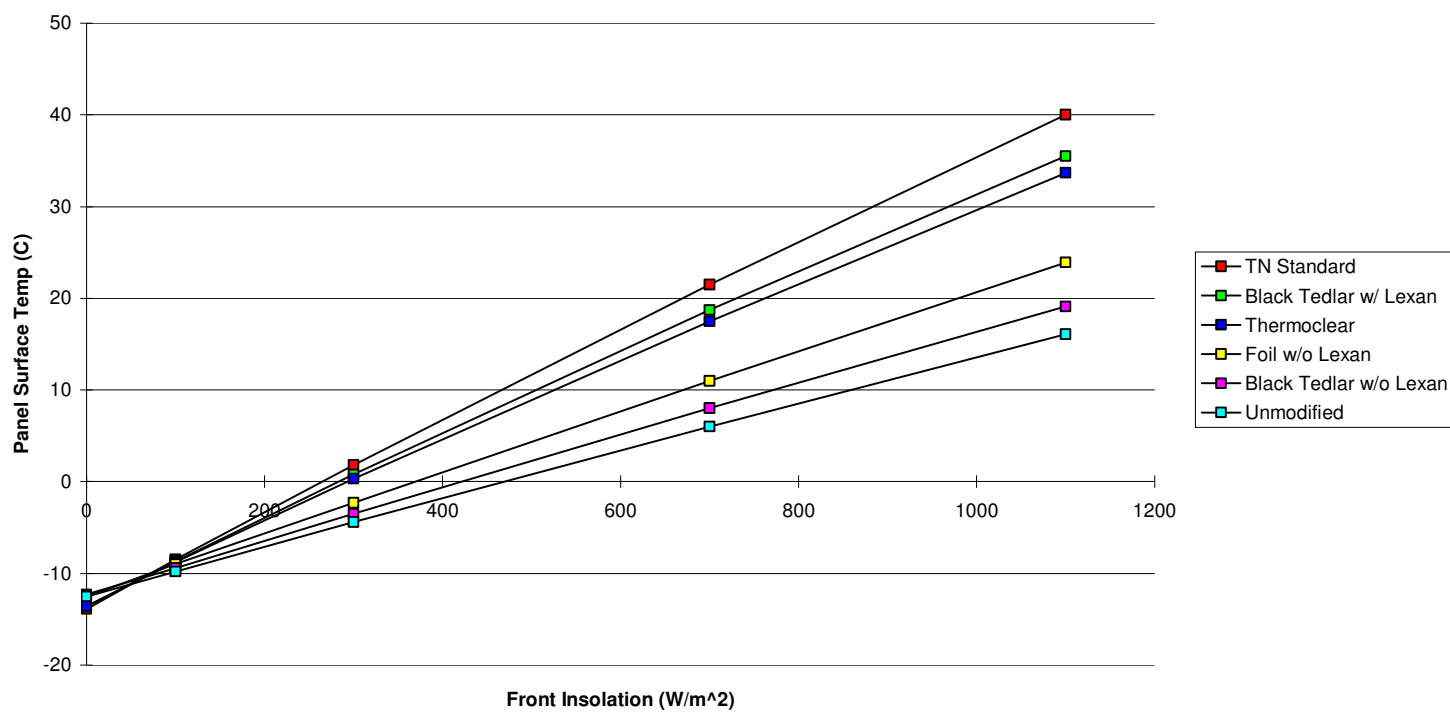


Figure 6.16 Comparison of Modelled Panel Surface Temperature, $T_{amb} = -10\text{ C}$, Wind = 10 km/h, Back Insol = Front/5



6.2.9 Model Deficiencies

As with all models, the thermal models developed here do not reflect perfectly the real world. The models have three principal failings. First, they treat convective cooling by wind in an overly simplified manner. Second, the models assume that the panel is at uniform temperature in the plane of the panel. Third, for the models of a panel with a Lexan back cover or with Thermoclear, the natural convection in the air cavity is treated in a very approximate manner.

The wind flow around a PV array and the resulting cooling of the panels in the array is poorly understood. The relation used in the models of this chapter is an empirical relation that does not account for the direction of the wind with respect to the array, the size of the array, or the turbulence caused by surrounding obstacles. Determining such a relation might be impossible; nevertheless, a more accurate convective cooling coefficient might significantly increase the model's accuracy. While this would aid in comparing the performance of different panel configurations under specified conditions, it probably could not be used to predict the performance of a PV array at a particular location, since in most cases the wind velocity at the site would be unknown.

The panel surface temperature is not uniform in the plane of the panel. As documented in Section 6.1.5, there exist temperature gradients, caused by natural convection in the air cavity of the TN Conseil-modified panels and heat transfer to the panel frame. In addition, if a panel were partially covered in snow, the areas covered in snow would have a different temperature from those that were uncovered; a similar effect would occur for areas shaded by obstructions, leaves, or bird droppings. Due to obstacles behind the panels and shading of the ground by the array itself, the back panel insulation will not usually be uniform, either. The models can not account for these phenomena, which are "two dimensional" in the plane of the panel.

The natural convection in the air cavity of the TN Conseil-modified panel models is treated in a rather approximate manner. The model finds an average heat loss for the panel. This ignores the temperature gradients caused by the natural convection. Further, it has not been verified that the method used for the Thermoclear is accurate. In studies of honeycomb insulation [Charters et al., 1972], researchers found that under some conditions natural convection "roll cells" became established in the compartments. These roll cells efficiently circulated the air in the compartment and resulted in a higher heat loss. This possibility has not been investigated here.

CHAPTER 7

SNOW AND ICE REMOVAL FROM PHOTOVOLTAIC PANELS

To evaluate the TN Conseil Technology, its ability to hasten the removal of snow and ice from a PV panel must be determined. In order to do this, models developed in Chapter 6 were modified to account for a uniform cover of snow or ice on the front face of the panel. These models were used to compare the performance of the different panel configurations.

As observed previously, snow and ice are extraordinarily complex phenomena. The models, however, can not account for much of this complexity and therefore the predicted performance of the panel may not match that observed in the field. Thus, the differences between real-life operation and the panel operation predicted by the models developed previously are discussed herein. This entails an examination of the thermal performance of the PV panel's aluminum frame and an investigation into the effects of rime icing on both the front and back faces of the panel.

7.1 Background

7.1.1 Natural Mechanisms of Snow and Ice Removal

There are a number of mechanisms that contribute to snow and ice removal from any PV panel. Many of these cannot be factored into the models that follow, since the mechanisms are extraordinarily difficult to quantify.

The panel tilt angle not only affects snow and ice accumulation on a PV panel, but, through gravity, it determines the force motivating the snow or ice to slide off the panel. As discussed in Section 2.2.3.3, the tendency of snow or ice to slide off the panel is related to the sine of the panel tilt angle.

When the surface of a snow- or ice-covered PV panel attains a temperature higher than that of the snow or ice on its surface, heat is transferred to the snow or ice. If the temperature of the snow or

ice is below the freezing point, this heat will warm the snow or ice. When the snow or ice attains the freezing point, the heat will cause melting. The mixture of water and snow or ice thus created on the panel surface will remain at zero °C and not sustain a temperature gradient across it (see Section 2.2.3.1)

As a significant layer of water forms, some water will be transported to other parts of the panel. For tilted panels, it will run down the panel, thus convecting heat to the snow or ice below it. Water will be drawn into nearby snow or rime crystals, causing them to become wet.

Should this water refreeze, a heat transfer with the environment equivalent to the latent heat of fusion will occur. Snow or ice in the vicinity of this freezing water will be warmed in the process.

Solar radiation incident on the snow or ice covering the front of the panel will be transmitted, reflected and absorbed by the cover. As discussed in Section 3.1.4, most of the solar energy will be either transmitted to the panel surface or back-scattered and returned to the environment. However, some of the radiation will be absorbed by the snow or ice, and this will cause warming within the accumulation, and not just at the panel-accumulation interface. This is especially true when the snow or ice is old and/or has many impurities in it.

Snow and ice have a high emissivity, and the surface of an accumulation will, in general, radiate energy to the sky.

Wind on the accumulation surface will cause heat transfer by convection and, if forceful enough, physical removal of snow and possibly ice.

Snow cover on the ground is subject to many of these removal mechanisms also. Snow cover that has remained on the ground for several weeks or more is stratified into layers having different properties that reflect the thermal history of the snow cover [Langham, 1981, p. 276]. Long-lived snow cover on PV panels may be similar.

7.1.2 Observed Snow Removal

The photographs in [TN Conseil, 1994] and observations of the roof-top array at the EDRL have shown that, broadly speaking, there are at least two ways in which freshly-fallen snow removes itself from PV panels.

"Shedding" is the first way in which snow removes itself from PV panels. The snow on the panel, acting as a sheet, slides down the panel *en masse*. The slide can be abrupt and the velocity of the sheet high, or, more rarely, the sheet of snow may slip very slowly down the face. Although the entire sheet of snow may fall off at once, sometimes the sheet stops part of the way down the face, and the panel remains partially covered. The snow that is protruding from the end of the panel either falls to the ground or rests on a panel below.

The second way that snow removes itself is by melting. The centre of the panel develops a "hole" where the snow cover has melted away. This hole enlarges itself towards the edges of the panel.

In general, snow is removed in a combination of these two ways. Often the result is a crescent of snow that remains at the bottom of the panel. The crescent runs part way up the edges of the panel, near the frame.

Snow removal by wind was not observed. This is probably a result of this being a gradual mechanism of snow-removal, and therefore less noticeable than the above mechanisms.

Unfortunately, there has been no occasion to observe either rime ice or aged snow removal. It is speculated that these accumulations would be more securely attached to the panel, and would have a tendency to melt rather than shed.

7.2 Modelled Panel Performance

The models of the unmodified panel and the standard TN Conseil-modified panel were altered to account for a layer of snow or ice on the front face of the panel. Only these two models were used. It was assumed that the snow-melting performance of the other panel configurations would rank between the performance of these two panels, roughly in the order indicated in Section 6.2.9.

Snow or ice on the front of the panel requires additional assumptions and idealizations in the thermal model. As will be shown, the predicted performance of the panels is highly dependent upon the properties of the snow or ice cover. However, for a specified set of properties, a comparison of the performance of the two different panel configurations should be valid, i.e., the comparison will indicate which configuration will remove the snow or ice more quickly.

7.2.1 Description of Model

The models used in this section are the unmodified panel model, described in Section 6.2.1.1, and the model of the panel equipped with the standard TN Conseil technology, described in Section 6.2.1.2, with the following alterations:

- 1) A node, "Snow surface temperature" has been added. This represents the temperature of the exterior surface of the snow or ice cover on the front face of the panel.
- 2) The terms for radiation to the ground and sky and convection to the ambient air that were previously associated with the glass temperature node have been moved to the snow surface temperature node.
- 3) An additional energy flow has been added. This energy flow represents the heat used to melt snow or ice at the glass surface when that snow or ice has reached a temperature of zero °C. That is, this heat is used to overcome the latent heat of fusion of the snow or ice.

- 4) An additional set of constraints has been added. The glass temperature node must remain at or below zero ° C. When it is below zero ° C, the heat transfer resulting in melting is zero. When it is at zero ° C, the heat transfer resulting in melting is greater than or equal to zero.
- 5) The solar radiation incident on the cell is equal to the radiation that penetrates the snow or ice cover, computed in the manner described in Section 3.1.4.2, multiplied by the transmittance-absorptance product for the snow-covered panel. Since light reflected from the cell surface will tend to be reflected back to the cell by the snow or ice cover, the transmittance absorptance product for a snow- or ice- covered panel will be higher than for a clear panel. It has been assumed that the transmittance-absorptance product for the front panel is 0.90, which is slightly higher than 0.87, the value of the transmittance absorptance product for diffuse radiation incident on a panel free of cover.

7.2.2 Impact of Accumulation Thickness on Panel Surface Temperature

An accumulation of snow or ice on the surface of a PV panel has two principal effects. First, it provides an insulative cover that reduces heat loss from the glass surface. Second, it attenuates the solar radiation incident on the panel.

The heat loss through the snow or ice cover is given by the conduction equation (Eq. 6.3) in Section 6.2.2.2. Thus, the heat loss is inversely proportional to the accumulation thickness. As discussed in Section 3.1.4.2, the fraction of the solar radiation transmitted through the snow or ice cover decreases exponentially with increasing cover thickness. The coefficient of thermal conduction for the particular type of snow or ice on the panel is the proportionality constant in the former; the accumulation's extinction coefficient appears in the exponent for the latter. Both these parameters vary widely for different types of snow and ice. Thus, the thickness of the accumulation is a critical determinant of the temperature of the panel and the energy available to melt the accumulation. In addition, the thermal behaviour of the panel will strongly depend on the type of snow or ice on the panel.

These conclusions are illustrated in Figure 7.1, which shows, as a function of snow or ice cover thickness, the ambient air temperature at which the glass surface of a covered, unmodified panel will be at zero ° C. Curves are shown for glaze and four types of snow. A front panel insolation level of 600 W/m², back panel insolation level of 200 W/m², wind speed of 3 m/s, ground temperature two ° C below the ambient air temperature, and sky temperature 20 ° C below ambient air temperature are assumed.

There are significant differences between the curves for the different accumulation types. The curve for glaze, slightly densified snow and fresh, light snow all have a minimum at a non-zero thickness, whereas this does not appear for the densified snows. The curves for densified snow, on the other hand, increase monotonically to a thickness of about ten cm, at which point they begin to gradually decrease.

Figure 7.1 Modelled Effect of Snow Cover Thickness on Critical Air Temperature for Melting (Unmodified Panel)

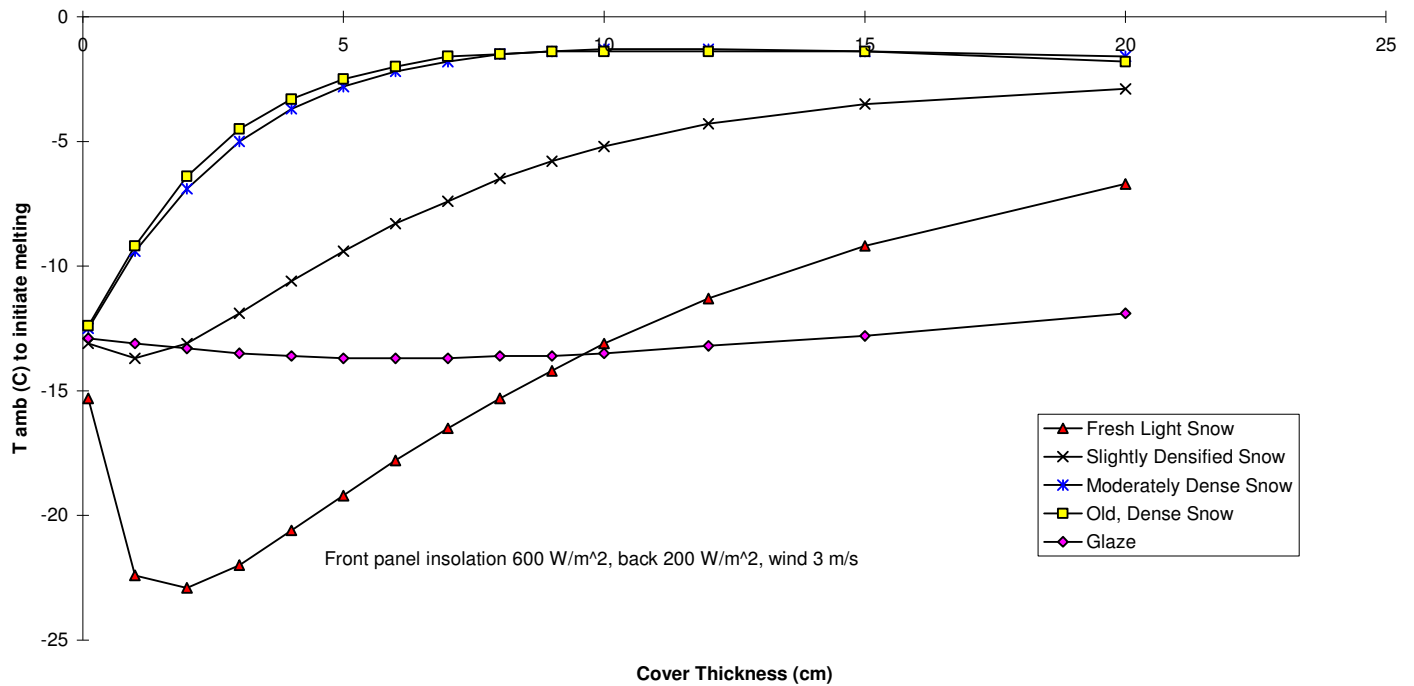
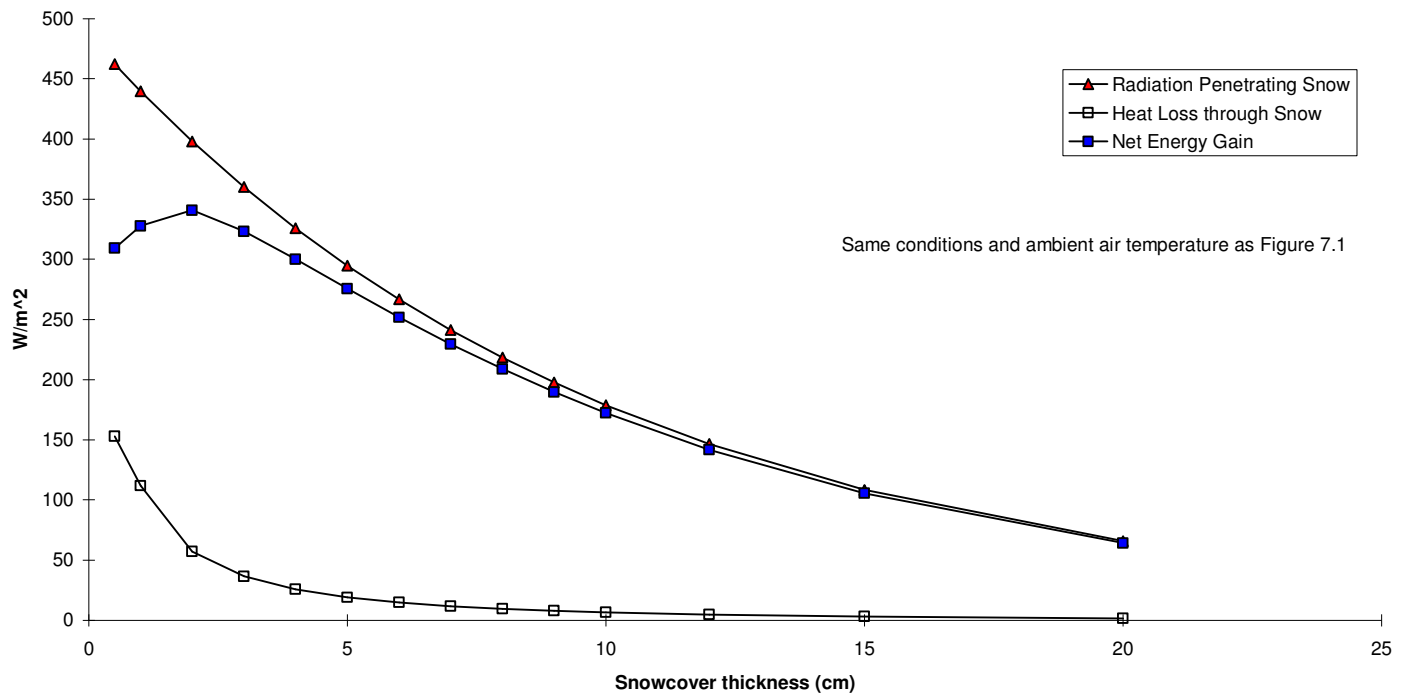


**Figure 7.2 Modelled Effect of Snowcover Thickness on Heat Conduction and Solar Radiation Penetration,
Fresh Light Snow (Unmodified Panel)**



The differences between these curves can be understood if one examines the role of the accumulation thickness on the net energy gain of the front panel. This is shown in Figure 7.2 for the case of fresh, light snow. The minimum observed in the ambient air temperature curve of Figure 7.1 is reflected as a maximum in the net heat gain through the snow cover. With the denser snow, this minimum disappears: the extinction coefficient and the coefficient of thermal conduction are larger, so the solar radiation that passes through the snow is lower while the heat losses are greater. This results in a net energy loss or an insignificant net gain. Glaze has a high coefficient of thermal conduction but a very low extinction coefficient. Thus, the fraction of solar radiation transmitted through glaze appears almost linear with thickness. This is reflected in the nearly flat curve for glaze observed in Figure 7.1. The decrease in the ambient air temperature required for melting for moderately dense and dense snow at thicknesses greater than 10 cm can be attributed to the fact that at these thicknesses radiation penetration is essentially insignificant, while heat losses continue to decrease with thickness.

The effect of accumulation thickness for rime will be similar to that of snow with similar extinction coefficient and coefficient of thermal conduction.

7.2.3 Critical Temperature Assumption

One way of modelling snow removal is to assume that once the entire surface of an inclined piece of glass reaches zero °C, all snow on the surface will be shed immediately [Schuyler]. This implies that there is a perfect bond between the snow and the glass at surface temperatures of less than zero °C and that at zero °C a very thin layer of meltwater lubricates the snow-glass interface, making it essentially frictionless.

To apply this critical temperature assumption to the models developed above, the locus of operating conditions that maintains the surface at zero °C is found. This is shown for light, fresh snow in Figure 7.3, for slightly densified snow, in Figure 7.4, for moderately dense snow, in Figure 7.5, and for rime, in Figure 7.6. The locus is plotted as a series of lines, each corresponding to a different combination of panel configuration (TN Conseil or unmodified), wind speed (two, five, or ten m/s), and accumulation thickness (two, five, or ten cm). The lines represent, for a given level of front panel insolation incident on the accumulation surface, the ambient air temperature at which the surface of the panel will be at zero °C. Melting, and therefore shedding, will occur at all ambient air temperatures above the line. The back panel insolation is assumed to be one-quarter of the front panel insolation. Ground and sky temperatures are assumed to be two and 20 °C below the ambient air temperature, respectively.

Several conclusions may be drawn from these results. First, regardless of the nature of the accumulation on the panel surface, for a given wind speed and insolation level, the TN Conseil modified panel will remove the accumulation at an ambient air temperature much lower than that required for melting by an unmodified panel. For example, with a 10 m/s wind, peak sun front panel insolation, and a 10 cm thick rime or moderately dense snow accumulation, the panel surface will reach zero °C at an ambient temperature of about -3 °C for the unmodified panel

Figure 7.3 Modelled Critical Ambient Air Temperature to Initiate Melting for Light, Fresh Snow

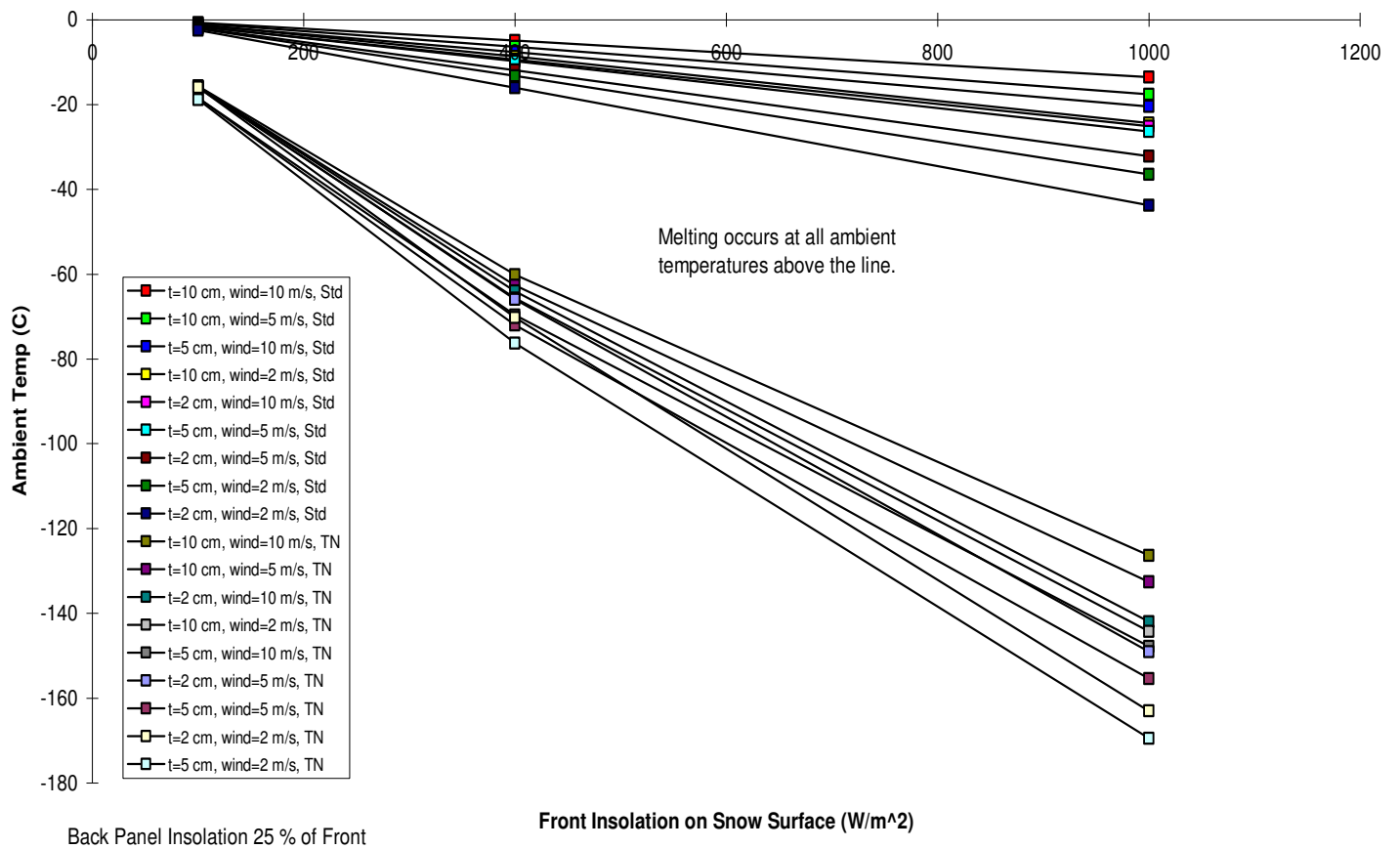
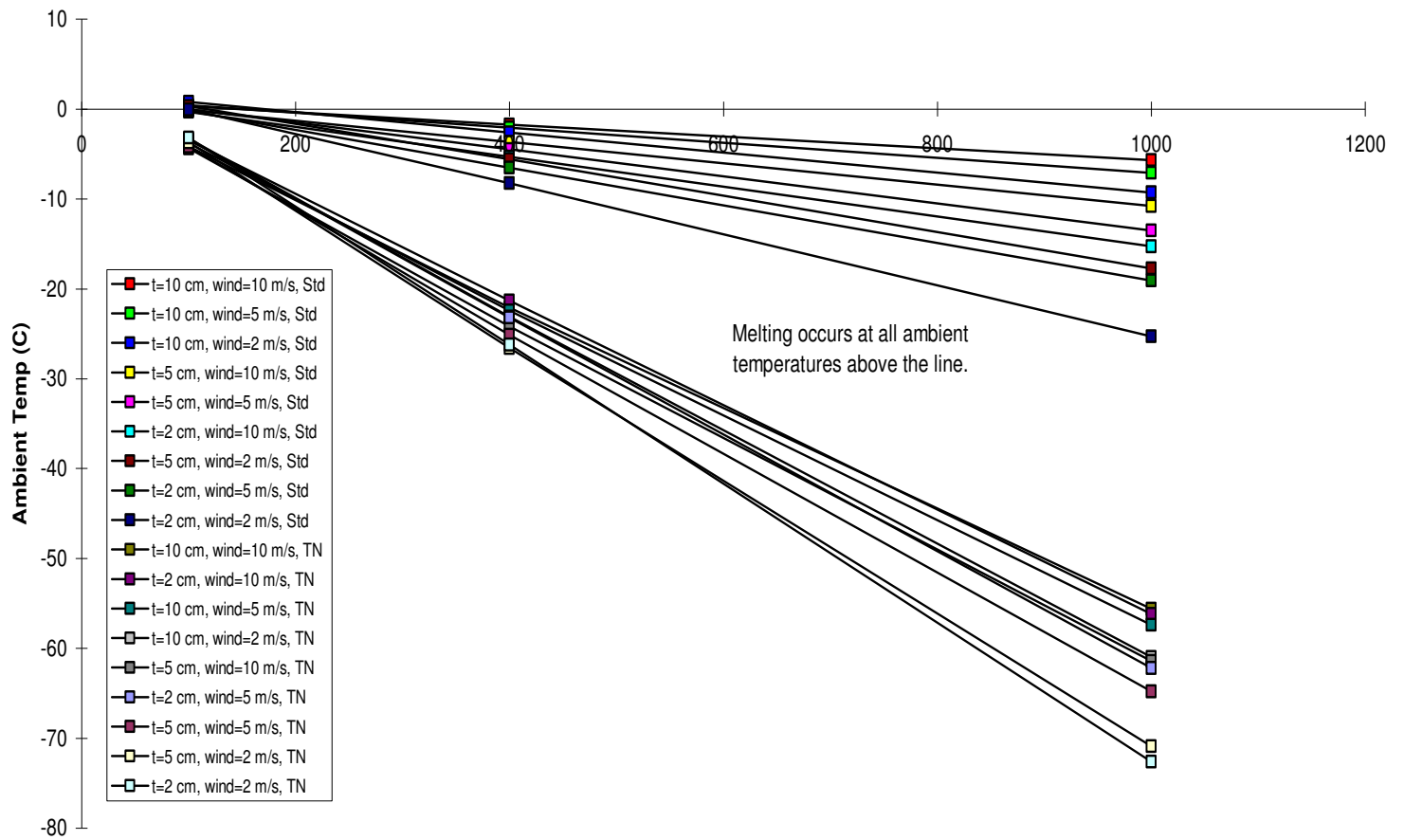


Figure 7.4 Modelled Critical Ambient Air Temperature to Initiate Melting for Slightly Densified Snow



Back Panel Insolation 25 % of Front

Front Insolation on Snow Surface(W/m²)

Figure 7.5 Modelled Critical Ambient Air Temperature to Initiate Melting for Moderately Dense Snow

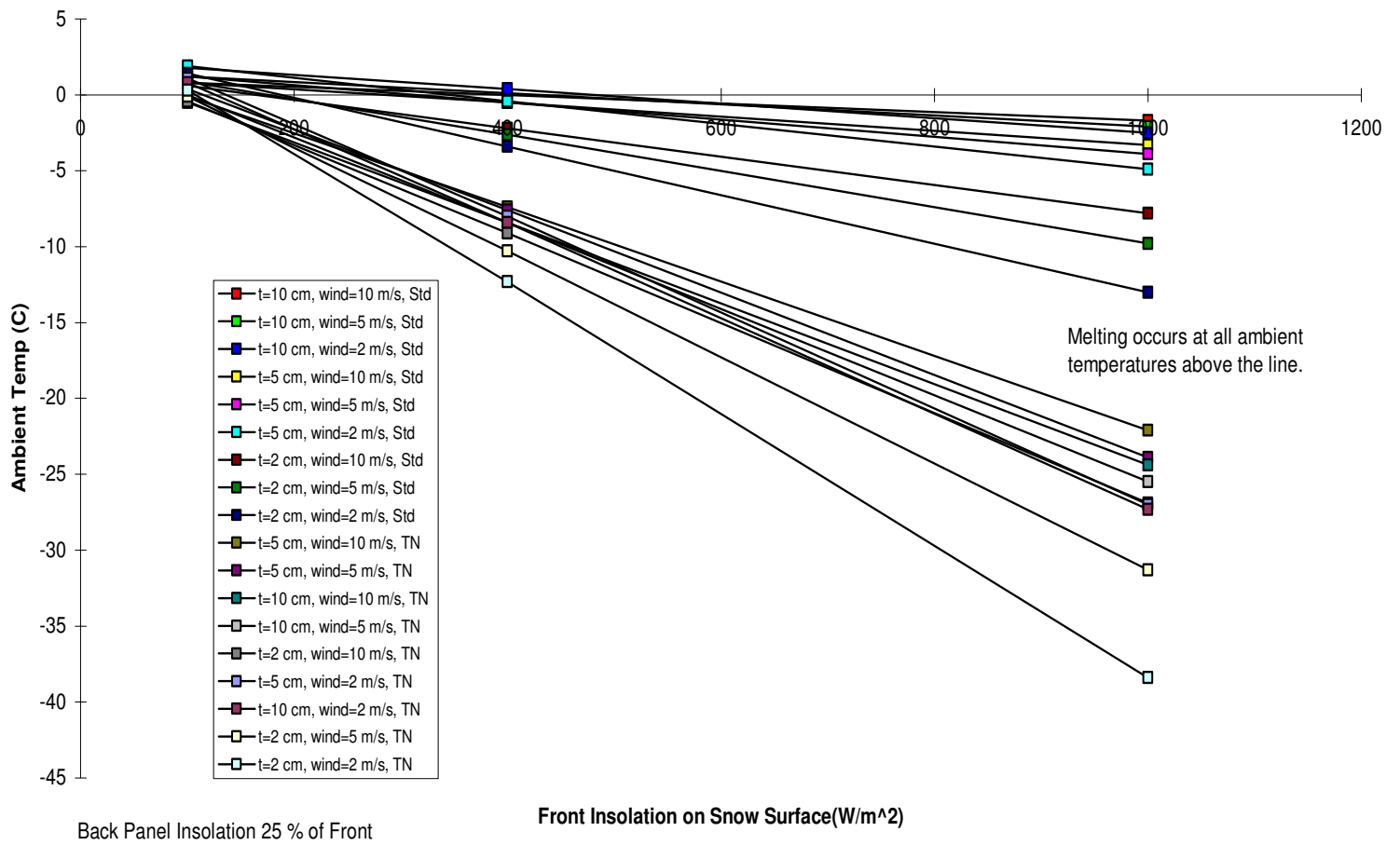
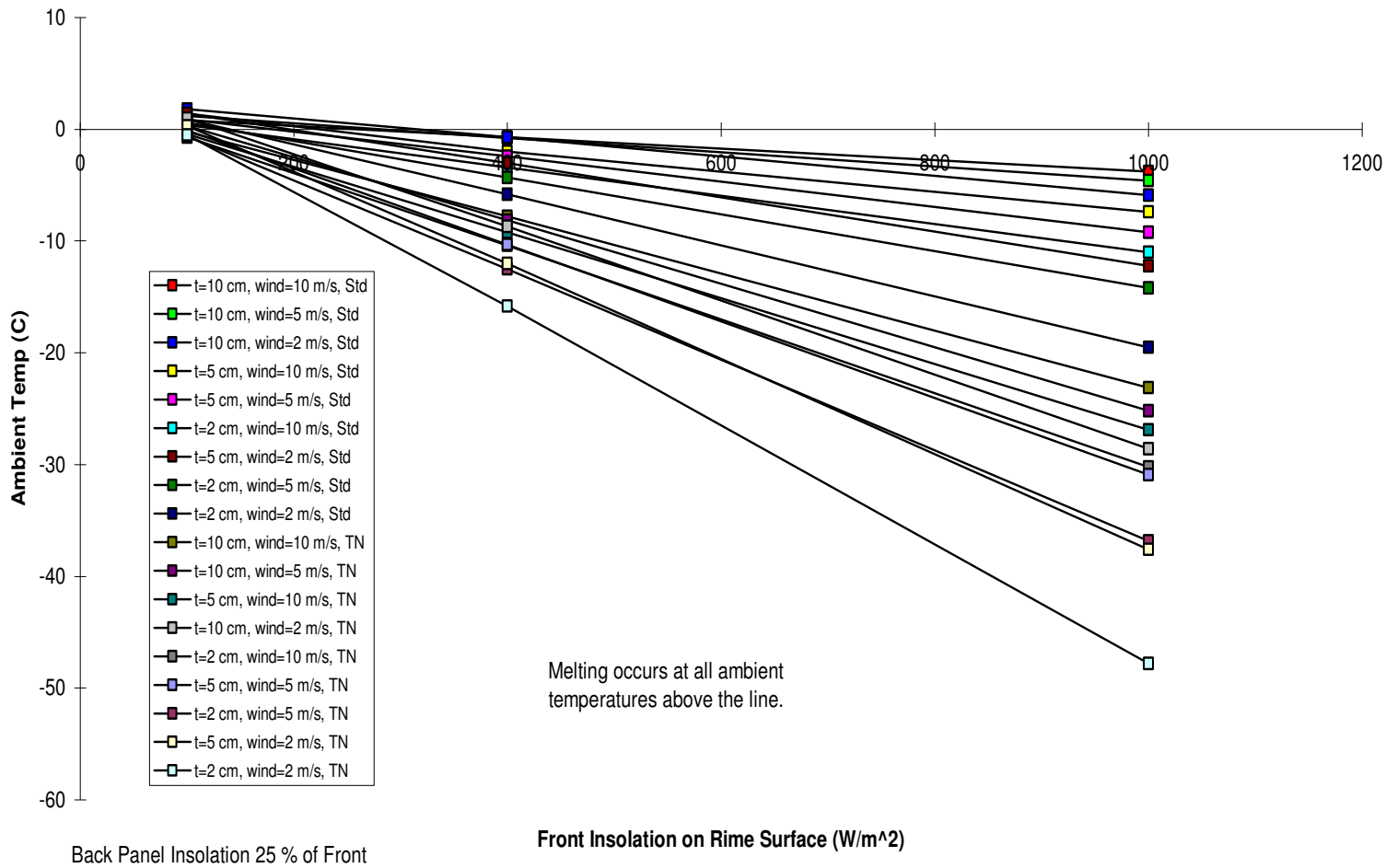


Figure 7.6 Modelled Critical Ambient Air Temperature to Initiate Melting for Rime



and about -23 °C for the TN Conseil equipped panel. This particular example represents the smallest difference between the performance of the unmodified panel and that of the TN Conseil panel; in other cases the difference is more exaggerated. Second, as expected, in most cases the ambient air temperature required to bring the panel surface to zero °C increases with increasing wind speed-- since there is increased convective cooling-- and increasing accumulation thickness-- since there is less radiation penetrating the accumulation and reaching the panel. An exception to this is found in the results for light, fresh snow, two and five cm thick, on the TN Conseil panels. This results from a reversal in the relative importance of the transmission of solar radiation and the insulative properties of the snow cover, as discussed in Section 7.2.2.

In most cases, the ambient air temperature at which the panel surface will be at zero °C decreases linearly with increasing insolation. The case of the TN Conseil panels covered in light, fresh snow is anomalous. It appears to result from the extreme temperature difference across the TN Conseil air cavity-- the Lexan back cover is just above ambient air temperature and the absorber foil will be about zero °C-- a difference of over 120 °C for peak sun front panel insolation but only 60 °C at 400 W/m². The convective heat transfer coefficient varies non-linearly with the temperature difference across the air cavity, and this nonlinearity becomes noticeable with high temperature differences. The effect is exaggerated by higher wind speeds, because these facilitate heat loss from the Lexan back cover.

The models developed in the previous section assume that the panel is at the same temperature everywhere on its surface. This is not the case. The ambient air temperature that initiates melting at the surface of the panel near the frame, for example, will be higher than that shown in the figures above. Furthermore, the frame temperature will be, in most cases, considerably lower than the panel temperature. According to the critical temperature assumption, the frame temperature will be limiting, and no shedding will occur until the entire frame reaches zero °C, regardless of the temperature of the glass surface of the panel. However, this assumes that the accumulation is perfectly bonded to a surface when the surface is below zero °C and that the accumulation is sufficiently strong not to break under its own weight. Neither of these is realistic; a heavy accumulation attached only to a small portion of the frame will slide off. Nevertheless, the frame temperature is important, and will be examined in Section 7.3.3.

7.2.4 Complete Melting Assumption

If an accumulation of snow or ice on the face of a PV panel does not slide off-- the assumption in Section 7.2.3-- it must be melted off. Thus, another way to compare the performance of the unmodified panel and the TN Conseil-modified panel is to determine the rate at which an accumulation will melt from their surfaces.

The snow or ice melt rate, R_{snow} , in cm/hr, is :

$$R_{\text{snow}} = \frac{360000 q_{\text{panel}} n_{\text{snow}}}{c_f} \quad (7.1)$$

where q_{panel} is the energy per unit time available for melting at the panel surface (W/m^2),
 U_{snow} is the specific volume of the accumulation (m^3/kg),
 c_f is the enthalpy of fusion for water, equal to 333000 J/kg ,
and the constant $360000 \text{ (cm}\cdot\text{s}\cdot\text{m}^{-1}\cdot\text{hr}^{-1})$ achieves consistent units.

The melting rate will be a function of a large number of variables: accumulation type, accumulation thickness, ambient air temperature, front insolation, back insolation, and wind speed. In order to make this comparison tractable, some simplifying assumptions were made. First, it was assumed that as long as it was greater than zero, q_{panel} was a linear function of the ambient air temperature. This was found to be a reasonable assumption. Thus, using only two points connected by a straight line, the ambient air temperature as a function of melting rate can be plotted. Second, the back panel insolation is assumed to be one-quarter of the front panel insolation. Third, it is assumed that the melting-rate for one accumulation thickness-- five cm-- is an adequate basis for a comparison of the performance of the panels for all thicknesses. Fourth, the effect of wind will not be significant compared with the effect of insolation level and accumulation type and a wind speed of five m/s will yield typical results. This, too, was tested and found to be a reasonable assumption.

Plots of ambient air temperature versus melting-rate are shown for slightly densified snow (Figure 7.7), moderately densified snow (Figure 7.8) and rime (Figure 7.9). Results are given for front panel insolation levels of 200 W/m^2 , 600 W/m^2 , and 1000 W/m^2 . The results are shown for ambient air temperatures at or below zero $^{\circ}\text{C}$: the model assumes that there is melting at the panel surface only, and melting will occur elsewhere for ambient air temperatures above zero $^{\circ}\text{C}$.

Under all conditions modelled, the TN Conseil-modified panel had a significantly higher melting rate than the unmodified panel. For example, for rime, at an ambient air temperature of -5°C and front panel insolation of 1000 W/m^2 , the melting rate for the unmodified panel is about 0.25 cm/hr and the melting rate for the TN Conseil-equipped panel is about 0.7 cm/hr . In addition, as suggested by the results of Section 7.2.3, melting begins at a much lower ambient air temperature for the TN Conseil panels than for the unmodified panels.

The melting rate given is the instantaneous melting rate. Because melting decreases the thickness of the accumulation, it also changes the melting rate.

The slopes of the curves for the TN Conseil panels are steeper than those for the unmodified panels. This is due to the insulating effect of the Lexan back cover. An increase in ambient air temperature results in a smaller temperature difference between the panel and the ambient air, and thus lower heat transfer through the back of the panel. In the unmodified panel, the resistance to this heat transfer is low, and a relatively large decrease in heat transfer through the back panel results. The resistance is higher in the TN Conseil panels, and the same increase in ambient air temperature produces a correspondingly smaller decrease in heat loss. A lower heat loss to the environment results in more energy available for melting at the panel surface.

Figure 7.7 Modelled Melting Rate for Slightly Densified Snow 5 cm Thick, Wind of 5 m/s

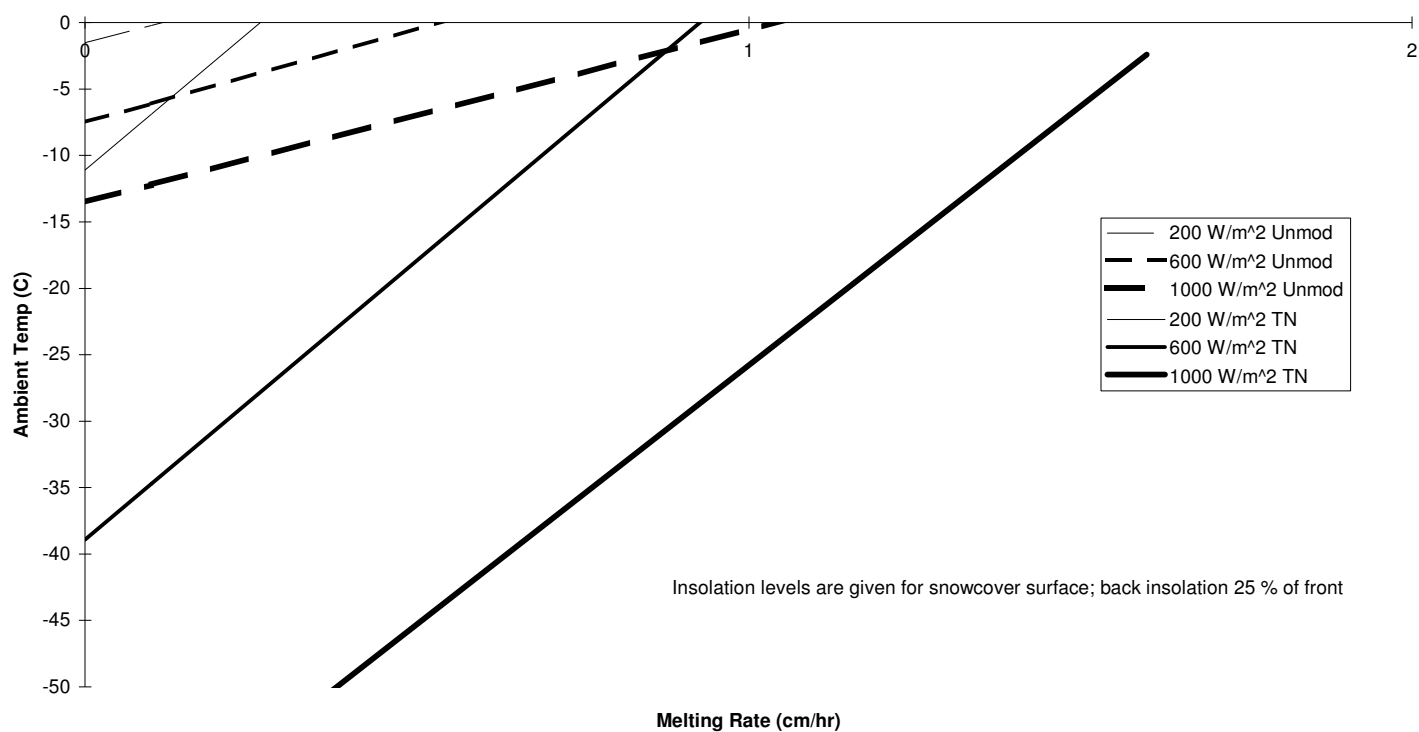


Figure 7.8 Modelled Melting Rate for Moderately Densified Snow 5 cm Thick, Wind of 5 m/s

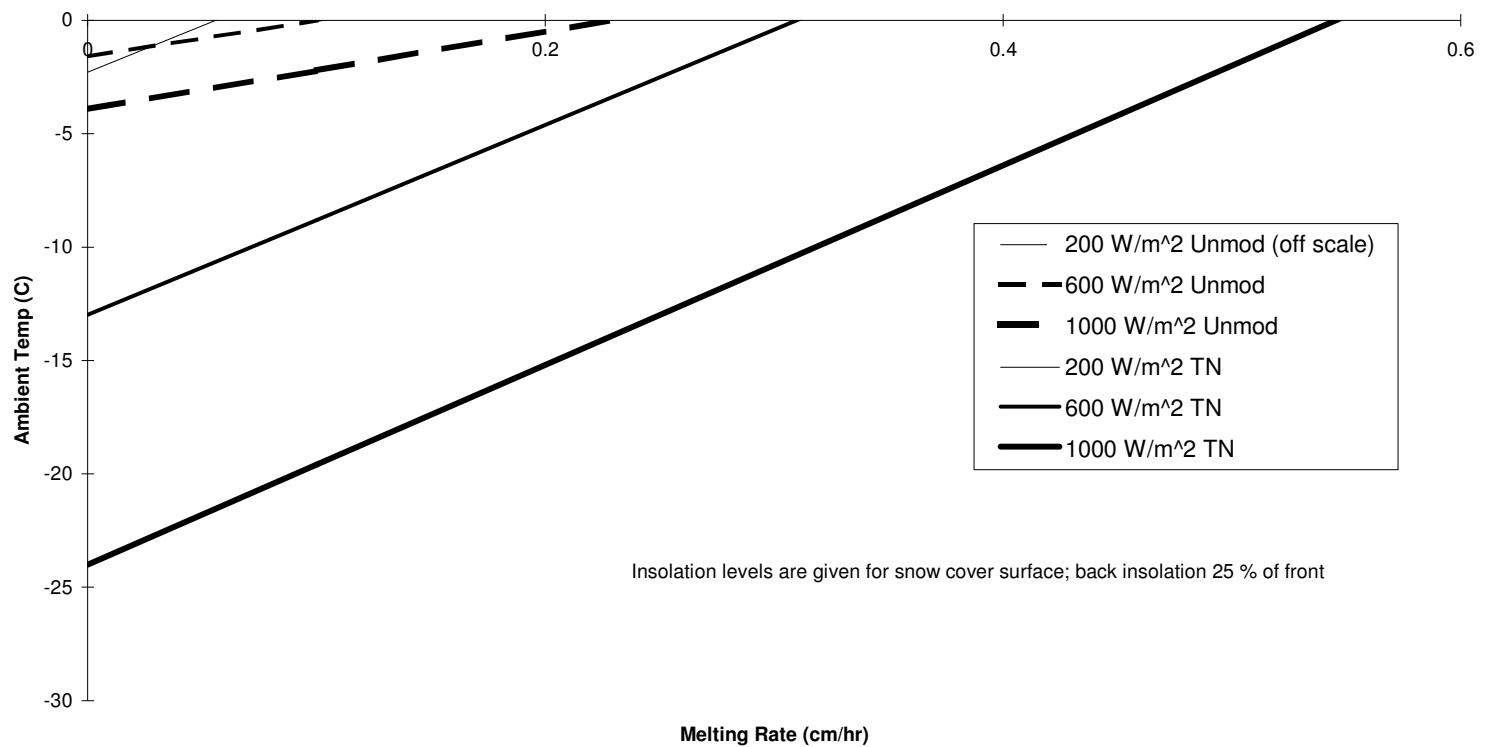
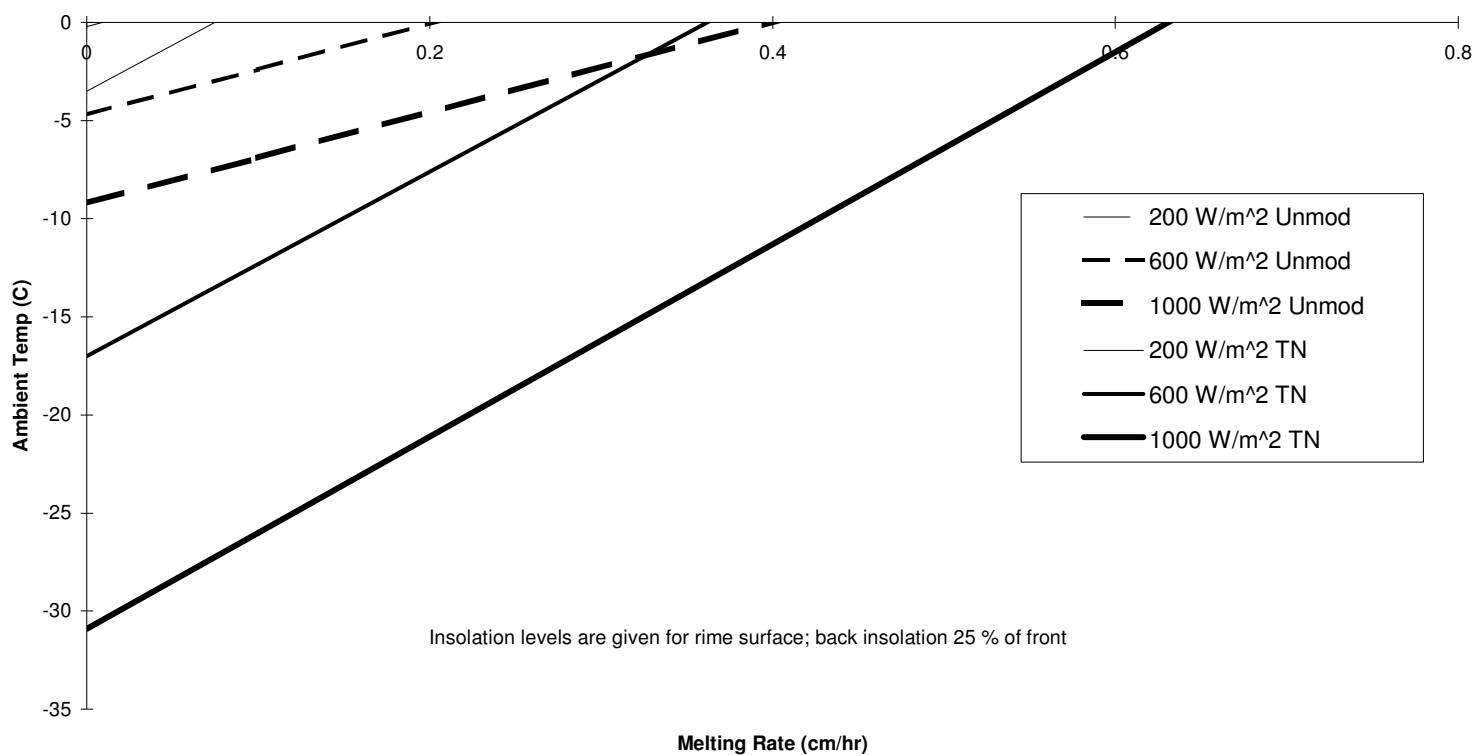


Figure 7.9 Modelled Melting Rate for Rime 5 cm Thick, Wind of 5 m/s



7.2.5 Discussion on the Operation of the TN Conseil Technology

The above results and the results presented in Section 6 clarify the respective roles of the black absorber foil and the Lexan back cover. The black absorber foil is principally responsible for higher melting rates, and the elevated temperature of the panel can be attributed to the Lexan back cover.

The temperature of the panel is governed by an energy balance on the system. The panel gains energy, in the form of solar radiation, from both the front and back face of the panel. The panel loses energy, in the form of heat, at the front and back of the panel also. In winter, the solar radiation incident on the front face of the panel is about three to five times that incident on the rear face of the panel. Thus, even if a layer of snow or ice reduces by 75 %³³ the radiation reaching the front side of the panel, the energy contributions of the front panel and back absorber foil will be roughly the same. On the other hand, adding the Lexan absorber foil greatly reduces the heat loss from the rear of the panel. With snow insulating the front of the panel and the Lexan insulating the back, heat losses are minimal and a small energy gain can raise the temperature of the panel greatly.

However, when the panel temperature reaches zero ° C and snow or ice begins to melt, the energy loss from the panel is greatly augmented by the heat required to turn ice to liquid water. The melting is the principal heat loss from the panel, and its rate will be closely related to the energy gain of the panel. The Lexan back cover does nothing to increase the energy gain of the panel; it simply reduces its loss. The black absorber foil, on the other hand, absorbs radiation incident on the back. The thicker the accumulation, the higher the fraction of the panel energy gain provided by the black absorber foil.

The amount of radiation incident on the back surface of the panel limits the improvement in melting rate realizable with the black absorber foil. Thus, the improvement in melting rate with the TN Conseil technology is less pronounced than the improvement in the ambient temperature at which melting will be initiated.

Thus, the Lexan back cover and the absorber foil fulfill different functions: the first minimizes heat losses, raising the panel temperature, and the latter maximizes energy gain, enhancing the melt-rate. It must be recognized that the system would not work with just one of the two components. If only the Lexan back cover were installed, melting would start at a low temperature but be very slow³⁴. If only the absorber foil were installed, heat losses at the back of the panel would prevent the panel temperature from rising.

³³This corresponds to a seven cm thick snow accumulation, approximately.

³⁴This might be sufficient to initiate shedding of snow in some cases, but well-attached deposits of rime and snow may have to be partially or fully melted for removal.

7.3 Ice Ledge Development

7.3.1 Observations

One of the aspects of the real-world operation of the TN Conseil panel that is not evident from the models above is the development of an "ice ledge". This is a lip of ice affixed to the panel at the line of intersection of the panel glass and bottom piece of the aluminum frame (see Figure 7.10).

This ledge develops when snow sheds incompletely from the panel surface, and a strip of snow, caught on the panel frame, covers the bottom five to 20 cm of the panel. The snow is generally quite wet as a result of melting; it may be that this wetness provides the adhesion necessary for the snow to remain stuck to the panel. If the ambient air temperature drops, as it does at night, this strip of snow can refreeze into a strong strip of ice firmly bonded to the frame. During the daytime, when the panel warms again, the portion of this accumulation that is in contact with the panel melts away. Because the strip is strong, however, the remaining accumulation doesn't collapse onto the panel, but remains suspended above the panel surface, attached only at the frame, which remains cold. Since it is no longer in thermal contact with the panel, the ledge can be removed only when it is broken off, the frame reaches zero ° C, or heat radiated from the sun and convected and radiated from the panel surface consume the ice.

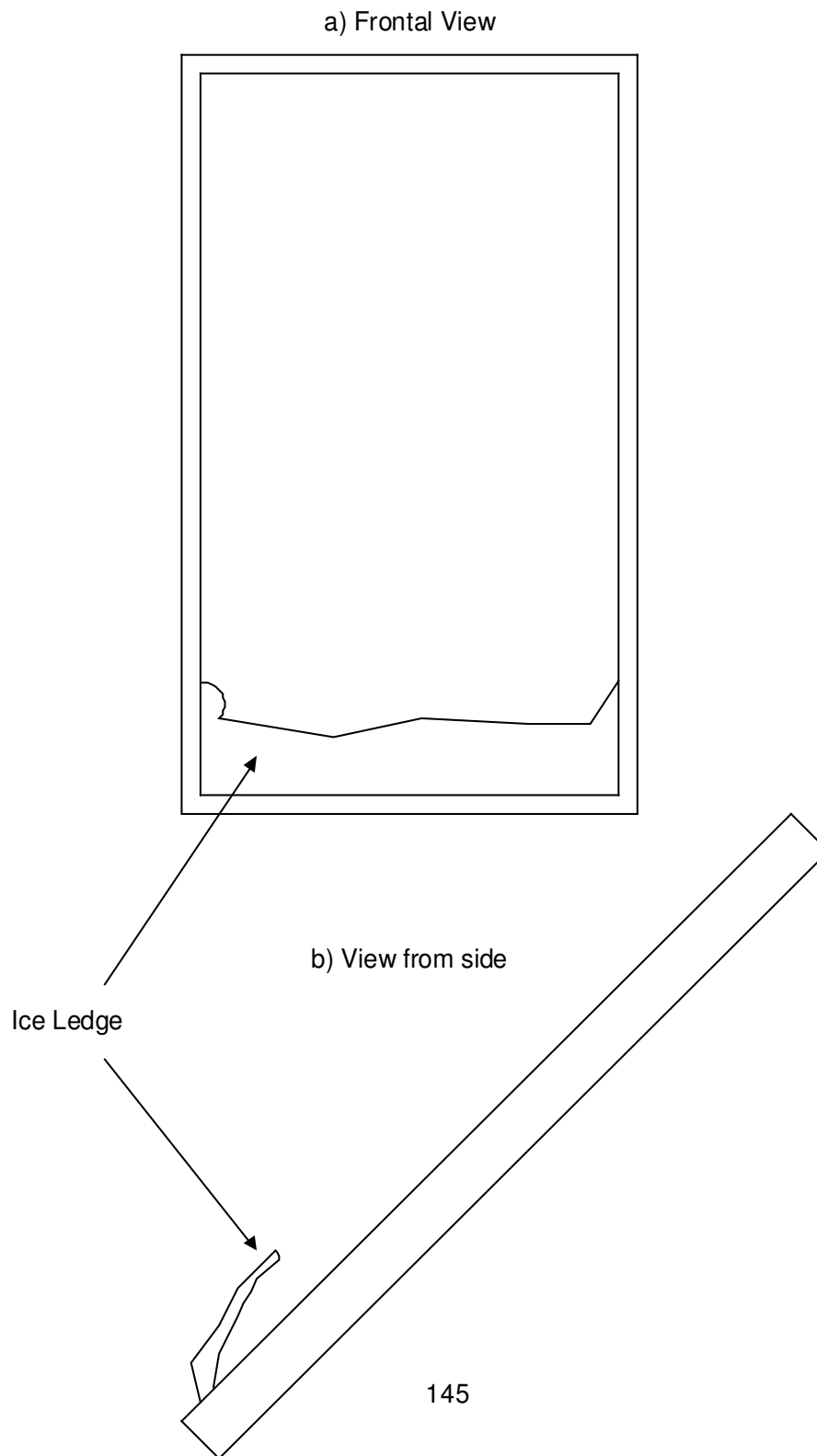
When it forms, the ledge may remain stuck to the panel for days after the snow has been removed from the other panels.

The ledge has two negative effects. First, it partially shades the panel. In general, this is not as serious as would be expected, since the ledge tends to become clearer-- that is, more like homogenous ice-- with time. Second, the ledge provides a foothold for further snow and ice accumulation. It is speculated that if snow falls on a panel with such a ledge, the panel will accumulate snow more effectively than a panel without a ledge. Further, the ledge may inhibit snow shedding.

On the panels in the roof-top array at the EDRL, the development of this ice ledge was observed only on the TN Conseil panels. This propensity to form an ice ledge may be partially attributed to the existence of unmodified panels directly below the TN Conseil panels. The TN Conseil panels shed their snow cover much sooner than the unmodified panels; the passage of this snow is impeded by the snow on the unmodified panel below. However, the formation of this ice ledge on TN Conseil panels in other arrays has been reported.

There are two explanations for the tendency of the TN Conseil panels to form an ice ledge. First, the better melting performance of the TN Conseil panel permits snow shedding under marginal insolation conditions, such as the late afternoon, when the unmodified panels would not shed their snowcover. If shedding begins under low insolation levels, a change in insolation conditions, such as the coming of night, can arrest the shedding before it is complete. This may

Figure 7.10 Ice Ledge



lead to the formation of an ice ledge. Thus, the ice ledge is less likely to develop if strong insolation conditions are required to initiate shedding, as is the case for the unmodified panel. A second explanation involves the temperature gradients created by natural convection in the air cavity (see Section 6.1.5). If the bottom of the panel is much colder than the top of the panel, the snow at the bottom of the panel will impede shedding. More snow at the top of the panel will melt, and this snow may become quite wet. This will increase its adhesion to the panel, and make it more likely to become caught on the bottom piece of the frame. Further, once the snow is at the bottom of the panel, the temperature gradient results in a slower melting rate. Neither of these two explanations has been tested.

It is unknown whether such an ice ledge might form on a rime-covered panel. It seems unlikely that shedding is an important mechanism for rime removal; this suggests that the ice ledge will not form. However, [Jarvis] reported that ice "cups", not in contact with the panel but attached to the supporting structure around the panels, formed on heavily rimed panels. These arched over the entire panel surface and appear to have formed when the rime melted away from the panel but not from the surrounding support structure. This occurred when the panel frame had been anodized in black, to facilitate melting from the frame.

7.3.2 Use of Thermoclear

If, as suggested in the preceding section, the temperature gradients caused by natural convection are responsible for the formation of the ice ledges, the reduction of natural convection in the air cavity would be very desirable. One way to do this would be to use Lexan Thermoclear instead of a Lexan sheet back cover. This option is described in Section 6.2.1.5. The ribs in the Lexan Thermoclear would effectively eliminate the temperature gradient caused by natural convection in the cavity.

There are, however, a number of minor problems with the Lexan Thermoclear option. First, according to the model, the thermal performance of the Lexan Thermoclear panel is poorer than that of the standard TN Conseil Technology (Section 6.2.9). That is, the ambient air temperature at which the panel surface will be at zero °C is substantially higher for the Lexan Thermoclear, due to the fact that radiation incident on the rear surface must pass through two sheets of Lexan rather than just one. Second, the fact that convection is eliminated may result in "cold spots" on the panel, in particular at locations where the back panel insolation is low due to shading by the array's supporting structure. In a standard TN Conseil panel, convection might carry heat from warmer parts of the panel to these cooler parts; with the Lexan Thermoclear this heat transfer occurs only by conduction, principally in the panel sandwich. This will be especially problematic when the solar radiation reaching the cells is low. This will be the case for thick accumulations of snow or rime.

These deficiencies of the Lexan Thermoclear may be ameliorated in two ways. The Lexan sheet that is adjacent to the absorber foil has very little insulative value. A material with just the outer Lexan cover and the ribs existed, it would perform nearly as well as the standard TN Conseil

technology. In addition, the spacing of the ribs in the Lexan Thermoclear is probably sub-optimally close. If the ribs were spaced at about five cm on centre, the resulting temperature gradient would be minimal, but there would still be some convection to the cold-spots on the panel.

7.3.3 Frame Modifications

7.3.3.1 Background

As noted in Section 7.3.1, the ice ledge freezes onto the panel at the line of intersection of the frame and the glass surface of the panel. This suggests that the frame remains below freezing even when the panel surface is well above. In general, the low temperature of the frame impedes snow and ice removal, both by providing a site for snow and ice to remain attached to when the rest of the panel has reached zero °C, and by being a heat sink for the edges of the panel (see Section 6.1.5).

The simplest and possibly most effective way to eliminate the ice ledge and facilitate shedding would be to eliminate the bottom piece of the aluminum frame, or at least that portion that is raised above the glass surface. This option has been investigated elsewhere [TN Conseil, 1993]. Unfortunately, removing part of the frame may have negative structural ramifications and will void the warranty for the panel.

Another approach is to increase the temperature of the frame, either by insulating it or by increasing its solar absorption.

7.3.3.2 Models of the Frame

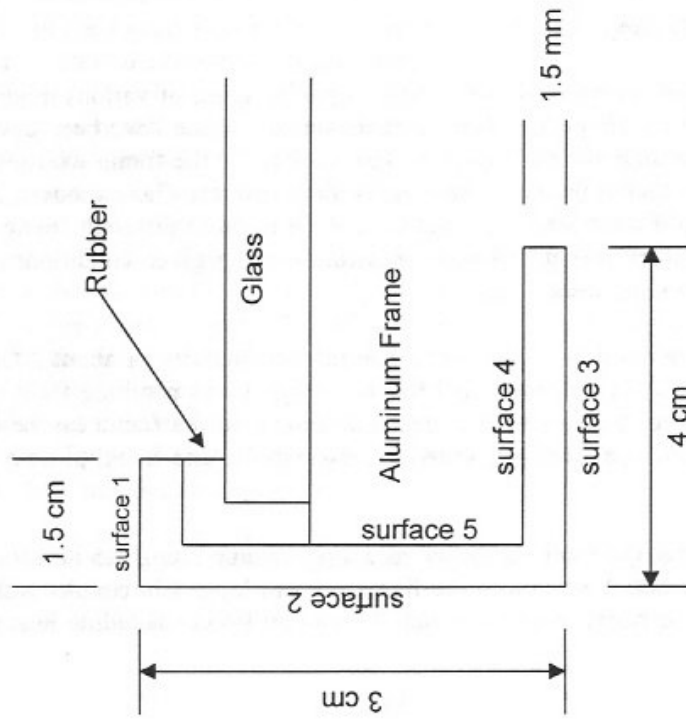
In order to facilitate the comparison of the thermal performance of various modifications to the panel frame, two very simplified thermal models of the frame have been developed. One model is for the frame without insulation, and the other is for the frame with insulation on all surfaces except the lip that is proud of the panel's glass surface. These models, being very rough approximations of the frame, are valid for comparisons of different frame options, but may not accurately predict the actual frame temperature under given conditions of wind, ambient air temperature and insolation.

The frame is made of aluminum, which has a thermal conductivity of about $200 \text{ Wm}^{-1}\text{K}^{-1}$. This thermal conductivity is very high, and for the energy flows resulting from solar radiation on the frame and heat conducted from the panel, all points on the frame can be considered as having the same temperature. This was tested experimentally, and found to be a good assumption.

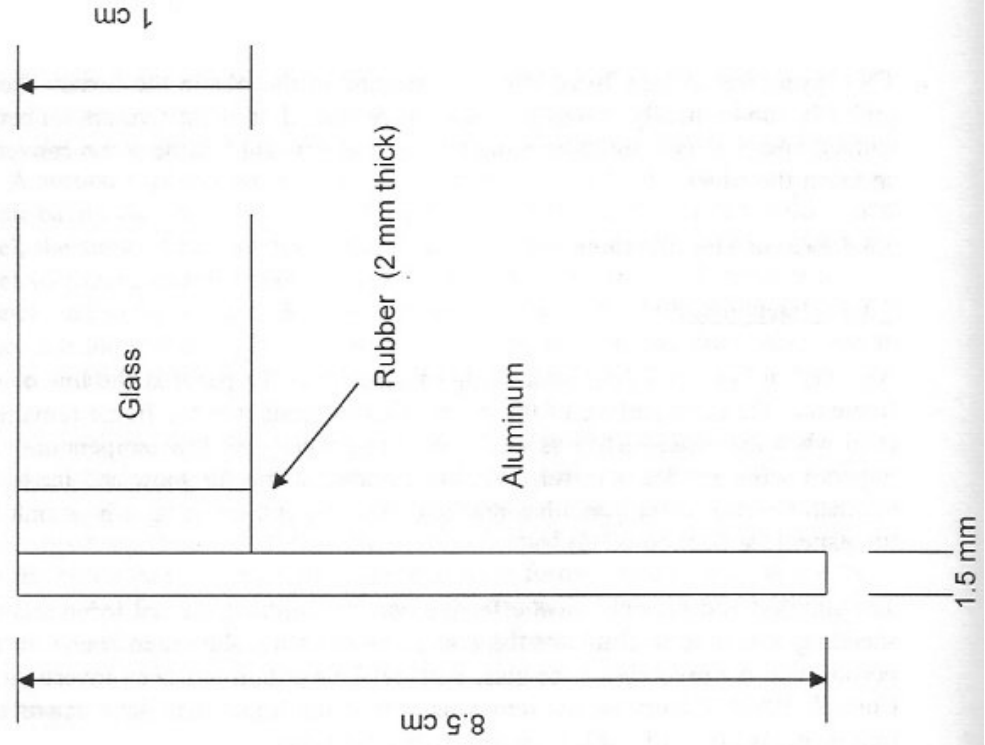
To simplify the analysis, the frame is treated as a strip of aluminum, 1.5 mm thick and 8.5 cm long (see Figure 7.11). A portion of the frame one cm long is in contact with the rubber gasket that separates the frame from the panel. All energy flows, including heat transfers, are treated on

Figure 7.11 Cross-Section of Frame (not to scale)

a. Diagram of Frame Cross-Section (Simplification)



b. Further Simplification for Model



a per unit length basis. For example, the irradiation on the frame is specified in units of W/m, instead of W/m².

The models are presented schematically in Figure 7.12 using the conventions of Section 6.2.1. The model of the unmodified panel has nodes for the temperature of the frame, the panel, the ground, the sky, and the ambient air; the model of the insulated panel has an additional node for the temperature of the air-insulation interface. Solar radiation is incident on the frame temperature node and the insulation surface temperature node. There is heat transfer between the frame and the panel by conduction, the frame and the ground by radiation, the frame and the sky by radiation, and the frame and the ambient air by convection. There are additional heat transfers for the model of the insulated frame: by conduction between the insulation surface and the frame, by convection between the insulation surface and the ambient air temperature by convection, and by radiation between the insulation surface and the sky and ground.

It is assumed that there will be no solar radiation incident on surface 2, 4, or 5 (the numbers refer to those indicated in Figure 7.11. Surface 1 will have the same irradiance as the front panel; surface 3 will have the same irradiance as the rear face of the panel. Thus, S_{frame} , the total solar radiation on the frame per unit length (W/m) is:

$$S_{\text{frame}} = \alpha_{\text{frame}} (L_1 I_{\text{front}} + \tau_{\text{ins}} L_3 I_{\text{rear}})$$

where α_{frame} is the solar absorptance of the frame material,
 L_x is the dimension of surface x (m), shown on Figure 7.11,
 τ_{ins} is the fraction of solar radiation transmitted through the insulation, set to one for the model of the unmodified frame,
 I_{front} is the front panel insolation (W/m²),
and I_{rear} is the rear face insolation (W/m²).

For the model of the frame with insulation, S_{ins} , the total solar radiation on the insulation per unit length (W/m) is:

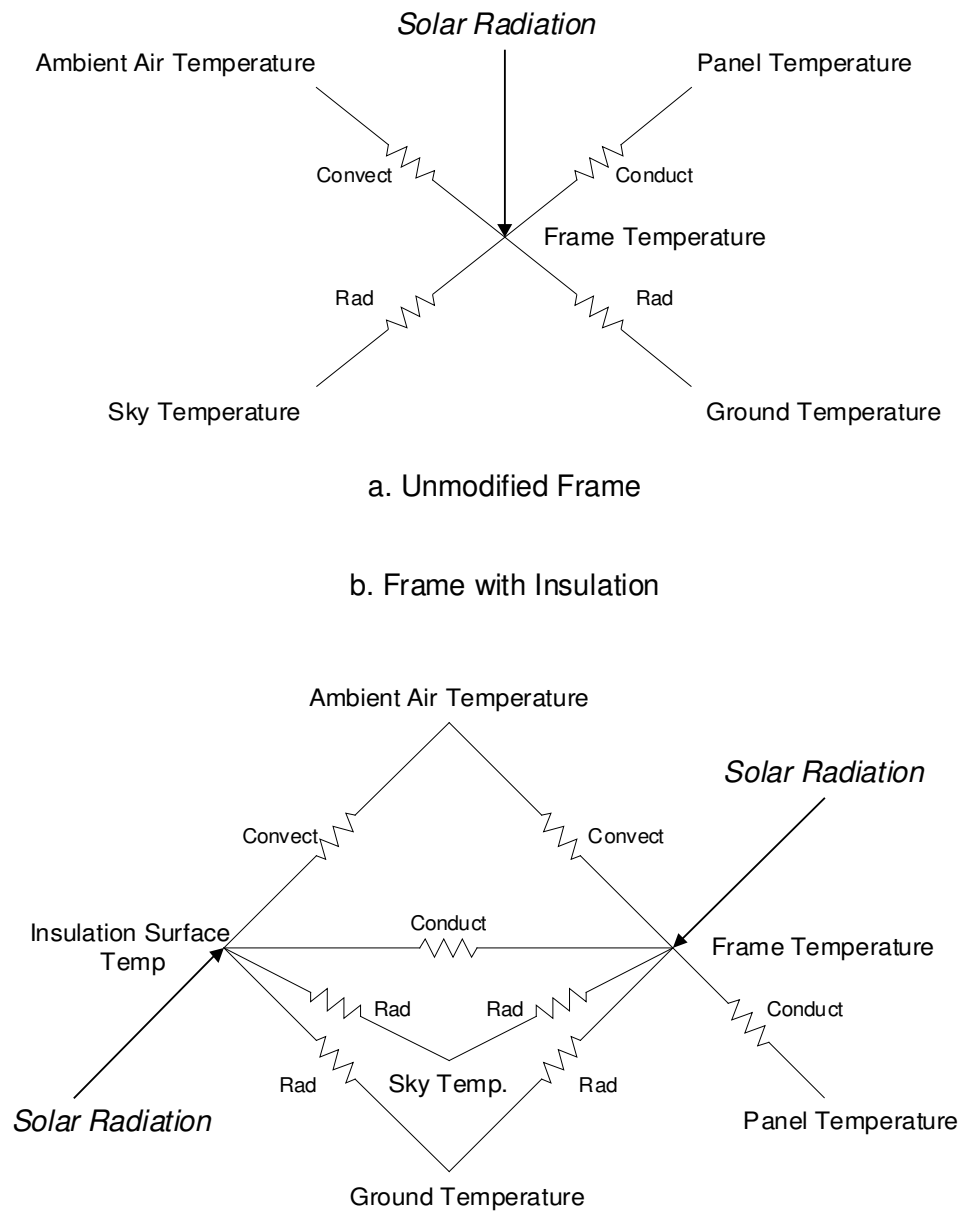
$$S_{\text{ins}} = \alpha_{\text{ins}} L_3 I_{\text{rear}}$$

where α_{ins} is the solar absorptance of the insulation.

It is assumed that "clear" insulation material absorbs an insignificant amount of radiation and the losses implied by τ_{ins} are attributed to reflection. Therefore, for the clear insulation α_{ins} is assumed to be zero.

From surface 1 and surface 3 there is heat transfer by radiation to the ground and sky. This is given by Equation 6.1 in Section 6.2.2.1, multiplied by L_1 for surface 1 or L_3 for surface 3 to convert to W/m. In this equation, the subscript "panel" is replaced by "frame" or "ins". It is assumed that the insulation is opaque to infra-red radiation; therefore, the parts of the frame that

Figure 7.12 Schematic Representations of the Frame Models



are covered in insulation do not participate in heat transfer by radiation.

In an array of PV panels, each panel will be adjacent to one or more panels. For a large or medium array this implies that in the majority of cases surface 2 of one panel's frame faces directly into surface 2 of another's. Using unity as an approximation for the view factor between the two facing surfaces, and assuming, by symmetry, that the two surfaces will be at the same temperature, there will be no infra-red loss or gain from surface 2.

The equation for heat transfer by conduction Equation 6.3 (Section 6.2.2.2) is utilized for heat transfer between the frame, the panel, and the surface of the insulation. To convert to units of W/m, the result from 6.3 is multiplied by 0.01 m, for the conduction between the frame and the panel, or 0.07 m, for the conduction between the frame and the insulation. The thermal conductivity of the rubber layer separating the panel and the frame is assumed to be $0.15 \text{ Wm}^{-1}\text{K}^{-1}$. The layer of rubber is assumed to be two mm thick.

Choosing an appropriate panel temperature for use with the conduction equation is complicated by a number of factors. First, the temperature gradients discussed in Section 6.1.5 suggest that the thermal models will provide an estimate of panel temperature that is higher than the actual panel temperature near the frame, especially at the bottom of the panel. Second, the panel temperature will depend on snow cover on the panel. A panel with snow cover will not attain a temperature much above zero °C, but the principal concern is the ice ledge, which is not in thermal contact with the panel. As a gross approximation, the panel temperature computed using the model of the unmodified frame without snow has been used; under most conditions this temperature is lower than that suggested by the model of the TN Conseil-equipped panels and is higher than that of the snow covered panel.

Heat transfer by convection is treated in the manner described in Section 6.2.2.3. The use of h_{wind} as the convection coefficient for wind losses from the frame is a very rough approximation; it has been used since the wind flow around and between the panels is unknown. The relation for q given in Section 6.2.2.3 is multiplied by 0.085 m to convert the heat transfer by convection to units of W/m.

Four modifications to the frame were compared using the above models. The basis for comparison was a silver anodized frame. Some frames have an anodized finish incorporating black dye; this increases the solar absorption. If a thin, clear plastic cover-- such as a sheet of Lexan-- is placed over this, the frame will benefit from the insulative value of the cover. The heat loss from the frame can be minimized with a thick layer of insulation, which may be either opaque or transparent. The parameters assumed in each case are found in Table 7.1.

7.3.3.3 Results

The above models were used to compare frame temperatures for conditions of ambient air temperature of -10 °C, 1000 W/m^2 front panel insolation, 250 W/m^2 back panel insolation, sky

Table 7.1 Parameters For Frame Models

	α_{frame}	$\varepsilon_{\text{frame}}$	L_{ins} (cm)	k_{ins} ($\text{Wm}^{-1}\text{K}^{-1}$)	α_{ins}	ε_{ins}	τ_{ins}
Silver Anodized	0.15	0.2	NA	NA	NA	NA	NA
Black Anodized	0.8	0.6	NA	NA	NA	NA	NA
Black + Thin Ins	0.8	0.6	0.5	0.2	0.0	0.5	0.8
Black + Thick Opaque Ins	0.8	0.6	2	0.05	0.8	0.5	0.0
Black + Thick Clear Ins	0.8	0.6	2	0.1	0.0	0.5	0.6

temperature of -35 °C, ground temperature of -12 °C, and wind speeds of two, five, and 10 m/s. For a wind speed of two m/s the panel temperature was 16 °C, for five m/s it was nine °C, and for 10 m/s it was four °C. To test for conditions of low insolation, the models were run with a front panel insolation of 400 W/m^2 , back panel insolation of 100 W/m^2 , and wind speed of five m/s. Under these conditions the panel temperature was found to be -4 °C.

The results are presented in Figure 7.13. The silver anodized framed has a temperature significantly lower than that of the other frame configurations; using a black anodized frame results in significantly higher frame temperatures. The thin, clear plastic cover yields a minor increase in frame temperature. A major improvement is realized with the addition of either the thick opaque or thick clear insulations.

7.3.3.4 Discussion

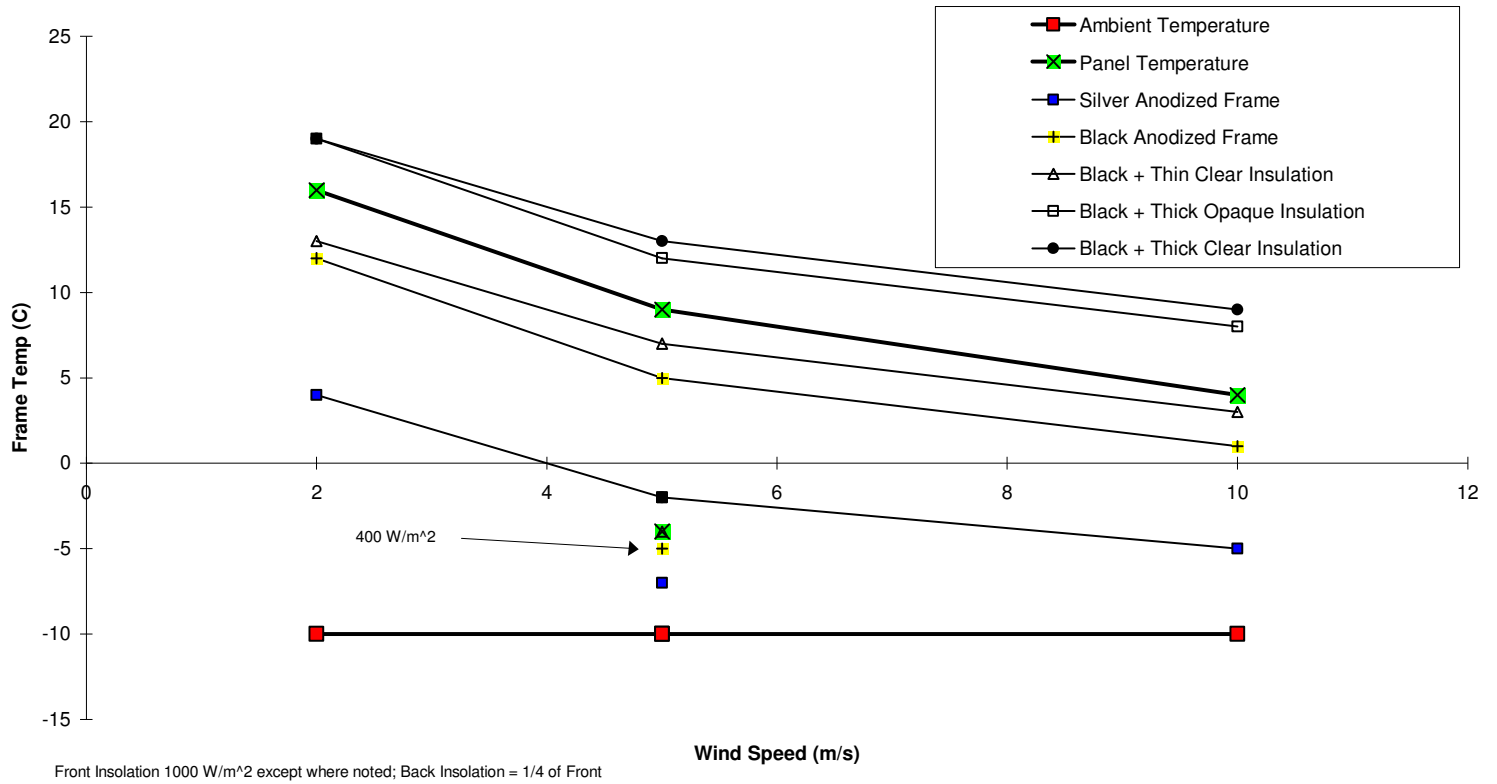
The models required many assumptions about the frame and its environment. This suggests that results computed from the models may err significantly.

The suspect assumptions and simplifications are:

- 1) That h_{wind} can be used for the convection coefficient.
- 2) That for surface 2 there is no insolation and no heat transfer by radiation.
- 3) That the panel temperature can be found from the model of the unmodified panel without snow cover.
- 4) The term for heat conduction through the rubber layer.

If the second assumption was incorrect, and the level of insolation on surface 2 was reasonably high, the black anodized frames would "collect" more energy and therefore have better results

Figure 7.13 Modelled Temperature of Frame for Various Configurations (Without Snow)



than reported above. If the insolation was low but the radiation losses high, the silver anodized frame, with its lower emittance, would fare better, relative to the other configurations. If h_{wind} overestimated the convection coefficient, the advantage of the panels with insulation has been overstated.

Only assumptions one and two will affect a comparison of the results-- if assumptions three and four are incorrect all the frames will be affected in the same way. If the value that has been used for h_{wind} is, in reality, too high, then the advantage of the insulation has been overstated. If, for example, the value used for h_{wind} is three times its proper value, the true temperature, for 1000 W/m^2 front panel insolation, 250 W/m^2 back panel insolation, and wind of 5 m/s, is about 15 °C, and not 5 °C as stated, for the black anodized frame. For the frame with thick clear insulation, the true temperature is 18 °C, and not 13 °C. In general it appears that there is a reasonable margin for error in the value of h_{wind} .

The radiation losses are small compared with the convective losses and solar energy gains; therefore it can be concluded that even if assumption two is not warranted, the conclusion that black anodizing improves the performance of the frame is still valid.

Not only will raising the temperature of the frame improve the frame's ability to melt ice and snow, but it will also lessen the heat loss from the panel to the frame. The heat transfer by conduction between the panel and the frame is proportional to the difference between the temperatures of the two. If the frame temperature is close to the panel temperature, there will be little heat transfer between the two. This will decrease the temperature gradient observed at the edges of the panel, and may improve the melting at the edges of the panel.

7.4 Rime Icing Considerations

7.4.1 Background

If there is rime ice on the front of the PV panel but the rear face is clear, the TN Conseil technology should perform as envisaged. However, in sites of severe rime icing there exists the danger that both the front and the rear face of the panel will be covered in rime. When this is the case, the solar radiation absorbed by the cell and the foil will be curtailed, and the ability of the panel to clear itself of the rime will be diminished.

[Jarvis] and others report that structures located at sites prone to severe rime icing are often completely covered in rime on all sides. This suggests that both the front and back of a PV panel at such a site will become rimed. This is borne out by inspection of pictures taken of the PV panels at the Lookout Hills RCMP repeater station in Gros Morne National Park, Newfoundland.³⁵

³⁵ At a site of less severe riming, it was reported that the back side of the panel remained free of rime ice [Bergevin]. It is not clear why this was the case.

7.4.2 Probability of Rear Face Rime Icing

[Morris] points out that the probability of riming on both the front and the back faces may be lower for panels which operate at an elevated temperature. The wind can only blow on one face of the PV panel at a time; therefore, at any point in time rime accretion can occur on one face of the panel only. For both faces to become covered in rime, the wind must first blow on one face, and then change direction and blow on the other face. For this a change in wind direction of at least 90° must occur. If there is a period of strong insolation between the rime accretion on the one face and the wind change, there will be an opportunity for the panel to melt off the accreted rime before further riming occurs. As long as one face is free of rime, considerable collection of solar energy will be possible. The more quickly the panel is capable of melting off the accreted rime, the lower the probability that both faces of the panel will become covered in rime. Therefore, a performance gain may be realized with the TN Conseil panel even in environments where unmodified panels become covered in rime on both the front and the rear face.

The principal weakness in this argument is that the air cavity in the TN Conseil technology is such an effective insulator that the temperature of the Lexan back cover is generally very close to the ambient air temperature. Rime that accumulates on the Lexan back cover will be even less likely to melt than the rime that accumulates on the front or back of an unmodified panel. This may result in a serious accumulation of rime on the rear surface of the panel.

7.4.3 Impact of Rear Face Rime Icing on Thermal Performance

To investigate the impact of rime ice accretion on the rear face of the panel, the models for the snow- and ice-covered unmodified panel and panel with TN Conseil technology were altered so that they reflected the thermal and optical effects of rime on the rear face of the panel. The alterations required for this were exactly the same as those required to adapt the models of Section 6 so that they were applicable to panels with snow- or ice-cover on their front surface. These changes were outlined in Section 7.2.1.

The resulting models were applied to conditions of high insolation and moderate wind. A front panel insolation of 1000 W/m^2 , a back panel insolation of 250 W/m^2 , sky temperature 25°C below the ambient air temperature, ground temperature 2°C above the air temperature, and a wind speed of 10 m/s were assumed. A higher wind speed than in previous tests was chosen because sites of severe riming tend to be windy.

The tests were run for two different types of rime. Both had a thermal conductivity of $1.5 \text{ W/m}^\circ \text{K}^{-1}$, but "Rime A" had an extinction coefficient of 20 m^{-1} and "Rime B" had an extinction coefficient of 40 m^{-1} . It is speculated that most rime has an extinction coefficient between these two values.

Four different scenarios were compared for each type of rime: the unmodified panel with rime on

the front and back, the TN Conseil-equipped panel with rime on the front and back, the TN Conseil-equipped panel with rime on the front only, and the TN Conseil-equipped panel with a "rime shield", a modification proposed and discussed in Section 7.4.4., with rime on the front face of the panel only.

The results are presented in Table 7.2 and Figure 7.14. The ambient air temperature required for the panel surface to be at zero ° C is given as a function of rime thickness; for those cases where there is rime on the front and the back of the panels, the thickness of the rime on the back is the same as that on the front.

The TN Conseil-equipped panels perform better than the unmodified panels. For thicker accumulations of rime, less radiation penetrates the rime and the insulative effect of the rime itself becomes more significant. Thus, the advantage of the TN Conseil panel decreases with increasing rime thickness.

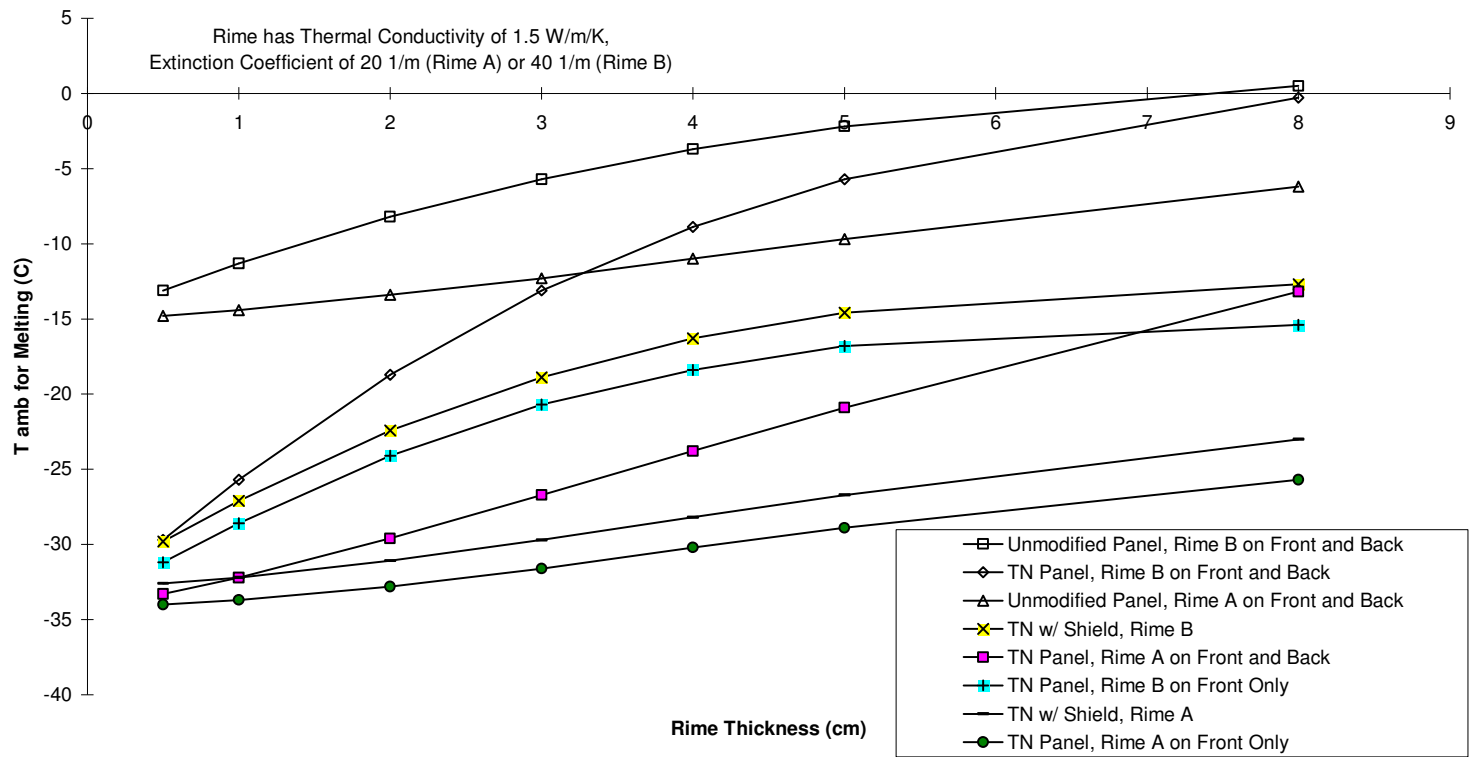
Rime on the back panel considerably reduces the radiation reaching the panel, and results in a considerably cooler panel. This is reflected in the much higher ambient temperatures required to initiate melting at the panel surface when there is rime on the rear panel surface. The difference in the performance of the panels with and without rime on the rear surface becomes more exaggerated with increasing rime thickness.

The difference between the two types of rime is very significant. Rime A, having a lower extinction coefficient than Rime B, permits more solar radiation to pass through it. The result is a considerably warmer panel.

7.4.4 Modification to Panel Installation

This section, including pages 159, 160, 161, and 162, are omitted from the public version of this report.

Figure 7.14 Modelled Effect of Rime: Wind 10 m/s, Front Insol 1000 W/m², Back 250 W/m²



CHAPTER 8

SIMULATION OF SYSTEM PERFORMANCE AT FOUR SITES

8.1 Introduction

The thermal models developed in the previous sections were used to estimate the time required for snow or ice to remove itself from unmodified panels, panels with the standard TN Conseil system, and panels outfitted with both the standard TN Conseil system and the rime shield (described in Section 7.4.4). This assessment was conducted using measured weather data from four weather stations. For three of the four sites an initial accumulation of five centimetres of rime was assumed; for the remaining site an eight centimetre accumulation of densified snow was assumed. The weather data were used, in conjunction with the thermal models, to gauge how long it would take for the accumulation to either melt-off completely or shed catastrophically as a sheet.

Three of the four sites were chosen on the basis of them being representative of "rime-prone" sites. These were Norman Wells, Northwest Territories; Prince George, British Columbia; and Daniels Harbour, Newfoundland. All of these sites are located in or near mountain ranges, and the Newfoundland and B.C. sites are in areas where riming problems have been reported.

The fourth site was Bagotville, Québec, a site that tends to have cold winters and receive heavy snowfalls.

There are two reasons for the selection of three rime sites but only one snow site. The ability of the TN Conseil modification to hasten snow removal has already been experimentally verified (see Chapter 10 and [TN Conseil, 1994]), whereas its efficacy under conditions of riming has not yet been tested. Thus, modelling its ability to remove rime has more value than modelling its ability to remove snow. Further, for PV panels in Canada rime appears to be a more serious problem than snow accumulation (see Chapter 2).

8.2 Method

A computer program was written to step through the hourly data files and determine when shedding (i.e., the critical temperature criterion of Section 7.2.3) and complete melting (Section 7.2.4) would occur. For each hour, the program read the insolation, temperature, and windspeed data, and used these to determine whether the critical ambient air temperature at which melting is initiated had been reached, and if so, to what extent melting had occurred. The thickness of the accumulation was adjusted according to the melting during the hour. The program indicated in an output file the first hour in each year during which the critical temperature was reached. It also indicated the hour when the thickness reached zero, i.e., the accumulation was completely melted off.

The critical ambient air temperature and melting rate for a particular accumulation thickness, insolation, and windspeed, were determined using the thermal models developed in Chapter 7. However, these models were not used at program run-time. Rather, before running the program, they were used to create a matrix of melting rates and critical temperatures at various thicknesses, insolation levels, and windspeeds. This matrix was incorporated into the program. At run-time, the actual insolation level, windspeed, and thickness were used to linearly interpolate among the values in the matrices.

8.2.1 Weather Data

The weather data used for these sites came from [Environment Canada, 1993], which lists actual hourly weather conditions for the years 1953 to 1989 (Prince George and Bagotville), 1956 to 1989 (Norman Wells), and 1966 to 1989 (Daniels Harbour). These data sets indicate whether precipitation occurred during an hour, but do not indicate how much precipitation occurred. Attempts at using this data to predict actual rime and snow accumulation levels were unsuccessful. Therefore, it was assumed that on January 1st the panels had an initial accumulation of five centimetres of rime at the three rime sites and eight centimetres of snow at Bagotville. Then the hourly insolation, wind, and temperature readings were used as parameters for the thermal model, which indicated how much of the accumulation melted during the hour. It was also assumed that there was no further rime or snow accumulation after January 1st. Obviously, this assumption is unrealistic. However, it was necessitated by the impossibility of predicting further accumulation levels based on the data available.

The weather data were modified in several ways before being used in the program:

1. The windspeed was doubled for the rime sites and halved for the snow sites to account for the fact that the weather stations are located at airports, which are far less windy than the mountaintops where riming will occur and far windier than the sheltered clearings where snow accumulation will be likely.

2. The rime sites were assumed to be at the top of mountains. Ambient air temperature drops roughly 6.5 °C per 1000 m of elevation. The Norman Wells and Daniels Harbour temperatures were lowered by 5 ° C, and the Prince George temperature lowered by 10 ° C. This corresponds to elevations of about 750 m and 1500 m above the weather station, respectively.

3. The global insolation and diffuse insolation values given in the data sets are for horizontal surfaces. The thermal models were run on the basis of insolation on the plane of the panel. Thus, the insolation needed to be transformed to the insolation at the panel tilt angle. This entailed four steps:

i. The beam portion of the solar radiation, equal to the global minus the diffuse, was multiplied by R_b , the ratio of beam radiation on a tilted surface to that on the horizontal. R_b is equal to the cosine of the angle of incidence divided by the cosine of the zenith angle [Duffie et al., 1991, p. 25]. At times when the sun is low in the sky, the zenith angle approaches 90 ° and its cosine tends to zero. Dividing by this near-zero value often yields unreasonably large values for R_b . Thus, when the zenith angle was greater than 85 °, R_b was set to unity.

ii. The diffuse portion of the sky was assumed to be isotropic, and the diffuse radiation was multiplied by the view factor of the sky, that being

$$((1 + \cos\beta) / 2)$$

where β is the panel tilt angle.

iii. The ground reflected radiation was calculated from Eq. 5.8 in Section 5.3.1. An albedo of 0.7 was assumed.

iv. The beam, diffuse, and ground-reflected radiation values were summed, yielding the global radiation on the panel.

The global insolation for the panel with the rime shield was further multiplied by a factor of 0.85 as a rough measure to account for the decreased radiation on the rear face of the panel.

There are about 50 hours in the 132 years of data for which temperature, radiation, and insolation are not available. For these hours, the data sets have a value of "9999". When the program encountered these hours, it ignored them entirely. This will affect the results very little, since these hours are so infrequent.

8.2.2 Use of the Thermal Model

The thermal model was used to create a matrix of values for the critical ambient air temperature and the melt-rate at various thicknesses, windspeeds, and insolation levels. In essence, this matrix represented a point-wise definition of the critical air temperature and melt-rate functions.

For all runs of the thermal model, a sky temperature 25 °C below the ambient air temperature and a ground temperature 2 °C below the ambient air temperature were assumed. In addition, the radiation on the rear surface of the panel was assumed to be 20 % of that on the front.

For snow, the thermal models were run for the unmodified panel and the standard TN Conseil panel. A snow cover, initially eight centimetres thick (on the front side of the panel only), with a density of 300 kg/m³, an optical extinction coefficient of 30 m⁻¹, and a thermal conductivity of 0.2 Wm⁻¹K⁻¹ was assumed. The critical air temperature at which melting would be initiated was calculated for windspeeds of two, five and 10 m/s, snow thicknesses of eight, five, three, and one cm, and insolation levels of 300 and 1000 W/m² (see Table 8.1).

In previous modelling, the melt-rate was observed to increase linearly with temperature at temperatures greater than the critical temperature. Thus, the melt-rate at an ambient air temperature above the critical temperature can be found from:

$$R_{\text{snow}}(T_{\text{amb}}, w, G_T, t) = m(w, G_T, t) \cdot [T_{\text{amb}} - T_{\text{crit}}] \quad (8.1)$$

where R_{snow} is the melt-rate (cm/hr),
 T_{amb} is the ambient air temperature (°C),
 w is the windspeed (m/s),
 G_T is the average global insolation on the panel over the hour (W/m²),
 t is the thickness (cm),
 m is the partial derivative of R_{snow} with respect to temperature (cm°C⁻¹hr⁻¹),
and T_{crit} is the critical ambient air temperature to initiate melting (°C).

In Figures 7.7, 7.8, and 7.9, the melt-rate lines, graphed as a function of ambient air temperature, are roughly parallel. This indicates that m is not a function of G_T , and the value for m at 1000 W/m² can be used for all insolation levels. Thus, to calculate m at a given windspeed and thickness one needs only the melt-rate at two different temperatures. We know that the melt-rate at T_{crit} is zero. An obvious second temperature is zero °C. To find the melt-rate at zero °C, the energy available for melting, q_{panel} , is used to calculate R_{snow} by Eq. 7.1. In this way, m was calculated for windspeeds of two, five and 10 m/s, snow thicknesses of eight, five, three, and one cm, and an insolation level of 1000 W/m² (see Table 8.1).

The same procedure was followed for the rime covered panels. The thermal models were run for the unmodified panel, the panel with the standard TN Conseil modification, and the panel with the TN Conseil modification and a rime shield. The rime was assumed to have a density of

Table 8.1 Parameters for Snow Removal										
For Snow, density = 300 kg/m ³ , extinction coefficient = 30 1/m, thermal conductivity = 0.2 W/mK										
Wind = 2 m/s										
Thickness (cm)			1	1	3	3	5	5	8	8
Insolation (W/m ²)			300	1000	300	1000	300	1000	300	1000
Unmod.	Tambcrit	(C)	-5.6	-27.3	-3.7	-19.1	-2	-12.3	-0.5	-6.6
	q @ 0 C	(W/m ²)	112	536	60	310	24.9	182	1	90
	MR @ 0C	(cm/hr)	0.244364	1.169455	0.130909	0.676364	0.054327	0.397091	0.002182	0.196364
	Slope	(cm/hr/C)	0.043636	0.042837	0.035381	0.035412	0.027164	0.032284	0.004364	0.029752
TN Stand	Tambcrit	(C)	-17.5	-70.8	-18.2	-69.2	-15.9	-60.7	-13.3	-51.7
	q @ 0 C	(W/m ²)	173	688	115	449	80	314	55	217
	MR @ 0C	(cm/hr)	0.377455	1.501091	0.250909	0.979636	0.174545	0.685091	0.12	0.473455
	Slope	(cm/hr/C)	0.021569	0.021202	0.013786	0.014157	0.010978	0.011287	0.009023	0.009158
Wind = 5 m/s										
Thickness (cm)			1	1	3	3	5	5	8	8
Insolation (W/m ²)			300	1000	300	1000	300	1000	300	1000
Unmod.	Tambcrit	(C)	-4.5	-20.5	-3	-14.5	-1.6	-9.4	-0.5	-5.1
	q @ 0 C	(W/m ²)	115	529	61	307	28	181	3.5	90
	MR @ 0C	(cm/hr)		1.154182		0.669818		0.394909		0.196364
	Slope	(cm/hr/C)		0.056302		0.046194		0.042012		0.038503
TN Stand	Tambcrit	(C)	-15.4	-59.4	-17.4	-63	-15.7	-56.8	-13.4	-49.2
	q @ 0 C	(W/m ²)		694		455		319		220
	MR @ 0C	(cm/hr)		1.514182		0.992727		0.696		0.48
	Slope	(cm/hr/C)		0.025491		0.015758		0.012254		0.009756
Wind = 10 m/s										
Thickness (cm)			1	1	3	3	5	5	8	8
Insolation (W/m ²)			300	1000	300	1000	300	1000	300	1000
Unmod.	Tambcrit	(C)	-3.7	-16.3	-2.6	-11.7	-1.4	-7.5	-0.5	-4
	q @ 0 C	(W/m ²)		521		303		179		89
	MR @ 0C	(cm/hr)		1.136727		0.661091		0.390545		0.194182
	Slope	(cm/hr/C)		0.069738		0.056503		0.052073		0.048545
TN Stand	Tambcrit	(C)	-14.1	-53	-16.9	-59.5	-15.6	-54.6	-13.5	-47.7
	q @ 0 C	(W/m ²)		700		458		322		223
	MR @ 0C	(cm/hr)		1.527273		0.999273		0.702545		0.486545
	Slope	(cm/hr/C)		0.028816		0.016794		0.012867		0.0102

500 kg/m³, an optical extinction coefficient of 30 m⁻¹, and a thermal conductivity of 1.5 Wm⁻¹K⁻¹. The critical temperature and m were calculated for windspeeds of five, 10 and 20 m/s, rime thicknesses of five, three, and one cm and insolation levels of 300 W/m² (for the critical temperature only) and 1000 W/m² (see Table 8.2).

For the panel with the rime shield, it was assumed that there was no rime on the rear face of the panel. For the unmodified panel and the panel with the TN Conseil system, it was assumed that at any given time the thickness of the rime accumulation on the front face was equal to that on the rear face. This is probably a weak assumption. In the case of the TN Conseil modified panel, the airspace is such a good insulator that the outer surface of the Lexan back cover stays at a temperature very close to the ambient. Thus, rime removal from this surface may be severely retarded. On the other hand, the rear face of the unmodified panel is generally at a temperature very close to the temperature of the glass front cover. Thus, melting should occur roughly equally at the front and back. While the assumption of equal front and back rime thicknesses is good in this case, it suggests that for the unmodified panel the melt-rate should be halved, since half the melting is occurring at the rear face. However, this was not done here. This suggests that for both these configurations, the modelled performance reported here is probably optimistic, at least in comparison with the modelled performance of the panel with the rime shield. This assumption will not affect the time required to shed (i.e., for the critical temperature assumption to be satisfied), since shedding occurs before any melting does. It will affect the time required for complete melting, but since the radiation on the front surface is assumed to be five times stronger than that incident on the rear face, the effect will not be too great.

The program interpolates among the values calculated for the critical temperatures and melt-rates. For insolation levels between 300 W/m² and 1000 W/m², the change in critical temperature is linear, so interpolation yields the model value exactly. The melt-rate and critical temperature vary non-linearly with thickness and windspeed. Therefore, linear interpolation introduces some error.

8.2.3 Software Description

A printout of the C program used to perform the analysis is located in Appendix E. A number of different variations of the program were developed; each differed only by some hardcoded constants. Each variation was written for a specific combination of panel technology (unmodified, TN Conseil modified, TN Conseil modified with rime shield), accumulation type (rime or snow) and location (high mountains, low mountains, or valley).

8.3 Results

The results for the four sites are presented in Tables 8.3 through 8.6 and in Figures 8.1 through 8.8. In the graphs, the vertical axis shows the elapsed time, in hours, between January 1 and the point at which shedding or complete melt-off occurred. A month contains approximately 720 hours.

Table 8.2 Parameters for Rime Removal							
For Rime, density = 500 kg/m ³ , extinction coefficient = 30 1/m, thermal conductivity = 1.5 W/mK							
Wind = 5 m/s							
Thickness (cm)			1	1	3	3	5
Insolation (W/m ²)			300	1000	300	1000	300
Unmod.	Tambcrit	(C)	-2.8	-16.1	-1	-9.6	0.3
	q @ 0 C	(W/m ²)	88	509	25	260	-8
	MR @ 0C	(cm/hr)	0.192	1.110545	0.054545	0.567273	-0.017455
	Slope	(cm/hr/C)	0.068571	0.068978	0.054545	0.059091	0.058182
TN Stand	Tambcrit	(C)	-7.6	-34.7	-3.8	-21.5	-1.1
	q @ 0 C	(W/m ²)	143	642	59	333	15.2
	MR @ 0C	(cm/hr)	0.312	1.400727	0.128727	0.726545	0.033164
	Slope	(cm/hr/C)	0.041053	0.040367	0.033876	0.033793	0.030149
TN Shield	Tambcrit	(C)	-8.3	-37	-5.6	-27.7	-3.9
	q @ 0 C	(W/m ²)	144	672	79	420	45
	MR @ 0C	(cm/hr)	0.314182	1.466182	0.172364	0.916364	0.098182
	Slope	(cm/hr/C)	0.037853	0.039627	0.030779	0.033082	0.025175
Wind = 10 m/s							
Thickness (cm)			1	1	3	3	5
Insolation (W/m ²)			300	1000	300	1000	300
Unmod.	Tambcrit	(C)	-2.2	-12.5	-1	-8.3	0
	q @ 0 C	(W/m ²)	89	502		262	
	MR @ 0C	(cm/hr)	0.194182	1.095273		0.571636	
	Slope	(cm/hr/C)	0.088264	0.087622		0.068872	
TN Stand	Tambcrit	(C)	-6.2	-27.7	-3.4	-18.2	-1.3
	q @ 0 C	(W/m ²)		645		338	
	MR @ 0C	(cm/hr)		1.407273		0.737455	
	Slope	(cm/hr/C)		0.050804		0.040519	
TN Shield	Tambcrit	(C)	-6.7	-29.5	-5	-23.3	-3.7
	q @ 0 C	(W/m ²)		675		425	
	MR @ 0C	(cm/hr)		1.472727		0.927273	
	Slope	(cm/hr/C)		0.049923		0.039797	
Wind = 20 m/s							
Thickness (cm)			1	1	3	3	5
Insolation (W/m ²)			300	1000	300	1000	300
Unmod.	Tambcrit	(C)	-1.8	-9.8	-1	-7	-0.2
	q @ 0 C	(W/m ²)		493		265	
	MR @ 0C	(cm/hr)		1.075636		0.578182	
	Slope	(cm/hr/C)		0.109759		0.082597	
TN Stand	Tambcrit	(C)	-5	-22	-3.2	-15.6	-1.5
	q @ 0 C	(W/m ²)		648		344	
	MR @ 0C	(cm/hr)		1.413818		0.750545	
	Slope	(cm/hr/C)		0.064264		0.048112	
TN Shield	Tambcrit	(C)	-5.5	-23.4	-4.4	-19.8	-3.6
	q @ 0 C	(W/m ²)		679		432	
	MR @ 0C	(cm/hr)		1.481455		0.942545	
	Slope	(cm/hr/C)		0.06331		0.047603	

Table 8.3 Modelled Snow Melt-off Times in Bagotville, Quebec					
Tilt Angles: Unmodified-- 60 deg., TN Standard-- 60 deg.					
Latitude: 48.33					
	Time to Shed (Hrs)		Time to Melt (Hrs)		
Year	Unmod	TN Stand	Unmod	TN Stand	
53	366	9	1333	181	
54	802	9	1212	302	
55	1116	10	1641	254	
56	190	9	1404	154	
57	483	9	1573	156	
58	587	11	1715	203	
59	385	9	1595	326	
60	492	9	1809	229	
61	1258	33	1599	181	
62	178	10	1622	298	
63	1524	35	1979	397	
64	83	9	1553	230	
65	198	9	1520	106	
66	394	9	1089	276	
67	850	34	2001	371	
68	803	10	1835	228	
69	536	58	1162	206	
70	756	9	1501	109	
71	109	9	1381	254	
72	60	34	516	180	
73	12	11	1544	230	
74	512	33	1355	204	
75	155	9	1215	299	
76	35	33	1405	225	
77	34	13	1600	302	
78	200	9	1045	132	
79	130	9	1401	251	
80	262	9	1523	109	
81	624	9	1115	274	
82	100	34	1550	227	
83	12	9	659	182	
84	82	9	1113	204	
85	997	10	1281	156	
86	282	9	1020	178	
87	35	33	853	224	
88	10	10	542	132	
89	180	9	1189	206	
Average	400.8649	16	1363.514	220.973	
SD	381.6306	12.16108	350.778	68.88709	

Figure 8.1 Modelled Time to Shedding, Bagotville, Qc., for Eight cm Snowcover on January 1

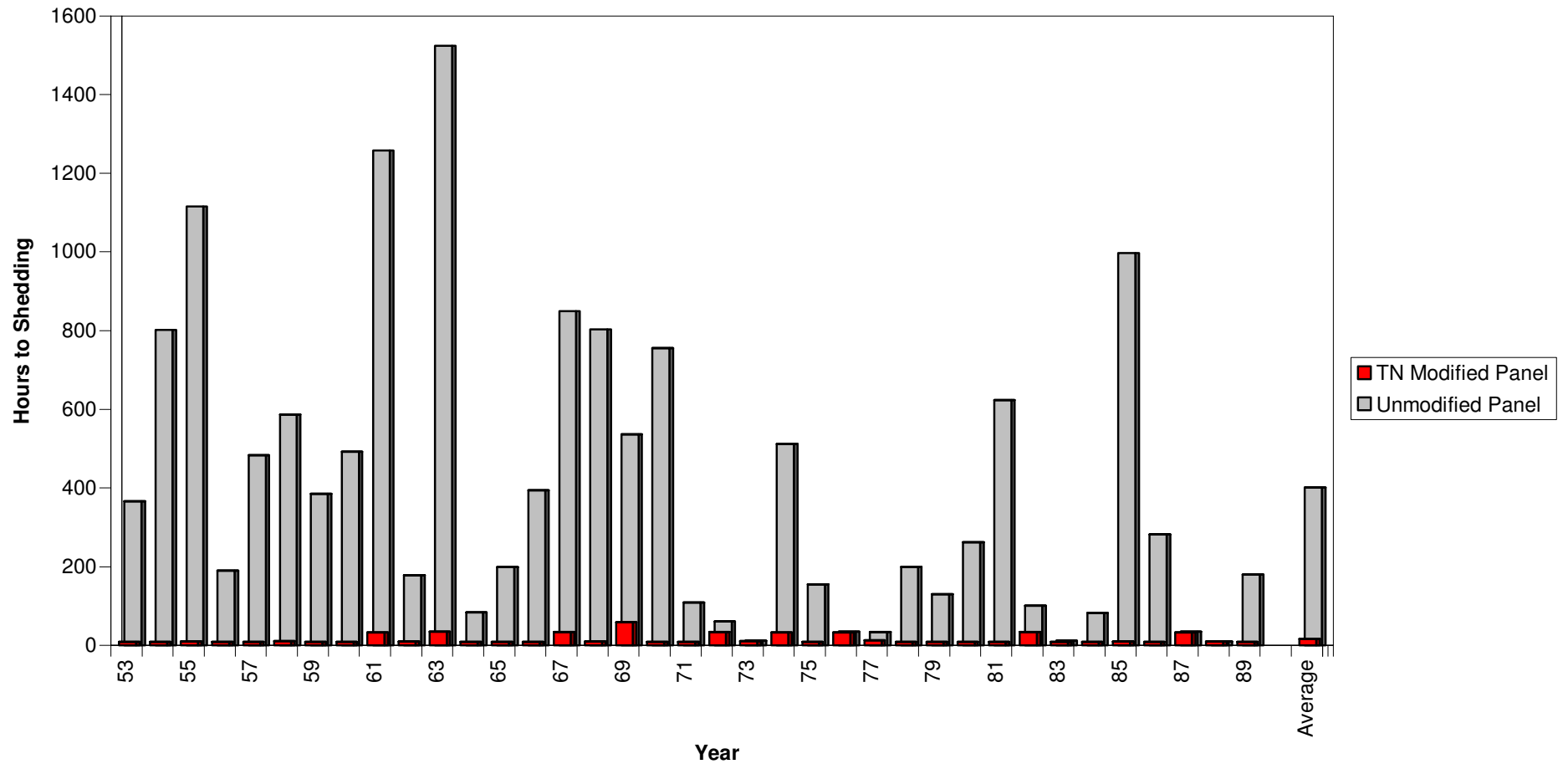


Figure 8.2 Modelled Time to Melt-off, Bagotville, Qc., for Eight cm Snowcover on January 1

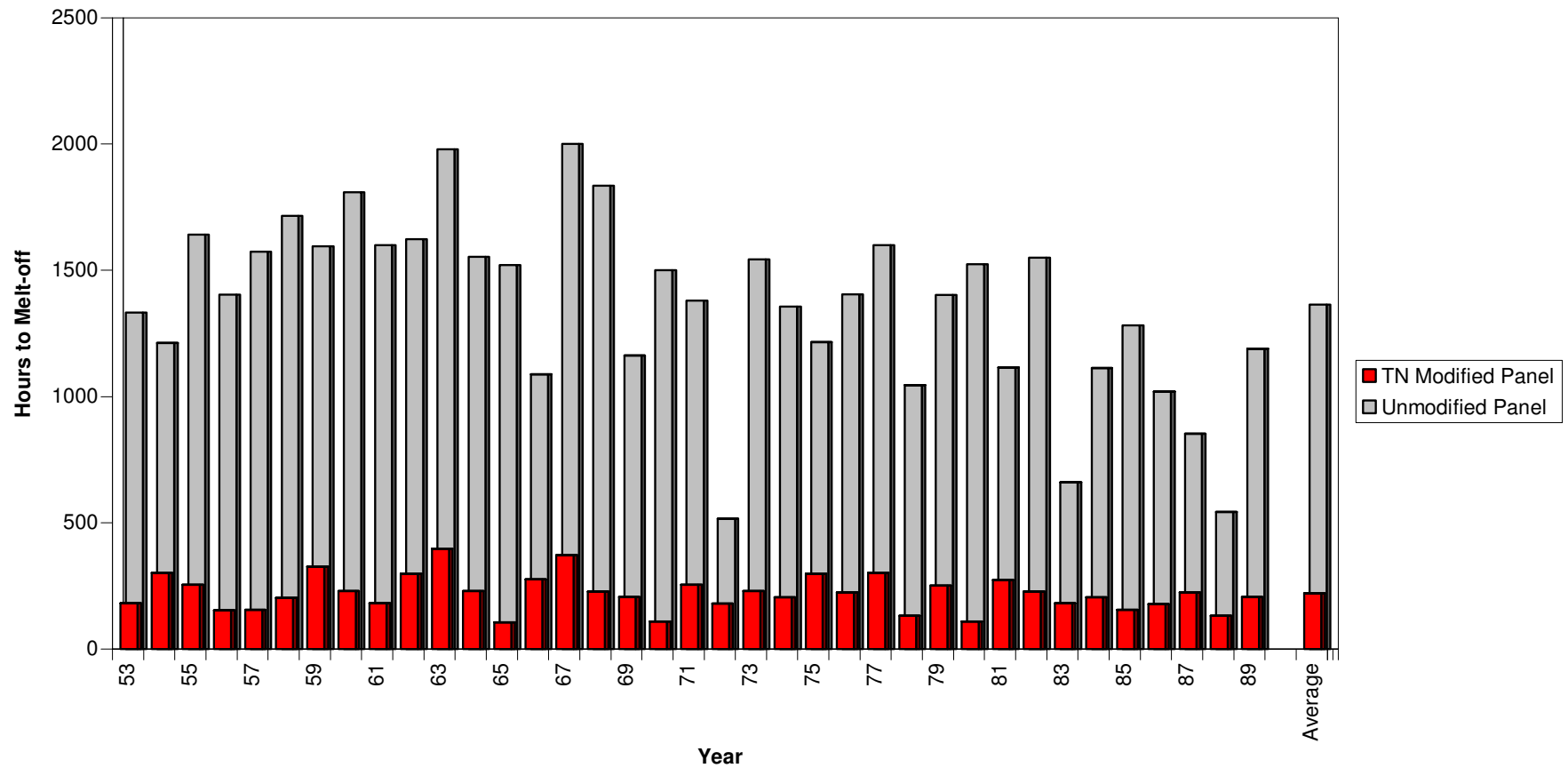


Table 8.4 Modelled Rime Melt-off Times in Mountains Near Daniels Harbour, Nfld.							
Tilt Angles: Unmodified-- 60 deg., TN Standard-- 60 deg., TN w/ Rime Shield-- 45 deg.							
Latitude: 50.23							
	Time to Shed (Hours)			Time to Melt (Hours)			
Year	Unmod	TN Stand	TN w/ RS	Unmod	TN Stand	TN w/ RS	
66	1563	1402	517	1934	1596	1548	
67	2052	1307	1283	2600	1980	1933	
68	852	825	493	1523	1380	1378	
69	622	34	34	1163	1140	1113	
70	802	802	227	823	829	828	
71	948	948	587	2146	1739	1525	
72	315	315	315	1858	1839	1835	
73	809	810	539	2217	1835	1666	
74	516	516	516	2459	1978	1837	
75	1859	1572	204	2246	1885	1762	
76	670	537	467	1923	1208	1210	
77	180	180	180	2144	1452	1331	
78	227	226	226	2313	1238	1281	
79	52	52	52	59	62	62	
80	279	282	276	2364	1617	1334	
81	246	178	178	950	1009	999	
82	1715	10	10	2316	1836	1716	
83	261	251	251	829	1067	1114	
84	139	1186	131	1828	1832	1809	
85	1666	372	371	2241	1690	1666	
86	634	633	326	648	659	659	
87	1879	276	276	2122	1931	1835	
88	1449	1448	1356	1666	1524	1523	
89	188	188	188	2219	1884	1765	
Average	830.125	597.9167	375.125	1774.625	1467.083	1405.375	
SD	638.7255	479.277	326.6377	661.648	475.8956	439.2099	

Figure 8.3 Modelled Time to Shedding, Daniels Harbour, Nfld., for Five cm Rime Deposit on January 1

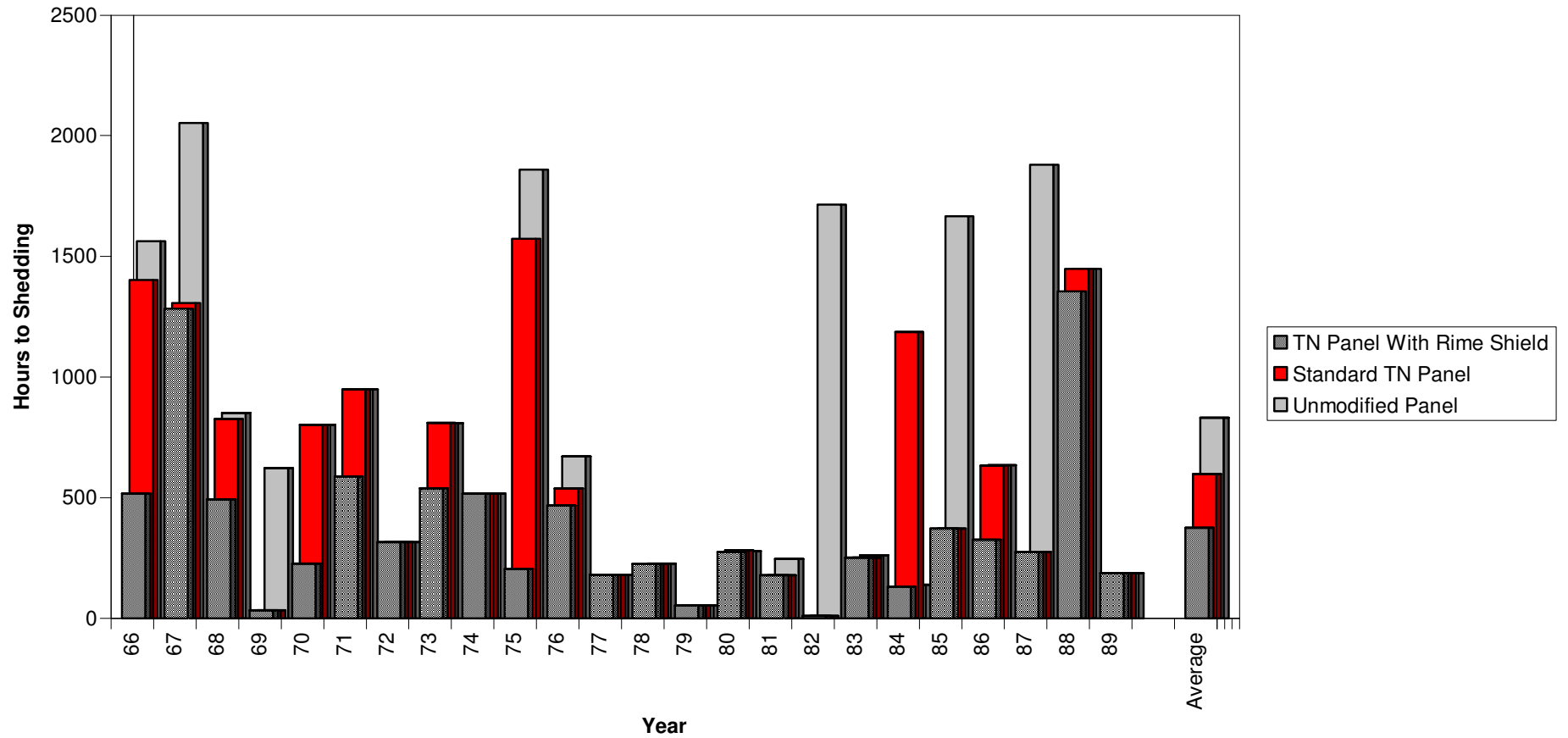


Figure 8.4 Modelled Time to Melt-off, Daniels Harbour, Nfld., for Five cm Rime Deposit on January 1

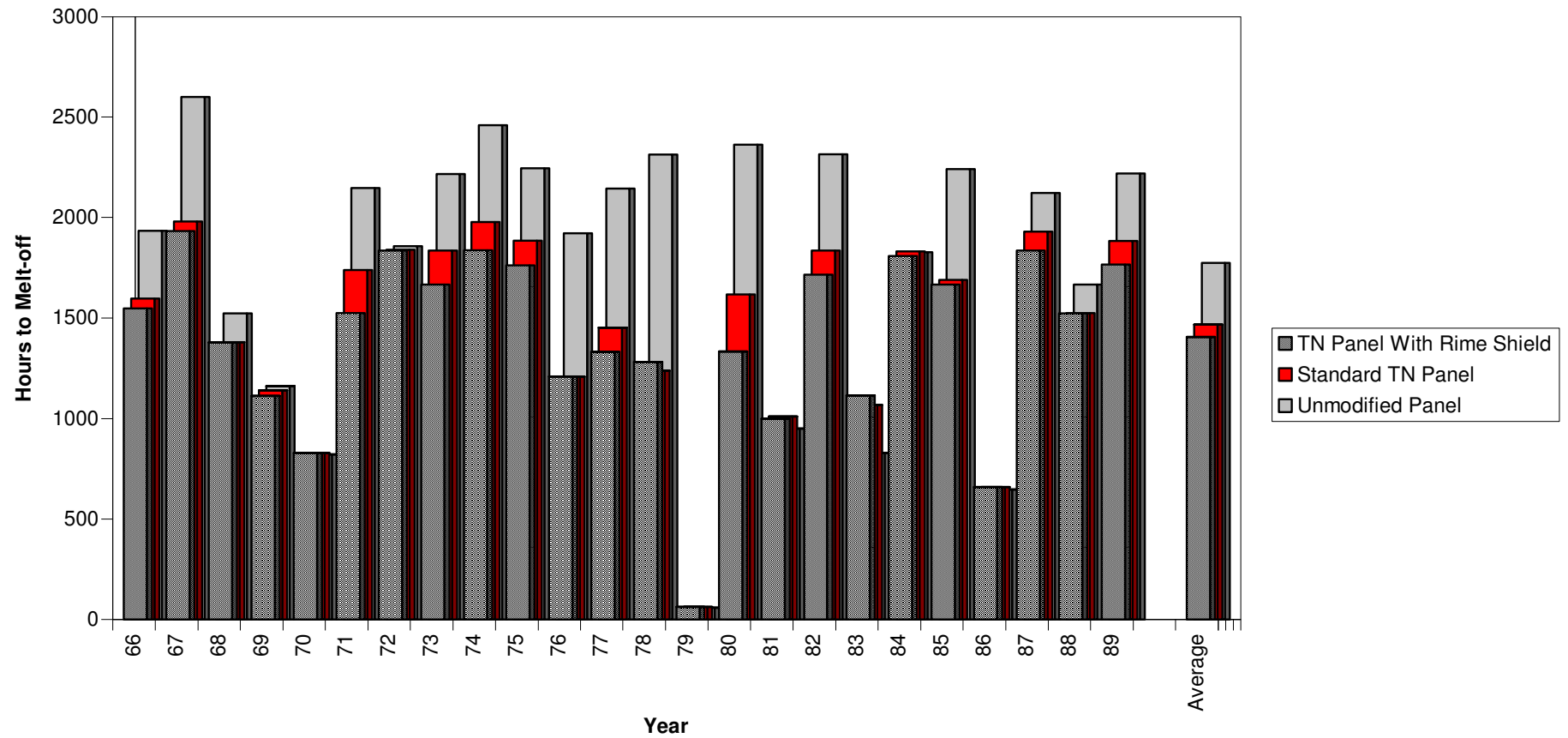


Table 8.5 Modelled Rime Melt-off Times in Mountains Near Norman Wells, NWT							
Tilt Angles: Unmodified-- 90 deg., TN Standard-- 90 deg., TN w/ Rime Shield-- 45 deg.							
Latitude: 65.28							
	Time to Shed (Hours)			Time to Melt (Hours)			
Year	Unmod	TN Stand	TN w/ RS	Unmod	TN Stand	TN w/ RS	
56	1787	1786	1786	2413	1907	1906	
57	344	344	344	2529	2317	2147	
58	2649	1689	1666	2796	2628	2220	
59	2315	2172	2171	2359	2341	2315	
60	2388	2388	1310	2727	2605	2533	
61	2700	2675	1934	2751	2726	2701	
62	2100	2054	2052	2148	2124	2103	
63	531	1622	1621	2413	2341	2321	
64	2581	2579	1981	2724	2654	2604	
65	1597	1501	1478	2271	1646	1644	
66	2198	2149	2005	2821	2224	2198	
67	2413	1836	1835	2632	2485	2390	
68	1022	1021	1021	2654	1838	1932	
69	2222	1358	1358	2342	1595	1573	
70	1334	1334	1334	2508	2244	2197	
71	2483	1813	1812	2629	2507	2485	
72	2412	1933	1886	2485	2436	2270	
73	2341	2005	2004	2630	2173	2124	
74	2532	2270	2222	2892	2556	2508	
75	2364	1356	1356	2532	2391	2368	
76	2244	2220	1549	2296	2269	2247	
77	2412	2124	2124	2610	2415	2389	
78	2509	1046	1046	2605	2507	2294	
79	2582	2316	2029	2650	2604	2414	
80	2698	1335	1335	2797	2558	2148	
81	347	347	347	2199	1696	1696	
82	1863	1861	1861	2607	1983	1936	
83	2486	2244	2198	2628	2533	2487	
84	2196	2103	1933	2295	2221	2218	
85	2726	1644	1596	2892	1984	1861	
86	2868	974	974	2894	2675	2221	
87	2605	1909	1645	2774	2029	1960	
88	1380	1311	1310	2387	1452	1454	
89	973	972	829	2369	2315	2223	
Average	2064.765	1714.441	1586.824	2566.441	2264.088	2179.029	
SD	696.4967	566.8691	483.0875	204.5019	332.5633	291.7464	

Figure 8.5 Modelled Time to Shedding, Norman Wells, for Five cm Rime Deposit on January 1

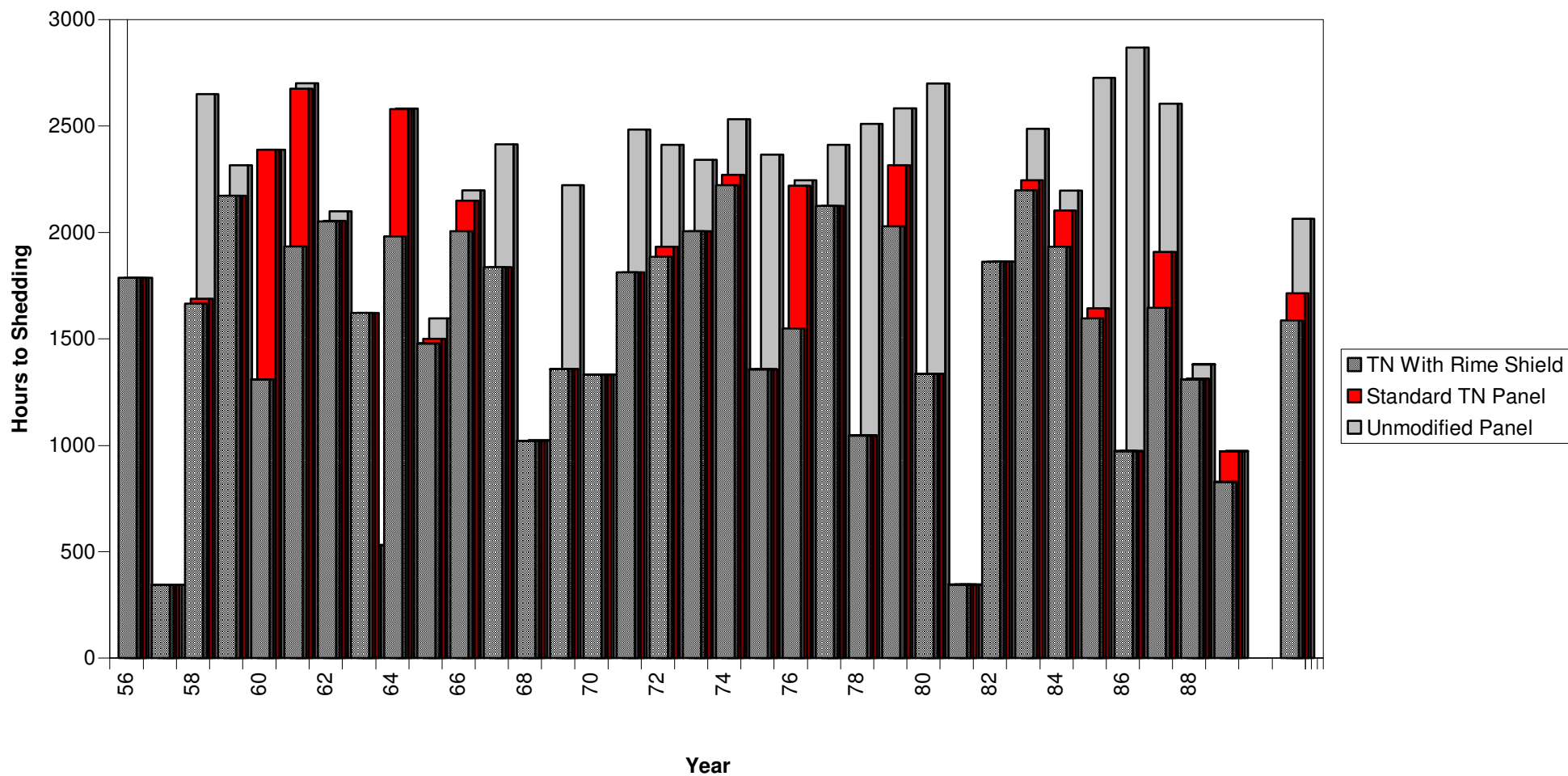


Figure 8.6 Modelled Time to Melt-off, Norman Wells, for Five cm Rime Deposit on January 1

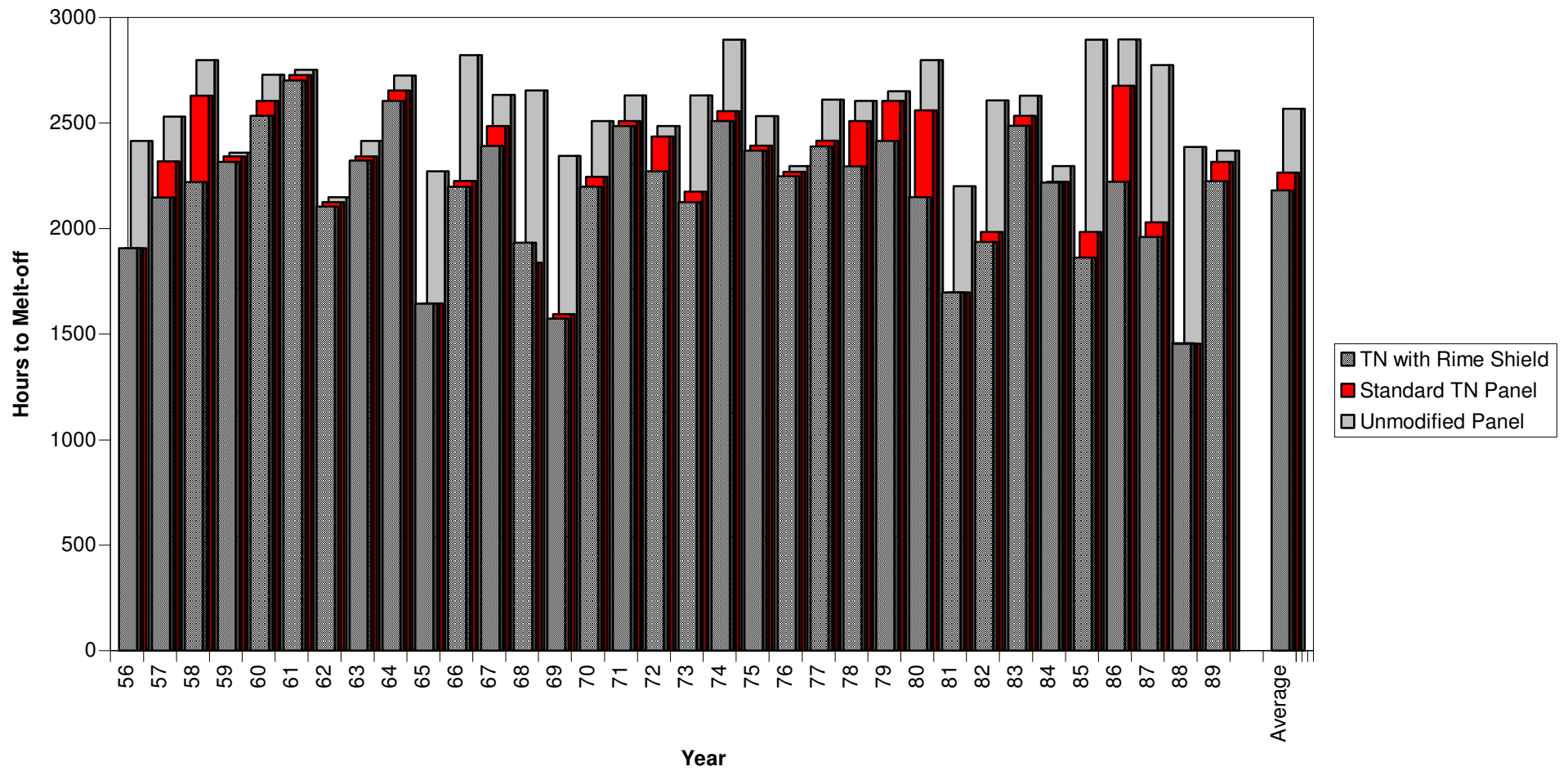


Table 8.6 Modelled Rime Melt-off Times in Mountains Near Prince George, BC								
Tilt Angles: Unmodified-- 85 deg., TN Standard-- 85 deg., 60 deg., TN w/ Rime Shield-- 45 deg.								
Latitude: 53.88								
	Time to Shed (Hours)				Time to Melt (Hours)			
Year	Unmod	TN @ 85	TN @ 60	TN w/ RS	Unmod	TN @ 85	TN @ 60	TN w/ RS
53	805	804	804	12	2531	1380	1404	1260
54	900	733	733	733	1764	948	949	926
55	2074	852	852	708	2313	1594	1597	1188
56	1811	1811	1811	874	2415	1859	1839	1837
57	1691	1046	1046	995	2342	1454	1454	1429
58	84	83	83	82	2222	1359	1402	1287
59	1525	804	804	804	2318	1569	1528	1473
60	1884	709	709	708	1910	1835	1886	1286
61	1211	901	1210	107	1836	1622	1619	1500
62	1767	1620	1620	949	2102	1860	1857	1767
63	873	830	830	830	1309	926	926	926
64	1212	12	12	12	2127	1239	1257	1236
65	1142	1142	1142	996	1595	1522	1504	1498
66	1282	1259	1259	900	1885	1331	1331	1308
67	1524	228	228	228	2198	1380	1402	1235
68	324	324	324	299	1432	923	925	925
69	1693	994	994	972	2169	1261	1282	1235
70	1260	541	541	541	1837	1257	1258	1212
71	420	158	158	158	2409	1190	1263	1190
72	1692	923	923	923	1884	1694	1715	1667
73	1237	301	1138	301	2146	1263	1283	1260
74	1642	1067	1067	997	2314	1836	1835	1522
75	2316	446	1263	446	2388	1979	1933	1619
76	636	397	397	397	2290	1019	1188	1019
77	947	419	419	419	2222	949	1092	945
78	875	587	588	516	1932	927	1019	926
79	1550	851	877	851	1716	1599	1598	1595
80	1332	827	827	826	2078	1382	1382	1379
81	491	466	467	466	1164	518	539	538
82	1165	1163	1163	300	2125	1743	1742	1668
83	1236	253	253	252	1789	1239	1284	1237
84	1188	35	35	35	1621	855	971	854
85	1069	1068	1068	1068	2269	1406	1406	1402
86	227	226	226	226	1645	1358	1383	1353
87	1070	1069	1069	468	1858	1331	1332	1286
88	1332	540	540	539	2198	1383	1384	1333
89	2004	467	467	373	2367	1838	1839	1501
Average	1229.486	701.5135	755.3243	548.9459	2019.459	1373.73	1394.811	1292.486
SD	520.8913	420.8419	433.4793	327.0632	327.3768	335.0178	314.0787	274.9347

Figure 8.7 Modelled Time to Shedding, Prince George, for Five cm Rime Deposit on January 1

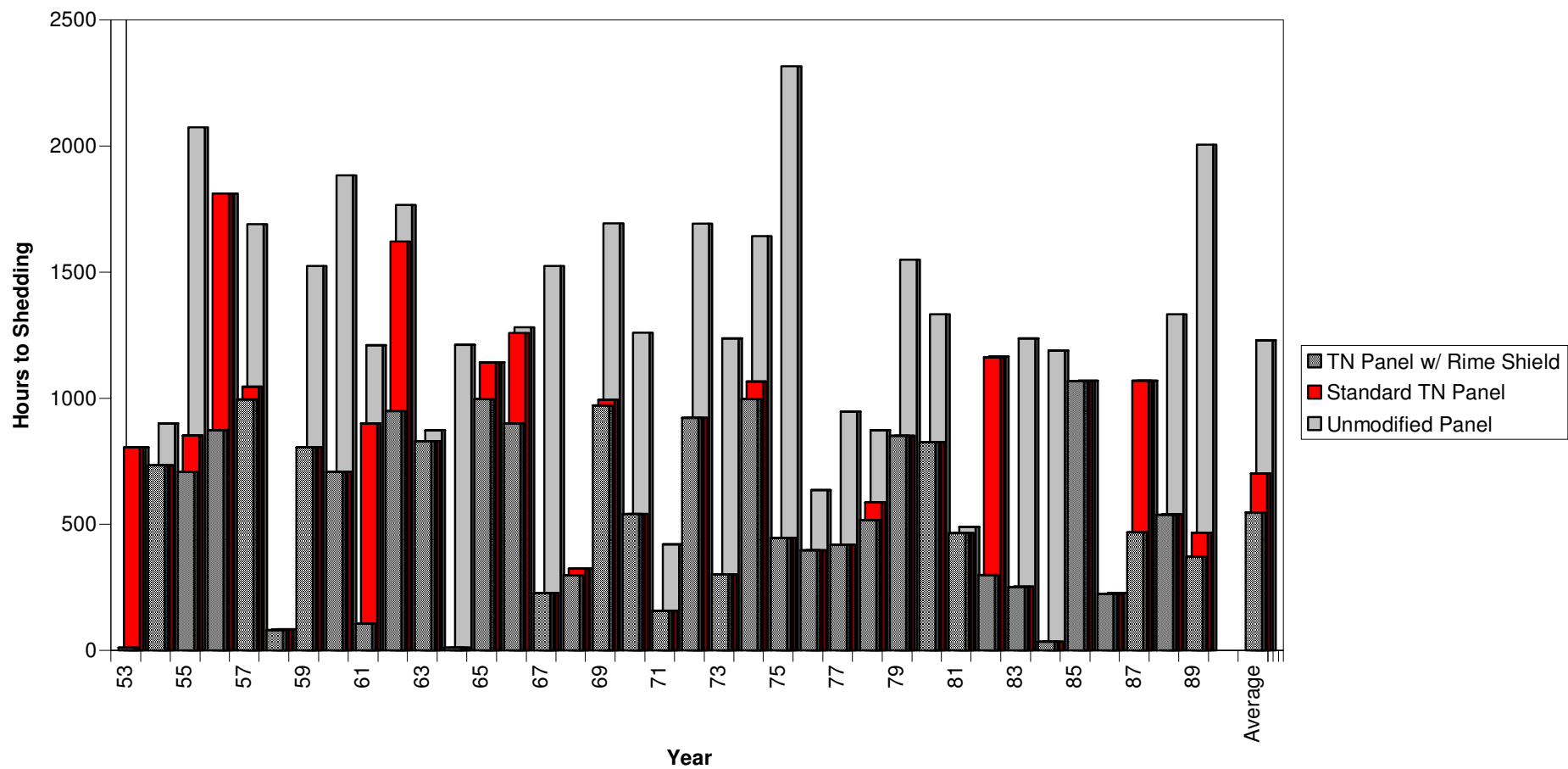
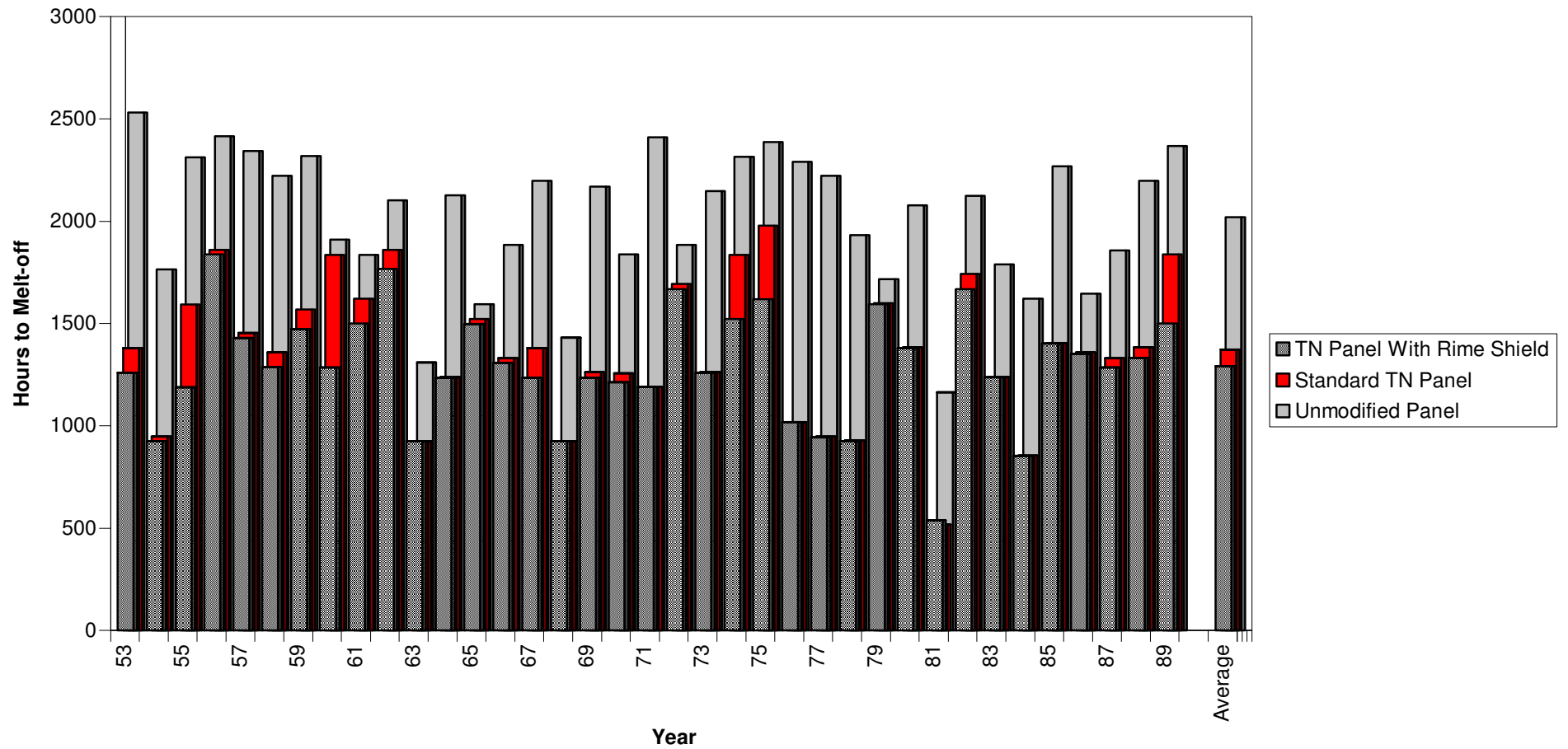


Figure 8.8 Modelled Time to Melt-off, Prince George, for Five cm Rime Deposit on January 1



At all four sites, the program predicts that the TN Conseil system consistently reduces the time to shedding and melt-off when compared with an unmodified panel.

In several instances (at Norman Wells in 1963, for example) the model reports that the unmodified panel sheds before the TN Conseil modified panels. These instances occur when the air temperature rises well above zero ° C during the night. The program calculates T_{crit} , the air temperature for shedding, on the basis of an insolation level of zero W/m^2 . Since the derivative of T_{crit} with respect to insolation is steeper for the TN Conseil modified panels (i.e., an increase in insolation raises their temperatures more than it does for the unmodified panel), at zero W/m^2 , T_{crit} for the TN Conseil modified panel is higher than that for the unmodified panel. The model predicts that the unmodified panel sheds before the TN Conseil modified panels when the insolation level is at or near zero, T_{crit} for the unmodified panel is lower than T_{crit} for the TN Conseil modified panel as a result, and the ambient air temperature rises to a level between the two T_{crit} temperatures. However, in real life, when the temperature is above zero ° C, melting may occur not just at the interface of the accumulation and the panel (as is assumed by the model), but all over the exterior surface of the accumulation. Thus, under these conditions, the model is no longer accurate, and the instances when the unmodified panel sheds sooner than the TN Conseil modified panels should be ignored. In reality, it is probable that both panels would have shed at this point.

There are a number of ways to summarize this data and compare the performance of the different technologies. The average shedding and melting times, the standard deviations for these times, and the worst-case scenarios can be compared. The worst-case scenarios are the longest shedding and melt-off times for all the years for which the program was run. These measures are given in the Tables 8.7 and Tables 8.8.

Tables 8.7 Modelled Time to Shed for Different Sites and Different Technologies

	Average (hours)			Worst-case (hours)			Standard Deviation (hours)		
Site	Un-mod	TN	TN RS	Un-mod	TN	TN RS	Un-mod	TN	TN RS
Prince George	1229	702	549	2316	1811	1068	521	421	433
Norman Wells	2065	1714	1587	2868	2675	2222	696	567	483
Daniels Harbour	830	598	375	2052	1572	1356	639	479	327
Bagotville	401	16	NA	1524	58	NA	382	12	NA

"Unmod" indicates unmodified panel; "TN" indicates standard TN Conseil modified panel; "TN RS" indicates TN Conseil modified panel with rime shield.

Tables 8.8 Modelled Time to Complete Melt-off for Different Sites and Different

Technologies

	Average (hours)			Worst-case (hours)			Standard Deviation (hours)		
Site	Un-mod	TN	TN RS	Un-mod	TN	TN RS	Un-mod	TN	TN RS
Prince George	2019	1374	1292	2531	1979	1837	327	335	275
Norman Wells	2566	2264	2179	2894	2726	2701	205	333	292
Daniels Harbour	1775	1467	1405	2600	1980	1933	662	476	439
Bagotville	1364	221	NA	2001	397	NA	351	69	NA

"Unmod" indicates unmodified panel; "TN" indicates standard TN Conseil modified panel; "TN RS" indicates TN Conseil modified panel with rime shield.

Table 8.9 Shedding and Melt-off Times as a Percentage of Time Required for Unmodified Panel

	Prince George	Norman Wells	Daniels Harbour	Bagotville
Shedding				
Ave. TN	57	83	72	4
Ave. TN RS	45	77	45	NA
Worst TN	78	93	77	4
Worst TN RS	46	77	66	NA
Melt-off				
Ave. TN	68	88	83	16
Ave. TN RS	64	85	79	NA
Worst TN	78	94	76	20
Worst TN RS	73	93	74	NA

"Ave" refers to average values, "Worst" refers to worse-case values.

"TN" refers to standard TN Conseil modified panel, "TN RS" refers to TN Conseil modified panels with a rime shield.

8.4 Discussion

8.4.1 Why the Shedding and Melt-off Times seem Very Long

The times required for melt-off and shedding seem improbably long-- it is a rare panel that is covered in snow for two months, a scenario suggested by the Bagotville results. Part of this may be due to inaccuracies in the models. However, the densities, thermal conductivities, and optical extinction coefficients chosen for the snow and rime accumulations modelled here are those for worst-case snow and rime: dense accumulations that will insulate poorly and not permit much light to pass through them. In terms of real-life conditions, the snow modelled here might best correspond to a heavy, wet snow that froze onto the array after several days; the rime might correspond to a hard rime that densified and froze to a fairly solid mass. These accumulations-- especially the frozen, wet snow-- are fairly rare, suggesting that the models may be accurate, but our intuitive expectations about the longevity of snow and rime deposits may be based on much less troublesome types of accumulation.

If it is the case that most rime and snow accumulations will be less dense, better insulators, and more transparent than the accumulations modelled here, the actual shedding and melt-off times may be significantly shorter than those reported. It is important to note that the melting rate of the panels at a given insolation level, windspeed, and thickness is a non-linear function of the ambient air temperature: a certain threshold must be reached before melting occurs. Changing the thermal conductivity and optical extinction coefficient moves this threshold significantly. Thus, a less dense and more transparent snow accumulation might move the critical temperature for the unmodified panel into the range of temperatures that occurs on most winter days. This could radically alter the results for the unmodified panel, which under the modelled conditions has a very high critical temperature, but would be less apparent for the TN Conseil modified panels, which already have a low critical temperature. This would bring the melt-off times for the panels more in line with those commonly observed (i.e., within a week or two). For rime, a less dense and more transparent accumulation may result in drastically better performance from the TN Conseil-modified panels. If the TN Conseil technology lowers the critical temperature into the range of average daily temperatures, an improvement in panel shedding and melting times greater than the one suggested by the above results will be observed. On the other hand, it is known from the longevity of rime on unmodified panels in the field that the critical temperature for the unmodified panels with real rime accumulations is quite high.

8.4.2 Performance for Rime versus Snow

It appears that the TN Conseil system performs much better for panels with snowcover than those covered in rime. There are several reasons for this. First, in the case of rime, it is assumed that the rear face of the panel is covered in accumulation. This blocks radiant energy from reaching the rear absorber foil. Second, the rime has a much higher thermal conductivity than the snow, and therefore insulates poorly against heat loss. Third, the rime is considerably denser than the snow, and therefore takes more energy to melt it off.

8.4.3 Shedding versus Complete Melt-off Times

The times required to satisfy the "shedding" (critical temperature) and complete melt-off criteria are very different. This can be attributed to the high enthalpy of fusion for water: the phase change from ice to liquid water requires a vast amount of energy that comes only from the solar energy penetrating the accumulation. Put another way, while the temperature of the panel may easily reach zero ° C, only under conditions of strong insolation will there be significant melting. The actual time required to remove the accumulation probably lies somewhere between the shedding and the complete melt-off time. Because rime may have an occasion to completely wet the panel surface before freezing, it will probably adhere better than snow. It could be argued that the shedding times should be used with the snow accumulation and the complete melt-off times be used for the rime accumulations.

8.4.4 Melting Performance in the Far North

When comparing the three rime sites, the performance of the TN Conseil System at the Norman Wells site is noticeably poorer than its performance at the more southern sites. There are two explanations for this. First, the Norman Wells site is considerably colder, and it is therefore more difficult to melt off the rime. Second, with the site being just above the Arctic Circle, during the winter there is much less insolation available to raise the temperature of the panel. This suggests that installations in the far north will not greatly benefit from the TN Conseil technology during the winter months. However, as the vernal equinox approaches, the TN Conseil technology will rapidly become more effective, and will promote earlier melting.

8.4.5 Utility of the Rime Shield

The performance of the standard TN Conseil technology and that of the TN Conseil-modified panel with rime shield appears to be very similar in the above results. This is deceptive, because it is based on the assumption that the rime on the rear face of the TN Conseil panel will clear itself from the Lexan back cover. Since the airspace between the panel and the back cover is an effective layer of insulation, this rime will not be easily melted off. Thus, it is probable that with each riming occurrence the rime accumulation on the rear face of the standard TN Conseil technology will thicken. This will seriously degrade the melting and shedding performance of the technology over the winter. On the other hand, the rime shield ideally prevents rime accumulation on the Lexan back cover, and the performance of the system will be unchanged over the winter.

When comparing the performance of the standard TN Conseil technology and that of the TN Conseil-modified panel with rime shield, it must be remembered that the above results are based on the assumption that rime will accumulate on the rear face of a panel. This appears to be a good assumption, based on observations of panels in the field. If, for some reason, it turns out that rime does not accumulate on the rear face, the rime shield has no utility and the shedding and melting performance of the standard TN Conseil technology, when compared with the unmodified panel, will be better than that reported above.

8.4.6 Interpreting the Results

The reader must be careful when interpreting the above results. The above analysis assumes that there is a certain accumulation on the panels on January 1, and then no further rime or snow accumulation on the panel occurs until melt-off. This is an unrealistic assumption-- rime and snow accumulation may occur with varying severity at various times throughout the autumn, winter and early spring. Thus, while the results can be used to compare the abilities of the unmodified panel and panel with TN Conseil technology to melt snow and rime, they must not be construed as the actual improvement in the availability of the panel to generate electricity. Further, since the probability of rime and snow accumulation is unknown, there is no way to use the above results to estimate the loss-of-load probabilities for the various technologies.

8.4.7 Further Work

It is unlikely that further efforts at modelling the melting ability of the panels with and without the TN Conseil modifications will yield many valuable results. There are too many unknowns: the variability of weather, the properties of rime, the adhesion and friction of rime and snow on glass, the role of convective cooling by wind, etc. Researching these unknowns would be prohibitively difficult and expensive.

It will be much cheaper, and the results more reliable, to experimentally test the performance of the TN Conseil Technology. This has already been done in the case of snow (see Section 10, [TN Conseil, 1994]), and the technology is presently being further tested at a site in Northern Québec. However, this experimental work has not been done in the case of rime.

There are two ways to experimentally test the melting performance of rime-covered panels. A laboratory cold chamber can be used to simulate natural rime accumulation; then either lamps or natural sunlight can be used to monitor the melting performance. Alternatively, the various technologies can be installed at rime-prone sites and monitored over one or more winters.

While it has some risks, testing the technology at a rime-prone site is probably the preferred alternative. It will be impossible to simulate all the natural conditions associated with a mountain-top site inside a laboratory cold chamber. The differences between the natural and the simulated environment may be very significant. Further, the laboratory experiment gives no indication of the likelihood of rime accumulation in the first place, and therefore can not be used to estimate loss-of-load probabilities. On the other hand, if the winters during which the monitoring occurs are unusually mild, a real site may yield no useful results. In addition, monitoring equipment at a mountaintop site may be prone to failure.

If rime accumulation on the panels at remote sites is a serious problem, as suggested in Chapter 2, the value of testing and developing this technology may be quite large. The eventual reduction in costs associated with improved system reliability and/or lower autonomy requirements could be very significant.

CHAPTER 9

SUMMER BATTERY CHARGING PERFORMANCE

9.1 Introduction

The TN Conseil snow removal technology, being a passive device, can not be turned off during the summer, even though there is no danger of snow accumulation during this time. As a result, panel temperatures are elevated not only for the winter, but also for the summer. For a given current, increasing the temperature of a PV panel has the effect of decreasing its output voltage. Therefore, there is a danger that the TN Conseil system could hinder battery charging during the summer months. Using the thermal model of the TN Conseil system, it is possible to determine whether this is likely to be a problem. Specifically, it is important to investigate whether a single panel or a parallel arrangement of panels will be capable of charging a nominally twelve volt battery bank under worst-case summer conditions.

9.2 Worst-Case Meteorological Conditions

In general, a PV panel with the TN Conseil technology operates at a higher temperature than an unmodified panel. This occurs for two reasons: first, the Lexan back cover insulates against heat loss, and second, the selective surface on the back of the panel absorbs ground reflected radiation more efficiently. During summer, when there will be no snow on the ground, the ground reflected radiation will be much lower than during the winter. The insulative effect of the back cover will be undiminished, however, and solar radiation absorbed at the front of the panel will cause the panel to operate at an elevated temperature.

The principal factors influencing the panel temperature are ambient air temperature, wind speed, and the short-wave radiation incident on the front and back of the panel. Panel temperatures will be highest when there is no convective cooling (i.e., wind speed of zero), high ambient air temperatures, and bright sun on the front of the panel (approximately 1000 W/m^2) and on a bright surface underneath or behind the array, causing a high radiation flux on the back of the array

(assume 200 W/m^2)³⁶. A high sky temperature (perhaps 10°C below the ambient air temperature) and a high ground temperature (two $^\circ \text{C}$ above the ambient air temperature) will also slightly raise the panel temperature. This is a worst-case scenario: if the voltage of the array is sufficient to charge the battery at the panel temperature resulting from these conditions, it will be sufficient under all conditions of reasonable insolation. Lowering the front panel insolation, for example, will significantly lower the panel temperature, but will decrease the panel voltage by a small amount related to the natural logarithm of the insolation level.

9.3 Method of Investigation

Usually, the battery bank and PV array are connected via a charge controller. The charge controller charges at voltages up to the voltage regulation setpoint (VR), at which point the charger enters a trickle- or cycle- charge mode of operation. This setpoint is often derated on the basis of battery temperature, since a warmer battery is charged at a lower voltage. That is, the voltage regulation setpoint decreases with increasing temperature [Energy Diversification Research Laboratory, 1995].

Between the array and the charge controller there is a voltage drop due to ohmic resistance and blocking diodes. This voltage drop, or "lead loss", may be as large as 1.5 V.

It is important that the panel be able to bring the charge controller to its voltage regulation setpoint. This is possible only when the array open circuit voltage exceeds the sum of the voltage regulation setpoint and the voltage drop between the array and the charge controller. The open circuit voltage is used because it is the maximum voltage attainable by the panel. The voltage regulation setpoint is a function of battery temperature and the panel open circuit voltage is a function of the solar cell temperature. These temperatures are, in turn, dependant on the ambient air temperature; for the remainder of this section it is assumed that the battery temperature is equal to the air temperature.

Stated formally, battery charging can occur only when the following inequality is satisfied.

$$(V_{\text{panel}} - D_{\text{panel}}\Delta T) - V_{\text{loss}} > (V_{\text{cc}} - D_{\text{cc}}\Delta T) \quad (9.1)$$

where V_{panel} is the open circuit voltage (V) of the array when the air temperature (not the cell temperature) is 25°C ,
 D_{panel} is the temperature derating for the panel open circuit voltage, in V per $^\circ \text{C}$ that the air temperature exceeds 25°C ,
 ΔT is equal to the air temperature ($^\circ \text{C}$) minus 25°C ,
 V_{loss} is the voltage drop between the panel and the charge controller (V),
 V_{cc} is the rated voltage regulation set point (V) for the charge controller at an air temperature of 25°C ,

³⁶ A wall covered in a reflective white paint might produce such a high back panel insolation.

and D_{cc} is the temperature derating for the charge controller voltage regulation set point, in V per °C that air temperature exceeds 25 °C.

For a twelve volt battery system with an on/off charge controller, a typical value for D_{cc} is 0.03 V/°C, and V_{cc} ranges from 13.8 V to 14.9 V, with an average value of 14.4 V [Energy Diversification Research Laboratory, 1995].

D_{panel} and V_{panel} must be determined using the thermal model. They are functions of the make and model of panel, the insolation, and the windspeed. The operating temperature of the cells at a specified windspeed and insolation level and an air temperature of 25 °C can be found from the thermal model. V_{panel} is determined by derating the open circuit voltage for standard operating conditions on the basis of the operating temperature of the cells. For Siemens M55 and M75 panels, the open circuit voltage of each cell must be derated by 2.3 mV for every degree that the cell temperature exceeds 25 °C [Siemens Solar Industries, 1990]. This derating factor should not be confused with D_{panel} , which is for the entire panel and is referenced to the air temperature, not the cell temperature. An M55 panel has 36 cells; an M75 module has 33.

To find D_{panel} , the thermal model is used to determine the cell temperature for an air temperature of T_1 , but the same insolation and windspeed conditions as for V_{panel} . The open circuit voltage at this operating temperature is then calculated. Since the cell temperature, and therefore the open circuit voltage, varies linearly with ambient air temperature,

$$D_{panel} = \frac{V_{oc}(25) - V_{oc}(T_1)}{T_1 - 25} \quad (9.2)$$

where $V_{oc}(T)$ is the open circuit voltage of the panel at an air temperature of T (°C).

In this section, a value of 35 °C is used for T_1 .

When investigating the ability of the panel to charge a battery during the summer, it is instructive to determine T_{max} , the maximum ambient temperature for which full charging will occur. T_{max} is a function of wind and insolation conditions. By changing the above inequality to an equality and solving for ΔT , one can find T_{max} as follows.

$$T_{max} = 25 + \frac{V_{panel} - V_{cc} - V_{loss}}{D_{panel} - D_{cc}} \quad (9.3)$$

Note that while V_{cc} and V_{loss} are independent of one another, it is really their sum that is of interest.

The battery voltage determines the voltage at which the panels operate. Ideally, this operating voltage would be at the maximum power point. However, the panel's IV curve will shift towards

lower voltages at higher panel temperatures. Thus, the operating voltage dictated by the battery will move towards the open circuit voltage at higher temperatures. T_{\max} is the air temperature, for given wind and insolation conditions, at which the operating voltage dictated by the battery is at the panel open circuit voltage. At lower air temperatures the operating voltage will be lower than the open circuit voltage and charging will occur at a higher rate. Ideally, the air temperature would be sufficiently low that the operating voltage would be at or below the maximum power point voltage. The maximum air temperature which will permit charging at V_{op} , an operating voltage below the open circuit voltage, will be lower than T_{\max} . We can find $T_{V_{\text{op}}}$, the ambient air temperature at which the operating voltage of the panel will be V_{op} , from:

$$T_{V_{\text{op}}} = 25 + \frac{V_{\text{op}} - V_{\text{oc}} - V_{\text{loss}}}{D_{\text{panel}} - D_{\text{oc}}} \quad (9.4)$$

Clearly, Eq. 9.3 is just a special case of Eq. 9.4.

9.4 Results

The ability of Siemens M55 and M75 panels to fully charge a 12 Volt battery system was investigated. The maximum temperature for full charging was calculated as a function of setpoint voltage plus lead losses for various conditions. Typical peak insolation conditions were assumed to be 1000 W/m^2 and 50 W/m^2 solar radiation on the front and back of the panel, respectively, and a 2 m/s wind; for worst-case conditions a back panel insolation of 200 W/m^2 was used instead. A twenty percent diffuse fraction for the front panel insolation, and a panel efficiency of zero at the open circuit voltage (since no power can be extracted from the panel when it is operating at its open circuit voltage) and ten percent at the maximum power point were used. A ground temperature two °C above the ambient air temperature, a sky temperature 10 °C below the ambient air temperature, and a panel tilt angle of 60 ° were assumed.

Figure 9.1 shows the results for the unmodified M55 and M75 panels at typical peak insolation conditions. As long as the air temperature remains below 50 °C, they both will be able to fully charge the battery. However, if the sum of the voltage regulation set point and the lead losses is high, the panels will be operating at voltages well above their maximum power points. For example, for lead losses of 1.5 V and a voltage regulation set point of 14.4 V, the M55 will operate at its maximum power point only at roughly zero °C; for the M75 the temperature must be about -30 °C. Thus, for summer temperatures, the panels will be able to fully charge the batteries during typical peak sun conditions, but the rate of charging will be low if the sum of the lead losses and the voltage regulation setpoint is high.

Figure 9.1 Modelled Maximum Ambient Air Temperature for Full Battery Charging with Unmodified Panel, M55 and M75

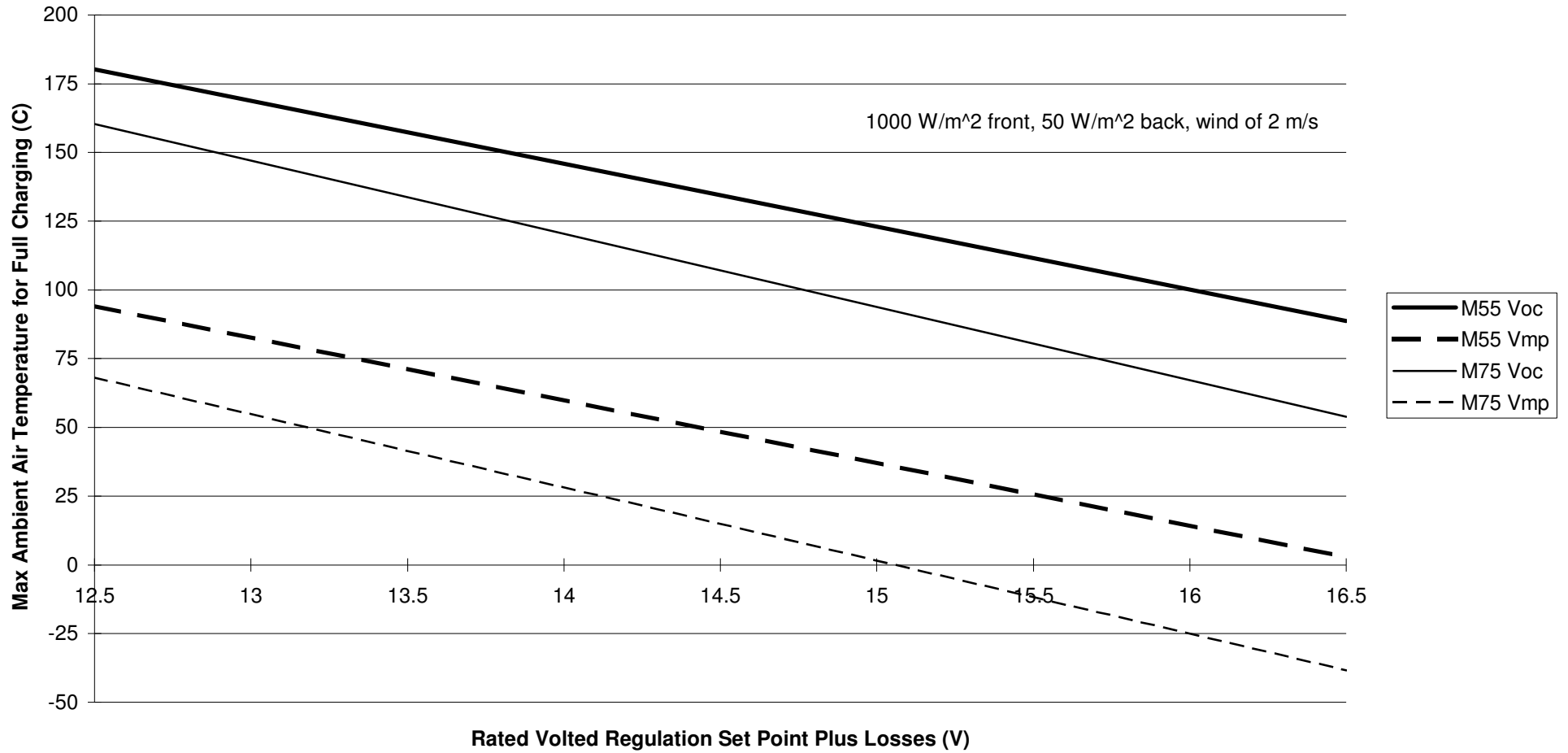


Figure 9.2 shows the results for the M55 with the TN Conseil modification. As long as the air temperature remains below about 40 ° C, even under the worst-case conditions the panel will be able to charge the battery. However, except when temperatures are very low and/or the sum of the voltage regulation setpoint and losses is low, the operating voltage will be above the maximum power point. Thus, charge rates will be slower than for the unmodified panel.

For the M75 with the TN Conseil modification (Figure 9.3), on the other hand, the panel will not be able to fully charge the battery under worst-case conditions when the sum of voltage regulation setpoint and lead losses is very high. Charge rates will be even lower than with the M55.

At first glance, this result suggests that TN Conseil-equipped panels will have poor summer charging performance, because under most conditions the panel will be operating at voltages well above its maximum power point. However, two factors should be considered. First, the IV curve (and power versus voltage characteristic) of the panel is very steep at voltages near the operating circuit voltage. Thus, a significant increase in current (and power) will accompany a minor decrease in the operating voltage. Second, as the operating voltage drops below the open circuit voltage, the power output of the panel increases, and by conservation of energy, less solar radiation is converted into internal energy. Thus, the cell operates slightly cooler. For example, for an M55 with a cell temperature of 25 ° C, the open circuit voltage is rated at 21.7 V and the typical voltage at load is rated at 17.4 V-- a difference at 4.3 V. But the electrical efficiency of the cell is zero in the former case and about ten percent in the latter. This indicates that, for steady-state operation and all other conditions remaining the same, the ambient air temperature must be higher in the former case. Put another way, for identical environmental operating conditions and cell temperatures above 25 ° C, the rated open circuit voltage will be derated by an amount greater than that for the typical voltage at load or the maximum power point voltage. According to the thermal model, for environmental conditions held constant, the difference between open circuit voltage and the typical voltage at load for a Siemens M55 panel will not be 4.3 V, but rather 3.9 V, 4.0 V, and 4.1 V for a wind speed equal to zero, two, and six m/s, respectively.

The results are sensitive to wind speed. Even a slight wind cools the panels significantly and greatly facilitates charging. This can be seen in Figures 9.2 and 9.3, where the curve for a high front and back insolation level but a six m/s wind has been plotted. When there is no wind, the maximum ambient air temperature for full charge will be considerably lower than that for winds of two m/s. Unfortunately, the observed inaccuracy of the model at low wind speeds precludes any firm conclusions for the no-wind condition.

The results are probably conservative. As noted in Section 6.2.8, the models are increasingly inaccurate with decreasing windspeed and appear to overestimate the actual panel temperature. Charging will probably occur at temperatures higher than those indicated.

Figure 9.2 Modelled Maximum Ambient Air Temperature for Full Battery Charging with TN Conseil Panel, M55 with 1000 W/m² on Front

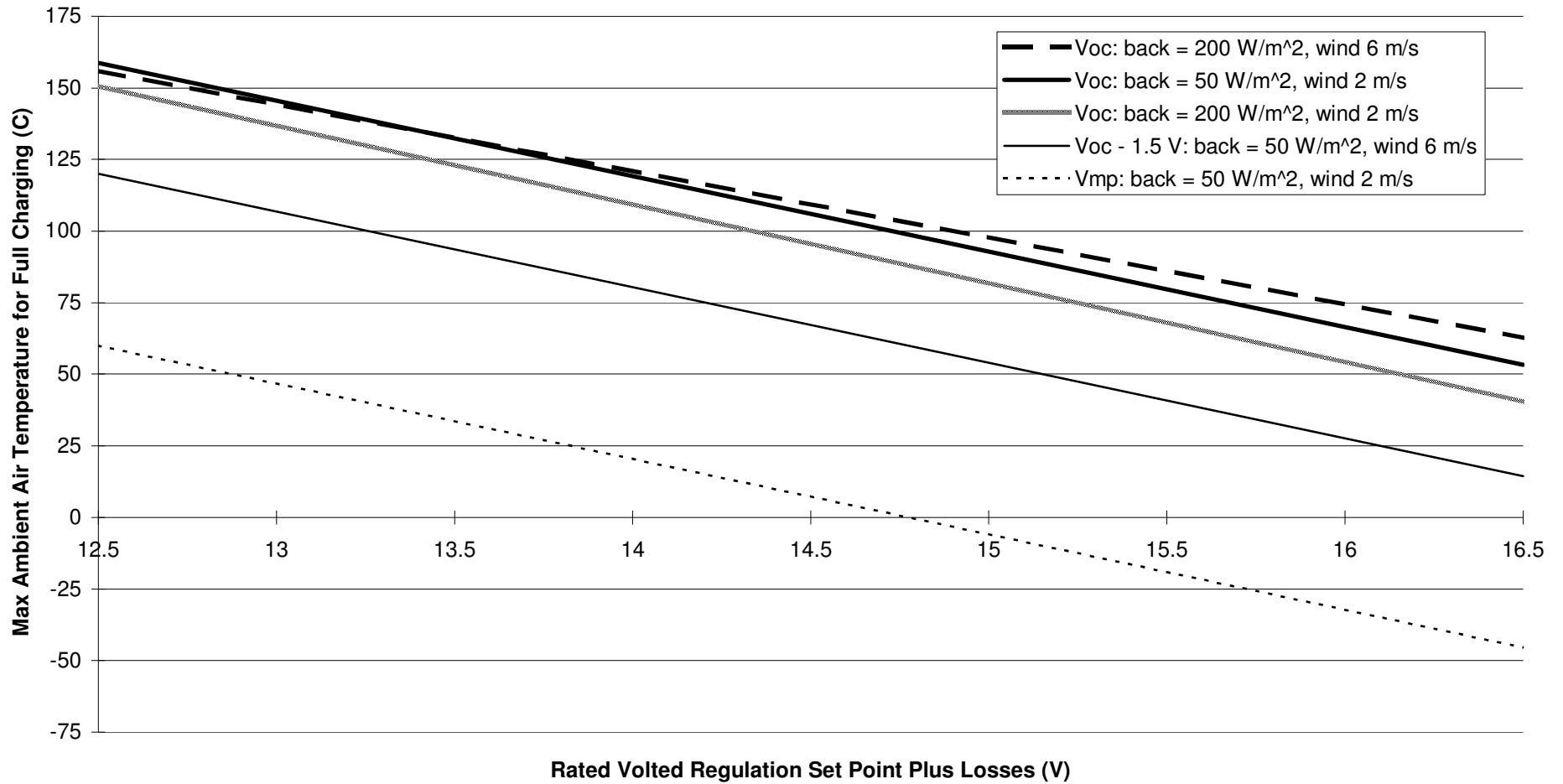
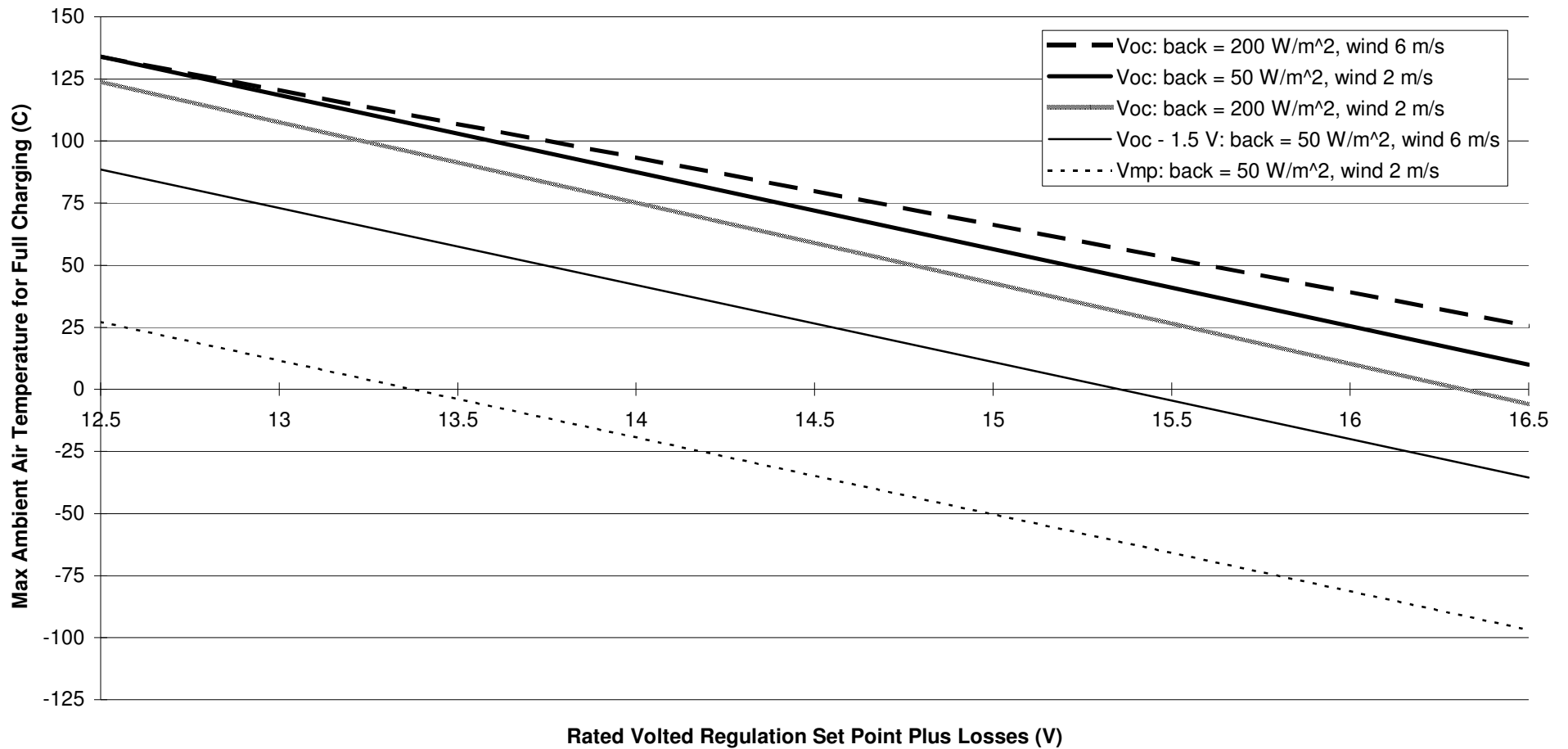


Figure 9.3 Modelled Maximum Ambient Air Temperature for Full Battery Charging with TN Conseil Panel, M75 with 1000 W/m² on Front



9.5 Effect of Charge Controller Temperature Derating

The results in Section 9.4 were calculated assuming a charge controller temperature derating, D_{cc} , of $0.030 \text{ V/}^\circ\text{C}$. This is an average value; different manufacturers use different values for D_{cc} . Changing D_{cc} will alter the maximum air temperature at which charging will occur.

For D_{cc} not equal to $0.030 \text{ V/}^\circ\text{C}$, the maximum ambient air temperature at which charging will occur is given by Eq. 9.4. For an M55 panel with the TN Conseil technology, this relation is plotted as a function of the sum of voltage regulation setpoint and lead loss for a range of values for the charge controller temperature derating (Figure 9.4). A windspeed of two m/s, front panel insolation level of 1000 W/m^2 , and back panel insolation of 50 W/m^2 . The M75 and lower wind speeds will have slightly more exaggerated results. The effect of changing the temperature derating is non-linear. The effect is less pronounced for larger sums of V_{cc} and V_{loss} . Increasing D_{cc} has a positive impact on the ability of the panels to charge the battery.

9.6 Maximum Monitored Temperatures

The TN Conseil panels that are installed in the roof-top array at the EDRL were monitored over the summer of 1995. The highest recorded temperature for the TN Conseil panel was 78°C , at 2:30 PM, August 14. At this point in time the ambient air temperature was 29°C ³⁷, the front panel insolation was 960 W/m^2 , the back panel insolation was 46 W/m^2 , and the windspeed was 3.5 km/hr . The temperature of the unmodified panel was 59°C ³⁸.

At this panel temperature, the open circuit voltage of M55 and M75 panels will be approximately 17.3 V and 15.8 V , respectively, based on the derating of $2.3 \text{ mV/}^\circ \text{C}$ (see Section 9.3). Thus, the M55 would be able to fully charge any 12 V battery system. The M75 would be able to fully charge systems for which the sum of the voltage regulation setpoint and the lead losses were less than 15.8 V .

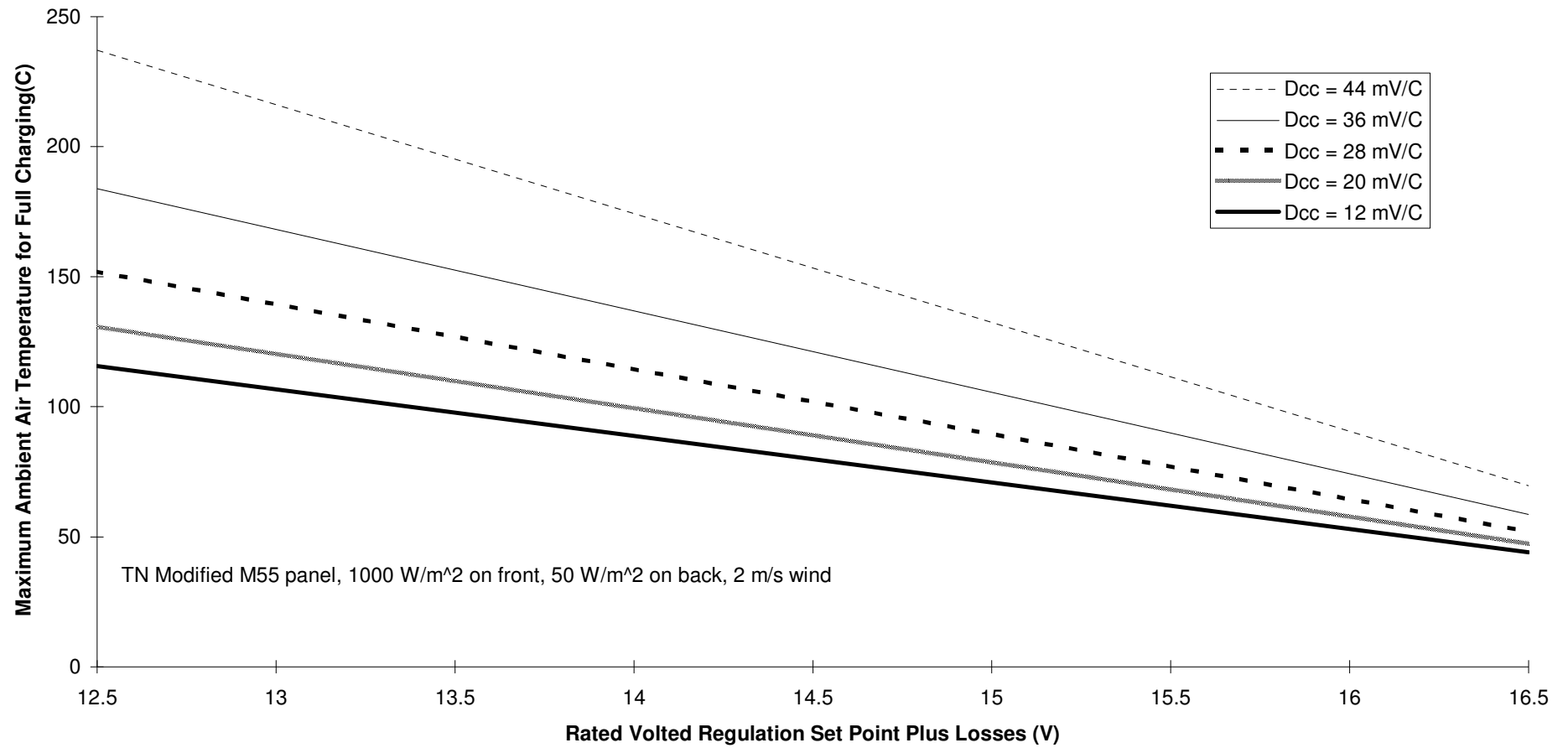
9.7 Conclusions

The results presented above suggest that for wind speeds of two m/s or greater, the M55's ability to achieve full charge will not be compromised by the TN Conseil System. The M75 may be compromised when the voltage regulation set point and the voltage drop between the array and the charge controller are both relatively large.

³⁷ The highest ambient air temperature observed at the site was on July 14, when it reached 36°C .

³⁸ For these environmental conditions, the thermal models of Chapter 6 predict a panel temperature of 77°C for the TN Conseil modified panel and 56°C for the unmodified panel, showing good agreement with the monitored values.

Figure 9.4 Maximum Ambient Air Temperature for Full Battery Charging at Various Charge Controller Temperature Deratings (Dcc)



In perfectly still air, the M55 and M75 may have difficulty achieving full charge; this can not be accurately verified with the thermal model. Based on the results of a two m/s wind, it seems unlikely that the M55 would have any problem achieving full charge except when the voltage regulation set point and the voltage drop between the array and the charge controller are both relatively large.

It is probable that the results presented here are conservative, since the thermal model appears to overestimate panel temperatures. Further, it is difficult to imagine that an entire summer would be nearly windless and extremely hot. Moderate insolation levels will still allow charging but not heat the panels so greatly. These factors suggest that the actual maximum ambient air temperature for full charging will be higher than suggested herein.

An operating voltage below the open circuit voltage for the same ambient air temperature significantly decreases the maximum ambient air temperature for full charging. Thus, under some conditions the TN Conseil equipped panel will charge at a lower rate than an unmodified panel.

The M55 is more likely to maintain panel voltages sufficient for full charging than the M75. This is a result of the M55 having thirty six cells in series and the M75 having only thirty-three. If summer charging capability is a concern, the TN Conseil technology should be used with thirty-six cell panels.

For most locations where this technology will be of interest, summer charging performance is not critical, whereas winter performance is. The TN Conseil Technology does not appear to compromise the former, at least for wind speeds at or above two m/s, but may significantly improve the latter.

CHAPTER 10

OBSERVED SHORT-TERM OPERATION OF THE SNOW REMOVAL TECHNOLOGY

10.1 Background

The TN Conseil snow removal system was installed on two panels in the roof-top array at the EDRL in Varennes; the panels and the environmental conditions were monitored as detailed in Section 6.1.1. On a number of occasions, snow accumulated on the array and permitted the comparison of the rate of snow removal with and without the TN Conseil Snow Removal System. The snow cover of March 6 and 7, 1995 was one such occasion.

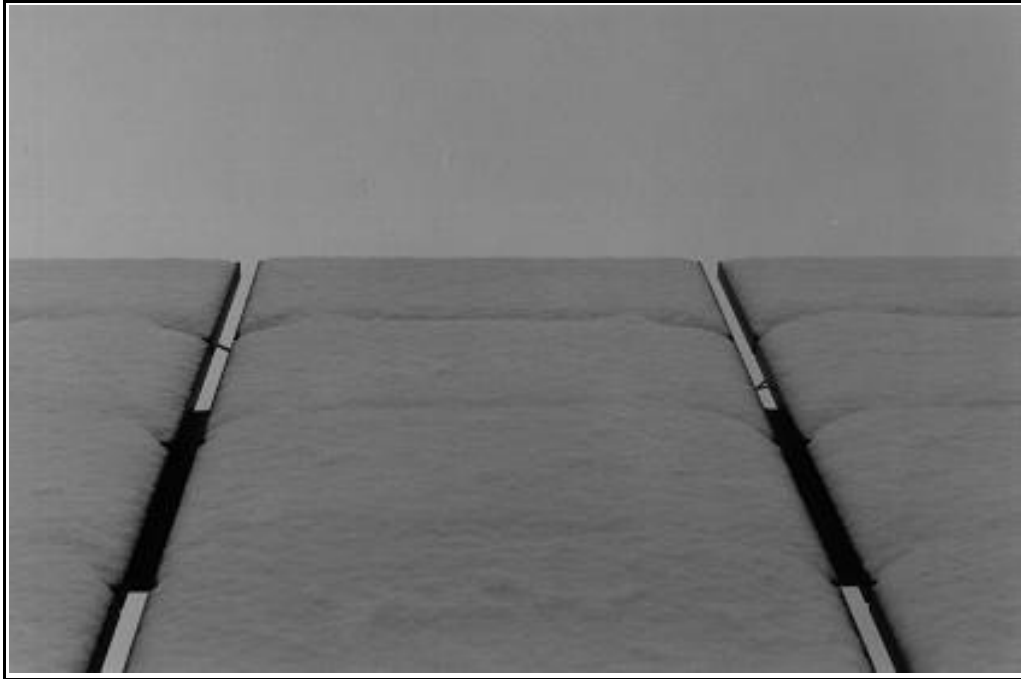
On the morning of March 6, 1995, most of the PV array was covered by a blanket of wet snow that had fallen overnight. The western half of the array, where the TN Conseil test panels are located, was uniformly covered in a layer of snow about 2.8 cm thick. The ambient temperature stayed between zero and -5 ° C until the afternoon of March 7; the two days were dark and overcast.

10.2 Photographs of Panels

A series of photographs (see Figure 10.1) taken during March 6 and 7 demonstrate that snow quickly began to melt from the TN Conseil panels while it remained on the unmodified panels. In each photograph, the TN Conseil panel is the top panel in the centre of the photograph. All other panels are unmodified panels; Control 1 appears on the right of TN1 and Control 2 appears on the left of TN2. TN2 showed the fastest rate of snow-removal, a result consistent with previous and subsequent observations. TN1, while slower to remove snow than TN2, significantly outperformed both the control panels.

Figure 10.1 Performance of TN Conseil-Modified Panels on March 6 and 7

a) TN2 at 9:07 am 95/03/06.



b) TN2 at 11:05 am 95/03/06.

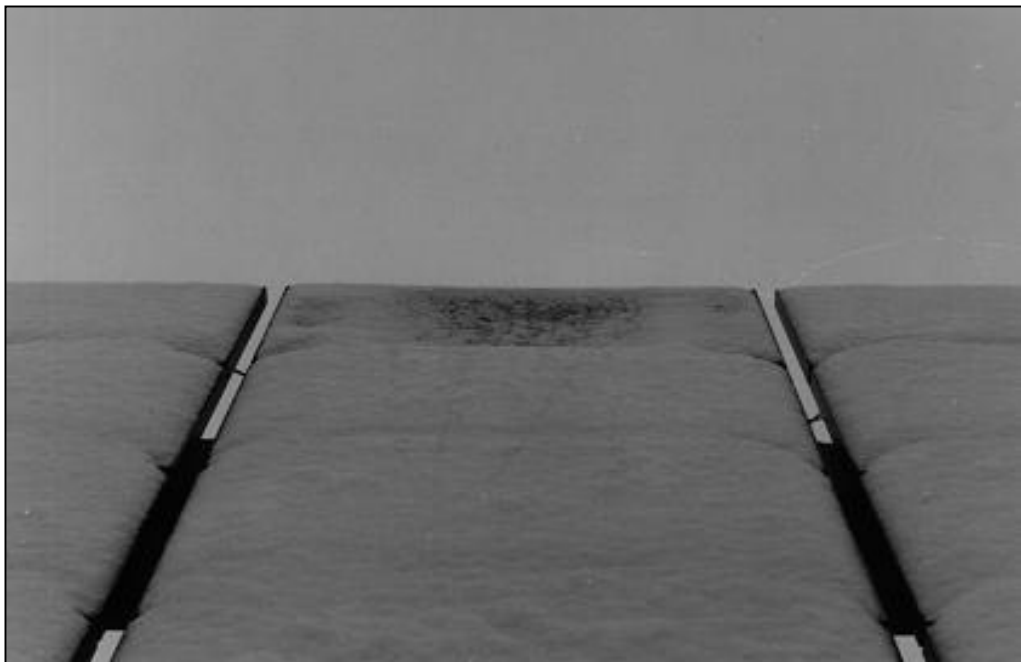
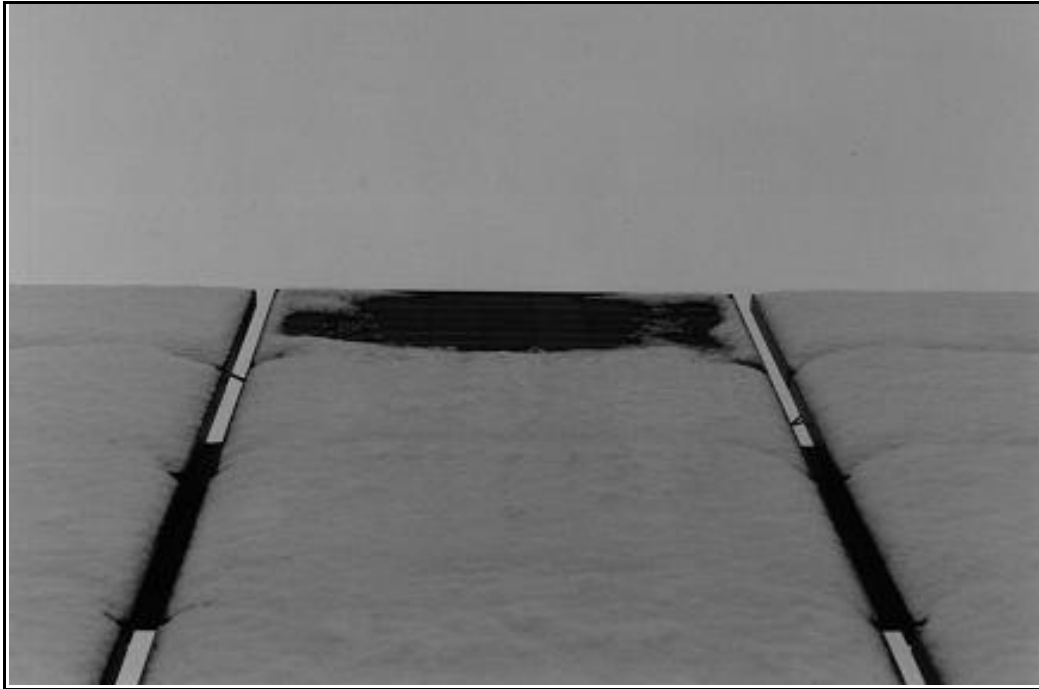


Figure 10.1 Performance of TN Conseil-Modified Panels on March 6 and 7

c) TN2 at 1:10 pm 95/03/06.



d) TN2 at 3:20 pm 95/03/06.

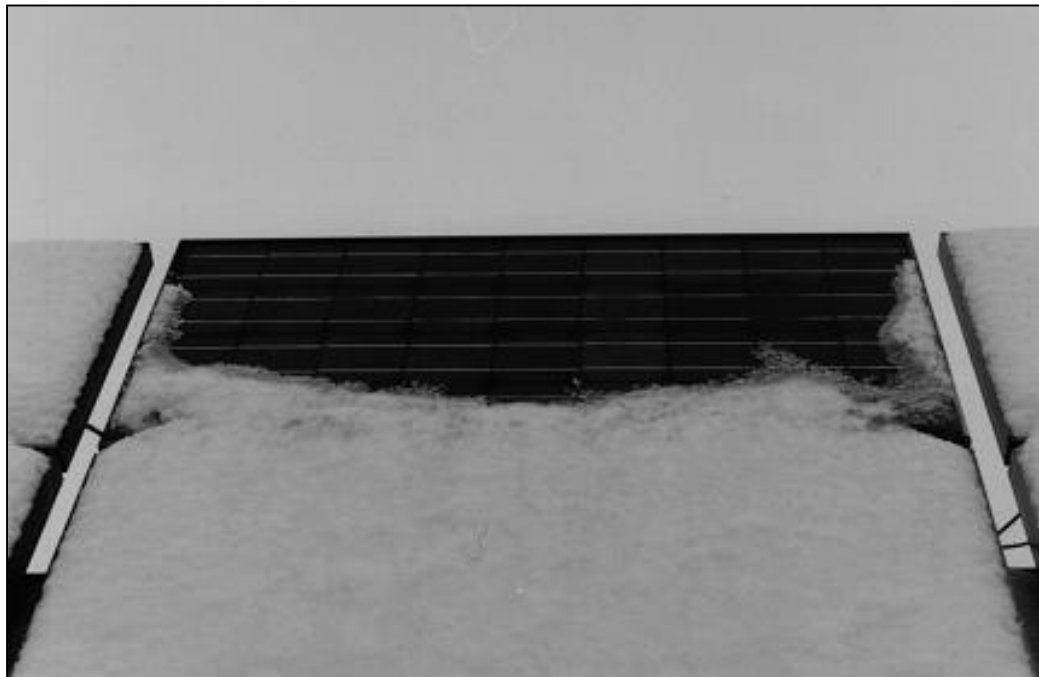
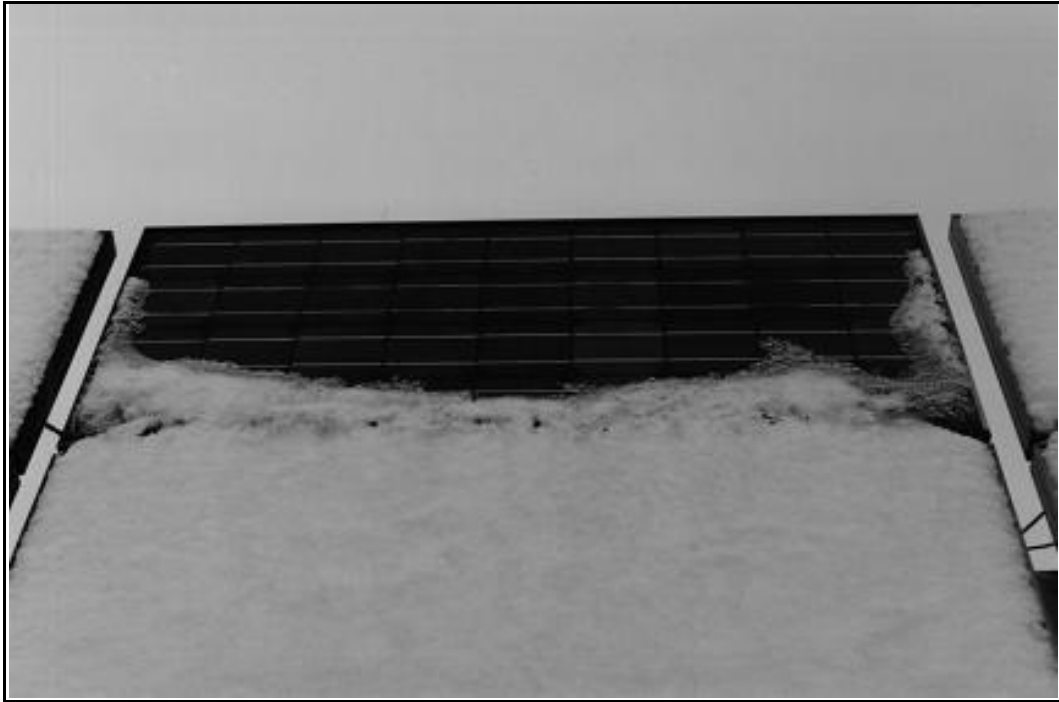


Figure 10.1 Performance of TN Conseil-Modified Panels on March 6 and 7

e) TN2 at 9:10 am 95/03/07.



f) TN2 at 3:00 pm 95/03/07



10.3 Monitored Data

10.3.1 Insolation Levels

As discussed in Section 6.1.1, an incompatibility between the data acquisition system and the pyranometer amplifier introduced errors into the readings of insolation levels. When snow was not present on the array, the short-circuit current of the monitored panels could be used to estimate the insolation level. However, since there was snow on the array on March 6 and 7, this could not be done.

As can be seen in the photographs of Figure 10.1, there was heavy cloud cover during the two days. From this it can be concluded that insolation levels were low.

10.3.2 Wind Speed

The wind speed measured at the weather station, located about five metres from one end of the array, is plotted in Figure 10.2. During most of March 6 and 7 the wind speed stayed below 15 km/hr. Late in the afternoon of March 7 the weather changed and wind speed averaged around 50 km/hr.

10.3.3 Temperature

Figure 10.3 shows the panel temperatures and ambient air temperatures over the two day period. Ambient air temperatures remained between -5°C and 0°C most of the time. In the late afternoon the air temperature rose abruptly to about 10°C , which resulted in the panels melting off their snowcover very quickly.

During March 6 and the early part of March 7, the temperature of the TN Conseil-equipped panels rose well above the freezing point while the control panels remained near ambient air temperature. There is a marked difference between the temperature of TN 1 and TN 2 on March 6. As noted in Section 6.1.3, the nickel absorber foil on TN 2 performs better than the copper absorber foil on TN 1, and, to a certain degree, this explains the temperature difference. But on March 7 the temperature difference is less pronounced. It can be inferred that on March 6 the snow covering the panel near the thermocouple melted sooner on TN2 than TN1; while there is snow on the front of the panel, the panel is held at a temperature close to 0°C . Thus, once the snow had melted from most of TN 2, the panel temperature rose in the vicinity of the thermocouple. TN 1 was still covered in snow and remained near 0°C .

During the night, all the panels dropped slightly below the ambient air temperature. This is explained in Section 6.1.2.

Figure 10.2 Wind Speed, March 6-7, 1995

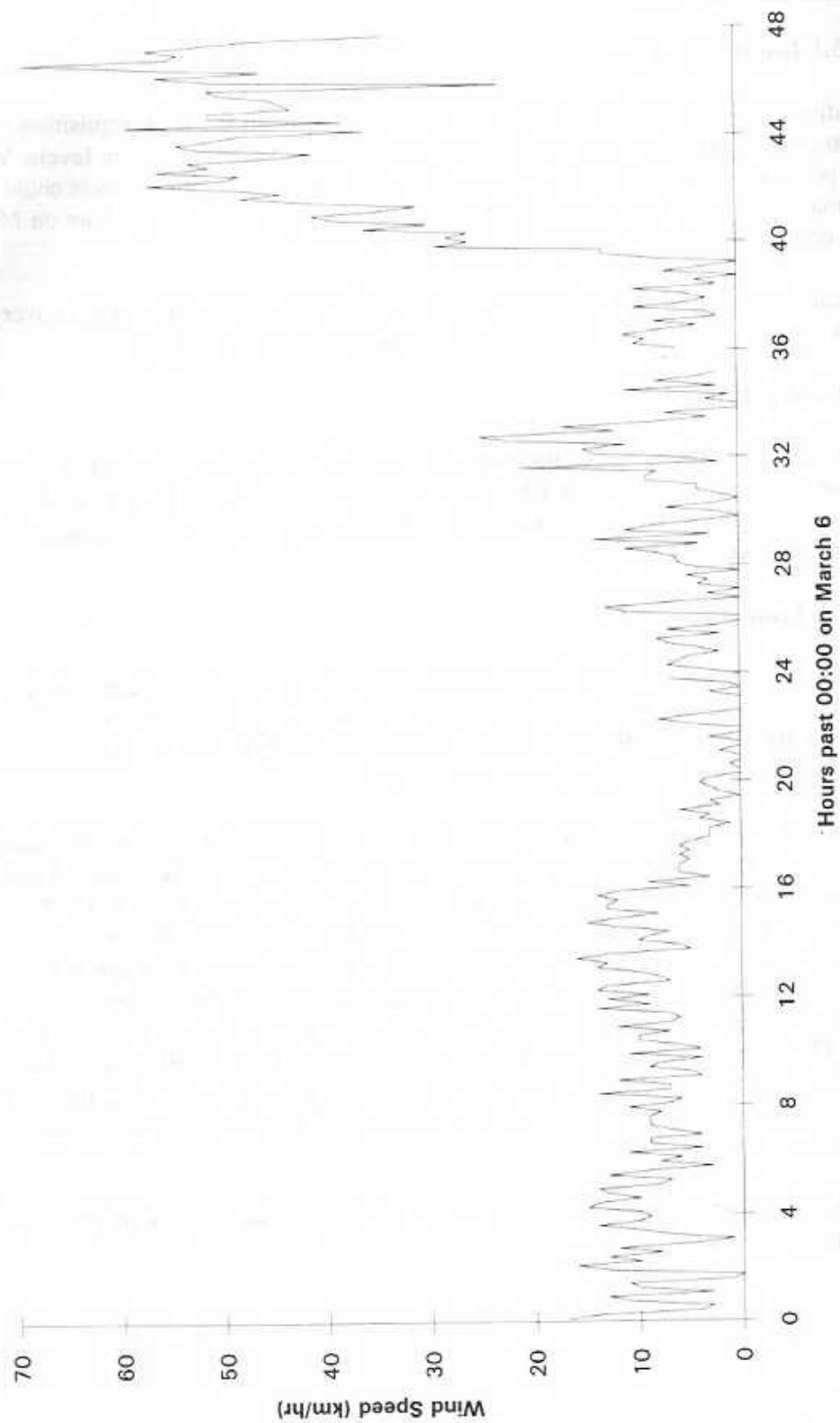
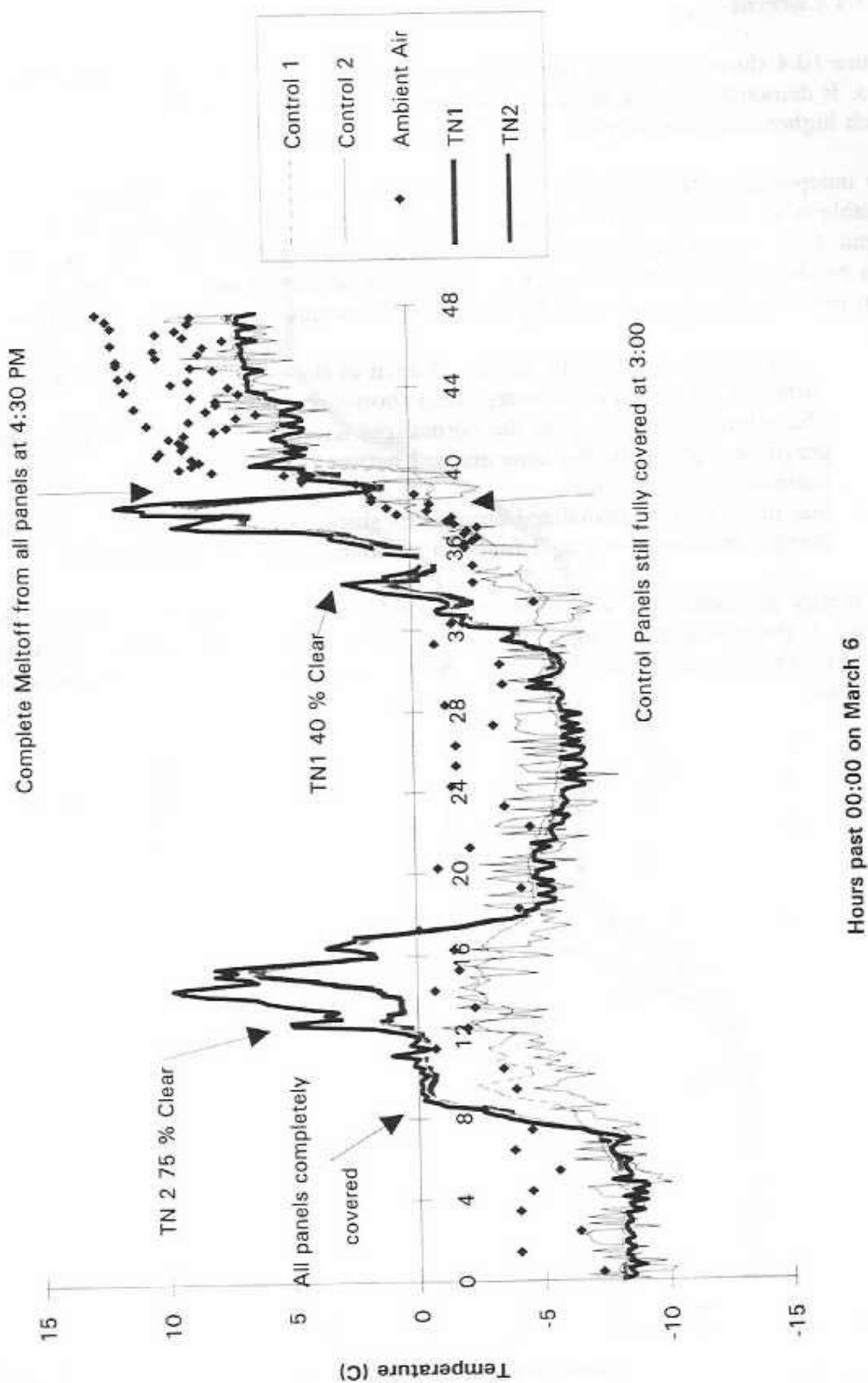


Figure 10.3 Temperatures of Panels and Ambient Air, March 6-7, 1995



10.3.4 Current

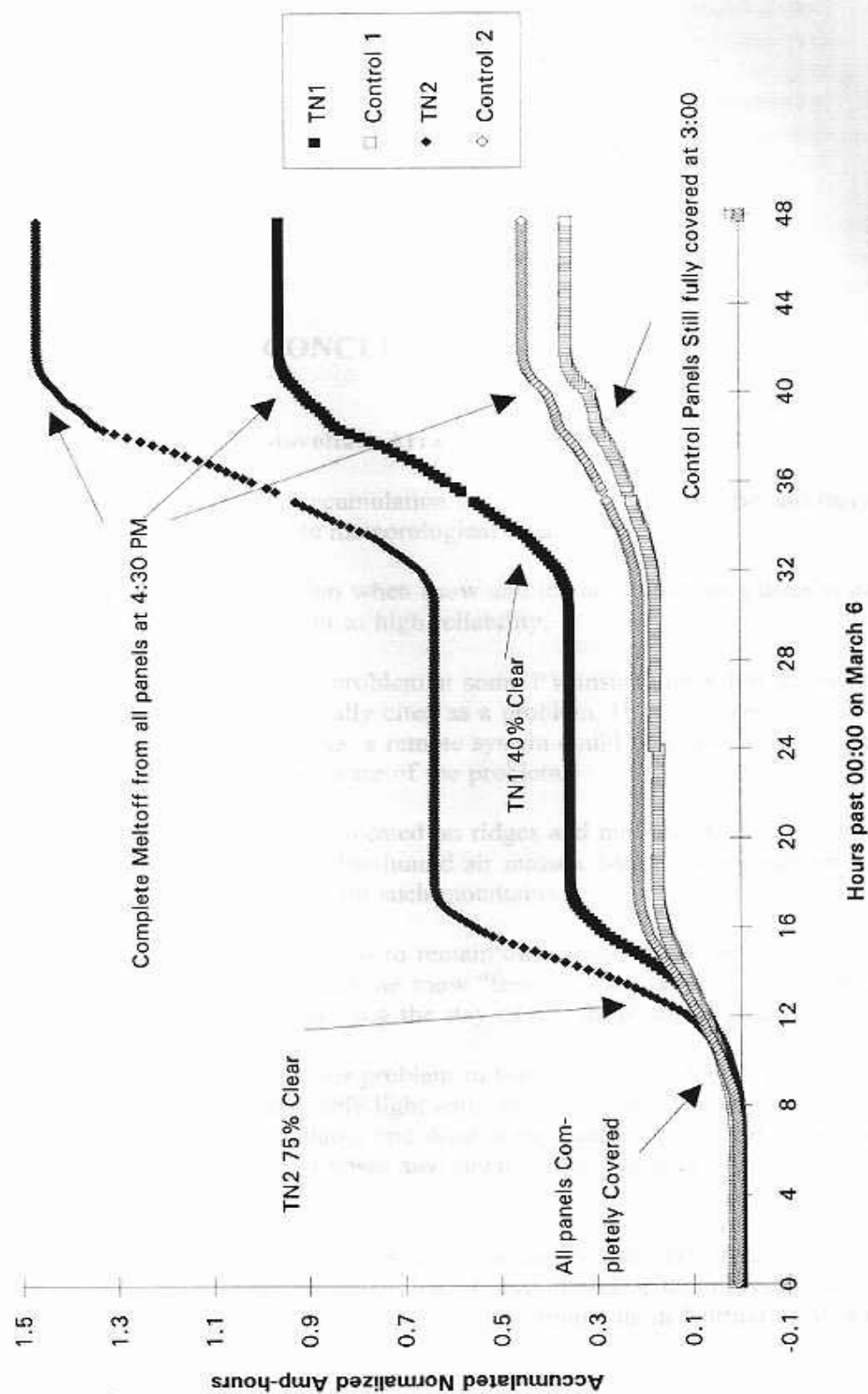
Figure 10.4 shows the cumulative normalized amp-hour output for the panels over the two days. It demonstrates that the increased rate of snow-removal of the TN panels translated into much higher electrical output.

The independent variable is the number of hours past midnight on March 6; the dependent variable is accumulated normalized amp-hours, a measure roughly proportional to energy output. One accumulated normalized amp-hour is equivalent to the amp-hours produced in one hour by the panel when short-circuited with peak sun conditions. This quantity was calculated from periodic measurements of the short-circuit current of each of the panels by:

1. Dividing the short-circuit current of each of the panels by its reference short-circuit current, thus yielding the normalized short-circuit current.
2. Multiplying the average of the normalized short-circuit current reading and the previous reading by the time elapsed between the two readings, to give a rating, in normalized amp-hours.
3. Summing all the normalized amp-hours since 00:00 on March 6, giving cumulative normalized amp-hours as a function of hours past 00:00 on March 6.

The energy provided by TN2 during this period of two days was over three times that of Control 2, the unmodified panel with the best performance. The energy collected by unmodified panels can be attributed to solar radiation penetrating the 2.8 cm layer of snow on the panels.

Figure 10.4 Cumulative Normalized Amp-Hrs, March 6-7, 1995



CONCLUSIONS

Snow and Ice Accumulation on Photovoltaic Arrays

- The probability of snow and ice accumulation on an array is site-specific and can not be predicted from readily available meteorological data.
- Although it is rare, the rare occasion when snow and ice accumulation causes system failure belies the PV system's claim to high reliability.
- Rime is a recognized and recurrent problem at some PV installations, but persistent snow accumulation is only occasionally cited as a problem. However, because PV systems have oversized battery banks, a remote system could be covered in snow for a long period without anyone being aware of the problem.
- Rime may accumulate on PV arrays located on ridges and mountaintops over 650 m in elevation, especially those encountering humid air masses. Many communication systems with PV panels are situated on such mountains.
- Wet snow is more likely than dry snow to remain on a photovoltaic array, especially if the ambient air temperature drops and the snow "freezes" onto the array. Nevertheless, there exist mechanisms that may prolong the stay of dry snow on the panel.
- Glaze does not appear to be a serious problem in the operation of PV arrays in Canada, since it transmits considerable light and, in most places in Canada, is followed by warm temperatures. Newfoundland, and Avalon especially, may be an exception. It is highly improbable that hoarfrost poses any threat to the winter operation of PV panels.
- In Northern Canada, riming of PV panels has been observed in the Arctic; these rime deposits, especially problematic on Baffin Island, may not clear themselves until June. Mountainous areas, such as the Yukon, the Torngat Mountains in Northern Labrador,

Devon Island, and Ellesmere Island, and areas prone to heavy Arctic fog, will probably have problems with rime. Severe riming occurs in the coastal mountains of British Columbia and the mountains just to the west of the Rockies. In these areas the rime "season" may last from October to early May, and can severely curtail PV panel output during this period. Riming is also a problem in mountainous regions of Québec, including the north shore of the St. Lawrence, the Sept-Iles area, and the Gaspé Peninsula. Heavy riming occurs in the Long Mountains of Newfoundland and moderate riming probably occurs in Cape Breton Island.

- One PV installer reported snow accumulation on PV panels on the Prairies, another reported problems in Québec.
- In most cases, mounting PV panels at high tilt angles is an effective solution to the problem of snow accumulation.
- Presently, many panels in rime-prone areas are mounted vertically and purposely situated at the windiest site. Since this maximizes the flux of supercooled water onto the panel, in theory this will exacerbate the problem of rime accumulation.
- Where snow and ice accumulation are problematic, a common practice is to drastically increase the capacity of the battery bank. It is not uncommon for the systems in British Columbia to have "three month autonomy". This increases the capital costs of the system, but at remote sites accessible only by helicopter, installation, operating, and maintenance costs may be far more significant.
- Soltek Solar Energy Ltd. has developed a solar panel for flush mounting directly onto comshells. Users report that this reduces, but does not eliminate, rime accumulation.
- Icephobic coatings, which purportedly reduce the adhesion of ice and snow to glass, wear off quickly and are unanimously dismissed by researchers and field personnel alike.

Pertinent Properties of Snow and Ice

- The transmission of solar radiation through snow can be modelled by the Bouguer-Lambert law; thus, the level of radiation penetrating a layer of snow decreases with thickness in an exponential manner.
- The properties of rime are poorly documented and must be inferred from those of snow.

Electrical Performance of a Snow or Ice Covered Array

- The electrical performance of a uniformly covered array will be linearly related to the level of solar radiation penetrating the snow cover. However, the electrical performance of a nonuniformly covered array will be highly nonlinearly related to the average level of solar radiation penetrating the snow cover.
- In a series string of cells, the current passing through the cells is limited by the most severely shaded cell. The less-shaded cells force this cell to operate at a current above its short circuit current, and thus the cell becomes reverse-biased, acts like a resistive component, and dissipates electrical energy as heat.
- In an experiment on Siemens and Astropower modules, shading one cell in the module by 60 to 75 % reduced the irradiance of the panel by only 2 % but reduced the peak power output by 40 to 50 %.

Solar Energy Incident on the Rear Face of a Panel

- A sensitivity analysis was performed on the model for the radiation incident on the rear face of an array, accounting for the array shadow. The diffuse radiation incident on the rear face of the array was only 5 to 15 % of the intensity of the ground-reflected radiation incident on the rear face of the array. The radiation incident on the rear face of an array was found to be 8 to 34 % of the total radiation incident on the front face of an array, with 24 % a typical value.
- For most small- and medium-sized arrays (up to one kW), the shadow of the array does not significantly affect the radiation incident on the rear face of the array.

Thermal Performance of a PV Panel with the TN Conseil Snow Removal Technology

- The monitored panels showed that with moderate to strong insolation levels, the TN Conseil-modified panels operated at temperatures 15 to 30 ° C higher than the unmodified panels.
- Free convection causes a temperature gradient to develop within the air cavity formed between the absorber foil and the Lexan back cover. Thus, during the daytime the top half of the panel is warmer-- by up to 10 ° C-- than the bottom half of the panel. In addition, the panel's aluminum frame acts as a heat sink and depresses the temperature of the panel in the vicinity of the frame.
- A sensitivity analysis of the thermal models of the unmodified panel and the panel with the TN Conseil technology indicated that the significant variables affecting the thermal performance of the panels are windspeed, insolation on the front and back of the panel,

and ambient air temperature. Windspeed has a nonlinear effect.

- Models of the thermal performance of various panel configurations were compared. In order of hottest to coolest, these configurations were: the standard TN Conseil technology, the Lexan back cover mounted on a panel with a black Tedlar encapsulant on the rear face, the absorber foil covered in Lexan Thermoclear (a transparent corrugated material), the absorber foil without a Lexan back cover, a panel with a black tedlar encapsulant on the rear face, and an unmodified panel (with white Tedlar encapsulant on the rear face).

Snow and Ice Removal From Photovoltaic Panels

- For a given windspeed and insolation level, the TN Conseil modified panel will initiate snow or ice removal at an ambient temperature much lower than that required for melting by an unmodified panel. For example, the model indicates that with peak sun and a 10 m/s wind, a ten cm thick rime or moderately dense snow accumulation will start melting at an ambient air temperature of -23°C on the TN Conseil modified panel but only at -3°C for an unmodified panel; the TN Conseil panel performs even better at lower windspeeds and with thinner accumulations.
- Under all modelled conditions, the TN Conseil-modified panel had a significantly higher melting rate than the unmodified panel. For example, for rime at an ambient air temperature of -5°C and peak sun insolation, the melting rate for the unmodified panel is about 0.25 cm/hr whereas the melting rate for the TN Conseil modified panel is about 0.7 cm/hr.
- The TN Conseil modified panel tends to form a ledge of densified snow or ice at its bottom lip. This ledge partially shades the panel and provides a foothold for further snow or ice accumulation. It is hypothesized that this ledge arises either from the temperature gradients along the panel or from the TN Conseil panel initiating melting under marginal conditions such that the ledge freezes onto the panel overnight.
- The use of Lexan Thermoclear, a corrugated transparent plastic, in place of the Lexan back cover sheet and associated air cavity, is proposed as a way to reduce the temperature gradients across the panel and thus decrease the modified panel's tendency to form an ice ledge.
- Very simple mathematical models of the panel frame are used to roughly estimate the effect of various modifications to the frame on the frame temperature. It was found that using a black anodized frame, or more effectively, insulating the frame (excluding its front surface) would significantly raise the frame's temperature. This would help maintain the panel temperature near the frame and also hasten snow and ice removal from the frame.

- It is possible that rime will accumulate on the rear as well as the front surface of the panel. Rime accumulation on the rear face of the panel will decrease the radiation incident on the black absorber foil and reduce the efficacy of the TN Conseil system considerably, especially for thicker rime deposits.

Simulation of System Performance at Four Sites

- The modelled performance for a site at Bagotville, Québec, suggests that the TN Conseil modification is highly effective for snow, reducing the average time to snow removal by about 95 % (if shedding occurs) to 80 % (if complete melt-off occurs). For rime, the model suggests that the TN Conseil technology is somewhat less effective. For mountainous sites in B.C. and Newfoundland, the average time to shedding was reduced by about 30 to 40 % and the average time to melting by about 20 to 30 %. The technology was less effective at a site just above the Arctic Circle in the Northwest Territories. However, if the parameters used to model the rime accumulation are incorrect, these results probably underestimate the improvement realizable with the TN Conseil technology.
- The times required for melting and shedding for the TN Conseil panel with the rime shield are only slightly better than those for the TN Conseil panel without the rime shield. This is misleading, however, since it was assumed that rime would be removed from the rear face of the panel at the same rate that it was removed from the front face of the panel. In reality, however, the air cavity in the TN Conseil technology insulates the panel sufficiently well that the Lexan back cover does not heat up. This suggests that rime will not remove itself from the rear of the TN Conseil technology, and therefore the performance of the TN Conseil Technology without the rime shield will degrade over the winter as rime accumulates on the rear face.
- The large number of assumptions and unknowns required to model the removal of rime and snow from the panel suggest that the results presented above can be used only as a rough comparison of thermal performance. A more accurate assessment will require experimentation, preferably in the field, at rime-prone sites.

Summer Battery Charging Performance

- According to the models, during worst-case summer conditions of very low wind, peak sun, and high ambient air temperatures, the M55 panel and other 36 cell panels will be able to charge the panels, although the rate of charging may be lower than that for an unmodified panel. Under worst-case conditions, the M75 and other panels with 33 or fewer cells may be unable to fully charge the panels. However, in locations where snow and ice accumulation is a concern, it is unlikely that worst-case conditions will persist for the duration of the summer.

REFERENCES

Adams, W. P., "Snow and Ice on Lakes", Handbook of Snow: Principles, Processes, Management and Use, (D. M. Gray and D. H. Male, eds.), Pergamon Press, Toronto, 1981, pp. 437-474.

Admirat, P., Dalle, B., "Experimental Studies of Wet Snow Accretion on Overhead Lines", Seminar on Overhead Lines and the Climatic Environment, Gif-sur-Yvette, (1985) p. 43.

Advanced Glazing System Laboratory, VISION3 Glazing System Thermal Analysis Reference Manual, University of Waterloo, Waterloo, Ontario, 1992.

American Meteorological Society, "Glossary of Meteorology", American Meteorological Society, Boston, Mass., 1959.

Arnold, J.N., Bonaparte, P.N., Catton, I., and Edwards, D.K., "Experimental Investigation of Natural Convection in a Finite Rectangular Region Inclined at Various Angles from 0 to 180 Degrees", Proceedings of the 1974 Heat Transfer and Fluid Mechanics Institute, Corvallis, OR, Stanford University Press, Stanford, CA, 1974.

ASHRAE, "1993 ASHRAE Handbook: Fundamentals", American Society of Heating, Refrigerating, and Air-Conditioning Engineers, Inc., Atlanta, GA, 1993.

Auger, Tim: Parks Canada, Alberta, personal communication.

Barnes, P., Tabor, D., Walker, F.R.S., Walker, J. C. F., "The Friction and Creep of Polycrystalline Ice", Proceedings of the Royal Society of London, Vol. 324 (1971), pp. 127-155.

Berdahl, P., Martin, M., "Emissivity of Clear Skies", Solar Energy, Vol. 32 (1984), p. 5.

Bergevin, Benoit: TN Conseil, Montréal, Québec, personal communication.

Boyd, D. W., "Icing of Wires in Canada", Tech. Paper No. 317 of the Division of Building Research, National Research Council of Canada, Ottawa, 1970.

Boyd, D. W., Williams, G. P. "Atmospheric Icing of Structures", Tech. Paper No. 275 of the Division of Building Research, National Research Council of Canada, Ottawa, 1968.

Bryazgin, N. N., Koptev, A. P., "O spektral'nom al'bedo snezhno-ledyanogo pokrova (Spectral Albedo of Snow-Ice Cover)", Problemy Arktiki i Antarktiki, Vol. 31 (1969) pp. 79-83.

Charters, W. W. S., Peterson, L. F., "Free Convection Suppression Using Honeycomb Cellular Materials", Solar Energy, Vol. 13 (1972), pp. 353-361.

Corotis, R. B., Dowding, C. H., Rossow, E. C., "Snow and Ice Accumulation at Solar Collector Installations in the Chicago Metropolitan Area", United States National Bureau of Standards, 1979.

Dodd, Mike: Technical Administration Services Branch, Ministry of Forests, Victoria, B.C., personal communication.

Drewes, Per: Ontario Hydro, Toronto, Ontario, personal communication.

Duffie, J. A., Beckman, W. A., "Solar Engineering of Thermal Processes", John Wiley & Sons, Inc., New York, 1991.

Egles, Dave: President, Soltek Solar Energy Ltd., Victoria, B.C., personal communication.

Energy Diversification Research Laboratory, "PV Charge Controller Survey, Report # EDRL 95 - 34 (TR)", CANMET, Dept. of Natural Resources Canada, Varennes, Quebec, 1995.

Environment Canada-- Atmospheric Environment Service, "Canadian Weather Energy and Engineering Data Sets (CWEEDS) CD-ROM", 1993.

Farzaneh, M., Melo, O. T., "Properties and Effect of Freezing Rain and Winter Fog on Outline Insulators", Cold Regions Science and Technology, 19 (1990) pp. 33-36.

Frampton, Glen: RCMP, Gros Morne National Park, Newfoundland, personal communication.

Gilbride, David: Weather Telemetry Equipment, Parks Canada, Alberta, personal communication.

Haldar, Asim: Newfoundland and Labrador Hydro, St. John's, Newfoundland, personal communication.

Hollands, K. G. T., Marshall, K. N., Wedel, R. K., "An Approximate Equation for Predicting the Solar Transmittance of Transparent Honeycombs", *Solar Energy*, Vol. 21 (1978), pp. 231-236.

Incropera, F. P., DeWitt, D. P., "Fundamentals of Heat and Mass Transfer, Third Edition", John Wiley & Sons, New York, 1990.

Iqbal, M., "An Introduction to Solar Radiation", Academic Press, 1983, Don Mills, Ontario.

Jantsch, M., Stoll, M., Roth, W., Kaiser, R., Schmidt, H., Schmid, J. "The Effect of Tilt Angle and Voltage Conditions on PV System Performance: An Experimental Investigation", *Proceedings of the 10th European Photovoltaic Solar Energy Conference*, Lisbon, April 1991, Kluwer Academic Publishers, pp. 431-434.

Jarvis, Roy: Communications Section, B. C. Ministry of Transportation and Highways, Victoria, B.C., personal communication.

Kalmbach, Eric: Lenbrook Energy Systems, Pickering, Ontario, personal communication.

Kennedy, Ken: Gros Morne National Park, Newfoundland, personal communication.

Klucher, T. M., "Evaluation of Models to Predict Insolation on Tilted Surfaces", *Solar Energy*, 23 (1979), pp. 111-114.

Kobayashi, D., "Snow Accumulation on a Narrow Board", *Cold Regions Science and Technology*, 13 (1987), pp. 239-245.

Kociuba, Peter: Atmospheric Environment Service, Environment Canada, Edmonton, personal communication.

Kondratyev, K., "Luchistaya Energiya Solntsa (The Radiant Energy of the Sun)", *Gidrometeoizdat*, Leningrad, 1954.

Kuroiwa, D., "Icing and Snow Accretion on Electric Wires", *Cold Regions Science and Technology*, Res. Report 123, 1965.

Kuroiwa, D., Mizuno, Y., Takeuchi, M., "Micromeritical Properties of Snow", *Proceedings of the International Conference on Low Temperature Science: Conference on Physics of Snow and Ice*, August, 1966 Sapporo, Japan, Vol 1, Part 2 (H. Oura, ed.), The Institute of Low Temperature Science, Hokkaido University, 1967, pp. 751-772.

LaPlace, Ron: President, Photron Canada, Inc., Colinton, Alberta, personal communication.

- Langham, E. J., "Physics and Properties of Snowcover", Handbook of Snow: Principles, Processes, Management and Use (D. M. Gray and D. H. Male, eds.) Pergamon Press, Toronto, 1981, pp. 275-337.
- Lide, D. R., ed., "CRC Handbook of Chemistry and Physics, 75th Edition", CRC Press, Boca Raton, Florida, 1994.
- Lock, G. S. H., "The Growth and Decay of Ice", Cambridge University Press, Cambridge, 1990.
- Maguire, R. J., "Light Transmission Through Snow and Ice", Environment Canada Technical Bulletin No. 91, 1975.
- Makkonen, L., "Estimating Intensity of Atmospheric Ice Accretion on Stationary Structures", Journal of Applied Meteorology, Vol. 20 (1981), pp. 595-600.
- Makkonen, L., "Estimation of Wet Snow Accretion on Structures", Cold Regions Science and Tecnology, 17, (1989) pp. 83-88.
- Male, D.H., Gray, D. M., "Snowcover Ablation and Runoff", Handbook of Snow: Principles, Processes, Management and Use (D. M. Gray and D. H. Male, eds.) Pergamon Press, Toronto, 1981, pp. 360-436.
- McKay, G. A., Gray, D. M., "The Distribution of Snowcover", Handbook of Snow: Principles, Processes, Management and Use (D. M. Gray and D. H. Male, eds.) Pergamon Press, Toronto, 1981, pp. 153-190.
- McKay, G. A., Thompson, H. A., "Estimating the Hazard of Ice Accretion in Canada from Climatological Data", Journal of Applied Meteorology, 8 (1969), pp. 927-935.
- Mellor, M., "Engineering Properties of Snow", Journal of Glaciology, Vol. 19 (1977), pp. 15-65.
- Mellor, M., "Some Optical Properties of Snow", Publication No. 69 of the AIHS: Proceedings of the International Symposium on Scientific Aspects of Snow and Ice Avalanches, April 5-10, 1965, Davos, Switzerland, 1966.
- Meyer, B. A., El-Wakil, M. M., Mitchell, J. W., "Natural Convection Heat Transfer in Small and Moderate Aspect Ratio Enclosures-- An Application to Flat-Plate Collectors", Thermal Storage and Heat Transfer in Solar Energy Systems (F. Kreith, R. Boehm, J. Mitchell, R. Bannerot, eds.), American Society of Mechanical Engineers, New York, 1978.
- Minsk, L.D., "Icing on Structures", CRREL report 80-31. U. S. Cold Regions Research and Engineering Laboratory, Hanover, New Hampshire, 1980.

Morris, Bob: Atmospheric Environment Service, Environment Canada, Downsview, Ontario, personal communication.

Mostrel, M., Givoni, B., "Windscreens in Radiant Cooling", *Passive Solar Energy Journal*, Vol. 1 (1982), pp. 229-238.

Nentwich, A., Szeless, A., "The 'Alpsolar' Project-- field Testing and Optimization of European Photovoltaic Power Plant Equipment at High-Elevation and Nordic Sites", *Progress in Photovoltaics: Research and Applications*, Vol 1, 55-66 (January 1993).

O'Neill, A. D. J., Gray, D. M., "Solar Radiation Penetration Through Snow", *The Role of Snow and Ice in Hydrology: Proceedings of the Banff Symposium*, 1972.

O'Rourke, M. J., "Snow and Ice Accumulation around Solar Collector Installations", United States National Bureau of Standards, 1979.

Overstraeten, R. J., Mertens, R. P., "Physics, Technology and Use of Photovoltaics", Adam Hilger Ltd., Bristol, England, 1986.

Perez, R., Ineichen, P., Seals, R., Michalsky, J., Stewart, R., "Modeling Daylight Availability and Irradiance Components from Direct and Global Irradiance", *Solar Energy*, 44 (1990), pp. 271-289.

Real, Markus: Alpha Real AG Energy Systems and Engineering, Zurich, Switzerland, personal communication.

Real, M., "The Behaviour of Large Solar Power Stations in the Swiss Alps", *Proceedings of the 4th European Photovoltaic Solar Energy Conference*, Stresa, Italy, 1982, pp. 51-56.

Reynolds, W. C., Perkins, H. C., "Engineering Thermodynamics", McGraw-Hill Publishing Company, New York, 1977.

Schadel, J., "The 4 kW Pilot Plant 'Muttler'", *Proceedings of the 10th European Photovoltaic Solar Energy Conference*, Lisbon, April 1991, Kluwer Academic Publishers, pp. 763-765.

Schuyler, Glen: Rowan, Williams, Davies and Irwin Inc., Guelph, Ont., personal communication.

Shellard, H. C., "The Meteorological Aspects of Ice Accretion on Ships", Report No. 10 on Marine Science Affairs, World Meteorological Organization, Geneva, 1974.

Siemens Solar Industries, "Photovoltaic Technology and System Design: Training Manual", Siemens Solar Industries, Camarillo, CA, 1990.

Stallabrass, J. R., "Airborne Snow Concentrations and Visibility". Second International Symposium on Snow Removal and Ice Control Research, Hanover, N. H. U.S. Army Cold Regions Research and Engineering Laboratory, 1978 , pp. 192-199.

Stewart, R. E., Crawford, R. W., Donaldson, N. R., Low, T. B., Sheppard, B. E., "Precipitation and Environmental Conditions during Accretion in Canadian East Coast Winter Storms", Journal of Applied Meteorology, Vol 29 (1990), pp. 529-538.

Taylor, D. A., "Snow on Sloping Roofs", Proceedings of the 1987 CSCE Centennial Conference, Montreal, Quebec, 1987, v. 1, pp. 145-158.

Thomas, C. W., "On the Transfer of Visible Radiation through Sea Ice and Snow", Journal of Glaciology, Vol 4 (1963) pp. 481-484.

TN Conseil, "Prevention de l' accumulation et elimination de la neige et du verglas sur les capteurs photovoltaïques utilises au Canada", TN Conseil, Montreal, March, 1994.

TN Conseil, "Test de comportement a la neige et au verglas de prototypes de capteurs photovoltaïques de la compagnie Astropower", TN Conseil, Montreal, March, 1993.

U.S. Army Corps of Engineers, "Snow Hydrology", Portland, Oregon, North Pacific Div., Corps of Engineers, 1956.

Wakahama, G., Kuroiwa, D., Goto, K., "Snow Accretion on Electric Wires and its Prevention", Journal of Glaciology, Vol. 19 (1977), pp. 479-487.

Warren, S. G., "Optical Properties of Snow", Reviews of Geophysics and Space Physics, Vol. 20 (1982), pp. 67-89.

Waszkiewicz, Mike: Campbell Scientific, Edmonton, Alberta, personal communication.

Watsun Simulation Laboratory, "Watsun-PV User's Manual and Program Documentation Version 4.0", University of Waterloo, Waterloo, Ontario, 1992.

APPENDIX A

ICING ON WIRES AND STRUCTURES

ICING ON WIRES, BY PROVINCE

Prov.	Location	Elev., ft	Year	Date	Hr	Wind, mph	Wind Later, mph	Type	Thickness in.	Exposure
B. C.	* Langley	200	1935	Jan. 21	6	No	-	Glaze	2.5	Flat
	* Matsqui	30	1949	-	3	No	-	Glaze	1/2	Flat
	Vanderhoof	2100	1959	Dec.	48	No	-	Sleet	2.5	Sheltered
	Fort St. John	2200	1960	May 23	48	40	-	Snow	1.75	Flat
	* Terrace	300	1963	Dec. 21	24	No	-	Rime	2	Hilly
	* Alberni	1000	1964	Dec. 18	24	No	-	S&ZR	3	Mountain
	* Sandspit	60		Dec. 26	3	60	-	Glaze	1/2	Varied
	* Bella Coola	50		Dec. 31	18	5	-	S&ZR	1.5	Sheltered
	Terrace	700	1965	Dec. 3	11	G15	No	Snow	2	Benches
	* Courtenay	2000		Dec. 8	6	Yes	No	Rime	1.5	Mountain
	Campbell R.	Low		Dec. 24	24	15	No	Snow	2.5	Flat
	Sutton Pass	800		Dec. 27	4	No	No	Snow	5	Mountain
	Sunset Beach	400	1966	Jan. 4	-	No	No	Snow	2	Hilly
	L. Cowichan	800		Jan. 9	10	No	No	Snow	2	Hilly
	* Fraser Mtn.	3758		Feb. 1	144	20	30	Glaze	1/2	Plateau
	Mica Creek	1850		Dec. 16	48	No	No	Snow	1.25	Valley
	* Osoyoos	6100	1967	Mar. 21	41	19	15	Rime	1.5	Mountain
	* Clearwater	2500		Oct. 27	16	No	No	Rime	1.25	Hilly
	Alta Lake	2200		Oct. 27	-	Yes	Yes	Snow	4	Valley
	Pemberton	600		Oct. 27	-	Yes	Yes	Snow	4	Valley
	* Cheakamus	100	1968	Jan. 10	84	No	No	Rime	1	Valley
	Cheekye	50		Jan. 12	20	No	No	Rime	1/2	Delta
	Tisdall	1700		Jan. 18	31	No	No	Snow	4.5	Mountain
	* Kitimat	300		Jan. 19	7	-	-	Glaze	1/2	Mountain
ALTA.	* Calgary	3500	1965	Feb. 27	-	-	-	Glaze	1/4	-
	* Sedgewick	2300		May 16	9	40G55	Yes	S&ZR	1	-
	* Stettler	2700	1966	Mar. 13	72	No	No	Rime	1/4	Flat
	Stettler	2700		Apr. 11	48	No	-	Glaze	1/4	Flat
SASK.	* Lewvan	-	1965	Dec. 11	72	No	No	Rime	1.25	Flat
	North Portal	-		Dec. 11	10	No	No	Hoar	1.5	Flat
	* Regina	1885		Dec. 13	72	No	-	Rime	3/4	Flat
	* Central Butte	2065	1966	Mar. 10	-	-	-	Rime	3/4	Flat
MAN.	Deloraine	1640	1965	Dec. 11	72	No	No	Hoar	2	Flat
	* Minnedosa	1800	1967	Mar. 29	12	Yes	Yes	Glaze	1/2	Flat
ONT.	* White River	1243	1940	Dec. 9	4	Yes	No	Glaze	3/8	Exposed
	* Guelph	1100	1959	Feb. 14	48	No	No	Glaze	3/4	City
	Guelph	1100		Mar. 14	48	Yes	Yes	Glaze	1/4	City
	Guelph	1100		Dec. 28	72	Yes	Yes	Glaze	3/4	City
	* Marathon	1000	1964	Oct. 8	31	20	No	S&ZR	1	Low Flat
	* Haycroft	-		Dec. 4	7	Yes	No	Glaze	1/2	Flat
	Guelph	1100	1965	Feb. 10	48	No	No	Glaze	1/4	City
	* Millgrove	825		Feb. 25	18	20	40	Glaze	1/2	Flat
	* Bells Corners	250		Nov. 17	10	Yes	Yes	Glaze	3/8	Flat
	* Manotick	325		Nov. 17	10	Yes	Yes	Glaze	1/4	Flat
	Guelph	1100		Dec. 11	48	Yes	No	Glaze	1/4	City
	* Toronto	350		Dec. 11	20	No	-	Glaze	1/4	City
	* Milton	550		Dec. 12	16	No	Yes	Glaze	1/2	Hilly
	* Scarborough	514	1966	Mar. 12	14	No	No	Glaze	3/16	Nr. Bluff
	* St. Thomas	750		Apr. 27	-	-	-	Glaze	1/2	Flat
	* Ballantrae	-	1968	Jan. 14	28	Yes	Yes	Glaze	1/2	Rolling
	* Feneion Falls	850	1969	Jan. 29	14	No	No	Glaze	3/8	Hilly

from [Boyd, 1970].

ICING ON WIRES, BY PROVINCE

Prov.	Location	Elev., ft	Year	Date	Hr	Wind, mph	Wind Later, mph	Type	Thickness in.	Exposure
QUE.	* Dorval	98	1965	Feb. 10	10	20G40	No	Glaze	3/8	Flat
	* Lacolle	-		Feb. 10	2	Gusty	Gusty	Glaze	2	Flat
	* St. Hilaire	125		Feb. 10	2	Yes	Yes	Glaze	1/4	Flat
	* Bethanie	650		Feb. 25	1	75	-	-	1/4	Flat
	* Joliette	108		Nov. 15	12	No	-	Rime	1/4	Flat
	* Berthierville	-	1966	Nov. 17	12	Yes	Yes	Glaze	1/2	Flat
	* Hull	200		Nov. 27	12	Yes	Yes	Glaze	1/4	Flat
	* Ste. Scholastique	225		Nov. 27	24	No	No	Glaze	1/2	Flat
	* Ste. Therese	-		Nov. 27	8	Yes	Yes	Glaze	1/2	Flat
	* Ste. Jean de Matha	-		Mar. 5	2	Yes	Yes	Glaze	3/8	Hilly
	* St. Calixte Nord	-		Mar. 6	8	No	No	Rime	1/2	Hilly
	* Trois Rivières	-		Dec. 11	48	-	-	Glaze	1	-
	* Anjou	-		Nov. 28	17	10	No	Glaze	1/4	Flat
	* Pont Viau	-		Nov. 28	14	35	5	Glaze	5/8	Flat
	* St. Laurent	125		Nov. 28	12	20	No	Glaze	1/4	Flat
	* St. Vincent de Paul	-		Nov. 28	15	No	No	Glaze	3/8	Flat
	* St. Bruno	460		Dec. 23	8	30	15	Rime	1/2	Flat
	* "Saguenay"	3000		Nov. 13	192	Yes	-	Rime	3. 5	Hilly
N. B.	* Moncton	248	1964	Nov. 20	4	20	30	Glaze	3/8	Flat
	* Moncton	248		Dec. 27	4	No	20G27	Glaze	1/4	Flat
	* Spruce L.	MSL		Dec. 28	18	No	Yes	Glaze	3/8	Flat
	* Baie Ste. Anne	150	1967	Dec. 4	12	No	No	Glaze	3/8	Flat
N. S.	* Antigonish	30	1961	Mar.	168	-	-	Rime	4. 25	-
	* Cheticamp	1750	1964	Dec. 29	10	90	30	Glaze	2	Flat
	* Antigonish	920	1965	Jan. 1	24	Yes	No	Glaze	1. 5	Hilly
	* Cape Mabou	1050		Jan. 2	7	35	20	Glaze	2	Flat
	* Bay St. Lawrence	1250		Jan. 4	22	40	15	Glaze	2	Flat
	* Whitehead	100	1966	Mar. 5	17	No	No	Glaze	1	Flat
	* Port Hawkesbury	100		Mar. 5	16	-	No	Glaze	1	Hilly
	* Port Hawkesbury	100	1968	Feb. 9	12	30	30	Rime	1/2	Coast
NFLD.	* St. John's	125	1958	Feb. 27	46	-	-	Glaze	1	-
	* Conception Bay	950	1964	Jan. 24	-	No	No	Glaze	5	Severe
	* Twillingate	150	1965	Dec. 26	12	38-48	30-35	Glaze	1/4	Hilly
	* Kenmount Hill	500	1966	Jan. 9	24	Yes	Yes	Rime	1/2	Hilltop
	* White Bay	1600		Jan.	-	-	-	Rime	3	Hilltop
	* Roddickton	500		Jan. 18	24	Yes	Yes	Rime	3/4	Plateau
	* Kenmount Hill	600		Jan. 19	24	25	-	Rime	1. 5	Hilltop

ICING ON STRUCTURES OTHER THAN WIRES, BY PROVINCE

Prov.	Location	Elev., ft	Year	Date	Hr	Wind, mph	Wind Later, mph	Type	Thickness in.	Exposure
B. C.	Fraser Mtn.	3758	1966	Feb. 1	144	20	30	Glaze	1/2	Plateau
*	Osoyoos	6100		Nov. 15	240	13	20	Rime	20	Mountain
	Osoyoos	6100	1967	Mar. 21	41	19	15	Rime	4	Mountain
*	Cheakamus	100	1968	Jan. 10	84	No	No	Rime	1	Valley
ALTA*	Sedgewick	2300	1965	May 16	9	40G55	Yes	S&ZR	6	-
ONT. *	Little Current	975	1954	Mar. 1	-	29	-	S&ZR	1.5	Hilly
	Guelph	1100	1959	Feb. 14	48	No	No	Glaze	3/4	City
	Guelph	1100		Mar. 14	48	Yes	Yes	Glaze	1/4	City
	Guelph	1100		Dec. 28	72	Yes	Yes	Glaze	3/4	City
	Guelph	1100	1965	Feb. 10	48	No	No	Glaze	1/4	City
	Millgrove	850		Feb. 25	18	20	40	Glaze	1/2	Flat
	Guelph	1100		Dec. 11	48	Yes	No	Glaze	1/4	City
	Toronto	400		Dec. 11	20	No	-	Glaze	1/4	City
	Milton	550		Dec. 12	16	No	Yes	Glaze	1/2	Hilly
	St. Thomas	750	1966	Apr. 27	-	-	-	Glaze	1/2	Flat
	North Bay	850		Nov. 3	8	30	-	Glaze	1/2	Flat
*	St. Thomas	750	1967	Jan. 27	-	60	-	Glaze	1.25	Flat
	Ballantrae	-	1968	Jan. 14	28	Yes	Yes	Glaze	1/2	Rolling
*	Leaside	-		Jan. 14	28	Yes	Yes	Glaze	2	Flat
QUE. *	St. Constant	100	1961	Feb. 25	-	G70	-	Glaze	2	Flat
	Dorval	98	1965	Feb. 10	10	20G40	No	Glaze	1/4	Flat
*	Lacolle	-		Feb. 10	2	Gusty	Gusty	Glaze	4	Flat
*	St. Scholastique	225		Nov. 27	24	No	No	Glaze	2.5	Flat
	Ste. Therese	150		Nov. 27	8	Yes	Yes	Glaze	1/2	Flat
	St. Vincent de P.	-	1968	Nov. 28	15	No	No	Glaze	3/4	Flat
	St. Bruno	460		Dec. 23	8	30	15	Rime	3/4	Flat
*	"Saguenay"	3000	1969	Nov. 13	192	Yes	-	Rime	8	Hilly
N. B. *	Caledonia Mtn.	1300	1956	Jan.	168	No	-	Glaze	5	Hilly
	Moncton	248	1964	Nov. 20	4	20	30	Glaze	3/8	Flat
	Moncton	248		Dec. 27	4	No	20G27	Glaze	1/4	Flat
N. S. *	Ecum Secum	100	1964	Mar. 27	-	Yes	-	Glaze	3	Hilly
	Halifax	461		Dec. 28	21	G25	G25	Glaze	1/2	Rolling
	Antigonish	920	1965	Jan. 1	24	Yes	No	Glaze	4	Hilly
*	Antigonish	1020		Jan. 3	-	No	-	Glaze	10	Hilly
	Brown's Mtn.	-		Jan. 5	-	G40	-	Glaze	10	Hilly
NFLD	St. John's	125	1958	Feb. 27	46	-	-	Glaze	1.25	-
	St. Lawrence	96	1962	Feb.	-	40	-	Glaze	3/4	-
*	Conception Bay	950	1964	Jan. 24	-	No	No	Glaze	8	Severe
*	Torbay	525		Feb.	-	G75	-	Glaze	12	Flat
*	Gander	488	1965	Jan. 2	38	No	No	Glaze	1.5	Flat
*	Lascie	330		Jan. 6	-	40	-	Glaze	15	Flat
*	Port aux Basque	185		Feb.	-	50	-	Glaze	1	Hilly
*	Cook's Harbour	450		Mar. 5	-	G105	-	Glaze	12	Hilly
*	Kenmount Hill	500	1966	Jan. 9	24	Yes	Yes	Rime	1	Hilltop
*	White Bay	1600		Jan.	-	-	-	Rime	6	Hilltop
*	Gaff Topsails	1100		Jan. 13	48	40-50	No	Rime	2	Hillside
	Gaff Topsails	1100		Jan. 18	24	Yes	Yes	Rime	2	Hillside
	Kenmount Hill	600		Jan. 19	24	25	-	Rime	3	Hilltop
*	Heart's Cont't	900		Jan. 20	36	30-40	30-40	Glaze	6	Hilltop
	Gander	482	1967	Apr. 12	5	Yes	Yes	Glaze	1/4	Flat

APPENDIX B

MATHCAD FILE: FRONT PAN.MCD

This Mathcad file contains an implementation of the Temps, Coulson and Klucher model for diffuse radiation, an implementation of the Perez model for diffuse radiation, and various equations for determining sun angles.

Calculation of Sun Angles:

See "Solar Engineering of Thermal Processes", Duffie and Beckman, pp. 13-16 for following relations on sun angles for beam radiation.

$$\omega(H, M) := \left[(H - 12) + \frac{M}{60} \right] \cdot 15 \cdot \frac{\pi}{180} \quad \text{Hour angle, (radians, morning negative)}$$

(see Duffie and Beckman p. 13,16)

$$\delta(D) := 23.45 \sin \left(360 \frac{284 + D}{365} \cdot \frac{\pi}{180} \right) \cdot \frac{\pi}{180} \quad \text{Declination (radians, north positive)}$$

$$\text{Zenith}(L, D, H, M) := \arccos(\cos(L) \cdot \cos(\delta(D)) \cdot \cos(\omega(H, M)) + \sin(L) \cdot \sin(\delta(D))) \quad \text{Zenith angle (radians)}$$

$$\omega_{ew}(L, D) := \arccos \left(\frac{\tan(\delta(D))}{\tan(L)} \right) \quad \text{Hour angle when sun is due east or west (radians)}$$

$$C_1(L, D, H, M) := \text{if}(|\omega(H, M)| \leq \omega_{ew}(L, D), 1, -1) \quad \text{Constants for pseudo solar azimuth}$$

$$C_2(L, D) := \text{if}([L - \delta(D)] \geq 0, 1, -1)$$

$$C_3(H, M) := \text{if}(\omega(H, M) \geq 0, 1, -1)$$

$$\gamma_{s_pseudo}(L, D, H, M) := \arcsin \left(\frac{\sin(\omega(H, M)) \cdot \cos(\delta(D))}{\sin(\text{Zenith}(L, D, H, M))} \right) \cdot \frac{180}{\pi} \quad \text{Pseudo solar azimuth (rad)}$$

$$\text{DB_Sol_Az}(L, D, H, M) := \left[C_1(L, D, H, M) \cdot C_2(L, D) \cdot \gamma_{s_pseudo}(L, D, H, M) \dots \right. \\ \left. + C_3(H, M) \cdot \left(\frac{1 - C_1(L, D, H, M) \cdot C_2(L, D)}{2} \right) \cdot 180 \right] \cdot \frac{\pi}{180}$$

Solar Azimuth (rad) as calculated by Duffie and Beckman (east of south is negative.)

Calculation of Diffuse Radiation Incident on Rear of Array:

$$H_H := 1000 \quad (\text{W/m}^2) \quad \text{Peak Sun insolation.}$$

$$\text{Albedo} := 0.7$$

Equations from [Duffie et al., 1991] and [Watsun, 1992].

$$\theta(L, D, H, M, \beta) := \arccos \left(\cos(\text{Zenith}(L, D, H, M)) \cdot \cos(\beta) \dots \right. \\ \left. + \sin(\text{Zenith}(L, D, H, M)) \cdot \cos(\text{DB_Sol_Az}(L, D, H, M)) \cdot \sin(\beta) \right) \quad \text{Angle of incidence, south facing array}$$

$$\theta_s(L, D, H, M, \beta) := \arccos \left(\cos(\text{Zenith}(L, D, H, M)) \cdot \cos(\beta) \dots \right. \\ \left. + \sin(\text{Zenith}(L, D, H, M)) \cdot \cos(\text{DB_Sol_Az}(L, D, H, M) - \pi) \cdot \sin(\beta) \right) \quad \text{Angle of incidence, north facing array.}$$

Temps and Coulson Model with Modulating Function By Klucher.

$$H_{dt}(L, D, H, M, \beta, k_d) := H_H \cdot k_d \cdot \left(\frac{1 + \cos(\beta)}{2} \right) \cdot \left[1 + (1 - k_d^2) \cdot \sin\left(\frac{\beta}{2}\right)^3 \right] \cdot \left[1 + (1 - k_d^2) \cdot \cos(\theta(L, D, H, M, \beta))^2 \cdot \sin(\text{Zenith}(L, D, H, M))^3 \right]$$

Diffuse radiation

$$H_{bt}(L, D, H, M, \beta, k_d) := H_H \cdot (1 - k_d) \cdot \frac{\cos(\theta(L, D, H, M, \beta))}{\cos(\text{Zenith}(L, D, H, M))}$$

Beam radiation.

$$H_{gt}(\beta) := H_H \cdot \text{Albedo} \cdot \left(\frac{1 - \cos(\beta)}{2} \right)$$

Ground Reflected Radiation, standard model.

$$H_{tt}(L, D, H, M, \beta, k_d) := H_{dt}(L, D, H, M, \beta, k_d) + H_{bt}(L, D, H, M, \beta, k_d) + H_{gt}(\beta)$$

Total radiation on a tilted surface

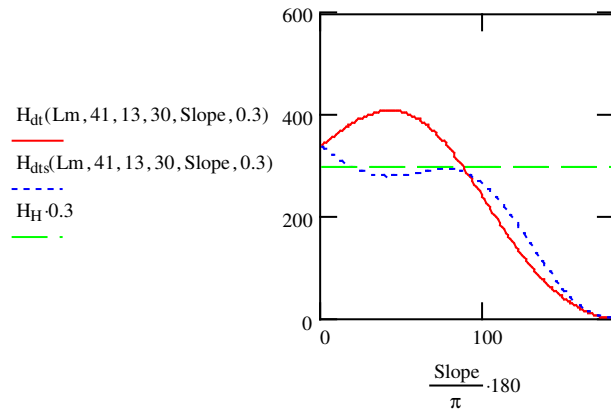
$$H_{dts}(L, D, H, M, \beta, k_d) := H_H \cdot k_d \cdot \left(\frac{1 + \cos(\beta)}{2} \right) \cdot \left[1 + (1 - k_d^2) \cdot \left(\sin\left(\frac{\beta}{2}\right)^3 \right) \right] \cdot \left[1 + (1 - k_d^2) \cdot \cos(\theta_s(L, D, H, M, \beta))^2 \cdot \sin(\text{Zenith}(L, D, H, M))^3 \right]$$

Diffuse radiation for north facing array according to Temps, Coulson, Klucher

$$Lm := \pi \cdot \frac{45}{180}$$

Latitude of 45 N

$$\text{Slope} := 0, \frac{\pi}{180} \dots \pi$$



Comparison of diffuse radiation incident on the face of south and north facing arrays, Feb 10, 13:30 at 45 degrees North. according to Temps, Coulson, and Klucher. The south facing array is solid line. The north facing array has higher irradiation at panel tilt angles > 90 degrees due to a bogus circumsolar region seen by the model in the direction perfectly opposite the sun.

panel tilt angle-- 0 horizontal, facing the sky
and 180 is horizontal, facing the ground

Perez Model

$$a(\theta) := \text{if}(\cos(\theta) > 0, \cos(\theta), 0)$$

$$b(\text{Zenith}) := \text{if}\left(\cos(\text{Zenith}) > \cos\left(\pi \cdot \frac{85}{180}\right), \cos(\text{Zenith}), \cos\left(\pi \cdot \frac{85}{180}\right)\right)$$

$$\varepsilon(L, D, H, M, k_d, I_H) := \frac{\frac{k_d + \frac{(1 - k_d)}{\cos(\text{Zenith}(L, D, H, M))}}{k_d} + 5.535 \cdot 10^{-6} \cdot \left(\text{Zenith}(L, D, H, M) \cdot \frac{180}{\pi}\right)^3}{1 + 5.535 \cdot 10^{-6} \cdot \left(\text{Zenith}(L, D, H, M) \cdot \frac{180}{\pi}\right)^3}$$

$$m_{\text{air}}(L, D, H, M) := \frac{1}{\cos(\text{Zenith}(L, D, H, M)) + 0.15 \left[93.885 - \left(\frac{180}{\pi}\right) \cdot \text{Zenith}(L, D, H, M) \right]^{-1.253}}$$

$$I_{on}(D) := 4.921 \cdot \left(1 + 0.033 \cos \left(\frac{360 \cdot D \cdot \pi}{365 \cdot 180} \right) \right)$$

$$I_0(L, D, H, M) := I_{on}(D) \cdot \cos(\text{Zenith}(L, D, H, M))$$

$$\Delta(L, D, H, M, k_d, I_H) := m_{air}(L, D, H, M) \cdot \frac{I_H \cdot k_d}{I_{on}(D)}$$

Constants for Perez model.

Range of brightness index, ε

$$f := \begin{pmatrix} -0.196 & 1.084 & -0.006 & -0.114 & 0.18 & -0.019 \\ 0.236 & 0.519 & -0.180 & -0.011 & 0.02 & -0.038 \\ 0.454 & 0.321 & -0.255 & 0.072 & -0.098 & -0.046 \\ 0.866 & -0.381 & -0.375 & 0.203 & -0.403 & -0.049 \\ 1.026 & -0.711 & -0.426 & 0.273 & -0.602 & -0.061 \\ 0.978 & -0.986 & -0.350 & 0.280 & -0.915 & -0.024 \\ 0.748 & -0.913 & -0.236 & 0.173 & -1.045 & 0.065 \\ 0.318 & -0.757 & 0.103 & 0.062 & -1.698 & 0.236 \end{pmatrix} \begin{matrix} 0 \text{ to } 1.065 \\ 1.065 \text{ to } 1.230 \\ 1.230 \text{ to } 1.500 \\ 1.500 \text{ to } 1.950 \\ 1.950 \text{ to } 2.800 \\ 2.800 \text{ to } 4.500 \\ 4.500 \text{ to } 6.200 \\ 6.200 \text{ to infinity} \end{matrix}$$

$$RI(\varepsilon) := \text{if}[\varepsilon < 1.065, 0, [\text{if}[\varepsilon < 1.23, 1, [\text{if}[\varepsilon < 1.5, 2, [\text{if}[\varepsilon < 1.95, 3, [\text{if}[\varepsilon < 2.8, 4, [\text{if}[\varepsilon < 4.5, 5, (\text{if}(\varepsilon < 6.2, 6, 7))]]]]]]]]]]]$$

$$\text{maxof}(a, b) := \text{if}(a > b, a, b)$$

$$F_1(L, D, H, M, k_d, I_H) := \text{maxof} \left(0, f_{RI}(\varepsilon(L, D, H, M, k_d, I_H)), 0 + f_{RI}(\varepsilon(L, D, H, M, k_d, I_H)), 1 \cdot \Delta(L, D, H, M, k_d, I_H) \dots \right. \\ \left. + \text{Zenith}(L, D, H, M) \cdot f_{RI}(\varepsilon(L, D, H, M, k_d, I_H)), 2 \right)$$

$$F_2(L, D, H, M, k_d, I_H) := f_{RI}(\varepsilon(L, D, H, M, k_d, I_H)), 3 + f_{RI}(\varepsilon(L, D, H, M, k_d, I_H)), 4 \cdot \Delta(L, D, H, M, k_d, I_H) \dots \\ + \text{Zenith}(L, D, H, M) \cdot f_{RI}(\varepsilon(L, D, H, M, k_d, I_H)), 5$$

$$I_{dT}(L, D, H, M, \beta, k_d, I_H) := I_H \cdot k_d \cdot \left[\left(1 - F_1(L, D, H, M, k_d, I_H) \right) \cdot \frac{1 + \cos(\beta)}{2} + F_1(L, D, H, M, k_d, I_H) \cdot \frac{a(\theta(L, D, H, M, \beta))}{b(\text{Zenith}(L, D, H, M))} \dots \right. \\ \left. + F_2(L, D, H, M, k_d, I_H) \cdot \sin(\beta) \right]$$

$$I_{dT_S}(L, D, H, M, \beta, k_d, I_H) := I_H \cdot k_d \cdot \left[\left(1 - F_1(L, D, H, M, k_d, I_H) \right) \cdot \frac{1 + \cos(\beta)}{2} + F_1(L, D, H, M, k_d, I_H) \cdot \frac{a(\theta_s(L, D, H, M, \beta))}{b(\text{Zenith}(L, D, H, M))} \dots \right] \\ + F_2(L, D, H, M, k_d, I_H) \cdot \sin(\beta)$$

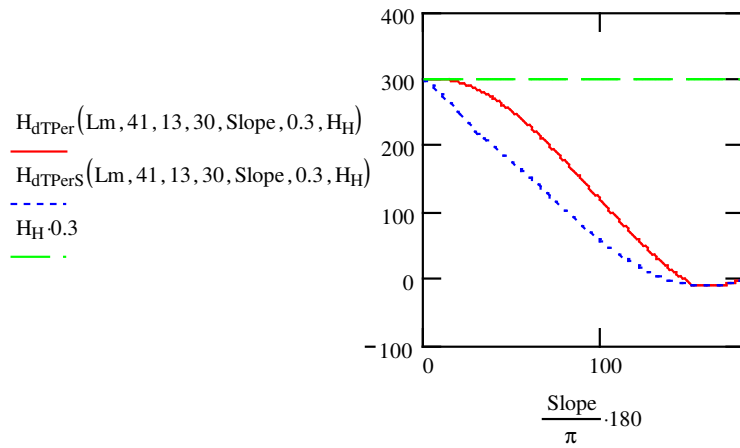
Diffuse radiation on south and north facing surfaces, in J/hour/m^2

$$H_{dT_{Per}}(L, D, H, M, \beta, k_d, H_H) := \left(I_{dT} \left(L, D, H, M, \beta, k_d, H_H \cdot \frac{3600}{10^6} \right) \right) \cdot \frac{10^6}{3600}$$

$$H_{dT_{PerS}}(L, D, H, M, \beta, k_d, H_H) := \left(I_{dT_S} \left(L, D, H, M, \beta, k_d, H_H \cdot \frac{3600}{10^6} \right) \right) \cdot \frac{10^6}{3600}$$

Diffuse radiation on south and north facing surfaces, in W/m^2

Comparison of diffuse radiation incident on the face of south and north facing arrays, Feb 10, 13:30 at 45 degrees North. according to Perez. The south facing array is in solid line.



panel tilt angle-- 0 horizontal, facing the sky
and 180 is horizontal, facing the ground

$$I_{dT}\left(40 \cdot \frac{\pi}{180}, 51, 9, 30, \frac{\pi}{3}, \frac{787}{1040}, 1.04\right) = 0.799 \quad \text{Check against Duffie and Beckman p. 101 -- 0.801}$$

Use I.dT for south facing surfaces, use I.dTS for north facing surfaces.

APPENDIX C

MATHCAD FILE: DIFFUNCM.MCD

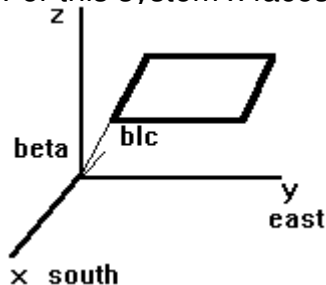
Radiation Incident on the Back of the Array due to Ground-Reflected Radiation

This model calculates the radiation incident on the rear face of the array due to beam and diffuse components of ground-reflected radiation. It accounts for the shading of the ground due to the array itself for both beam and diffuse radiation.

Model Input Parameters:

$h := 1.7$	m	Height of bottom edge of array
$\beta := \frac{\pi}{180} \cdot 45$	Rad	Array slope
$\text{width} := 1$	m	Width of a single panel
$\text{height} := 1$	m	Height of a single panel
$\text{Rows} := 3$		Number of panels in array in a vertical direction
$\text{Columns} := 42$		Number of panels in array in a horizontal direction
$H_{\text{Horiz}} := 615$	W/m ²	Insolation on an unobstructed horizontal surface
$k_d := 0.25$		
$\text{Albedo}_{\text{Diff}} := 0.7$		Spectrum averaged ground reflectance (Diffuse radiation)
$\text{Albedo}_{\text{Beam}} := 0.7$		Spectrum averaged ground reflectance (Beam radiation)

Note: The model assumes that the array faces due south. Points in space are expressed in two different coordinate systems. One, the "array-based" coordinate system, is a cartesian coordinate system that has z increasing with increasing elevation, x positive in the northern direction, and y positive in the easterly direction. For this coordinate system, the origin lies at the intersection of the plane of the ground and a line passing through the western edge of the array. The "ground-based" coordinate system has its origin at the ground at a specified distance from the bottom, west corner of the array. Points in space are expressed either in Cartesian or spherical coordinates. For this system x faces in the opposite direction as in the system above.



Lat := 43.8	degrees Latitude of installation
$\text{Lat} := \frac{\text{Lat}}{180} \cdot \pi$	Radians Latitude of installation
Hour := 14	Hour in 24 hour format
Minute := 35	Minute
Day := 69	Day of the year

Calculation of array corners:

$Y_{\text{blc}} := 0$	m	Y-coordinate of bottom left-hand (West) corner of array
$X_{\text{blc}} := \frac{-h}{\tan(\beta)}$	m	X-coordinate of bottom left-hand (West) corner of array
$fX_{\text{trc}}(X_{\text{blc}}) := X_{\text{blc}} - \text{height} \cdot \text{Rows} \cdot \cos(\beta)$		Functions to calculate the top rh (east) corner of the array.
$fY_{\text{trc}}(Y_{\text{blc}}) := Y_{\text{blc}} + \text{Columns} \cdot \text{width}$	$X_{\text{blc}} = -1.7$	
$X_{\text{trc}} := fX_{\text{trc}}(X_{\text{blc}})$	$X_{\text{trc}} = -3.821$	Test values.
$Y_{\text{trc}} := fY_{\text{trc}}(Y_{\text{blc}})$	$Y_{\text{trc}} = 42$	
$ta := \tan(\beta)$	$ta = 1$	Constants calculated from the array slope to speed calculations.
$si := \sin(\beta)$	$si = 0.707$	
$co := \cos(\beta)$	$co = 0.707$	
$b := h + X_{\text{blc}} \cdot ta \quad b = 0$		The z-intercept of the plane of the array. This should always be zero.
$z(x) := -x \cdot ta + b$		Function to calculate z, height above ground.
$z(X_{\text{blc}}) = 1.7$		Height of top and bottom array in metres
$z(X_{\text{trc}}) = 3.821$		

Calculation of Sun Angles:

See "Solar Engineering of Thermal Processes", Duffie and Beckman, pp. 13-16 for following relations on sun angles for beam radiation.

$\omega := \left[(\text{Hour} - 12) + \frac{\text{Minute}}{60} \right] \cdot 15 \cdot \frac{\pi}{180}$	Hour angle, (radians, morning negative)
	(see Duffie and Beckman p. 13,16)
$\delta := 23.45 \sin \left(360 \cdot \frac{284 + \text{Day}}{365} \cdot \frac{\pi}{180} \right) \cdot \frac{\pi}{180}$	Declination (radians, north positive)
$\text{Zenith} := \arccos(\cos(\text{Lat}) \cdot \cos(\delta) \cdot \cos(\omega) + \sin(\text{Lat}) \cdot \sin(\delta))$	Zenith angle (radians)
$\omega_{\text{ew}} := \arccos \left(\frac{\tan(\delta)}{\tan(\text{Lat})} \right)$	Hour angle when sun is due east or west (radians)

$C_1 := \text{if}(|\omega| \leq \omega_{ew}, 1, -1)$ Constants for pseudo solar azimuth

$C_2 := \text{if}[(\text{Lat} - \delta) \geq 0, 1, -1]$

$C_3 := \text{if}(\omega \geq 0, 1, -1)$

$\gamma_{s_pseudo} := \text{asin}\left(\frac{\sin(\omega) \cdot \cos(\delta)}{\sin(\text{Zenith})}\right) \cdot \frac{180}{\pi}$ Pseudo solar azimuth (rad)

$\text{DB_Sol_Az} := \left[C_1 \cdot C_2 \cdot \gamma_{s_pseudo} + C_3 \cdot \left(\frac{1 - C_1 \cdot C_2}{2} \right) \cdot 180 \right] \cdot \frac{\pi}{180}$ Solar Azimuth (rad) as calculated by Duffie & Beckman (east of south is -)

$\text{Sol_Az} := \text{DB_Sol_Az} \cdot (-1)$

$\text{Sol_Az} := \text{if}(\text{Sol_Az} < 0, \text{Sol_Az} + 2 \cdot \pi, \text{Sol_Az})$ Solar Azimuth in terms of conventional

$\text{Flag} := \text{if}\left(\text{Zenith} > \frac{\pi}{2}, 1, 0\right)$ spherical coordinates: $0 \leq \text{Sol_Az} < 2\pi$, increasing angle in counterclockwise direction, south is zero.

$\text{Sol_Az} := \text{if}(\text{Flag}, \text{Sol_Az} + \pi, \text{Sol_Az})$

$\text{Sol_Az} := \text{if}(\text{Sol_Az} \geq 2 \cdot \pi, \text{Sol_Az} - 2 \cdot \pi, \text{Sol_Az})$

$\text{Zenith} = 59.81\text{deg}$

$\text{Sol_Az} = 313.814\text{deg}$ $\text{DB_Sol_Az} = 46.186\text{deg}$ Verification Values

$H_{\text{Beam}} := (1 - k_d) \cdot H_{\text{Horiz}}$

$H_{\text{Diff}} := k_d \cdot H_{\text{Horiz}}$

Function to Calculate Diffuse Shading:

This function calculates, for a point on the ground, the fraction of:

(diffuse radiation striking that point/diffuse radiation striking that point if there was no array)

It assumes an isotropic sky. It reasons that the view, or shape, factor for the sky plus the

view factor for the array must equal one. It assumes that the array has zero thickness.

This function calculates, for a point on the ground (x0,y0), one minus the view factor for an array located by the x,y coordinates of its corners and its Z-intercept, B. The x,y coordinate system used for these corner points has its origin at the point on the ground (x0,y0). Positive X is to the south, positive y is to the east, and up is positive z.

$\text{TOL} := 0.001$ Tolerance for integral convergence

$$\text{Frac}_{\text{diff}}(X_{\text{Blc}}, X_{\text{Trc}}, B, Y_{\text{Blc}}, Y_{\text{Trc}}) := 1 - \left[\int_{Y_{\text{Blc}}}^{Y_{\text{Trc}}} \int_{X_{\text{Trc}}}^{X_{\text{Blc}}} \frac{|[x \sin i + (B - x \tan a) \cdot \cos i] \cdot (B - x \tan a)|}{[x^2 + y^2 + (B - x \tan a)^2] \cdot \cos i} dx dy \right] \cdot \frac{1}{\pi}$$

$\text{Frac}_{\text{diff}}(-1.7, -2.761, 0, 0, 10) = 1$

Test value-- a point on the ground on the line of the intersection of the plane of the ground and the plane of the array should yield a value of 1, since the ground sees only the infinitely thin edge of the array.

Function to Calculate Beam Shading:

This function returns zero if a point on the ground is in the shadow of the array and one otherwise. The point is defined by its x,y coordinates in the "array-based" coordinate system.

First the four corners of the shadow-- corresponding to the four corners of the array-- are calculated. Then, when the function is called, it checks whether the point lies within the parallelogram formed by connecting the four corners of the shadow with straight lines. If so, it returns zero.

Subscript of "s" indicates a coordinate on the array, and a subscript of "g" indicates a coordinate on the ground.

$$\rho(X_s, Y_s, Z_s, X_g, Y_g) := \sqrt{(X_s - X_g)^2 + (Y_s - Y_g)^2 + Z_s^2}$$

Function to calculate the distance between a point on the ground and a point on the array.

Solve Block for locating point on ground given point on array.

$X_g := 0$ Initial guess for ground coordinates

$Y_g := 0$

Given

$$X_s = X_g + \rho(X_s, Y_s, Z_s, X_g, Y_g) \cdot \sin(\text{Zenith}) \cdot \cos(\text{DB_Sol_Az})$$

$$Y_s = Y_g + \rho(X_s, Y_s, Z_s, X_g, Y_g) \cdot \sin(\text{Zenith}) \cdot \sin(\text{DB_Sol_Az})$$

$$Z_s = \rho(X_s, Y_s, Z_s, X_g, Y_g) \cdot \cos(\text{Zenith})$$

$$\text{G_Coord}(X_s, Y_s, Z_s) := \text{Find}(X_g, Y_g)$$

Function to find point on ground given point on array.

Calculation of the coordinates of the four corners of the shadow.

$$\begin{pmatrix} \text{Blc}_x \\ \text{Blc}_y \end{pmatrix} := \text{G_Coord}(X_{\text{blc}}, Y_{\text{blc}}, h) \quad \begin{pmatrix} \text{Blc}_x \\ \text{Blc}_y \end{pmatrix} = \begin{pmatrix} -3.723 \\ 2.109 \end{pmatrix} \quad X_{\text{blc}} = -1.7$$

$$\begin{pmatrix} \text{Tlc}_x \\ \text{Tlc}_y \end{pmatrix} := \text{G_Coord}(X_{\text{trc}}, Y_{\text{blc}}, z(X_{\text{trc}})) \quad \begin{pmatrix} \text{Tlc}_x \\ \text{Tlc}_y \end{pmatrix} = \begin{pmatrix} -8.369 \\ 4.74 \end{pmatrix}$$

$$\begin{pmatrix} \text{Brc}_x \\ \text{Brc}_y \end{pmatrix} := \text{G_Coord}(X_{\text{blc}}, Y_{\text{trc}}, h) \quad \begin{pmatrix} \text{Brc}_x \\ \text{Brc}_y \end{pmatrix} = \begin{pmatrix} -3.723 \\ 44.109 \end{pmatrix}$$

$$\begin{pmatrix} \text{Trc}_x \\ \text{Trc}_y \end{pmatrix} := \text{G_Coord}(X_{\text{trc}}, Y_{\text{trc}}, z(X_{\text{trc}})) \quad \begin{pmatrix} \text{Trc}_x \\ \text{Trc}_y \end{pmatrix} = \begin{pmatrix} -8.369 \\ 46.74 \end{pmatrix}$$

Function to Calculate Whether a point is in the array shadow or not.

$$X_{\text{diff}} := -\text{Brc}_x + \text{Trc}_x \quad X_{\text{diff}} = -4.646 \quad \text{Constants to speed up calculation; test values}$$

$$Y_{\text{diff}} := \text{Trc}_y - \text{Brc}_y \quad Y_{\text{diff}} = 2.631$$

$$\text{Alt_Frac}_{\text{beam}}(x, y) := \text{if} \left[\left(\text{Brc}_x > x \right) \cdot \left(\text{Trc}_x < x \right) \cdot \left[y > \left(\text{Blc}_y + \frac{x - \text{Brc}_x}{X_{\text{diff}}} \cdot Y_{\text{diff}} \right) \right] \cdot \left[y < \left(\text{Brc}_y + \frac{x - \text{Brc}_x}{X_{\text{diff}}} \cdot Y_{\text{diff}} \right) \right] \right], 0, 1$$

$\text{Alt_Frac}_{\text{beam}}(-3.3, 1.4) = 1$
 $\text{Alt_Frac}_{\text{beam}}(-6.1, 0.5) = 1$
Test values

Create vector of corner points so that the array and its shadow can be graphed.

$gi := 0, 1..4$

$gx_0 := \text{Blc}_x$ $gy_0 := \text{Blc}_y$ For the shadow

$gx_3 := \text{Brc}_x$ $gy_3 := \text{Brc}_y$

$gx_1 := \text{Tlc}_x$ $gy_1 := \text{Tlc}_y$

$gx_2 := \text{Trc}_x$ $gy_2 := \text{Trc}_y$

$gx_4 := gx_0$ $gy_4 := gy_0$

$gcx_0 := X_{\text{blc}}$ $gcy_0 := Y_{\text{blc}}$ For the array.

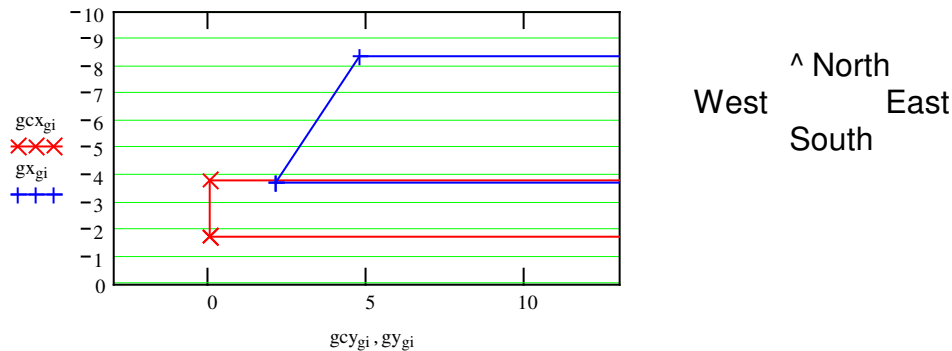
$gcx_1 := X_{\text{blc}}$ $gcy_1 := Y_{\text{trc}}$

$gcx_2 := X_{\text{trc}}$ $gcy_2 := Y_{\text{trc}}$

$gcx_3 := X_{\text{trc}}$ $gcy_3 := Y_{\text{blc}}$

$gcx_4 := X_{\text{blc}}$ $gcy_4 := Y_{\text{blc}}$

Plan view of array (red, x) and its shadow (blue, +).



Calculation of Matrix of Diffuse Radiation Values for Points on the Ground:

This procedure creates a grid of equally spaced points on the ground underneath the array. For each point in this grid it calculates the fraction of radiation on the ground to total diffuse radiation on an unobstructed horizontal surface. The grid extends to the centerline of the array, making use of the fact that with an isotropic sky, the shading of diffuse radiation will be symmetrical.

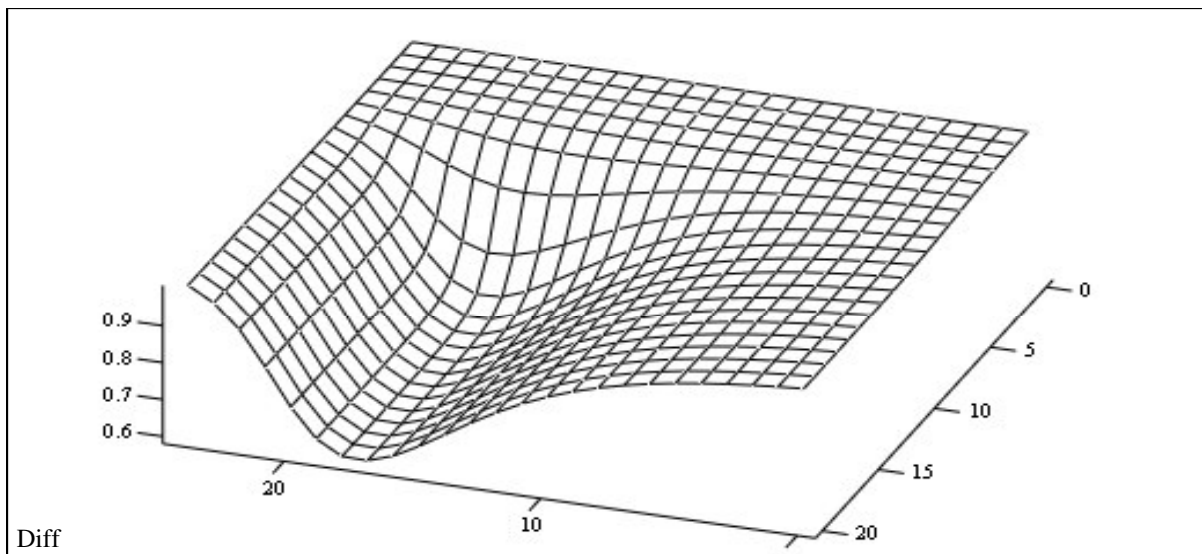
$y_{\text{lower}} := -10$ m The western boundary for the grid

$y_{\text{upper}} := \text{Columns} \cdot \frac{\text{width}}{2}$ m The eastern boundary for the grid.

```

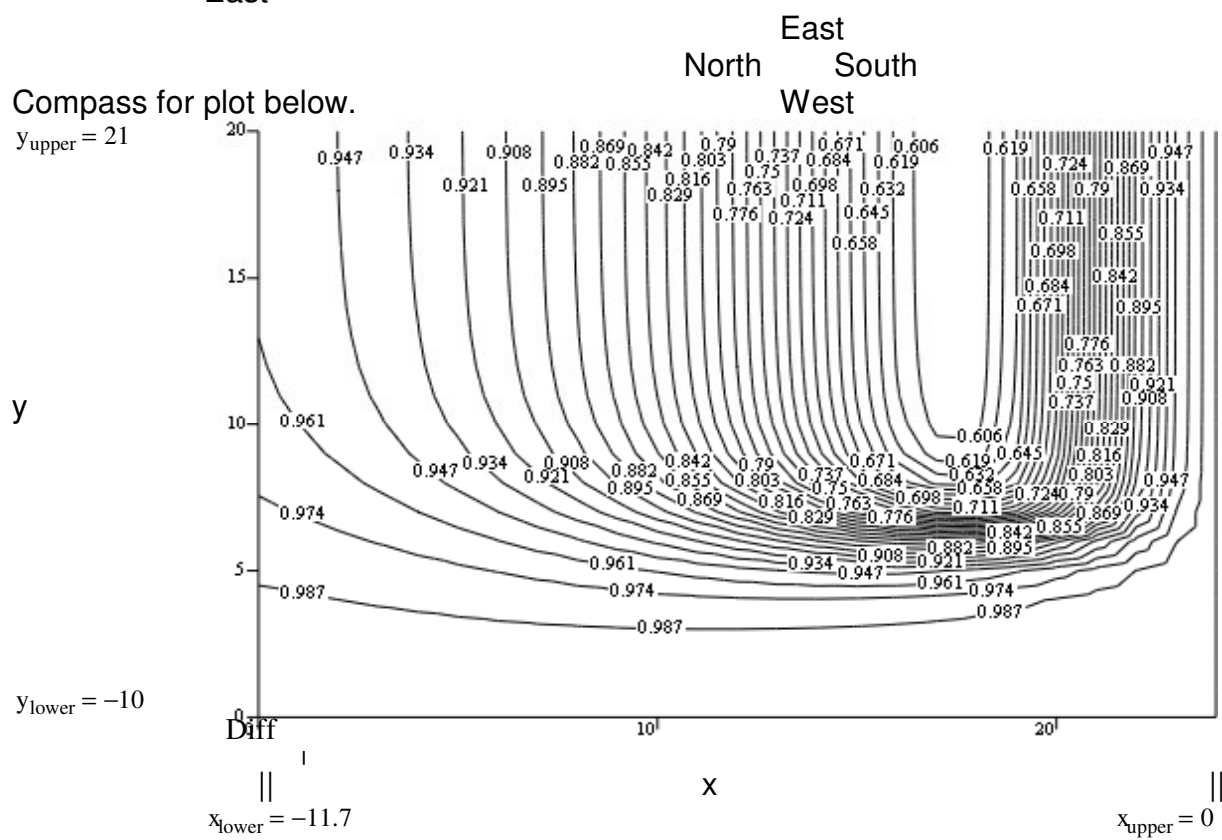
Num_Elementsy := 20      Number of points in the y direction
Δy :=  $\frac{(y_{upper} - y_{lower})}{Num\_Elements_y}$     m The difference in y between two adjacent points
xupper := 0              m The southern boundary of the grid.
                        xupper = 0
xlower := -10 + Xblc      m The northern boundary of the grid.
Num_Elementsx := 24      Number of elements in the x direction.
Δx :=  $\frac{-(x_{lower} - x_{upper})}{Num\_Elements_x}$     m The difference in x between two adjacent points
i := 0, 1.. Num_Elementsx
j := 0, 1.. Num_Elementsy
xi := xlower + i·Δx      Calculate grid
yj := ylower + j·Δy
Diffi,j := Fracdiff $\left[-x_i + X_{blc}, fX_{trc}(-x_i + X_{blc}), h + (-x_i + X_{blc}) \cdot ta, -y_j, fY_{trc}(-y_j)\right]$ 
WRITEPRN("dffbotta.prn" ) := Diff
Diff := READPRN("dffbotta.prn" )

```



South
East
West
North

Compass for graph above.



Calculation of Ground-Reflected Radiation Incident on Rear of Array:

This uses the matrix of diffuse radiation values calculated above and the Fracbeam function to calculate the total ground-reflected radiation incident on the rear of the array, in W/m², as a function of position on the array.

$$Z_{\text{panel}}(\text{Row_num}) := h + \text{si} \cdot (\text{Row_num} - 0.5) \cdot \text{height}$$

$$X_{\text{panel}}(\text{Row_num}) := X_{\text{blc}} - \text{co} \cdot (\text{Row_num} - 0.5) \cdot \text{height}$$

$$Y_{\text{panel}}(\text{Col_num}) := Y_{\text{blc}} + (\text{Col_num} - 0.5) \cdot \text{width}$$

$$\text{round}(x) := \text{if}(x - \text{floor}(x) < 0.5, \text{floor}(x), \text{ceil}(x))$$

$$\text{adjy}(y) := \text{if}\left[\left(y > y_{\text{upper}}\right), \left(2 \cdot y_{\text{upper}} - y\right), y\right]$$

Functions to calculate the x,y,z coords of the (Row,Col) panel. Row, Col = 1,1 is associated with the bottom left corner. Rounding function.

Adjustment to account for y values in eastern half of array, which is the mirror of the western half, in the matrix.

Functions to calculate the diffuse shading matrix indices given x, y coordinates on the ground.

$$\text{Ind}_i(x) := \text{if}\left[\left(x \geq x_{\text{lower}}\right) \cdot \left(x \leq x_{\text{upper}}\right), \text{round}\left(\frac{x - x_{\text{lower}}}{\Delta_x}\right), -1\right] \quad y_{\text{upper}} = 21 \quad y_{\text{lower}} = -10$$

$$\text{Ind}_j(y) := \text{if}\left[\left(\text{adjy}(y) \geq y_{\text{lower}}\right) \cdot \left(\text{adjy}(y) \leq y_{\text{upper}}\right), \text{round}\left(\frac{\text{adjy}(y) - y_{\text{lower}}}{\Delta_y}\right), -1\right]$$

Functions to calculate the diffuse and beam reflected radiation, in watts per metre².

$$J_D(x, y) := \text{Albedo}_{\text{Diff}} \cdot H_{\text{Diff}} \cdot \text{if}\left[\left(\text{Ind}_i(x) > -1\right) \cdot \left(\text{Ind}_j(y) > -1\right), \text{Diff}_{\text{Ind}_i(x), \text{Ind}_j(y)}, 1\right]$$

The "if" function returns 1 if the coordinate lies outside the grid of diffuse radiation points.

$$J_B(x, y) := \text{Albedo}_{\text{Beam}} \cdot H_{\text{Beam}} \cdot \text{Alt_Frac}_{\text{beam}}(x, y)$$

Calculation of the upper and lower limits of integration for the integral, based on the size of the array.

$$X_{\text{lim}} := -14.5$$

$$Y_{\text{lim}} := -50$$

$$Y_{\text{ulim}} := 70$$

$$\text{TOL} := 0.1$$

Tolerance for the convergence of the integral.

$$\text{Insol_P}(X_p, Y_p, Z_p) := \int_{Y_{\text{lim}}}^{Y_{\text{ulim}}} \int_{X_{\text{lim}}}^{-0.4} \frac{Z_p \cdot [\text{si} \cdot (-x + X_p) + \text{co} \cdot Z_p] \cdot (J_D(x, y) + J_B(x, y))}{\left[(x - X_p)^2 + (y - Y_p)^2 + Z_p^2\right]^2 \cdot \pi} dx dy$$

For all rows and columns of panels...

$\text{panel}_{\text{rows}} := 1, 2 \dots \text{Rows}$

$\text{panel}_{\text{cols}} := 1, 2 \dots \text{Columns}$

$\text{Panels}_{\text{panel}_{\text{cols}}-1, \text{panel}_{\text{rows}}-1} := \text{Insol_P}(X_{\text{panel}}(\text{panel}_{\text{rows}}), Y_{\text{panel}}(\text{panel}_{\text{cols}}), Z_{\text{panel}}(\text{panel}_{\text{rows}}))$ ■

Calculate the incident radiation for all panels.

West

Top

East

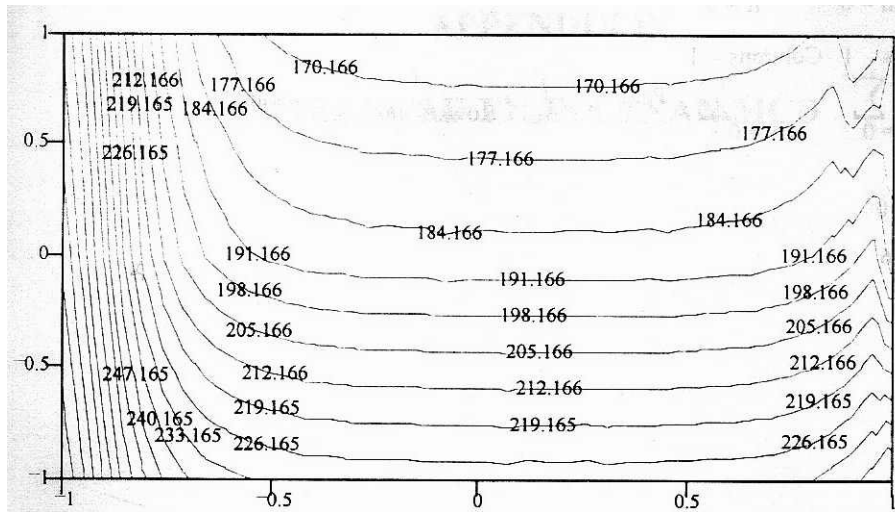
Tlc

Trc

Blc

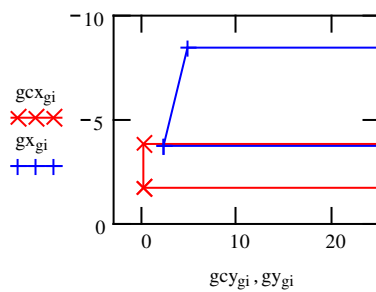
Brc

Bottom



For comparison, here is the...

Plan view of array (red, x) and it's shadow (blue, +).



West ^ North
 East
 South

Insol_P(-3,9,2.62)=184.511

$$\text{Mean} := \left(\sum_{m=0}^{\text{Rows}-1} \sum_{n=0}^{\text{Columns}-1} \text{Panels}_{n,m} \right) \cdot \frac{1}{\text{Rows} \cdot \text{Columns}} \quad \text{Mean}=204.931$$

$$\text{Var} := \left[\sum_{m=0}^{\text{Rows}-1} \sum_{n=0}^{\text{Columns}-1} (\text{Panels}_{n,m})^2 \right] \cdot \frac{1}{\text{Rows} \cdot \text{Columns}} - \text{Mean}^2$$

Var=1.198 · 10³

Var^{0.5}=34.616

APPENDIX D

MATHCAD FILE: LEXAN.MCD

Energy Balance for TN Conseil-modified Panel without Snow on Front

$T_{\text{ambient}} := 35$ Degrees Celsius

$\text{Wind} := 2.3.6$ km/h

$\text{Insol}_f := 1000$ W/m²

$\text{Insol}_b := \frac{\text{Insol}_f}{5}$ W/m²

$\text{Diff}_{\text{frac}} := 0.2$ () Diffuse Fraction

$\text{HR} := 0.42$ () Relative humidity

$\text{second} := 53101$ Seconds past midnight

$\text{hour} := \frac{\text{second}}{3600}$ Hours past midnight

$\beta := \frac{\pi}{3}$ Collector Slope

$\eta_{\text{ref}} := 0.1$ Reference efficiency of solar cell

$\text{Pyr}_{\text{corr}} := 1.0$ () Pyranometer Correction factor

$\tau_{f0} := 0.88$ () Normal incidence front panel transmission

$\tau_{f60} := 0.81$ () Diffuse front panel transmission

$\tau_{b60} := 0.79$ () Diffuse back panel transmission

Input Parameter Preprocessing

$\text{Front} := \text{Pyr}_{\text{corr}} \cdot \text{Insol}_f \cdot [\text{Diff}_{\text{frac}} \cdot \tau_{f60} + (1 - \text{Diff}_{\text{frac}}) \cdot \tau_{f0}]$

$\text{Back} := \text{Pyr}_{\text{corr}} \cdot \text{Insol}_b \cdot \tau_{b60}$

$V_{\text{wind}} := \frac{\text{Wind}}{3.6}$

$T := T_{\text{ambient}} + 273.15$

$\ln p_{\text{wsn}} := -\frac{5674.536}{T} + 6.3925 - 0.0096778T + 6.22115710^{-7} \cdot T^2 + 2.0747810^{-9} \cdot T^3 - 9.48410^{-13} \cdot T^4 \dots$
 $+ 4.1635 \ln(T)$

$\ln p_{\text{wsp}} := -\frac{5800.221}{T} + 1.3915 - 0.04864T + 4.176410^{-5} \cdot T^2 - 1.445210^{-8} \cdot T^3 + 6.545967 \ln(T)$

$p_{\text{ws}} := \text{if}(T_{\text{ambient}} > 0, e^{\ln p_{\text{wsp}}}, e^{\ln p_{\text{wsn}}})$ Pressure of saturated pure water, Pa

$p_{\text{w}} := \frac{p_{\text{ws}} \cdot \text{HR}}{1000}$ Partial pressure of water vapour, kPa

$\alpha := \ln(p_{\text{w}})$

$t_{\text{dpp}} := 6.54 + 14.526\alpha + 0.7389\alpha^2 + 0.09486\alpha^3 + 0.4569p_{\text{w}}^{0.1984}$

$t_{\text{dpn}} := 6.09 + 12.608\alpha + 0.4959\alpha^2$

$t_{\text{dp}} := \text{if}(T_{\text{ambient}} > 0, t_{\text{dpp}}, t_{\text{dpn}})$ Deg C Dew point

$$T_{\text{sky}} := T \cdot \left(0.711 + 0.0056 t_{\text{dp}} + 0.000073 t_{\text{dp}}^2 + 0.013 \cos\left(\frac{15 \cdot \text{hour} \cdot \pi}{180}\right) \right)^{\frac{1}{4}}$$

Deg K Sky Temperature

Variables and Constants

$g := 9.81$	m/s ² Gravitational acceleration
$R := 0.286$	kJ/kg/K Ideal gas constant for air at low pressures
$P_{\text{atm}} := 101325$	N/m ² Atmospheric pressure
$\sigma := 5.6697 \cdot 10^{-8}$	W/((m ²)(K ⁴)) Stefan-Boltzmann Constant
$\epsilon_{\text{foil}} := 0.08$	Emissivity of Absorber foil lies in range 0.08 to 0.11 at 100 deg C (p 77)
$\epsilon_{\text{glass}} := 0.88$	Emissivity of Glass from Duffie and Beckman p. 257
$\epsilon_{\text{lex}} := 0.7$	Emissivity of lexan sheet from General Electric Technical hot-line (T unspecified)
$F_{\text{glass_sky}} := \frac{1 + \cos(\beta)}{2}$	Snow-sky shape factor assuming infinite length panel
$F_{\text{glass_ground}} := \frac{1 - \cos(\beta)}{2}$	Snow-ground shape factor assuming infinite length panel
$F_{\text{lex_sky}} := \frac{1 - \cos(\beta)}{2}$	Back panel shape factor for sky assuming infinite length panel
$F_{\text{lex_ground}} := \frac{1 + \cos(\beta)}{2}$	Back panel shape factor for ground assuming infinite length panel
$k_{\text{glass}} := 1.00$	W/m/K CRC value for soda lime glass; same as for low iron soda lime (AFG)
$L_{\text{glass}} := 0.003$	m Thickness of glass-- Nominal, Kim Mitchell, Siemens
$k_{\text{eva}} := 0.29$	W/m/K Thermal conductivity of EVA, Dupont Hotline
$L_{\text{eva}} := 0.00046$	m Thickness of EVA, Dupont
$L_{\text{fp}} := L_{\text{glass}} + L_{\text{eva}}$	m Front panel thickness
$k_{\text{fp}} := \frac{L_{\text{fp}}}{\frac{L_{\text{glass}}}{k_{\text{glass}}} + \frac{L_{\text{eva}}}{k_{\text{eva}}}}$	W/m/K Thermal conduction of front panel
$k_{\text{panel}} := 0.349$	W/m/K Estimate based on component materials-- see page 245,271 lab book
$L_{\text{panel}} := 0.000912$	m Estimate based on component materials-- see page 245,271 labbook
$k_{\text{foil}} := 89.9$	W/m/K Absorber foil thermal conductivity, From TN Conseil Fax
$L_{\text{foil}} := 0.000013$	m from TN Conseil: the foil is 13 Microns
$k_{\text{adh}} := 0.29$	W/m/K Guess: thermal conductivity of adhesive
$L_{\text{adh}} := 0.000050$	m Nominal thickness of adhesive-- from TN Conseil Fax

$k_{lex} := 0.19$ W/m/K Lexan thermal conductivity From Telephone conversation with GE Hotline
 $L_{lex} := 0.0028$ m Measurement of existing lexan sheet
 $V := V_{wind}$ m/s Wind velocity

Empirical relation for convective losses from Watsun p6.2-6

$h_{c_glass_amb} := \text{if}(V < 0.45, 5.0, 0.6 + 6.64\sqrt{V})$
 $h_{c_lex_air} := \text{if}(V < 0.45, 5.0, 0.6 + 6.64\sqrt{V})$ W/m²/K
 $L_{cav} := 0.01$ m Thickness of airspace between absorber foil and Lexan
 $l_{panel} := 1.2$ m Length of M55 panel
 $AR_{IL} := \frac{l_{panel}}{L_{cav}}$ Aspect Ratio of Panel
 $S_{solar} := \text{Front}$ W/m² Solar insolation reaching panel
 $S_{tn} := \text{Back}$ W/m² Solar insolation reaching TN Conseil Foil
 $S_{rb} := 0$ W/m² Energy Input due to reverse biasing
 $T_{sky} := T - 10$
 $T_{amb} := T$ K Ambient air temperature
 $T_{sky} = 298.15$ K Sky temperature
 $T_{ground} := T_{amb} + 2$ K Ground snow-cover temperature--slightly lower than air

Initial Guesses for Variables

$$T_{\text{glass}} := 342$$

$$T_{\text{glass_panel}} := 346$$

$$T_{\text{foil}} := T_{\text{glass_panel}}$$

$$T_{\text{lex_int}} := 314$$

$$T_{\text{lex_ext}} := T_{\text{lex_int}}$$

Function To Solve for Convective Heat Loss Across Airspace

$$T_m(T_1, T_2) := \frac{T_1 + T_2}{2} \quad \text{K} \quad \text{Mean airspace temperature}$$

$$\rho_{\text{air}}(T) := \frac{P_{\text{atm}}}{R \cdot T \cdot 1000} \quad \text{kg/m}^3 \quad \text{Mean air density (assuming ideal gas)}$$

$$\beta_{\text{tec}}(T) := \frac{1}{T} \quad \text{1/K} \quad \text{Isobaric compressibility for ideal gas}$$

The following relations all from VISION software reference manual

$$k_{\text{air}}(T) := (0.0953286 + 0.0033086T) \cdot 2.414 \cdot 10^{-2} \quad \text{W/m/K} \quad \text{Thermal conductivity of air}$$

$$\mu_{\text{air}}(T) := \frac{0.0035165 + 0.0000498T}{1000} \quad \text{kg/m/s} \quad \text{Viscosity of air}$$

$$C_{p_air}(T) := (3.4898964 + 0.0000511T) \cdot 0.2870411000 \quad \text{J/kg/K} \quad \text{Specific heat at constant pressure for air}$$

$$Ra(T_1, T_2) := \frac{(\rho_{\text{air}}(T_m(T_1, T_2)))^2 \cdot L_{\text{cav}}^3 \cdot g \cdot \beta_{\text{tec}}(T_m(T_1, T_2)) \cdot C_{p_air}(T_m(T_1, T_2)) \cdot (T_1 - T_2)}{\mu_{\text{air}}(T_m(T_1, T_2)) \cdot k_{\text{air}}(T_m(T_1, T_2))} \quad \text{Rayleigh number}$$

$$aa := 1.759667810^{-10} \quad bb := 0.028154 \quad cc := 0.0673838 \quad dd := 2.2985 \quad ee := 5 \cdot 10^4$$

$$Nu_1(T_1, T_2) := \text{if}(Ra(T_1, T_2) \leq 10^4, 1 + aa \cdot Ra(T_1, T_2)^{dd}, \text{if}(Ra(T_1, T_2) \leq ee, bb \cdot Ra(T_1, T_2)^{0.4134}, cc \cdot Ra(T_1, T_2)^{0.333}))$$

$$Nu_2(T_1, T_2) := 0.242 \left(\frac{Ra(T_1, T_2)}{AR_{\text{IL}}} \right)^{0.272}$$

The Nusselt Number is the Maximum of Nu1 and Nu2

$$Nu_v(T_1, T_2) := \text{if}(Nu_1(T_1, T_2) < Nu_2(T_1, T_2), Nu_2(T_1, T_2), Nu_1(T_1, T_2)) \quad \text{For a vertical glazing}$$

$$Nu(T_1, T_2) := 1 + (Nu_v(T_1, T_2) - 1) \cdot \sin(\pi - \beta) \quad \text{Nusselt number for a glazing inclined at beta to horizontal}$$

$$h_{c_tn}(T_1, T_2) := Nu(T_1, T_2) \cdot \frac{k_{\text{air}}(T_m(T_1, T_2))}{L_{\text{cav}}} \quad \text{Heat loss coefficient} \quad \text{W/m}^2/\text{K}$$

Solve Block

Given

Equation at the Glass surface

$$\epsilon_{\text{glass}} \cdot F_{\text{glass_sky}} \cdot \sigma \cdot (T_{\text{glass}}^4 - T_{\text{sky}}^4) + \epsilon_{\text{glass}} \cdot F_{\text{glass_ground}} \cdot \sigma \cdot (T_{\text{glass}}^4 - T_{\text{ground}}^4) \dots = 0$$

$$+ h_{\text{c_glass_amb}} (T_{\text{glass}} - T_{\text{amb}}) - \frac{k_{\text{fp}}}{L_{\text{fp}}} \cdot (T_{\text{glass_panel}} - T_{\text{glass}})$$

Equation at the Glass-Cell interface

$$\frac{k_{\text{fp}}}{L_{\text{fp}}} \cdot (T_{\text{glass_panel}} - T_{\text{glass}}) - \frac{1}{\left(\frac{L_{\text{panel}}}{k_{\text{panel}}} + \frac{L_{\text{foil}}}{k_{\text{foil}}} + \frac{L_{\text{adh}}}{k_{\text{adh}}} \right)} \cdot (T_{\text{foil}} - T_{\text{glass_panel}}) \dots = 0$$

$$+ -S_{\text{solar}} - S_{\text{rb}} + \eta_{\text{ref}} S_{\text{solar}}$$

Equation at the Absorber Foil-Cavity interface

$$\frac{1}{\left(\frac{L_{\text{panel}}}{k_{\text{panel}}} + \frac{L_{\text{foil}}}{k_{\text{foil}}} + \frac{L_{\text{adh}}}{k_{\text{adh}}} \right)} \cdot (T_{\text{foil}} - T_{\text{glass_panel}}) + h_{\text{c_tn}}(T_{\text{foil}}, T_{\text{lex_int}}) \cdot (T_{\text{foil}} - T_{\text{lex_int}}) \dots = 0$$

$$+ \frac{\sigma \cdot (T_{\text{foil}}^4 - T_{\text{lex_int}}^4)}{\frac{1}{\epsilon_{\text{foil}}} + \frac{1}{\epsilon_{\text{lex}}} - 1} - S_{\text{tn}}$$

Equation at the Cavity-Lexan interface

$$h_{\text{c_tn}}(T_{\text{foil}}, T_{\text{lex_int}}) \cdot (T_{\text{foil}} - T_{\text{lex_int}}) + \frac{\sigma \cdot (T_{\text{foil}}^4 - T_{\text{lex_int}}^4)}{\frac{1}{\epsilon_{\text{foil}}} + \frac{1}{\epsilon_{\text{lex}}} - 1} - \frac{k_{\text{lex}}}{L_{\text{lex}}} \cdot (T_{\text{lex_int}} - T_{\text{lex_ext}}) = 0$$

Equation at the Lexan-outside air interface

$$h_{\text{c_lex_air}}(T_{\text{lex_ext}} - T_{\text{amb}}) + \epsilon_{\text{lex}} \cdot F_{\text{lex_ground}} \cdot \sigma \cdot (T_{\text{lex_ext}}^4 - T_{\text{ground}}^4) \dots = 0$$

$$+ \epsilon_{\text{lex}} \cdot F_{\text{lex_sky}} \cdot \sigma \cdot (T_{\text{lex_ext}}^4 - T_{\text{sky}}^4) - \frac{k_{\text{lex}}}{L_{\text{lex}}} \cdot (T_{\text{lex_int}} - T_{\text{lex_ext}})$$

Non-negativity Constraints

$$T_{\text{glass}} > 0$$

$$T_{\text{glass_panel}} > 0$$

$$T_{\text{foil}} > 0$$

$$T_{\text{lex_int}} > 0$$

$$T_{\text{lex_ext}} > 0$$

$$\text{Result} := \text{Find}(T_{\text{glass}}, T_{\text{glass_panel}}, T_{\text{foil}}, T_{\text{lex_int}}, T_{\text{lex_ext}})$$

$$\text{Result} = \begin{pmatrix} 352.50506 \\ 356.18499 \\ 356.24903 \\ 318.9667 \\ 316.97709 \end{pmatrix} \quad \begin{array}{l} \text{Results valid for Rayleigh numbers between 100 and 1 000 000} \\ \text{Ra}(\text{Result}_3, \text{Result}_4) = 143.08368 \quad h_{\text{c_tm}}(\text{Result}_3, \text{Result}_4) = 2.76979 \\ \text{Check on Rayleigh number} \end{array}$$

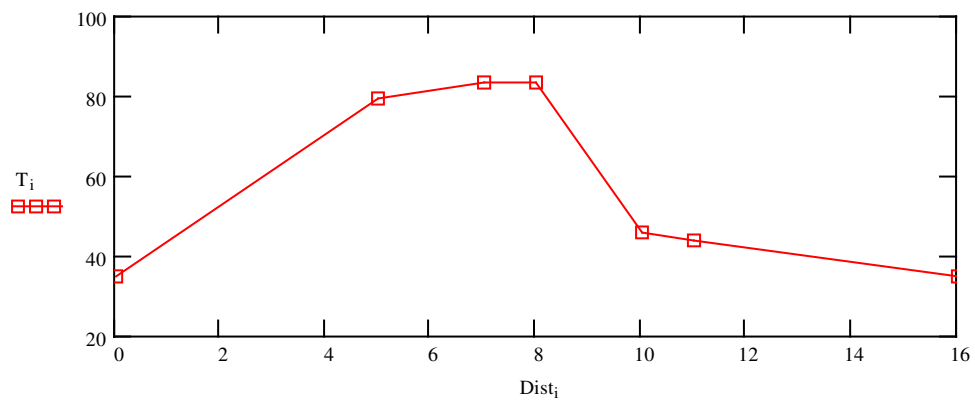
$$\text{Result} - 273.16 = \begin{pmatrix} 79.34506 \\ 83.02499 \\ 83.08903 \\ 45.8067 \\ 43.81709 \end{pmatrix}$$

$$\text{Dist} := \begin{pmatrix} 0 \\ 5 \\ 7 \\ 8 \\ 10 \\ 11 \\ 16 \end{pmatrix}$$

$$\text{T} := \begin{pmatrix} T_{\text{amb}} \\ \text{Result}_0 \\ \text{Result}_1 \\ \text{Result}_2 \\ \text{Result}_3 \\ \text{Result}_4 \\ T_{\text{amb}} \end{pmatrix} - 273.16$$

$i := 0, 1..6$

This is just for visualization



APPENDIX E

C PROGRAM TO SIMULATE RIME SHEDDING AND MELTOFF FROM TN PANEL AT NORMAN WELLS AND DANIELS HARBOUR

```

/*****
/*
/* TTM- Time to Melt
/* Program to analyse Canadian Meteorological Files
/*
/*
/* Michael Ross--Energy Diversification Research Laboratory
/*
/* This program searches through all the annual meteorological
/* files for a particular site. It assumes a rime/snow accum-
/* -ulation of 5cm/8cm starting Jan 1, then calculates how long
/* it will take to melt off, using the critical thickness and
/* complete melt-off assumption.
/*
/* Standard TN panel, rime, low mountains.
*****/

#include <stdio.h>
#include <stdlib.h>
#include <string.h>
#include <math.h>

/*
#define START_YR 59
#define LAST_YR 59
*/

#define GLOB_POS 18
#define DIFF_POS 30
#define TEMP_POS 89
#define WIND_POS 103
#define MON_POS 8
#define DAY_POS 10
#define HOUR_POS 12

#define FILE_N_LEN 60
#define LINE_LEN 250
#define PI 3.1415

#define WIND_CORR 2
#define TEMP_CORR -5
#define ALBEDO 0.7 /*must be float */
#define KOPT 30

#define AUTHOR "Michael Ross--EDRL 95/08/11\n"

/*****
/* Global variables
*****/

```

```

/* For Rime */

float ColV[3]={5.0,10.0,20.0}; /* Wind Speeds */
float RowV[3]={1.0,3.0,5.0}; /* Thicknesses */
float LayerV[2]={1080.0,3600.0}; /*Insolation, kJ/m^2 */

/* Parameter Matrices */
/* The parameters for the same wind value all appear in same row. */

/* For Rime, Unmodified Panel */
/*
float Slopes[3][3]={ {0.068978,0.059091,0.048397},
                    {0.087622,0.068872,0.056994},
                    {0.109759,0.082597,0.06497}};
float Tcrit[2][3][3]={ { {-2.8,-1.0,0.3},
                        {-2.2,-1.0,0.0},
                        {-1.8,-1.0,-0.2} },
                      { {-16.1,-9.6,-5.5},
                        {-12.5,-8.3,-4.9},
                        {-9.8,-7.0,-4.5} }};
*/
/* For Rime, Standard TN Panel */

float Slopes[3][3]={ {0.040367,0.033793,0.029326},
                    {0.050804,0.040519,0.033917},
                    {0.064264,0.048112,0.039008}};
float Tcrit[2][3][3]={ { {-7.6,-3.8,-1.1},
                        {-6.2,-3.4,-1.3},
                        {-5.0,-3.2,-1.5} },
                      { {-34.7,-21.5,-12.35},
                        {-27.7,-18.2,-11.0},
                        {-22.0,-15.6,-9.9} }};

/* For Rime, TN Panel with Rime Shield */

/*
float Slopes[3][3]={ {0.039627,0.033082,0.028586},
                    {0.049923,0.039797,0.033301},
                    {0.06331,0.047603,0.038214}};
float Tcrit[2][3][3]={ { {-8.3,-5.6,-3.9},
                        {-6.7,-5.0,-3.7},
                        {-5.5,-4.4,-3.6} },
                      { {-37.0,-27.7,-21.6},
                        {-29.5,-23.3,-19.0},
                        {-23.4,-19.8,-16.9} }};
*/
/* For Snow */

/* float ColV[3]={2.0,5.0,10.0}; /* Wind Speeds */

```

```

/* float RowV[4]={1.0,3.0,5.0,8.0}; /* Thicknesses */
/* float LayerV[2]={1080.0,3600.0}; /*Insolation, kJ/m^2 */

/* For Snow, Unmodified Panel */
/*
float Slopes[3][4]={ {0.042837,0.035412,0.032284,0.029752},
                     {0.056302,0.046194,0.042012,0.038503},
                     {0.069738,0.056503,0.052073,0.048545}};
float Tcrit[2][3][4]={ { {-5.6,-3.7,-2.0,-0.5},
                          {-4.5,-3.0,-1.6,-0.5},
                          {-3.7,-2.6,-1.4,-0.5} },
                       { {-27.3,-19.1,-12.3,-6.6},
                          {-20.5,-14.5,-9.4,-5.1},
                          {-16.3,-11.7,-7.5,-4.0} }};
*/
/* For Snow, Standard TN Panel */
/*
float Slopes[3][4]={ {0.021202,0.014157,0.011287,0.009158},
                     {0.025491,0.015758,0.012254,0.009756},
                     {0.028816,0.016794,0.012867,0.0102}};
float Tcrit[2][3][4]={ { {-17.5,-18.2,-15.9,-13.3},
                          {-15.4,-17.4,-15.7,-13.4},
                          {-14.1,-16.9,-15.6,-13.5} },
                       { {-70.8,-69.2,-60.7,-51.7},
                          {-59.4,-63.0,-56.8,-49.2},
                          {-53.0,-59.5,-54.6,-47.7} }};
*/

/*****
/* Function to Churn out a informative header for the output file */
*****/

int Out_Header(FILE *File_Ptr,char *Src_File)
{
    fprintf(File_Ptr,"Program to Predict Melt-off Time based on "
              "Meteorological Conditions.\n");
    fprintf(File_Ptr,"Standard TN panel, rime in low mountains.\n");
    fprintf(File_Ptr,AUTHOR);
    fprintf(File_Ptr,"\n\nInput File: %s \n\n",Src_File);
    fprintf(File_Ptr,"\n\n");
    fprintf(File_Ptr,"=====\n");

    return(0);
}

/*****
/* function to interpolate between 300 and 1000 w/m^2 Tcrit */
*****/

```

```

float CT(int col, int row, float Insol)
{
    return(Tcrit[0][col][row]+(Insol-1080.0)*
        ((Tcrit[1][col][row]-Tcrit[0][col][row])/2520.0));
}

/*****
/* function to calculate Rb, the ratio of beam radiation on a
/* tilted surface to that on a horizontal surface
*****/

float Calc_Rb(float Lat, int month, int day, int hour, float slope)
{
    int n_day;
    int Days_in_M[12]={0,31,59,90,120,151,181,212,243,273,304,334};
    float hour_ang;
    float declin;
    float cosZenith;
    float cosAngInc;
    float Rb;

    /*printf("Lat %f month %d day %d hour %d tilt %f\n",Lat,month,day,hour,slope);*/
    /* Calculate day of year */
    n_day=day+Days_in_M[month-1];

    /* Calculate declination */
    declin=23.45*sin(2.0*((float)(284+n_day))/365.0*PI);

    /* calculate hour angle */
    hour_ang=15.0*(((float)hour)-12.5);

    /* calculate zenith angle */
    cosZenith=cos(Lat*PI/180.0)*cos(declin*PI/180.0)*cos(hour_ang*PI/180.0)+
        sin(Lat*PI/180.0)*sin(declin*PI/180.0);

    /* calculate angle of incidence */
    cosAngInc=sin(declin*PI/180.0)*sin(Lat*PI/180.0)*cos(slope*PI/180.0);
    cosAngInc-=sin(declin*PI/180.0)*cos(Lat*PI/180.0)*sin(slope*PI/180.0);
    cosAngInc+=cos(declin*PI/180.0)*cos(Lat*PI/180.0)*cos(slope*PI/180.0)*cos(hour_ang*PI/180.0);
    cosAngInc+=cos(declin*PI/180.0)*sin(Lat*PI/180.0)*sin(slope*PI/180.0)*cos(hour_ang*PI/180.0);

    /*printf("\n %d declin %f hourang %f coszen %f cosanginc %f\n",n_day, declin,
    hour_ang,cosZenith,cosAngInc);*/

    /* calculate Rb, if sun is within 5 degrees of horizon, set Rb to 1 */
    if ((cosZenith>0.087)&&(cosAngInc>0.0))
        Rb = cosAngInc/cosZenith;
    else
        Rb = 1.0;
    return(Rb);
}

```

```
}
```

```

/*****
/* main */
*****/

main(int argc, char *argv[])
{
    char Src_File[FILE_N_LEN];
    char Src_File_Root[FILE_N_LEN];
    char Dest_File[FILE_N_LEN];

    FILE *Src_Ptr;
    FILE *Dest_Ptr;

    char Inp_Line[LINE_LEN];
    char Fin_String[LINE_LEN];
    char Bogus[LINE_LEN];

    int Start_Yr;
    int End_Yr;
    int Yr_Count;
    int Count;
    int Hours_Covered;
    float Acc_Insol;
    char Temp_Str[6];
    float Thickness;
    float OldThick;
    float Latitude;
    float Tilt;

    int windspeed; /* speed (m/s) times ten */
    int Temperature; /* temp times ten*/
    float windspeedf; /* speed, m/s */
    float Temperaturef; /* Temp, C */
    int Glob_Rad; /* kj/m2 */
    int Diff_Rad; /* kj/m2 */
    int Month;
    int Day_of_Month;
    int Hour;
    int ShedFlag;
    int DoneFlag;

    float Kd; /* diffuse fraction */
    float BeamT; /* Beam radiation on tilted surface */
    float DiffT; /* Diffuse radiation on tilted surface */
    float GrT; /* Ground-reflected radiation on a tilted surface */
    float TotT; /* Total radiation on a tilted surface. */
    int Col1,Col2,Row1,Row2; /* indices into matrix of slopes and Tcrits */

```

```

float TC_LW, TC_HW, FinalTc, Slope_LW, Slope_HW, Finalslope;

/* Check to see whether the correct number of input parameters was */
/* encountered. If not print a message. */
if (argc!=7)
{
    printf("\nProgram to Predict Time to Meltoff Based on");
    printf(" Meteorological Conditions.\n");
    printf("Standard TN Panel, Rime in low Mountains.\n");
    printf(AUTHOR);
    printf("\nUSAGE: TTMRTN <SRC_FILE_ROOT> <DEST_FILE> <START> <END> <LATITUDE> <TILT>\n");
    printf("where <SRC_FILE_ROOT> does not include extension.\n");
    printf("and <START> and <END> are the first and last years to be examined.\n");
    /* printf("Temp Crit = %f\n",CT(0,0,2343.0));
    printf("Ratio beam = %f\n",Calc_Rb(40.0,2,16,9,30.0));
    printf("Ratio beam = %f\n",Calc_Rb(40.0,2,16,10,30.0));*/
}
else
{

strcpy(Src_File_Root,argv[3]);
strcpy(Dest_File,argv[4]);
Start_Yr=atoi(Src_File_Root);
End_Yr=atoi(Dest_File);
strcpy(Dest_File,argv[5]);
strcpy(Src_File_Root,argv[6]);
Latitude = atof(Dest_File);
Tilt = atof(Src_File_Root);
strcpy(Src_File_Root,argv[1]);
strcpy(Dest_File,argv[2]);

strcpy(Temp_Str,"Garb");
strcpy(Fin_String,"12345123451234 ");

/* Open Output file */
if ((Dest_Ptr=fopen(Dest_File,"w"))!=NULL)
{
    printf("Creating output File...\n");
    Out_Header(Dest_Ptr,Src_File_Root);

    /* Loop through all the years of data files */
    for(Yr_Count=Start_Yr;(Yr_Count<=End_Yr);Yr_Count++)
    {
        Hours_Covered=0;
        Acc_Insol=0.0;
        Thickness=5.0;
        ShedFlag = 0;
        DoneFlag = 0;
        strcpy(Src_File,Src_File_Root);
    }
}

```

```

strcat(Src_File, ".y");
strcat(Src_File, itoa(Yr_Count, Bogus, 10));

if ((Src_Ptr=fopen(Src_File, "r"))!=NULL)
{
    printf("Processing input file %s\n", Src_File);
    while((fgets(Inp_Line, sizeof(Inp_Line), Src_Ptr)!=NULL) && (DoneFlag == 0))
    {

        /* Extract the data */
        for(Count=0; Count<4; Count++)
            Temp_Str[Count]=Inp_Line[GLOB_POS+Count];
        Glob_Rad=atoi(Temp_Str);
        for(Count=0; Count<4; Count++)
            Temp_Str[Count]=Inp_Line[DIFF_POS+Count];
        Diff_Rad=atoi(Temp_Str);

        for(Count=0; Count<4; Count++)
            Temp_Str[Count]=Inp_Line[TEMP_POS+Count];
        Temperature=atoi(Temp_Str);
        for(Count=0; Count<4; Count++)
            Temp_Str[Count]=Inp_Line[WIND_POS+Count];
        windspeed=atoi(Temp_Str);

        strcpy(Temp_Str, "12");
        for(Count=0; Count<2; Count++)
            Temp_Str[Count]=Inp_Line[MON_POS+Count];
        Month=atoi(Temp_Str);
        for(Count=0; Count<2; Count++)
            Temp_Str[Count]=Inp_Line[DAY_POS+Count];
        Day_of_Month=atoi(Temp_Str);
        for(Count=0; Count<2; Count++)
            Temp_Str[Count]=Inp_Line[HOURL_POS+Count];
        Hour=atoi(Temp_Str);
        /*printf("\nMonth %d Day %d Hour %d windx10 %d\n Tempx10 %d GInsol %d DInsol
        %d\n", Month, Day_of_Month, Hour, windspeed, Temperature, Glob_Rad, Diff_Rad); */
        if ((Temperature!=9999)&&(Glob_Rad!=9999)&&(Diff_Rad!=9999))
        {
            /* Adjust the windspeed and temperature so */
            /* that it matches the site. */

            windspeedf=((float) (windspeed*WIND_CORR))/10.0;
            Temperaturef=((float) (Temperature+(10*TEMP_CORR)))/10.0;
            /*printf("wind %f Temp %f Lat %f Tilt %f\n", windspeedf, Temperaturef, Latitude, Tilt); */
            /* Calculate radiation on the panel */
            /* angle from global, diffuse, direct. */

            if (Glob_Rad != 0)
            {
                Kd=((float) Diff_Rad)/((float) Glob_Rad);
            }
        }
    }
}

```

```

        /* calculate diffuse fraction */
        BeamT=(1.0-Kd)*((float) Glob_Rad)*Calc_Rb(Latitude,Month,Day_of_Month,Hour,Tilt);
        DiffT=((float) Diff_Rad)*((1.0+cos(Tilt*PI/180.0))/2.0);
        GrT=((float) Glob_Rad)*ALBEDO*((1.0-cos(Tilt*PI/180.0))/2.0);
        TotT=BeamT+DiffT+GrT;
    }
    else
        TotT=0.0;
    /*printf("TotT = %f\n",TotT);*/

    /* Find Indices into Parameter Matrices */

    Col1=0;
    Col2=0;
    if (( windspeedf > ColV[0]) && (windspeedf <= ColV[1]))
        Col2=1;
    if (( windspeedf > ColV[1]) && (windspeedf < ColV[2]))
    {
        Col1=1;
        Col2=2;
    }
    if ( windspeedf >= ColV[2])
    {
        Col1=2;
        Col2=2;
    }

    Row1=0;
    Row2=0;
    if (( Thickness > RowV[0]) && (Thickness <= RowV[1]))
        Row2=1;
    if (( Thickness > RowV[1]) && (Thickness < RowV[2]))
    {
        Row1=1;
        Row2=2;
    }
    if ( Thickness >= RowV[2])
    {
        Row1=2;
        Row2=2;
    }

    /*printf("Thickness %f\n",Thickness);*/
    /*printf("col1 = %d col2 = %d row1 = %d row2 = %d \n",Col1,Col2,Row1,Row2);*/
    /* Find the critical temperature.*/

    if (Row1 != Row2)
    {
        TC_LW = CT(Col1,Row1,TotT)+

```

```

        (Thickness-RowV[Row1]))*
        (CT(Col1,Row2,TotT)-CT(Col1,Row1,TotT))/
        (RowV[Row2]-RowV[Row1]);
    TC_HW = CT(Col2,Row1,TotT)+
        (Thickness-RowV[Row1))*
        (CT(Col2,Row2,TotT)-CT(Col2,Row1,TotT))/
        (RowV[Row2]-RowV[Row1]);
}
else
{
    TC_LW = CT(Col1,Row1,TotT);
    TC_HW = CT(Col2,Row1,TotT);
}
if (TC_LW != TC_HW)
    FinalTc=TC_LW+(windspeedf-ColV[Col1])*
        (TC_HW-TC_LW)/(ColV[Col2]-ColV[Col1]);
else
    FinalTc=TC_LW;

/* Check if ambient air temp is above crit temp. */
/*printf("Critical Temp is %f\n",FinalTc);*/
OldThick = Thickness;
if (Temperaturef > FinalTc)
{
    if (ShedFlag == 0)
    {
        fprintf(Dest_Ptr,"%d Shed: M %d D %d H %d (%d Hrs) T: %f
I:%f\n",Yr_Count,Month,Day_of_Month,Hour,Hours_Covered,Temperaturef,TotT);
    }
    ShedFlag = 1;

    /* Find melt rate and reduce thickness */

    if (Row1 != Row2)
    {
        Slope_LW = Slopes[Col1][Row1]+
            (Thickness-RowV[Row1))*
            (Slopes[Col1][Row2]-Slopes[Col1][Row1])/
            (RowV[Row2]-RowV[Row1]);
        Slope_HW = Slopes[Col2][Row1]+
            (Thickness-RowV[Row1))*
            (Slopes[Col2][Row2]-Slopes[Col2][Row1])/
            (RowV[Row2]-RowV[Row1]);
    }
    else
    {
        Slope_LW = Slopes[Col1][Row1];
        Slope_HW = Slopes[Col2][Row1];
    }
    if (Slope_LW != Slope_HW)

```

```

        FinalSlope=Slope_LW+(windspeedf-ColV[Col1])*
        (Slope_HW-Slope_LW)/(ColV[Col2]-ColV[Col1]);
    else
        FinalSlope=Slope_LW;
    /*printf("Melt-rate is %f\n", FinalSlope);*/
    Thickness = Thickness - FinalSlope*(Temperaturef-FinalTc);
    /*printf("Thickness is %f\n", Thickness);*/
}

/* check to see whether the accumulation is gone. */

if (Thickness > 0.0)
{
    /* if not, add another hour, add solar energy. */
    Hours_Covered++;
    /*printf("Accum Insol before: %f",Acc_Insol);*/
    Acc_Insol += TotT*exp(-KOPT*(Thickness+OldThick)/200);
    /*printf("Accum Insol after: %f\n",Acc_Insol);*/
}
else
{
    /* if so, print the result and finish the year. */
    fprintf(Dest_Ptr,"%d Melt: M %d D %d H %d (%d Hrs) T: %f
I:%f\n",Yr_Count,Month,Day_of_Month,Hour,Hours_Covered,Temperaturef,TotT);
    DoneFlag = 1;
}
}
else
    printf("Error in input file.\n");
} /*End "while there is input"*/
} /*end "if can open source file"*/

fclose(Src_Ptr);
} /*end "for all years"*/

fclose(Dest_Ptr);
} /*end "if can open destination file"*/
else
    printf("Couldn't open output file.\n");
} /*end "if command line makes sense"*/
return(0);
} /*end main*/

```